SUBSTANTIATION OF USING GEOPOLYMER IN DEEP MIXING METHOD: AN EXPERIMENTAL INVESTIGATION

By

Most. Mukta Banu

Student ID: 15MCE024P

A Thesis Submitted in Partial Fulfilment of the Requirements for the Degree of

MASTER of SCIENCE in CIVIL ENGINEERING

Department of Civil Engineering

CHITTAGONG UNIVERSITY OF ENGINEERING AND TECHNOLOGY

January, 2025

The thesis titled

Substantiation of Using Geopolymer in Deep Mixing Method: An Experimental Investigation

Submitted by

Most. Mukta Banu

Student ID: 15MCE024P; Session: 2015-16

has been accepted as satisfactory in partial fulfillment of the requirements for the degree of Master of Science in Civil Engineering on 5th January, 2025.

BOARD OF EXAMINERS

Dr. Md. Aftabur Rahman Professor, Department of Civil Engineering Chittagong University of Engineering and Technology	Chairman (Supervisor)
(Dr. Aysha Akter) Professor and Head, Department of Civil Engineering Chittagong University of Engineering and Technology	Member (Ex-Officio)
Sultan Mohammad Farooq Associate Professor, Department of Civil Engineering Chittagong University of Engineering and Technology	Member (Internal)
Dr. Md. Zoynul Abedin Professor, Department of Civil Engineering Military Institute of Science and Technology and Professor (Retired), Department of Civil Engineering Bangladesh University of Engineering and Technology	Member (External)

Declaration

I hereby declare that the work contained in this thesis has not been previously submitted to meet the requirements for an award at this or any other higher education institution. To the best of my knowledge and belief, the thesis contains no material previously published or written by another person except where due reference is cited. Furthermore, the Thesis complies with PLAGIARISM and ACADEMIC INTEGRITY regulation of Chittagong University of Engineering and Technology.

Most. Mukta Banu

Student ID: 15MCE024P

Department of Civil Engineering

Chittagong University of Engineering and Technology

January, 2025

Copyright © Most. Mukta Banu, 2025.

This work may not be copied without permission of the author or Chittagong University of Engineering and Technology.

Dedication

To my Parents

List of Publications

Conference Paper

1. **Most. Mukta Banu** and Md. Aftabur Rahman (2024). "**Experimental Investigation on Geopolymer-Based Deep Mixing Method on Soft Soils"** " in Proceedings of International Conference on Geo-Structures 2024 GSP 361 270. 270–279, November 17-20, 2024, Pittsburg, Pennsylvania. (https://doi.org/10.1061/9780784485842.026)

2. Md. Al Mamun, Md. Rakibul Hassan, **Most. Mukta Banu** and Md. Aftabur Rahman (2024). "**Sand-Geopolymer Mixture On Strength Development Of Soft Soils: An Experimental Investigation"** In Proceedings of 7th International Conference on Civil Engineering for Sustainable Development (ICCESD). February 07–09, KUET, Khulna-9203, Bangladesh. (www.iccesd.com/proc_2024/Papers/596.pdf)

3. Md. Habibun. Nabi , Sagarmoy Acharjee , **Most. Mukta Banu** and Md. Aftabur Rahman (2023). "**Effect of Geopolymer Contents on Strength Development of Soft Soils**" in Proceedings of 4th International Conference on Planning, Architecture and Civil Engineering (ICPACE). October 12–14, RUET, Rajshahi, Bangladesh. (https://icpaceruet.org/wp-content/uploads/2023/10/CE-0190.pdf)

Approval by the Supervisor

This is to certify that Most. Mukta Banu has carried out this research work under my supervision and that she has fulfilled the relevant Academic Ordinance of the Chittagong University of Engineering and Technology so that she is qualified to submit this thesis in the application for the degree of MASTER of SCIENCE in Civil Engineering. Furthermore, the thesis complies with the PLAGIARISM and ACADEMIC INTEGRITY regulations of Chittagong University of Engineering and Technology.

Dr. Md. Aftabur Rahman

Professor

Department of Civil Engineering

Chittagong University of Engineering and Technology

Acknowledgements

First and foremost, all praise and thanks are due to Allah, the Most Gracious and the Most Merciful. By His mercy and guidance, the author was granted the strength and perseverance to complete this research. Without His blessings, this work would not have been possible.

The author expresses her heartiest gratitude to her supervisor Dr. Md. Aftabur Rahman, Professor, Department of Civil Engineering, Chittagong University of Engineering and Technology, for his continuous guidance, support, inspiration and encouragement throughout this study. His dedication, valuable suggestions, proper directions, constructive advice at every stage made this study successful.

Laboratory assistance provided by the staff, the technicians and the officers of Geotechnical Engineering Laboratory, Department of Civil engineering, Chittagong University of Engineering and Technology, is duly acknowledged.

The author expresses her gratitude to the Instrument Engineers and Technical Officers of Multi Scale Characterization Laboratory of the Department of Nanomaterials and Ceramic Engineering, Bangladesh University of Engineering and Technology, and Atomic Energy Commission, Bangladesh, for all the technical supports.

The author acknowledges the assistance of her husband Mr. Md. Siddiqur Rahman, B.Sc. in Computer Science Engineering, Bangladesh University of Engineering and Technology, and brother Mr. Md. Manik Hossain, B.Sc. in Materials and Metallurgical Engineering, Bangladesh University of Engineering and Technology, in the statistical and mineralogical analysis of this study respectively.

The author would also like to thank her Parents for their continuous inspiration.

Abstract

(Thesis Title: Substantiation of Using Geopolymer in Deep Mixing Method: An Experimental Investigation)

Soft soils encounter a serious problem for the stability of the superstructure, and this has been a crucial issue since the beginning of the history. Among various ground improvement options, the Deep Mixing Method is one of the promising methods that can alter the soil matrix at close spacing and resemble pile-like responses that can provide sufficient reactions to the superimposed loads. Cement is generally mixed with problematic soils and has proven to be effective in many applications; however, environmental concerns have become substantial in cement-treated ground improvement options. Alternately, waste materials, mostly Fly Ash or Slag, have been considered as replacements of cement for possible applications. Fly Ash is being produced in high amount globally as an industrial byproduct; its disposal is a big concern and, hence, attracted concern of the geotechnical experts for its utilization especially in ground improvement. To date, fly ash has been mostly considered for shallow ground improvement, while its justification in deep mixing is seldom found in technical writings. The available applications mostly focus on treating granular materials. The present study, as such, aims to explore the possibility of utilizing fly ash in the deep mixing method. To enhance the bonding, a chemical additive, commonly known as an alkali activator, has been added to the fly ash to form a geopolymer that has been added with the parent soils at different fly ash proportions ranging from 10% to 25% of the dry weight of soils. In addition to the variation of geopolymer, three different moisture levels of soils, at the liquid limit and on both sides of the liquid limit, have been considered in this research. A number of samples of each considered case has been prepared at three different curing ages: 14 days, 28 days, and 56 days, in order to find the

effectiveness of the fly ash-based geopolymer treated deep mixing method in ground improvement.

The Unconfined Compressive Strength has been found to increase with the increase of fly ash content in all cases. The increase of strength has been found to depend on the optimum dosage of both alkali activator and precursor binder (fly ash). Moisture sensitivity has been seen as distinctive, and geo-polymerization of soil in the wet phase has no portrayed considerable strength development. In this study, the activator-to-precursor binder ratio of 0.5 with fly ash contents of 20-25% has shown the highest strength gain in approximately all scenarios. Based on the discrete datasets, predictive models, keeping the aim of estimating preliminary compressive strength, have been developed considering the non-linearity and influence of different properties. Several prediction models (both equation based and Machine Learning models) have been developed, and model performances have been compared with the experimental data. The highest accuracy has been observed from Exponential Gaussian Process Regression Model with an R^2 value of 0.97 which indicates that the model fits excellently with an ability to explain 97% of the experimental data. Furthermore, Mineralogical bond formation of stabilized soil has been observed from X-ray diffraction (XRD) pattern and Scanning Electron Microscope (SEM) image. Densification and void reduction due to geo-polymerization process in soil-geopolymer mix as well as the surface texture having no cracks in micro level have been observed from SEM image. XRD pattern analysis provided the information about the compounds present in the mix by which susceptible elements can be identified. Overall, this research provides a base for the use of waste-based geopolymer in deep mixing methods in alluvial deposition.

বিমূর্ত

(Thesis Title: Substantiation of Using Geopolymer in Deep Mixing Method: An Experimental Investigation)

ইতিহাসের শুরু থেকে কাঠামোর স্থিতিশীলতার ক্ষেত্রে নরম মাটির কারণে গুরুতর সমস্যার সম্মুখীন হতে হয়। মাটি উন্নতকরণের বিভিন্ন প্রক্রিয়ার মধ্যে গভীর মিশ্রণ (Deep Mixing) একটি প্রতিশ্রুতিশীল প্রক্রিয়া, যা মাটি ম্যাট্রিক্সকে পরিবর্তন করে স্বল্প ব্যবধান পরপর পাইল এর মত কার্যকর করে তোলে, যা উপরে চাপানো লোডের বিপরীতে যথেষ্ট প্রতিক্রিয়া দিতে পারে। সাধারণত সমস্যাযুক্ত মাটির সাথে সিমেন্ট মিশ্রিত করা হয় যা কার্যকর প্রমাণিত হয়েছে, কিন্তু সিমেন্ট দ্বারা মাটি উন্নতকরণ বিকল্পগুলোর ক্ষেত্রে যথেষ্ট পরিবেশগত উদ্বেগ রয়েছে। সম্ভাব্য ক্ষেত্রে বর্জ্য পদার্থ, বেশিরভাগ ক্ষেত্রে ফ্লাই অ্যাশ, স্ল্যাগ সিমেন্টের বিকল্প হিসেবে বিবেচিত হয়েছে। বিশ্বজুড়ে শিল্পকারখানায় অনেক বেশি পরিমাণে ফ্লাই অ্যাশ উপজাত হিসেবে উৎপাদিত হয়, এগুলোকে নিষ্কাশন করা বড় উদ্বেগের বিষয়, একারণে জিওটেকনিকাল অভিজ্ঞদেরকে আকর্ষণ করছে মাটি উন্নতকরণের কাজে এটার সঠিক ব্যবহারের জন্য। আজ পর্যন্ত অগভীর ভূমি উন্নতকরণের জন্যই ফ্লাই অ্যাশকে বিবেচনা করা হয়েছে, যেকারণে প্রযুক্তিগত লিখায় গভীর মাটি মিশ্রণের ন্যায্যতা খুব কমই পাওয়া যায়। একইভাবে, উপলব্ধ প্রয়োগের ক্ষেত্রে বেশিরভাগই দানাদার পদার্থের উন্নতকরণে গুরুত্ব দেয়া হয়। সীমাবদ্ধতার উপর লক্ষ্য রেখে এই গবেষণার উদ্দেশ্য হল গভীর মিশ্রণ পদ্ধতিতে ফ্লাই অ্যাশ এর সদ্ব্যবহারের সম্ভাবনা অন্বেষন করা। বন্ধন বাড়ানোর জন্য, একটি রাসায়নিক অ্যাডিটিভ, যা সাধারণত একটি ক্ষারীয় অ্যাক্টিভেটর নামে পরিচিত, জিওপলিমার তৈরি করতে যুক্ত করা হয়েছে ফ্লাই অ্যাশ এ যা শুষ্ক মাটির ওজনের ১০% থেকে ২৫% পর্যন্ত বিভিন্ন অনুপাতে মূল মাটির সাথে যোগ করা হয়েছে। এই গবেষণায় জিওপলিমার ভিন্নতা ছাড়াও, মাটির তিনটি ভিন্ন আর্দ্রতা স্তর, বিশেষ করে লিকুইড লিমিট এবং লিকুইড লিমিট এর উভয় পাশে, বিবেচনা করা হয়েছে। বর্ণিত রূপরেখা অনুসরণ করে, ফ্লাই অ্যাশ ভিত্তিক জিওপলিমার উন্নতকরন গভীর মিশ্রণ পদ্ধতির মেকানিক্স বোঝার জন্য প্রতিটি বিবেচিত ক্ষেত্রে অনেকগুলো নমুনা তিনটি ভিন্ন কিউরিং বয়স ১৪ দিন, ২৮ দিন এবং ৫৬ দিন এর জন্য প্রস্তুত করা হয়েছে।

সমস্ত ক্ষেত্রে ফ্লাই অ্যাশ পরিমাণ বৃদ্ধির সাথে অবরুদ্ধিত চাপ সহনশীলতা (Unconfined Compressive Strength) বৃদ্ধি পাওয়া গেছে। এদিকে, শক্তির বিকাশ নির্ভর করে অ্যাডিটিভ এবং প্রিকার্সর বাইন্ডার (ফ্লাই অ্যাশ) উভয়ের সর্বোত্তম ডোজ। আর্দ্রতা সংবেদনশীলতাকে স্বাতন্ত্র্যসূচক হিসাবে দেখা হয়েছে, এবং আর্দ্র পর্যায়ে মাটির জিওপলিমারিজেশন যথেষ্ট শক্তি বিকাশকে চিত্রিত করে না। এই গবেষণায়, ২০-২৫% এর ফ্লাই অ্যাশ এর সাথে ০.৫ এর অ্যাক্টিভেটর-টু-প্রিকার্সর বাইন্ডার অনুপাত প্রায় সমস্ত ক্ষেত্রে সর্বোচ্চ শক্তি বৃদ্ধি দেখায়। বিচ্ছিন্ন ডেটাসেটের উপর ভিত্তি করে বিভিন্ন অ-রৈখিক বৈশিষ্ট্যে এবং প্রভাব বিবেচনা করে অবরুদ্ধিত চাপ সহনশীলতা অনুমান করার লক্ষ্যে ভবিষ্যদ্বাণী (Prediction) মডেলগুলি তৈরি করা হয়েছে। বেশ কিছু ভবিষ্যদ্বাণী মডেল (সমীকরণ ভিত্তিক এবং মেশিন লার্নিং মডেল উভয়) তৈরি করা হয়েছে, এবং মডেলের কর্মক্ষমতা (Performance) পরীক্ষণকৃত ডেটার সাথে তুলনা করা হয়েছে। R^2 এর মান ০.৯৭ সহ এক্সপোনেনশিয়াল গাউসিয়ান প্রসেস রিগ্রেশন মডেল থেকে সর্বোচ্চ নির্ভুল ভবিষ্যদ্বাণী পরিলক্ষিত হয়েছে যা নির্দেশ করে যে মডেলটি পরীক্ষণকৃত ডেটার ৯৭% ব্যাখ্যা করার সক্ষমতা সহ চমৎকারভাবে ফিট করে। অধিকন্তু, এক্স-রে ডিফ্র্যাকশন (XRD) প্যাটার্ন এবং স্ক্যানিং ইলেক্ট্রন মাইক্রোস্কোপ (SEM) ইমেজ থেকে স্থিতিশীল মাটির খনিজ বন্ড গঠন লক্ষ্য করা গেছে। মাটি-জিওপলিমার মিশ্রণে জিও-পলিমারাইজেশন প্রক্রিয়ার কারণে ঘনত্ব এবং ভয়েড হ্রাস সেইসাথে SEM ইমেজ থেকে পরিলক্ষিত হয়েছে পৃষ্ঠের টেক্সচারে মাইক্রো পর্যায়ে কোন ফাটল নেই। XRD প্যাটার্ন বিশ্লেষণ মিশ্রণে উপস্থিত যৌগ সম্পর্কে তথ্য প্রদান করে যার দ্বারা সংবেদনশীল উপাদান সনাক্ত করা যায়। সামগ্রিকভাবে, এই গবেষণাটি পাললিক জমায় ডীপ মিক্সিং পদ্ধতিতে বর্জ্য-ভিত্তিক জিওপলিমার ব্যবহারের জন্য একটি ভিত্তি প্রদান করে।

Table of Contents

Declaration…….. i

Dedication……...ii

List of Publications……....iii

Approval by the Supervisor …….…...iv

Acknowledgements……v

Abstract..... vi

বিমূর্ত ……..viii

Table of Contents x

List of Figures..... ..xiiii

List of Tables……xxii

List of Notation……...xxiii

Chapter 1: INTRODUCTION.....1

1.1 General.....1

1.2 Background 1

1.3 Statement of Problem 2

1.4 Aims and Objectives.....3

1.5 Significance and Scope 3

1.6 Organization of Thesis 4

Chapter 2: LITERATURE REVIEW.....5

2.1 General.....5

2.2 Ground Improvement Methods 5

2.3 The Deep Mixing Method 5
2.3.1 Mechanism of Deep Mixing Method 6
2.3.2 History of Development of Deep Mixing Method 6
2.3.3 Applications of Deep Mixed Columns 7
2.3.4 Patterns of Deep Mixed Columns 7
2.3.5 Studies on Deep Mixing Method 13
2.4 Geopolymer 25
2.4.2 Geopolymer as an Alternate of Cement 28
2.4.5 Efficiency of Fly Ash by Various Investigations 37
2.5 Concluding Remarks 49
Chapter 3: TEST PROGRAMME AND PROCEDURES 51
3.1 General 51
3.2 Materials 51
3.2.1 Soil 51
3.2.2 Precursor Binder 54
3.2.3 Additives 56
3.2.4 Water 57
3.3 Fly Ash Geopolymerization Process 57
3.4 Experimental Program 59
3.4.1 Material Proportioning 59
3.4.2 Method of Sample Preparation 61
3.4.3 Test Procedures 62
Chapter 4: RESULTS AND DISCUSSIONS 65
4.1 General 65
4.2 Properties of Geopolymer Treated Soils 66
4.2.1 Effect of Precursor Binder on Unconfined Compressive Strength 66

4.2.2 Effects of Water on Unconfined Compressive Strength 72
4.2.3 Effects of Additives on Unconfined Compressive Strength 75
4.3 Variation of Index Properties 80
4.4 Variation of Unit Weight 82
4.5 Mineralogical Analysis 83
4.5.1 SEM Analysis 85
4.6.1 X-Ray Diffraction Pattern (XRD) Analysis 89
4.6 Development of Prediction Model 94
4.6.1 Linear Regression Model 98
4.6.2 Non-linear (Quadratic) Regression Model 101
4.6.3 Trial-based Non-linear Regression Model 102
4.6.4 Boosted Tree (BT) Model 113
4.6.5 Cubic Support Vector Machine (C-SVM) Model 114
4.6.6 Exponential Gaussian Process Regression (EGPR) Model 117
4.6.7 Tri-layered Artificial Neural Network (T-ANN) Model 121
4.6.8 Comparison of Model Performances 123
Chapter 5: CONCLUSIONS 127
5.1 General 127
5.2 Key Findings 127
5.3 Limitations of the Study 128
5.4 Recommendations for Further Study 129
References 130
Appendices 139

List of Figures

Fig. No. **Figure Caption** **Page**

Figure 2.1: The Process of Deep Mixing Method (Han, 2015) 6

Figure 2.2: Group Deep Mixing Columns (Kitazume et al., 2000) 8

Figure 2.3: Group Deep Mixing Columns In Tangent Wall (Kitazume et al., 2000) 8

Figure 2.4: Group Deep Mixing Columns in Tangent Block (Kitazume et al., 2000) 9

Figure 2.5: Wall Type Deep Mixing Columns (Kitazume et al., 2000) 9

Figure 2.6: Grid Type Deep Mixing Columns (Kitazume et al., 2000) 9

Figure 2.7: Block Type Deep Mixing Columns (Kitazume et al., 2000) 10

Figure 2.8: Development of Strength With Change in (a) Injection Pressure and (b) Cement Dose (Onur et al., 2022) 14

Figure 2.9: Experimental Ultimate Bearing Capacity (UBC); (a) End-bearing DCM, (b) Floating DCM (Dehghanbanadaki et al., 2022) 15

Figure 2.10: (a) Model with End-bearing Deep Mixing Columns; (b) Model with Floating Deep Mixing Columns. (c) Settlement vs Time Curve for End-bearing and Floating Deep Mixing Columns (Zakaria et al., 2020) 16

Figure 2.11: Triaxial Test Results of Deep Cement Mixing Column (Frikha et al., 2017) 17

Figure 2.12: Settlement Behavior Without Deep Cement Mixing (DCM) Column (Hamdhan et al., 2024) 17

Figure 2.13: Settlement with Lattice Pattern Deep Cement Mixing (DCM) Column (Hamdhan et al., 2024) 18

Figure 2.14: Settlement Time Reduction with Different Pattern of Deep Cement Mixing (DCM) Column (Hamdhan et al., 2024) 18

Figure 2.15: The Relationship Between Coefficient of Compressibility (Cc) and Void Ratio (e_i) (Raftari et al., 2024)..... 19

Figure 2.16: The Relationship between Consolidation Yield Pressure (P_y) and Unconfined Compressive Strength (Raftari et al., 2024)..... 19

Figure 2.17: (a) Settlement Reduction Ratio (SRR) and (b)Bearing Improvement Ratio (BIR) for Different Sized Group Piles, Cement and Lime Columns (Al-Qaisi and Al-Waily, 2022)..... 20

Figure 2.18: Shape Factors From 3D and 2D Analysis Performed on Images Collected Using Microtomography and High-Resolution Scanner (Bellato et al., 2020) 21

Figure 2.19: Classification of Pores According to Equivalent Sphere Diameter (Bellato et al., 2020)..... 22

Figure 2.20: Correlation Between Unconfined Compressive Strength at 125 Curing Days and Porosity with Microtomography Analysis (Bellato et al., 2020)..... 22

Figure 2.21: Correlation Between Unconfined Compressive Strength at 125 Curing Days and Porosity With Mercury Porosimetry Analysis (Bellato et al., 2020)..... 23

Figure 2.22: Unconfined Compressive Strength at Various Depth and Different Water Cement Ratio (W/C) (Usui et al., 2024) 24

Figure 2.23: Displacemnet of Deep Mix Column at Various Depth (Usui et al., 2024)..... 25

Figure 2.24: Frequency of various (a) Unconfined Compressive Strength (UCS), (b) Moisture Content, and (c) Density (Yin et al., 2022).....26

Figure 2.25: Variation of Unconfined Compressive Strength (UCS) with (a) Tidal Fluctuation, (b) Injection Rate, (c) Water Volume, (d) Slurry Volume, (e)Penetration Time, (f) Mixing Time, and (g) Moisture Content (Yin et al., 2022) 27

Figure 2.26: Formation of Geopolymer (Davidovits, 2005) 28

Figure 2.27: Effect of Water-to-Cement Ratio and Various Micro-Silica (MS) Percentages on (a) Unconfined Compressive Strength (UCS) and (b) Modulus of Elasticity of the Deep Mix Columns (Esmaeili et al., 2020).....30

Figure 2.28: Scanning Electron Microscopy (800x Enlarged) Images of Deep Mix Column Having 15% Microsilica (Esmaeili et al., 2020)...30

Figure 2.29: Scanning Electron Microscopy (800x Enlarged) Images of Deep Mix Column Having 20% Microsilica (Esmaeili et al., 2020)...31

Figure 2.30: (a) Development of Strength with Fly Ash Geopolymer; (Abdullah, Shahin, and Sarker, 2019). 32

Figure 2.31: Effect of Activator on Unconfined Compressive Strength (UCS) (Abdullah, Shahin, and Sarker, 2019).....33

Figure 2.32: Effect of Stabilizers on (a) Unconfined Compressive Strength (UCS), (b) Soaked California Bearing Capacity Ratio (CBR) (Adeyanju et al., 2020).....35

Figure 2.33: (a) Unconfined Compressive Strength (UCS) at Different Metakaolin (MK) Content Added to Cement, (b) Deviatoric Stress-Strain (Wassie and Demir, 2024) 36

Figure 2.34: Comparison Between 20, 30, 40 and 50% Fly Ash Mixtures (Cristelo et al., 2011) 38

Figure 2.35: Comparison between Cement and 12·5 Molal Cold Activator with Fly Ash at 28 Days Curing (Cristelo et al., 2011) 39

Figure 2.36: (a) Unconfined Compressive Strength (UCS); (b) Failure Strain(Liu et al., 2016) 39

Figure 2.37: Unconfined Compressive Strength Test Results for Clayey, Silty Sand Stabilized with Cement and the Addition of 20% Fly Ash; (a)Aw = 5%, (b) Aw = 10% (Ekmen et al., 2020) 40

Figure 2.38: Unconfined Compressive Strength Test Results for Clayey, Silty Sand Stabilized with Cement and the Addition of 20% Fly Ash; (a)Aw = 15%, (b) Aw = 20% (Ekmen et al., 2020) 41

Figure 2.39: Variation of Deviatoric Stress and Volumetric Strain with Axial Strain in Triaxial Compression Tests at 28 Days of Curing (Rios et al., 2016) 42

Figure 2.40: Variation of Deviatoric Stress and Volumetric Strain with Axial Strain in Triaxial Compression Tests at 28 Days of Curing (Rios et al., 2016) 43

Figure 2.41: Typical CU Triaxial Compression Test Results for Untreated and Treated Kaolin Clay with Various Geopolymer Contents at 100, 200, and 400 Kpa Confining Pressures (28 Days): (a) Untreated; (b) 10% Geopolymer (Abdullah, Shahin, and Walske, 2019) 45

Figure 2.42: Typical CU Triaxial Compression Test Results for Untreated and Treated Kaolin Clay with Various Geopolymer Contents at 100, 200, and 400 Kpa Confining Pressures (28 Days): 20% Geopolymer (Abdullah, Shahin, and Walske, 2019) 46

Figure 2.43: Soaked CBR Value of Geopolymer Treated Soils (Debanath, 2019)....47

Figure 2.44: Unsoaked Value of Geopolymer Treated Soils (Debanath, 2019)....47

Figure 2.45: Consolidation curve (Yenginar and Olgun, 2024)....48

Figure 2.46: XRD Analyses of (a) the Base Soil (< 75 μm), (b) Cement, (c) Soil Treated with Cement and Fly Ash, and (d) Fly Ash (Ekmen et al., 2020)....48

Figure 3.1: Flow Diagram of Test Programme....52

Figure 3.2: Grain Size Distribution Curve for Parent Soil....53

Figure 3.3: Grain Size Distribution of Fly Ash....54

Figure 3.4: (a) Fly Ash; (b) Scanning Electron Microscope (SEM) Image of Fly Ash....55

Figure 3.5: (a) Sodium Hydroxide (NaOH) and (b) Sodium Silicate (Na_2SiO_3) pellets....56

Figure 3.6: Broken spheres after activated with sodium hydroxide (Pacheco-Torgal et al., 2008)....58

Figure 3.7: Alkali Activation Process of Fly Ash....58

Figure 3.8: Geopolymerization Process (Singh, 2018)....59

Figure 3.9: (a) Geopolymer Slurry; (b) Soil-Geopolymer Mix....62

Figure 3.10: Sealed Sample in Mould....63

Figure 3.11: Samples in (a) Desiccator and (b) Water Bath for curing....63

Figure 3.12: (a) Cured Sample Prior to Test; (b) Sample Being Tested in Unconfined Compressive Strength Test Machine; (c) Broken Samples After Test....64

Figure 4.1: Variation of Unconfined Compressive Strength (UCS) with Fly Ash Content at Liquid Limit and Activator to Binder Ratio (L/P) of (a) 0.2, (b) 0.5, (c) 0.8 68

Figure 4.2: Variation of Unconfined Compressive Strength (UCS) with Fly Ash Content at 0.75xLiquid Limit and Activator to Binder Ratio (L/P) of (a) 0.2, (b) 0.5, (c) 0.8 70

Figure 4.3: Variation of Unconfined Compressive Strength (UCS) with Fly Ash Content at 1.25xLiquid Limit and Activator to Binder Ratio (L/P) of (a) 0.2, (b) 0.5, (c) 0.8 71

Figure 4.4: Variation of Unconfined Compressive Strength (UCS) with Water at Activator to Binder Ratio (L/P) = 0.2 73

Figure 4.5: Variation of Unconfined Compressive Strength (UCS) with Water at Activator to Binder Ratio (L/P) = 0.5 73

Figure 4.6: Variation of Unconfined Compressive Strength (UCS) with Water at Activator to Binder Ratio (L/P) = 0.8 74

Figure 4.7: Unconfined Compressive Strength (psi) vs. Water to Cement Ratio in Different Studies (FHA Manual, 2013) 74

Figure 4.8: Variation of Unconfined Compressive Strength (UCS) Ratio with Alkali Additive (Activator) to Binder Ratio (L/P) at Fly Ash =10% and MC of (a) 0.75LL (b) LL and (c)1.25LL 76

Figure 4.9: Variation of Unconfined Compressive Strength (UCS) Ratio with Alkali Additive (Activator) to Binder Ratio (L/P) at Fly Ash =15% and MC of (a) 0.75xLiquid Limit (b) Liquid Limit and (c)1.25xLiquid Limit 77

Figure 4.10: Variation of Unconfined Compressive Strength (UCS) Ratio with Alkali Additive (Activator) to Binder Ratio (L/P) at Fly Ash

=20% and MC of (a)) 0.75xLiquid Limit (b) Liquid Limit and (c)1.25xLiquid Limit 78

Figure 4.11: Variation of Unconfined Compressive Strength (UCS) Ratio with Activator to Binder Ratio (L/P) at Fly Ash =25% and MC of (a)) 0.75xLiquid Limit (b) Liquid Limit and (c)1.25xLiquid Limit ... 79

Figure 4.12: Variation of Liquid Limit (LL), Plastic Limit (PL) and Plasticity Index (PI) at Activator to Binder ratio (L/P) of (a) 0.2, (b) 0.5, (c) 0.8 81

Figure 4.13: Unit Weight at 56-Days Curing Period and Moisture Content of (a) 0.75LL, (b) LL, (c) 1.25LL 84

Figure 4.14: SEM image of parent soil 85

Figure 4.15: SEM image of stabilized soil at 25% Binder Content, L/P=0.2 and (a) w/LL=0.75 (b) w/LL=1.0 and (c) w/LL=1.25 86

Figure 4.16: SEM image of stabilized soil at 25% Binder Content, L/P=0.5 and (a) w/LL=0.75 (b) w/LL=1.0 and (c) w/LL=1.25 87

Figure 4.17 SEM image of stabilized soil at 25% Binder Content, L/P=0.8 and (a) w/LL=0.75 (b) w/LL=1.0 and (c) w/LL=1.25 88

Figure 4.18: XRD pattern of (a) soil and (b) Fly Ash 90

Figure 4.19: XRD Pattern of Stabilized Soil at MC = 0.75xLL and (a) L/P=0.2, (b)L/P=0.5, and (c) L/P=0.8 91

Figure 4.20: XRD Pattern of Stabilized Soil at MC =LL and (a) L/P=0.2, (b)L/P=0.5, and (c) L/P=0.8 92

Figure 4.21: XRD Pattern of Stabilized Soil at MC = 1.25xLL and (a) L/P=0.2, (b)L/P=0.5, and (c) L/P=0.8 93

Figure 4.22: Relationship between Unconfined Compressive Strength (UCS) and Fly Ash Content 96

Figure 4.23: Relationship between Unconfined Compressive Strength (UCS) and Activator to Binder Ratio 96

Figure 4.24: Relationship between Unconfined Compressive Strength (UCS) and Mixing Water to Binder Ratio 97

Figure 4.25: Relationship between Unconfined Compressive Strength (UCS) and Curing Day 97

Figure 4.26: Summary of Generated Prediction Models 98

Figure 4.27: Linear Regression Model Analysis on (a) Training, (b) Test, (c) All data 100

Figure 4.28: Comparison of Nonlinear Regression Model (NRM) and Step-wise Nonlinear Regression Model (S-NRM) on (a)Training Data ,(b) Test Data, (c) All Data 103

Figure 4.29: Comparison of Trial-based Nonlinear Regression Model (TNR) and Step-wise Trial-based Nonlinear Regression Model (S-TNR) on (a)Training Data ,(b) Test Data, (c) All Data 105

. Figure 4.30: UCS (kPa) at 14-days Curing period (a) Experimental UCS, kPa (b) Trial-based UCS, kPa (c) Step-wise Trial-based UCS, kPa... 106

Figure 4.31: UCS (kPa) at 28-days Curing period (a) Experimental UCS, kPa (b) Trial-based UCS, kPa (c) Step-wise Trial-based UCS, kPa... 107

Figure 4.32: UCS (kPa) at 56-days Curing period (a) Experimental UCS, kPa (b) Trial-based UCS, kPa (c) Step-wise Trial-based UCS, kPa... 108

Figure 4.33: Mechanism of Boosted Tree Model (Chen et al., 2021) 113

Figure 4.34: Boosted Tree Model Analysis on (a) Training, (b) Test, (c) All data 115

Figure 4.35: Mechanism of C-SVM Model(Source: https://medium.com/cube-dev/support-vector-machines-tutorial-c1618e635e93)....116

Figure 4.36: Cubic Support Vector Machine Model Analysis on (a) Training, (b) Test, (c) All data....118

Figure 4.37: Illustration of Gaussian Process Regression Model (Source: https://arxiv.org/html/2009.10862v5)....119

Figure 4.38: Exponential Gaussian Process Regression Model Analysis on (a) Training, (b) Test, (c) All data....120

Figure 4.39: Architecture of Tri-layered Artificial Neural Network Model. 121

Figure 4.40: Tri-layered Artificial Neural Network Model Analysis on (a) Training, (b) Test, (c) All data....124

Figure 4.41: Comparison of Prediction Models on (a)Training Data ,(b) Test Data, (c) All Data....125

Figure A.1: Stress vs Strain Curve for Water Content=0.75 x Liquid Limit (i) L/P=0.2 (ii) L/P=0.5 (iii) L/P=0.8....139

Figure A.2: Stress vs Strain Curve for Water Content = Liquid Limit (i) L/P=0.2 (ii) L/P=0.5 (iii) L/P=0.8....140

Figure A.3: Stress vs Strain Curve for Water Content =1.25 x Liquid Limit (i) L/P=0.2 (ii) L/P=0.5 (iii) L/P=0.8....141

List of Tables

Table No.	Table Caption	Page No
Table 2.1:	Characteristics of Various Types of Deep Mixing Improvement	11
Table 2.2:	Parameters of Deep Mix Column Panels	21
Table 2.3:	Proportioning of Deep Mix Column Panels (Abdullah, Shahin, and Sarker, 2019)	32
Table 2.4:	Mix Proportion of Soil with CKD and RHA (Adeyanju et al., 2020)	34
Table 2.5	Material Proportioning. (Rios et al., 2016)	42
Table 3.1:	Properties of Parent Soil	53
Table 3.2:	Chemical Composition of Parent Soil and Fly Ash	55
Table 3.3.	Water Quality Parameters	57
Table 4.1:	Summary of Analysis on Deep Mixing Method	65
Table 4.2:	Variation of Unconfined Compressive Strength at different proportion of materials	67
Table 4.3:	Variation of Index Properties at Different Proportion of Materials	80
Table 4.4:	Variation of Unit Weight at Different Proportion of Materials	83
Table 4.5:	Hyperparameters of Machine Learning Models	112

List of Notation

ASTM – American Standard for Testing Materials

CBR – California Bearing Capacity Ratio

CKD – Cement Kiln Dust

FA - Fly Ash

LL - Liquid Limit

PL - Plastic Limit

PI - Plasticity Index

RHA – Rice Husk Ash

UCS - Unconfined Compressive Strength

SEM - Scanning Electron Microscope

XRD - X-Ray Diffraction

Chapter 1 : INTRODUCTION

1.1 GENERAL

Infrastructural developments have become very challenging for Bangladesh, since the country has soft, low-bearing soils; most of the time, deep foundations are required, which are pretty expensive. Various ground improvement techniques are in practice, one of which involves deep mixing for enhancing the strength of the soil. However, some conventional methods using cement create environmental hazards. The study aimed at utilizing fly ash-based geopolymer—an effective alternative that reduces carbon-di-oxide (CO_2) emission and enhances soil properties. This chapter deals with the background, problem statement, aims and scope of the study.

1.2 BACKGROUND

The geological formation that created a layer of soft, thick soils having a low bearing capacity hinders infrastructure development to some extent and hence, a deep foundation, which is costlier compared to the shallow foundation is then required. The scenario is extensive in alluvial deposits when the downstream end of the geological basin is typically formed by transported fine sediments deposited prior to discharging to the sea. For the thick layer of soft soil deposition, foundation costs are higher even for low-rise structures that are sometimes difficult to afford for individuals in developing countries. To alleviate such antagonistic situations, different approaches of ground improvement techniques have been used that enhance the bearing capacity of weak soil. Alongside, deep mixing where the appropriate amount of binder is mixed with in-situ soils through a rotating system that eventually creates a pile-like structural column and provides significant strength gain and also provide thick layer of bearing stratum that implicitly reduces the chance of shear failure.

Where cohesive soils are encountered at shallow depth or where the fines content of soils is higher, the deep mixing method renders an affirmative response to the strength of the soils. Cement is the mostly used binder in the traditional deep mixing method. However, cement produces a substantial amount of carbon-di-oxide (CO_2) and can't be considered green materials against sustainable development (Kacemi et al., 2017). All the same, the potential use of waste products from different industries has got an attraction to minimize the hazard associated due to waste production or alleviate the problems of deposition of such waste materials. A large quantity of waste from coal-based power plant, namely Fly Ash has been produced every year around the globe. Fly ash based geopolymer can be an alternative of cement in soil stabilization as geopolymer is an environmentally friendly green building material with fast hardening, high strength, low shrinkage, low cost, and low carbon dioxide emission (Luo, 2022). Therefore, the alteration of cement by fly ash in conventional deep mixing methods needs to be explored so that the mechanism of strength gain can be extracted for a better understanding of soil behavior.

1.3 STATEMENT OF PROBLEM

Bangladesh, a deltaic country that lies at the downstream end of the Himalayan belt has faced problems in foundation design as the upper layer in most parts of the country is soft deposition. The country's infrastructure development has been booming over the last few years keeping an aim to achieve the sustainable development goal. However, the problems of soft soils in the shallow/top poor layer discussed in the preceding section slow the development progress in many instances. Therefore, the search for an alternate approach, to be exact, a rational approach of ground improvement suitable from perspective of a developing country, such as Bangladesh, is due in academia so that the academic findings can be rolled into reality. Besides that a

substantial amount of fly ash has been being produced every year after 2023 when several coal-based power plants will be in operation.

Therefore, compiling the possible generation of a large amount of fly ash waste and the need for a suitable ground improvement technique, this research has initiated the study to explore the justification of using fly ash instead of conventional cement in deep mixing methods. The subsequent section describes the literature review and the scope of the current research.

1.4 AIMS AND OBJECTIVES

The aim is to predict improvement of soil after the introduction of deep mixed column in terms of improvement in properties (from laboratory tests) and economy. Based on the literature review and problem stated, the specific objectives are as follows:

- To evaluate the performance of fly ash as an alternate of cement in deep mixing column
- To determine the best possible combination for deep mix column for a certain strength
- To develop prediction model

1.5 SIGNIFICANCE AND SCOPE

The deep mixing method (DMM) with fly ash-based geopolymer can present a revolutionary solution to the geotechnical problems created by the soft and weak soils of Bangladesh. Chemical ground stabilization by the geopolymer-based DMM leads to outstanding improvement in soil properties of bearing capacity, stiffness, and durability, making it competent to carry heavy structures such as bridges, embankments, and high-rise buildings. Further, this method addresses environmental concerns by utilizing fly ash-a major industrial by-product-as a key component. This will not only reduce

dependence on conventional cement, which is energy-intensive and emits a high level of CO_2, but also help in managing industrial waste, thus aligning with the goals of sustainable development. This technique, in the larger picture, has an impact on infrastructure and economic sectors in Bangladesh. It is an affordable and sustainable method, especially crucial for coastal and flood-prone areas where soil failure due to rising sea levels and climate change is highly risky. Besides its practical advantages, the method opens up opportunities for innovation, skill development, and local employment by the production and application of geopolymer materials. By incorporating geopolymer-based DMM into public and private construction projects, it would contribute to the betterment of Bangladesh's prevailing soil stabilization needs while promoting sustainable and resilient development.

1.6 ORGANIZATION OF THESIS

This thesis is arranged in five different Chapters. Chapter 1 provides an introduction and background of the proposed study and also the outline of the thesis.

Chapter 2 describes different soil improvement techniques using different methods and stabilizing additives. The review mainly includes the mechanisms and findings of previous research on relevant topics.

Chapter 3 deals with the material details used in the present study and the experimental procedures and techniques.

Chapter 4 graphically describes the strength development pattern, changes in properties, and microstructural characteristics found in laboratory investigations and also describes prediction models developed.

Chapter 5 presents the recommendations and conclusions of the present research and further scope for research in this field.

Chapter 2 : LITERATURE REVIEW

2.1 GENERAL

When a structure is to be supported on very soft clay grounds or dredged clays, there might be serious issues of instability and settlement. There are numbers of methods to improve ground condition that are developed over hundreds of researches. Deep Mixing Method is one of the recently developed methods of ground improvement which provides improvement in strength, stability, settlement, permeability. This chapter provides a brief description of ground improvement with geopolymer and deep mixing method adopted all over the world.

2.2 GROUND IMPROVEMENT METHODS

If the sub-soil condition of a site is unable to support a structure, one of the following approaches can be applied.

a) Adopting different type of foundation of the structure
b) Excavation and Replacement of soil
c) Improving the soil with stabilizing agents
d) Providing reinforcement into the soil

2.3 THE DEEP MIXING METHOD

Deep Mixing Method is a recently developed ground improvement technique in which stabilizing agents are used to improved soil strength. The method has been established in Japan in 1970's. There are several benefits and use of deep mixing method. Detail of this method has been discussed in subsequent sections.

2.3.1 Mechanism of Deep Mixing Method

Deep Mixing represents in situ mixing of soils in conjunction with the hardening agent-cement, lime, slag, fly ash, or other binder varieties- at some depth with regularly spaced augers. Wet or dry methods could be carried out for the aforementioned method. In a wet method, the application is made with the help of binder in slurry, whereas in dry methods the binder is applied in powder form. Deep Mixing is a very common technique to improve strength in soft cohesive soils, thus allowing superstructures to stand, embankments to support, and for maintaining stability in slopes. The treatment also reduces the soil permeability and avoids liquefaction hazards in cohesionless soils (Han, 2015).

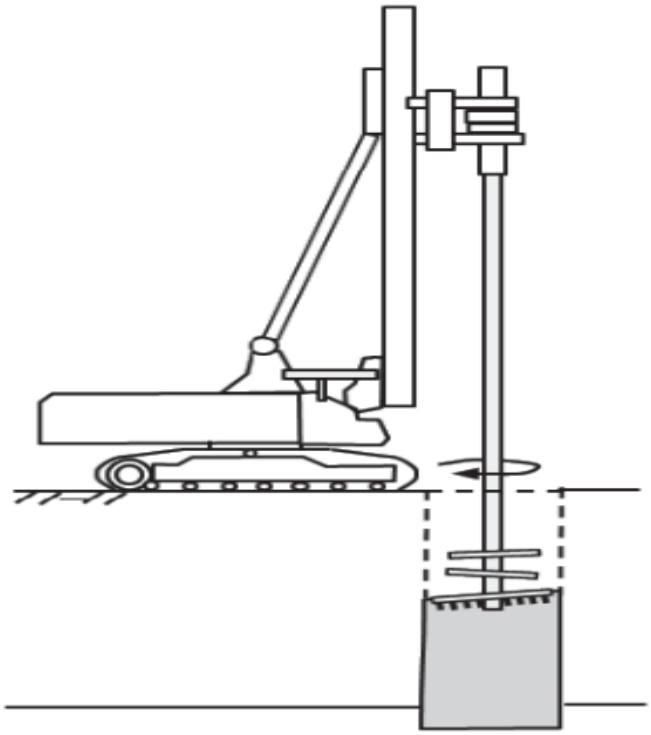


Figure 2.1: The Process of Deep Mixing Method (Han, 2015)

2.3.2 History of Development of Deep Mixing Method

The development of the Deep Mixing Method began with the Japanese Transport Ministry's efforts marked by the publication on lime stabilization of marine clay by the Port and Harbour Research Institute (PHRI) in 1968

(Yanase, 1968). In its initial phase, the focus was on investigating the stabilizing agents, advancing the construction equipment, testing the engineering properties of stabilized soils, and formulating design procedures to establish the method. Deep Mixing using cement mortar as a binder was first applied in 1974 under the name "Clay Mixing Consolidation Method (CMC)." Shortly after, in 1975, PHRI began developing the application of cement slurry as a binder, now known as the "Wet Method" of Deep Mixing. Later, in 2004, the method of utilizing powdered cement or lime binder was developed, which has been called the "Dry Jet Mixing (DJM) Method" and is the present method of dry Deep Mixing.

2.3.3 Applications of Deep Mixed Columns

Columns serve a variety of purposes, including: (1) providing structural support for buildings, bridges, embankments, and walls, (2) stabilizing slopes in waterfront and marine applications such as quay walls, wharf structures, and breakwaters, (3) offering lateral support, (4) containing water and pollutants, (5) mitigating liquefaction, (6) reducing vibrations, and (7) addressing other geotechnical challenges. Deep Mixed Columns have also been used for roadway widening to support new embankments (Han et al., 2007) and to address ground heave from expansive soils (Puppala et al., 2008). These uses take advantage of Deep Mixed Columns to increase bearing capacity, enhance slope stability, reduce settlement, mitigate liquefaction, provide lateral support, minimize vibration, and control water and pollutant movement.

2.3.4 Patterns of Deep Mixed Columns

Typically, deep mixed columns are installed in four different patterns such as group, wall, grid and block configurations. The Japanese practice commonly uses the block, wall or grid installation pattern to enhance ground in permanent or critical structures. In general, a group column pattern is generally applied to lightweight or temporary structures and embankments with the aim

of providing adequate stability and reducing the occurrence of vertical or horizontal displacements. However, in applications where a group of individual columns is used to stabilize embankment slopes, caution must be exercised in order to avoid progressive failure by bending of the columns due to the low tensile and bending strengths of the stabilized soil. (Kitazume et al., 2000).

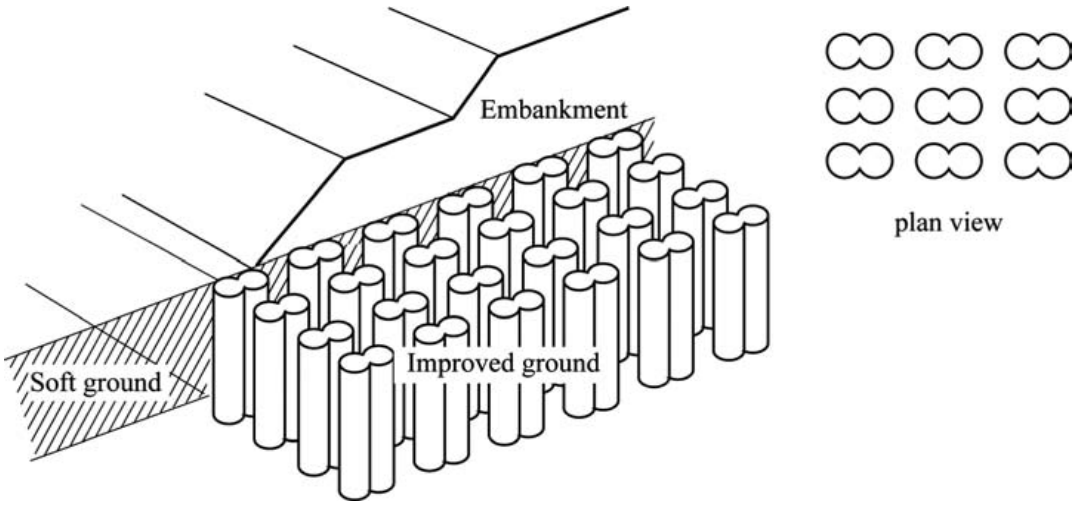


Figure 2.2: Group Deep Mixing Columns (Kitazume et al., 2000)

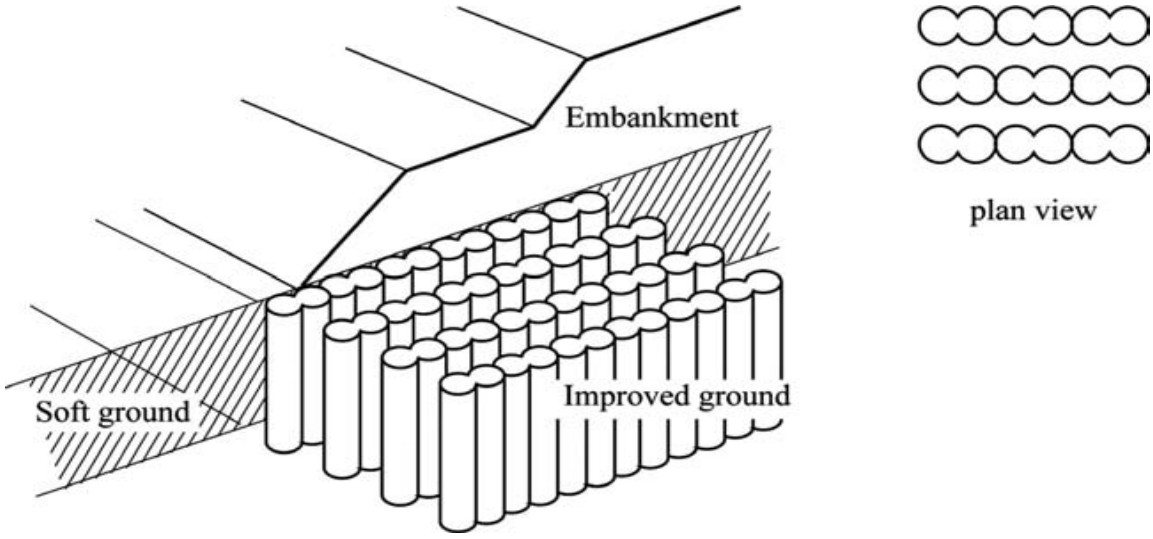


Figure 2.3: Group Deep Mixing Columns In Tangent Wall (Kitazume et al., 2000)

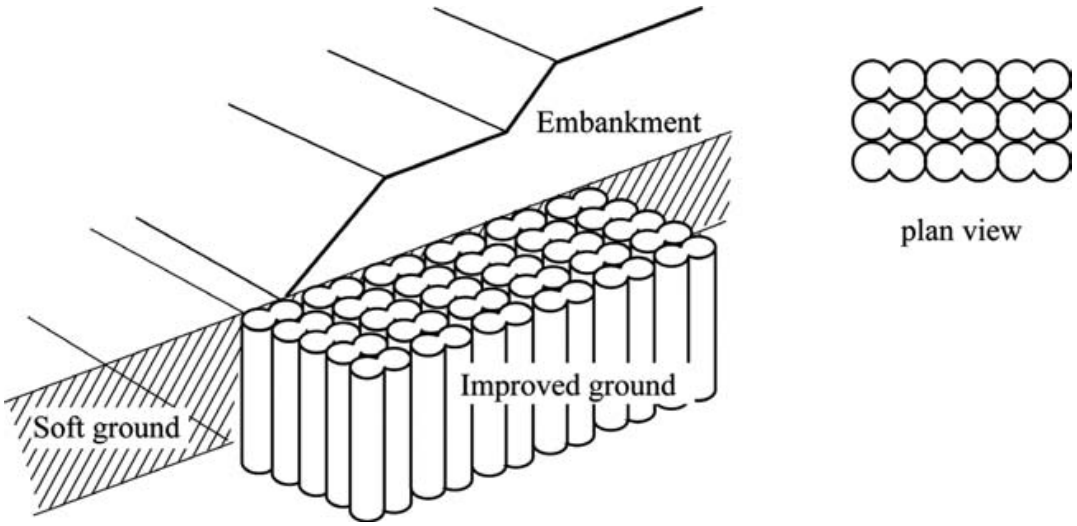


Figure 2.4: Group Deep Mixing Columns in Tangent Block (Kitazume et al., 2000)

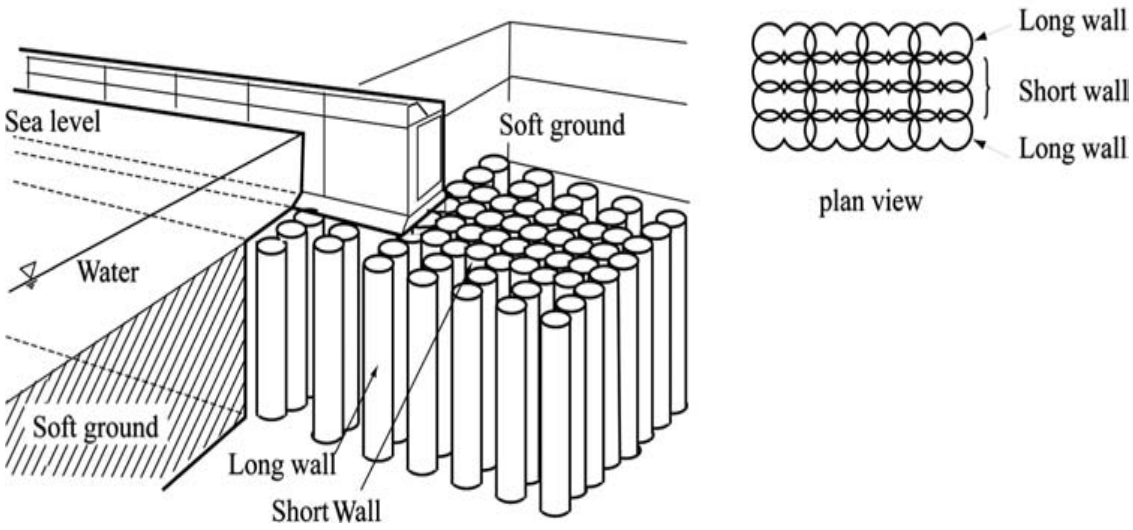


Figure 2.5: Wall Type Deep Mixing Columns (Kitazume et al., 2000)

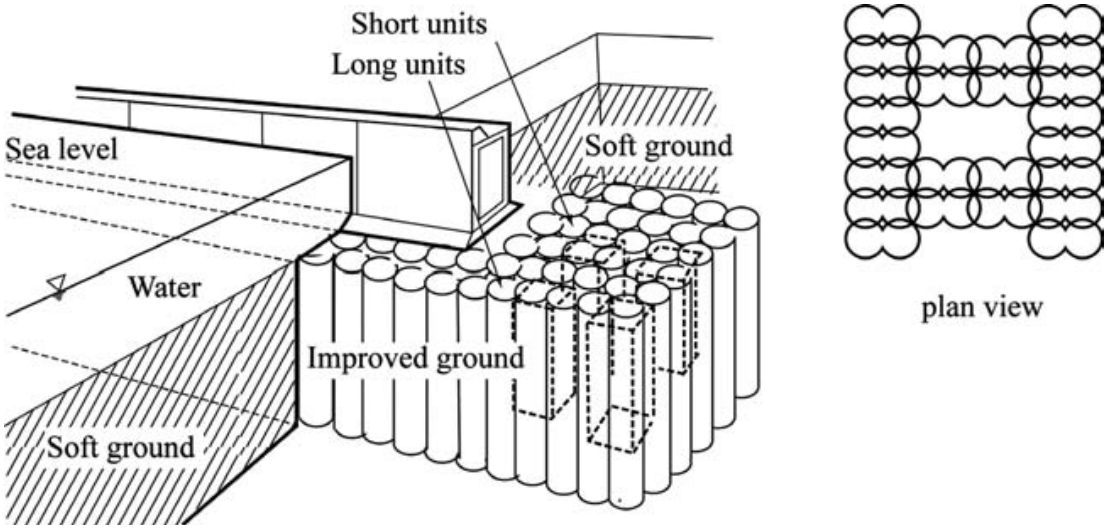


Figure 2.6: Grid Type Deep Mixing Columns (Kitazume et al., 2000)

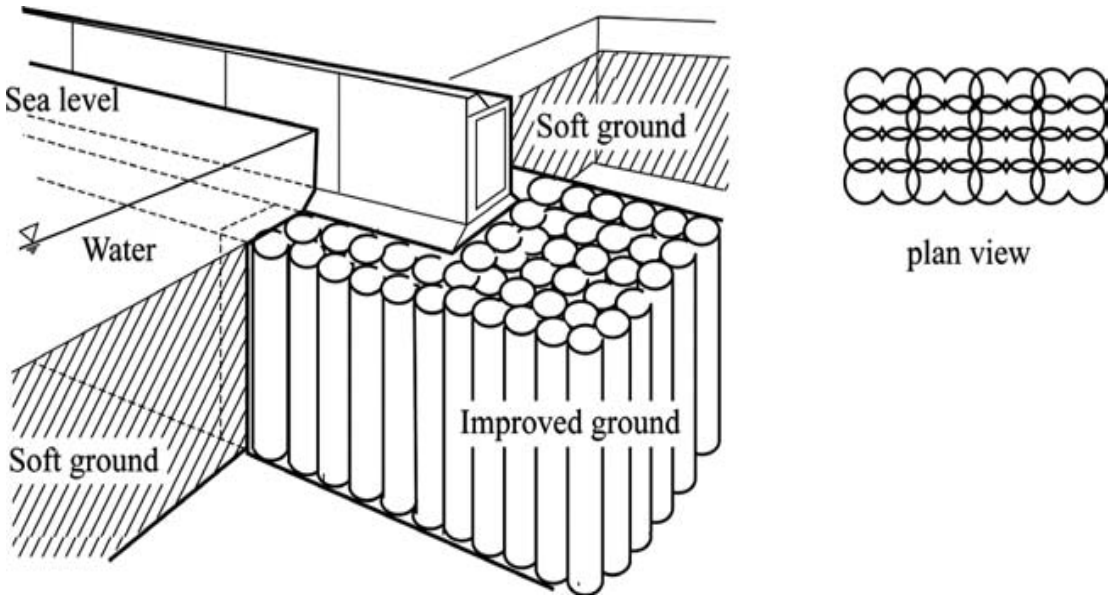


Figure 2.7: Block Type Deep Mixing Columns (Kitazume et al., 2000)

According to the type, size, and importance of the superstructure, purpose of the improvement, construction cost, and site conditions, the appropriate column installation pattern should be selected. Overlapping columns can be constructed only by a deep mixing machine with sufficient power and stability, high positioning and vertical alignment accuracy, and accurate monitoring of the position of the mixing shafts and blades during operation. Also, the pattern of installation must be chosen about locally available execution methods and quality control techniques.

Individual columns are usually applied for relatively low area replacement ratios below about 50%, to increase chiefly bearing capacity and reduce settlement. In contrast, block pattern columns are for area replacement ratio of more than 50%; their use is thus considered as to impart substantial vertical and/or horizontal loads. For instance, it has found use in block pattern is marine structure stabilization, and some forms of waste containment.

Table 2.1: Characteristics of Various Types of Deep Mixing Improvement

Type	Function	Cost	Installation	Design Consideration
Group column type .	Effective and efficient for settlement reduction under the full height of embankment.	Installation requires short period, and volume of improvement is small. Low cost.	Overlapping operation is not required.	Requires settlement analysis and bearing capacity of
Group column type by tangent arrangements	When lateral loads are small, very high stability is realized.	Volume improvement increases with the increase in the area ratio for the area improved. Less costly when compared to wall or grid or block types	Though overlaps are not required accurate locations and vertical alignments for the columns is of prime importance when they form a tangent arrangement.	Designs necessary both for overall stability, including the internal stability of tangent columns.
Wall Type	When external loads are primarily applied in a single	This method involves a smaller volume of improvement	Requires precise alignment and overlapping	the unimproved soil between the walls must be considered,

Table 2.1 continued…..

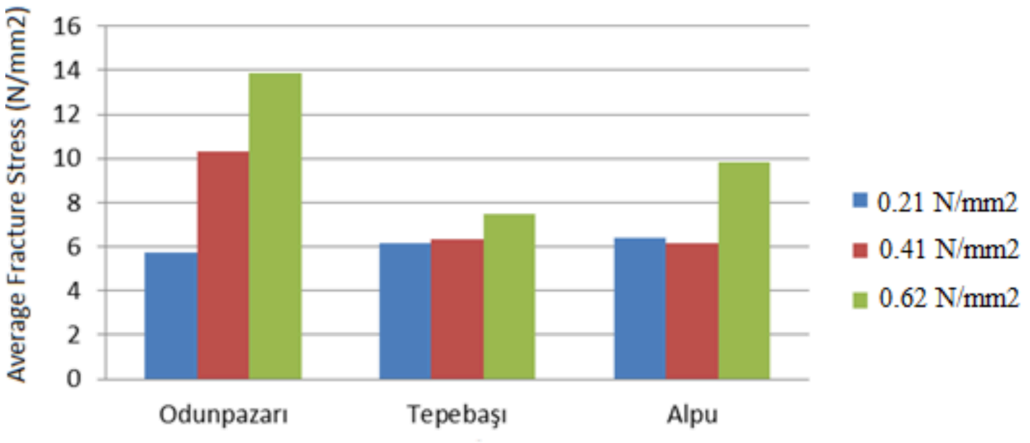
Type	Function	Cost	Installation	Design Consideration
	direction, walls are highly effective in improving stability	compared to block types and is more cost-efficient than grid or block systems.	of the long and short walls .	and the spacing and depth of the short walls must account for internal stability factors.
Grid Type	Highly stable as like as block Type.	Cost ranges between block type and wall type.	The installation process is complex due to the need to create a grid-like structure.	Needs design on 3-D internal stress.
Block type	The large solid block provides excellent resistance to external loads and ensures high stability.	The volume of improvement is larger compared to other types, but it comes with a high cost.	Longer installation time due to overlapping columns	Design is similar to gravity structures

2.3.5 Studies on Deep Mixing Method

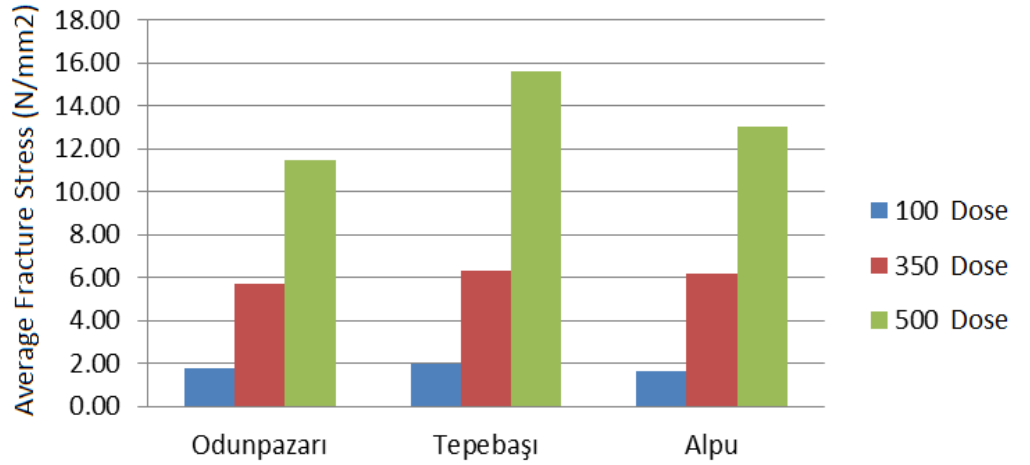
The strength development of deep-mixed soil depends on many factors, including curing age, binder type, binder content, water content, soil properties, mixing method and duration, and curing temperature and humidity. On the other hand, the strength development of cement-treated clay is mainly dominated by the ratio of water to cement content in relation to the fine-grained fraction of the soil (Yamashita et al., 2020). Many correlations have been developed to predict the strength of deep mixing columns for different parametric conditions.

A laboratory based experimental model was discussed on deep soil mix investigation on the strength development pattern depending on the variation of injection pressure, cement dose and mixing time (Onur et al., 2022). The unconfined compressive strength has been found to be increased about 240% with the increase of injection pressure from 0.21 N/mm^2 to 0.62 N/mm^2 while an 800% increase of strength was found for the increase of cement dose from 100 kg/m^3 to 500 kg/m^3 (Figure 2.8). Another study was carried out to evaluate and compare the rate of improvement in The Ultimate Bearing Capacity (UBC) of soil stabilized by Deep Cement Mix columns in selected experimental databases (Dehghanbanadaki et al., 2022). The UBC is primarily dependent on the end-bearing factor. The strength was found larger for the end-bearing column resting on treated hard soil mass than the floating column resting on the soft soil (Figure 2.9). Moreover, the settlement behavior of the end bearing column resting on treated hard soil mass and the floating column rests on soft soil were also observed (Zakaria et al., 2020) in laboratory scale model. The settlement decreases significantly for stabilized column where end bearing column shows more settlement resistant than floating column (Figure 2.10). Shear strength was

improved by cement stabilized deep mixing column on Tunis soft clay which has been shown in Figure 2.11 (Frikha et al., 2017).



(a)



(b)

Figure 2.8: Development of Strength With Change in (a) Injection Pressure and (b) Cement Dose (Onur et al., 2022)

Settlement behavior has also been studied in accordance with the standard of BS EN 14679:2005 by British Standards Institution, DCM column configuration has been designed into 8 configuration variations (Hamdhan et al., 2024). These shapes are rectangular patterns, triangular patterns, line patterns, wall patterns, block patterns, area patterns, lattice patterns, and overlaid column patterns. Among all the patterns, lattice pattern has been shown the most reduction in settlement (Figure 12 to Figure 14).

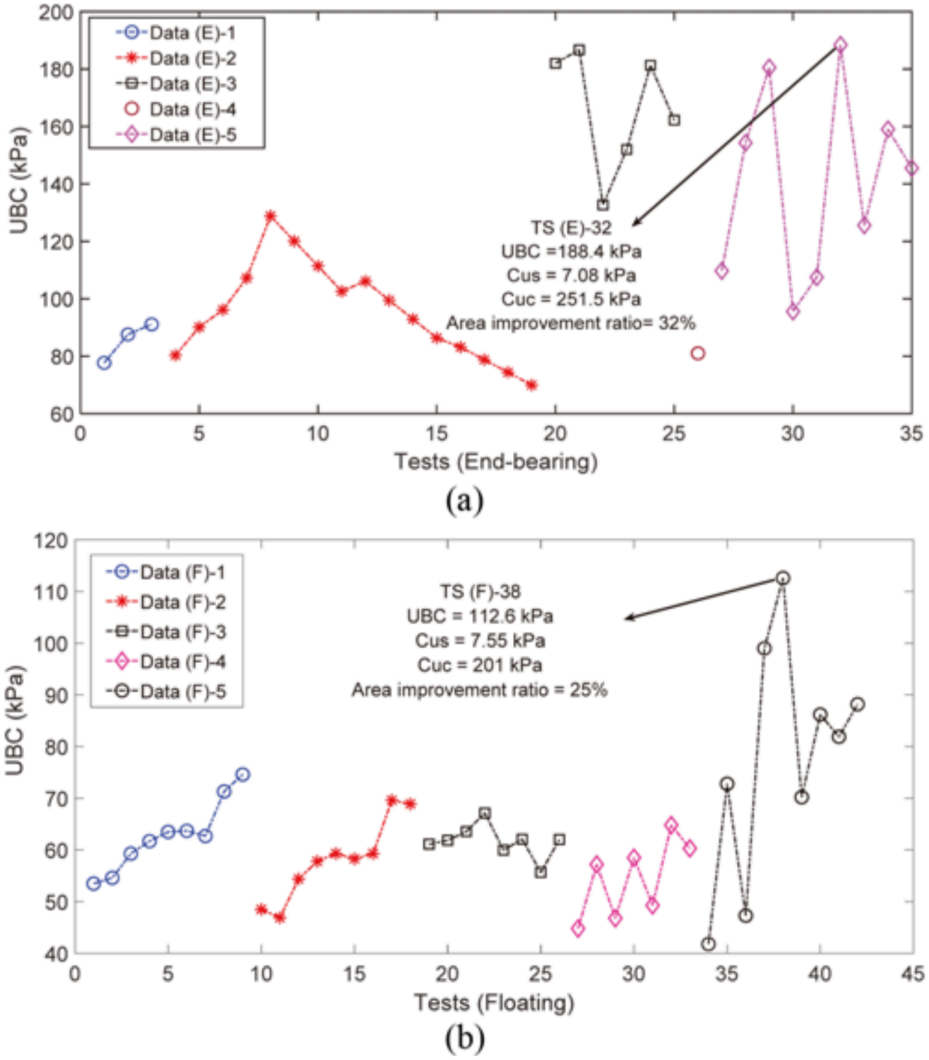
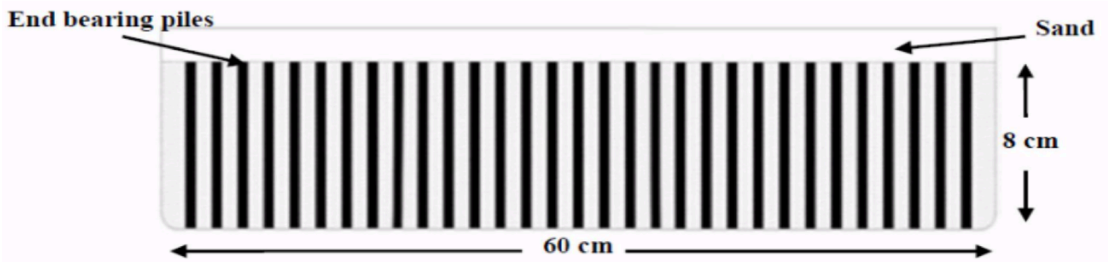


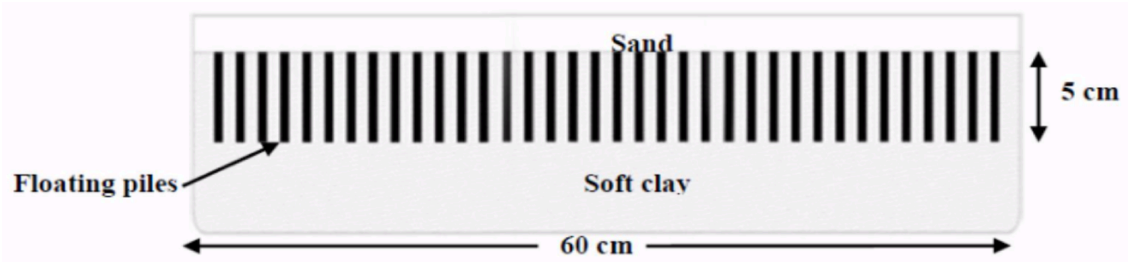
Figure 2.9: Experimental Ultimate Bearing Capacity (UBC); (a) End-bearing DCM, (b) Floating DCM (Dehghanbanadaki et al., 2022)

The proper explanation of the methodology adopted for carrying out the optimization of CDM column configuration to support the embankment on soft soil layer in Mekong Delta region (Nguyen, 2024). It introduced a specific approach, based on well-known relations of soil mechanics, applied to establish the first configuration of rehabilitation columns, which are installed inside weak soil. For rehabilitation columns the optimal configuration is found to be of 0.6 m diameter, 0.8 m spacing and 12.0 m length. The total settlement for this configuration is 0.180 m which is less than the permissible maximum settlement according to the Vietnamese Standard for transportation roads, TCVN 22TCN

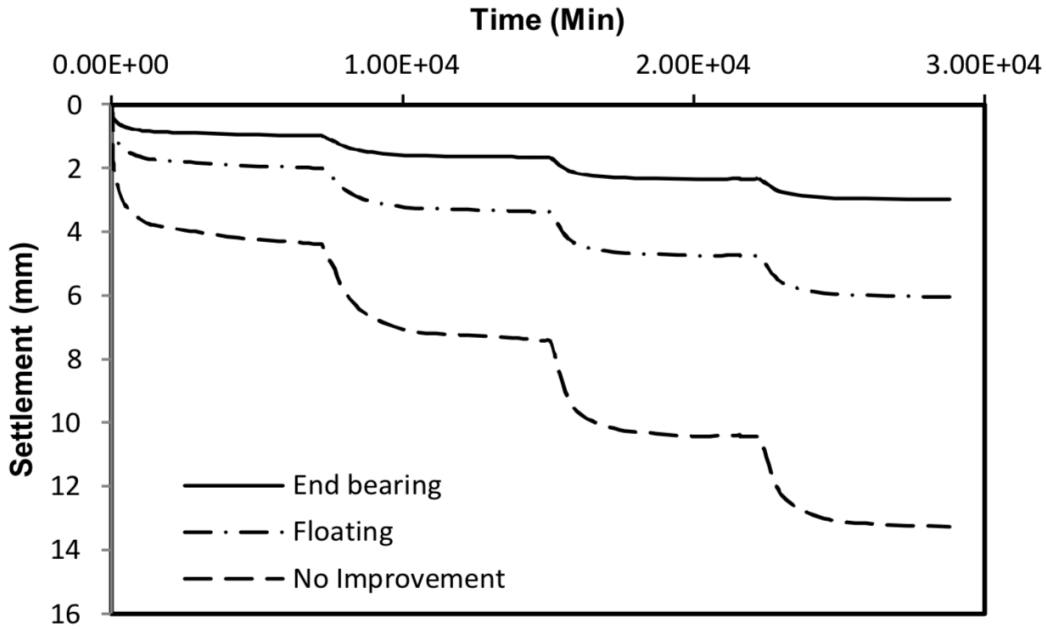
262-2000 [MOT Vietnam, 2020. 22TCN262-2000]. Regulations on survey and design of soft subgrade of roads and highways].



(a)



(b)



(c)

Figure 2.10: (a) Model with End-bearing Deep Mixing Columns; (b) Model with Floating Deep Mixing Columns. (c) Settlement vs Time Curve for End-bearing and Floating Deep Mixing Columns (Zakaria et al., 2020)

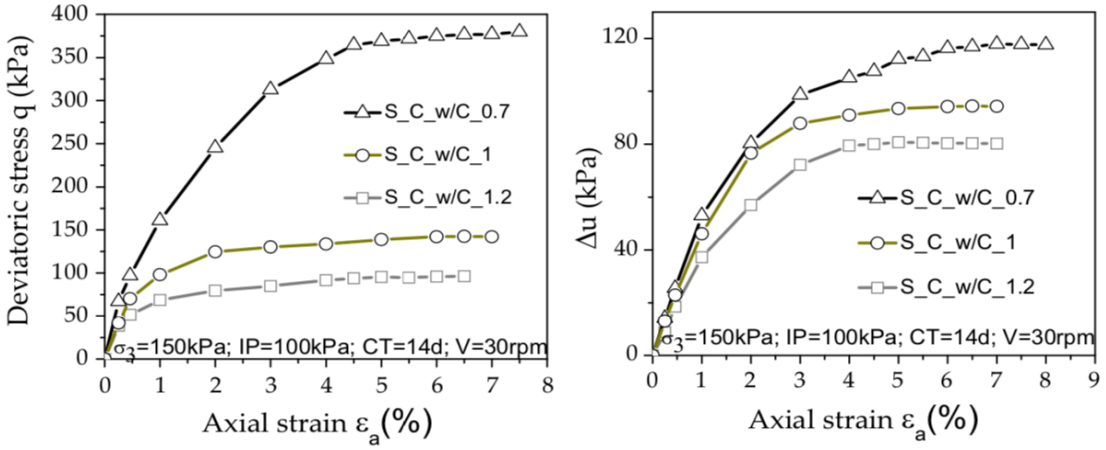


Figure 2.11: Triaxial Test Results of Deep Cement Mixing Column (Frikha et al., 2017)

The compressibility and shear strength of cement-stabilized clay for the long term were studied, prepared by the Deep Cement Mixing method. Properties such as UCS and consolidation behavior of Malaysian kaolin clays were investigated (Raftari et al., 2024). The aim was to simulate, as far as possible, practical conditions of deep mixing of soils with cement slurries in a curing period of almost 180 days. The cement content varied from 5% to 20% whereas the liquid content was varied between liquid limit and twice the liquid limit as shown in Figure 2.15 and 2.16.

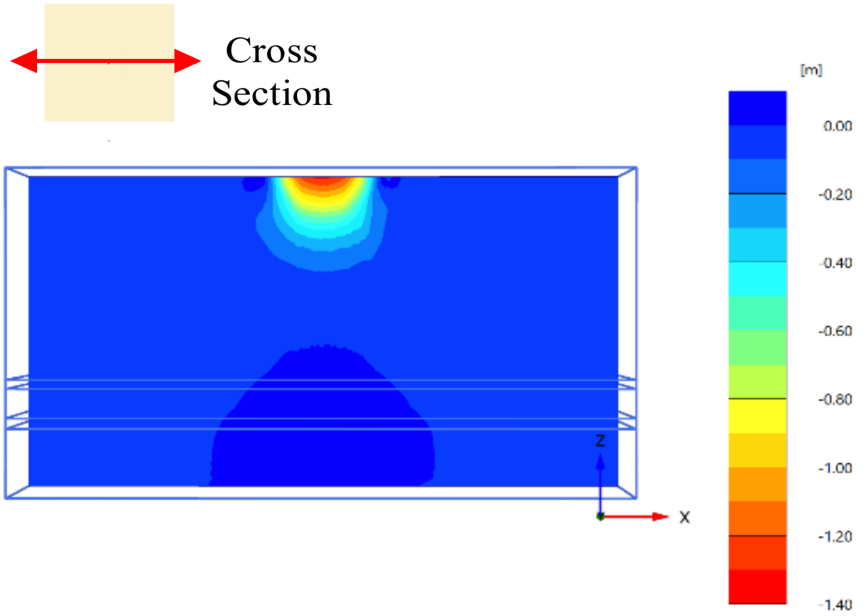


Figure 2.12: Settlement Behavior Without Deep Cement Mixing (DCM) Column (Hamdhan et al., 2024)

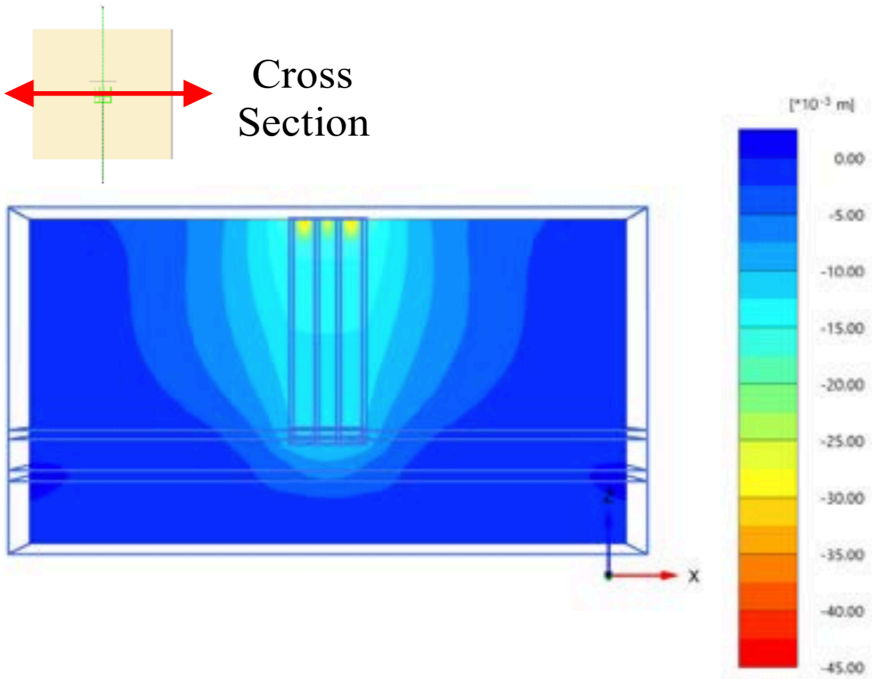


Figure 2.13: Settlement with Lattice Pattern Deep Cement Mixing (DCM) Column (Hamdhan et al., 2024)

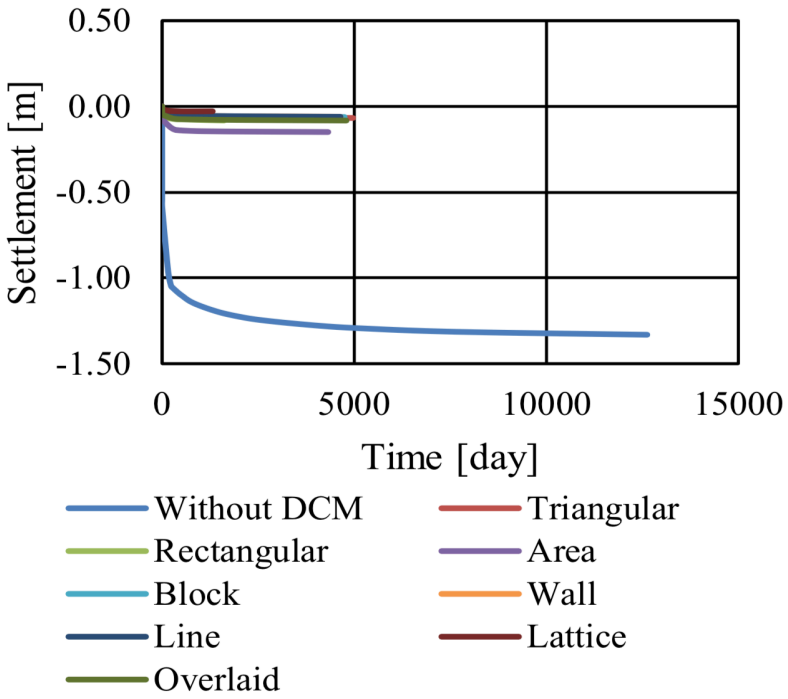


Figure 2.14: Settlement Time Reduction with Different Pattern of Deep Cement Mixing (DCM) Column (Hamdhan et al., 2024)

Experiments were made to analyse the settlement and bearing improvement on soft clay (Al-Qaisi and Al-Waily, 2022). Single and group piles (with 2, 3, and 4 columns) of lime cement and were installed and the 4-

pile group had the lowest settlement for the average SRR of 93% at all load levels, while that for the treated soil with cement or lime columns had an average SRR of 89% (Figure 2.17).

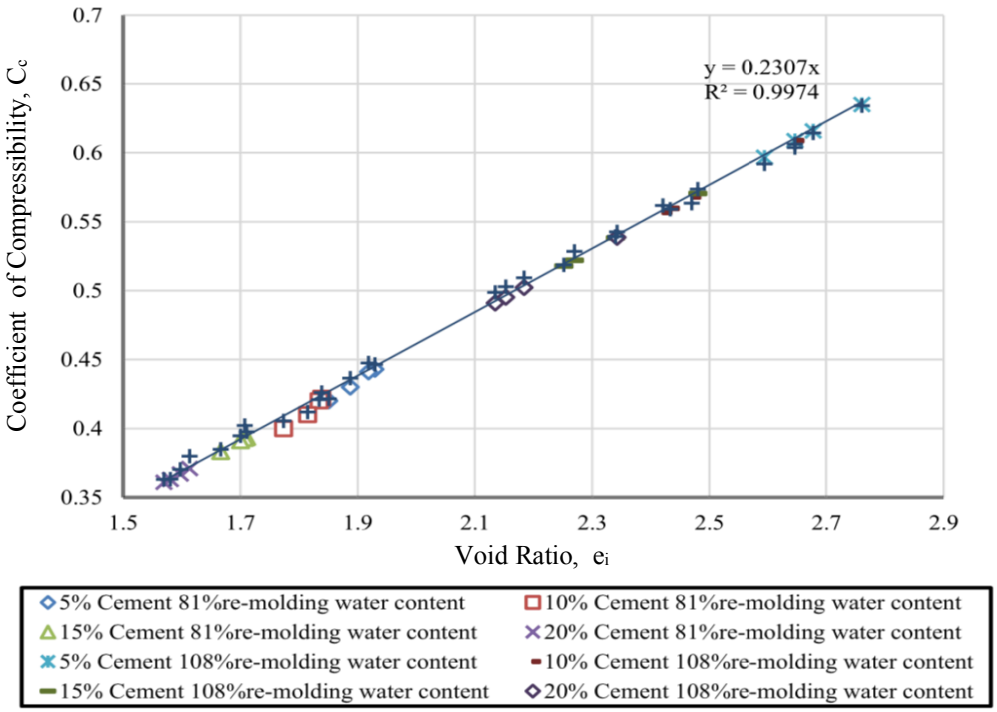


Figure 2.15: The Relationship Between Coefficient of Compressibility (Cc) and Void Ratio (e_i) (Raftari et al., 2024)

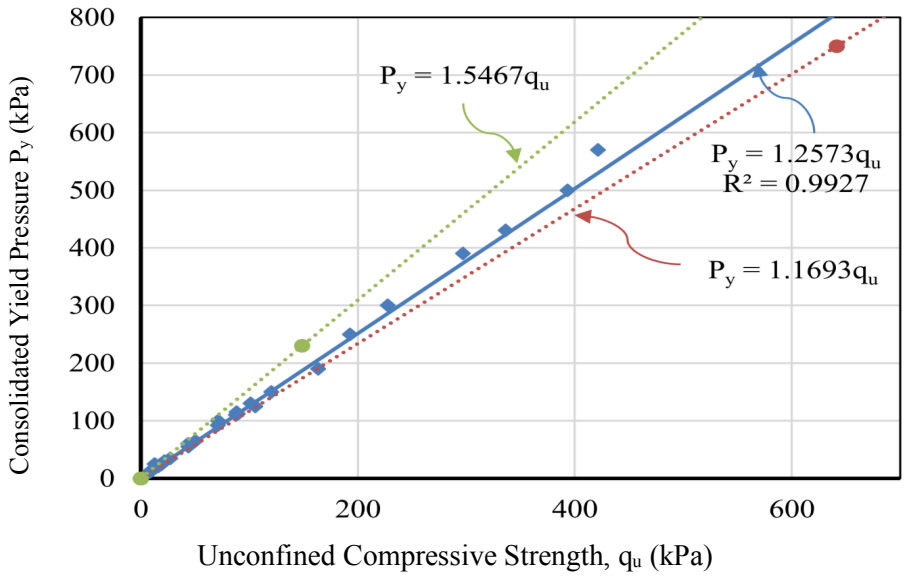
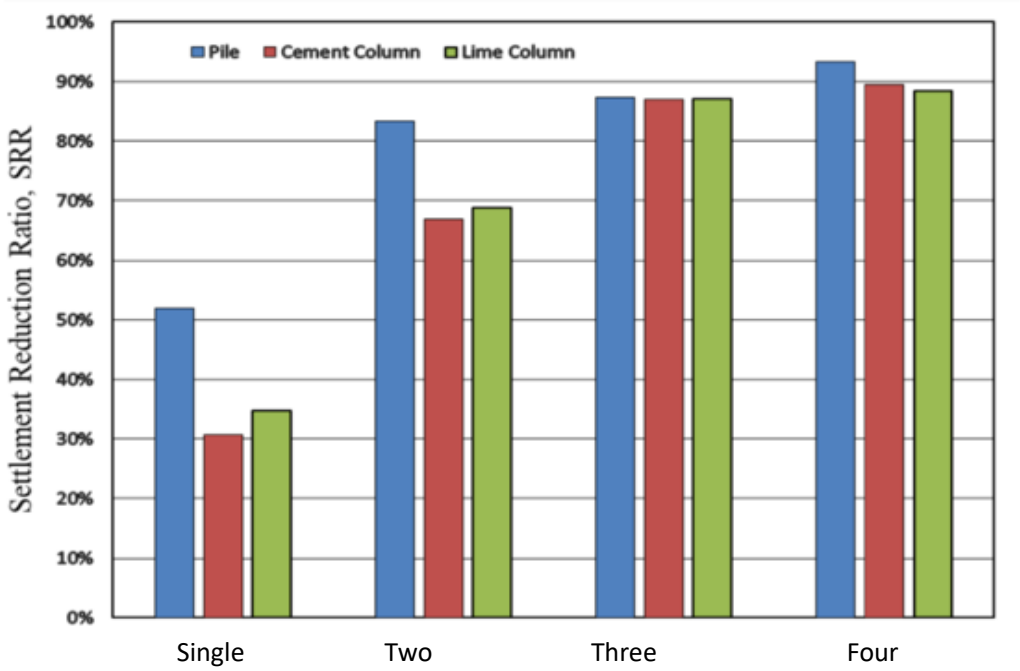
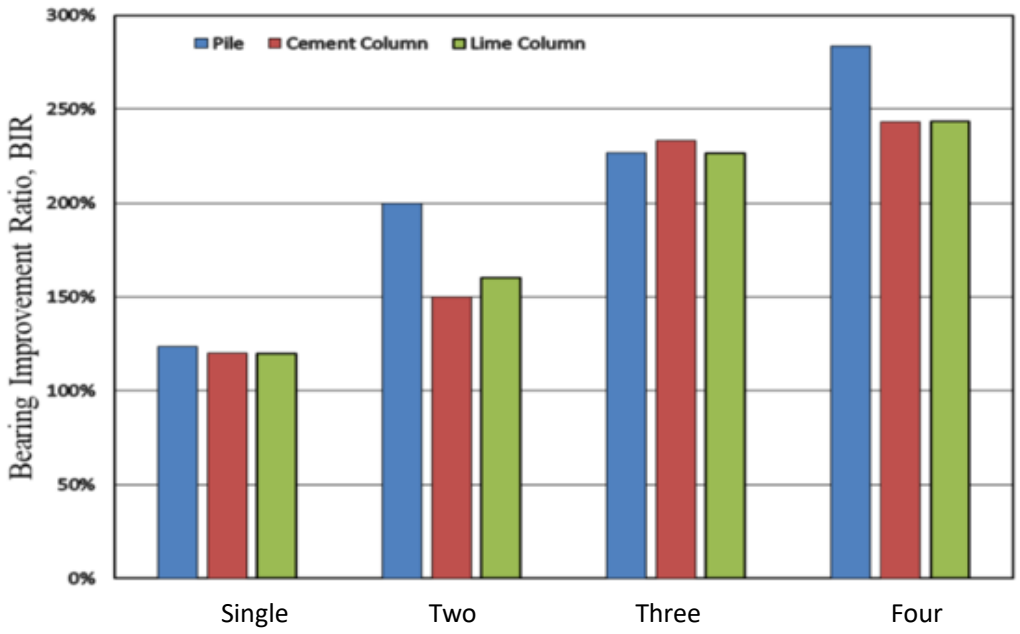


Figure 2.16: The Relationship between Consolidation Yield Pressure (P_y) and Unconfined Compressive Strength (Raftari et al., 2024)



(a)



(b)

Figure 2.17: (a) Settlement Reduction Ratio (SRR) and (b)Bearing Improvement Ratio (BIR) for Different Sized Group Piles, Cement and Lime Columns (Al-Qaisi and Al-Waily, 2022)

Pore structure network and volumes were studied on sand stabilized by various proportion stabilizing binders described in Table 2.2 (Bellato et al., 2020). The complementary nature of Mercury Intrusion Porosimetry (MIP) and

X-ray Computed Microtomography (μCT) is pointed out in this investigation. In fact, while μCT analyses in 3D showed a more general view with respect to total porosity and pore shape, the performed 2D analyses represented pores more irregularly shaped (Figure 2.18 and 2.19). Total porosity shows a positive relation with UCS (Figure 2.20 and 2.21), inverse linear in any case for the method adopted for measuring porosity.

Table 2.2: Parameters of Deep Mix Column Panels

Panel	P37	P38	P39	P40	P41	P44
w/c of the grout	1.25	1.25	1.12	1.12	1.12	1.17
Calculated cement factor, α (kg/m^3)	578	491	530	509	577	509
Average wheels rotational speed. (U/min)	32	30	33	31	30	33
Last 6 m average withdrawal speed (m/min)	0.74	0.61	0.92	0.76	0.75	0.77

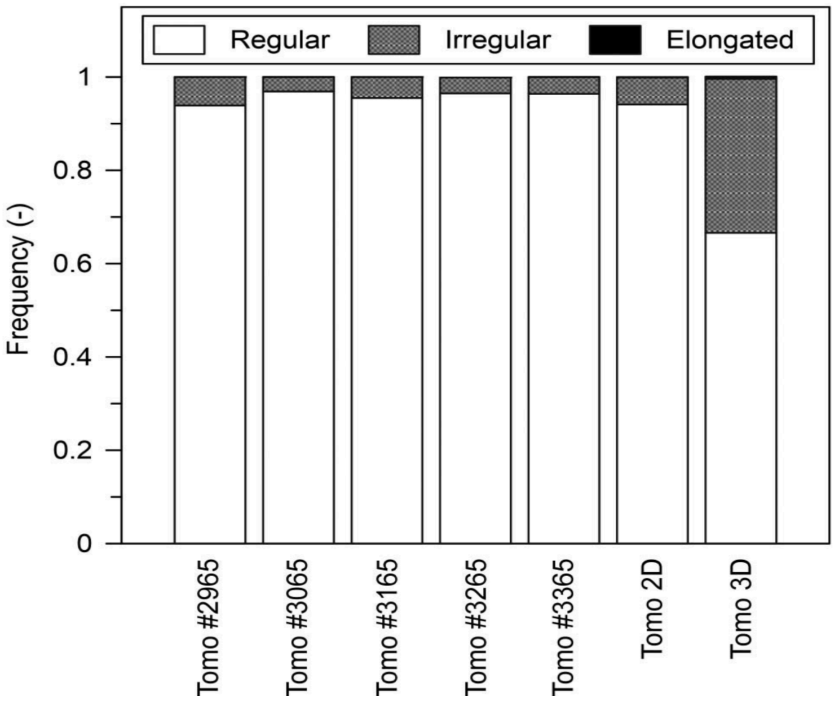


Figure 2.18: Shape Factors From 3D and 2D Analysis Performed on Images Collected Using Microtomography and High-Resolution Scanner (Bellato et al., 2020)

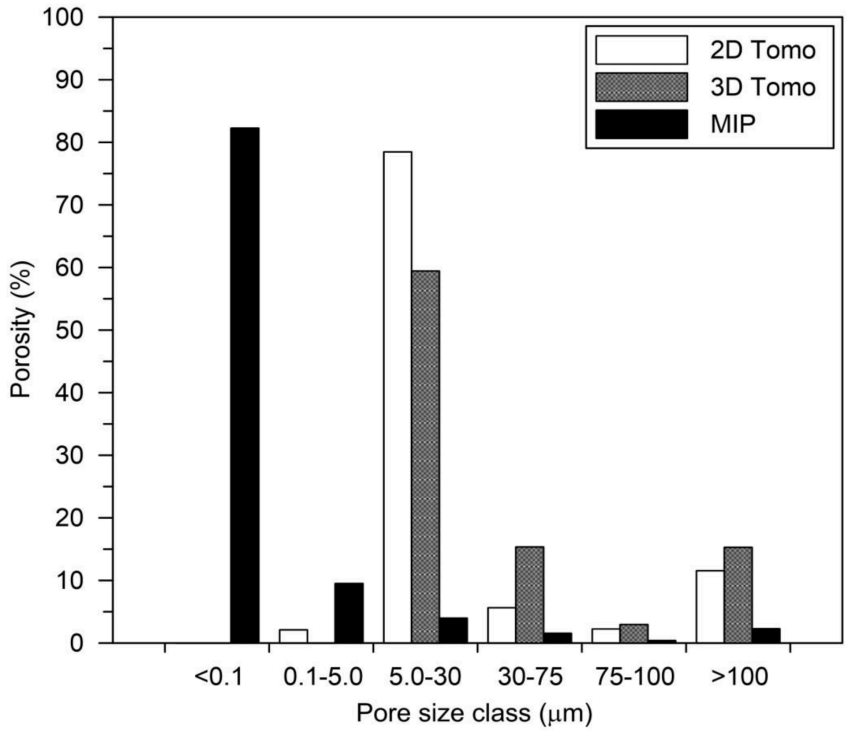


Figure 2.19: Classification of Pores According to Equivalent Sphere Diameter (Bellato et al., 2020)

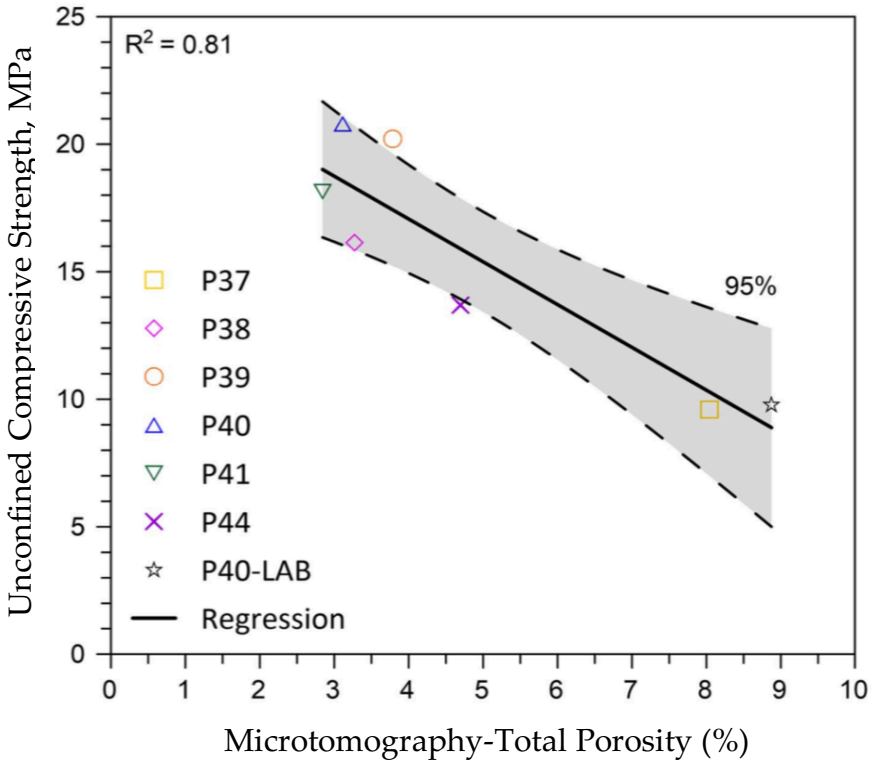


Figure 2.20: Correlation Between Unconfined Compressive Strength at 125 Curing Days and Porosity with Microtomography Analysis (Bellato et al., 2020)

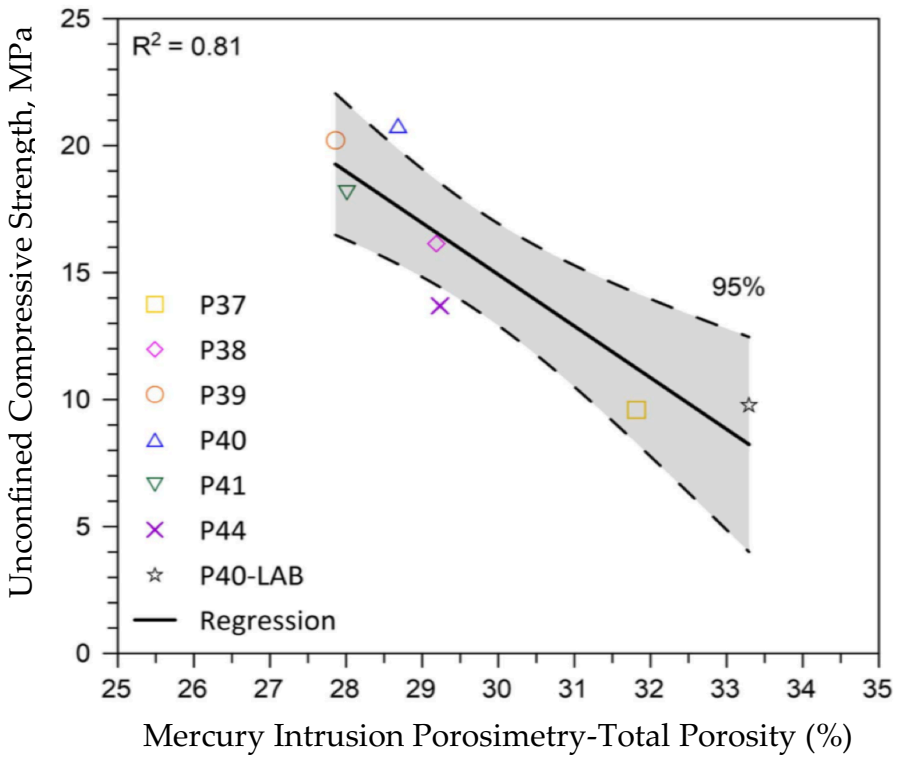


Figure 2.21: Correlation Between Unconfined Compressive Strength at 125 Curing Days and Porosity With Mercury Porosimetry Analysis (Bellato et al., 2020)

The microstructural analyses have proven to be a reliable tool in the assessment of porosity and pore networks in various soil stabilizations. Further, the analyses can be used in developing improved traditional soil acceptance criteria, including unconfined compression and permeability.

Research has been carried out on the implementation of deep mixing method (DMM) on cohesive soils in the Saga Lowland, Kyushu Japan with emphasis on the W/C ratio optimization and reducing the ground displacement effects during construction (Usui et al., 2024). In the experiment, three W/C ratios of 0.5, 1.0 and 1.5 were employed, using constant cement-based binder admixture. It was observed that increasing W/C ratio to 1.5 yielded a thinner cement slurry, resulting in better improved column quality. In particular, the Unconfined Compressive Strength after 28 days (q_u) was higher for this ratio with less Coefficient of Variation (CV) for column strength which implied more reliable columns (Figure 2.22). The defective rate for meeting the target strength

was least in W/C = 1.0, then 1.5 and 0.5 last. In terms of horizontal ground deformation (Sh), Case 3 (W/C = 1.5) had a Sh value of 2.0 – 6.5 mm, which was considerably lower than the Saga prefecture requirement of 20 mm (Figure 2.23). This was because of the high workability of the cement slurry that reduced sideways movement during mixing and helped to avoid lifting of the soil-cement columns.

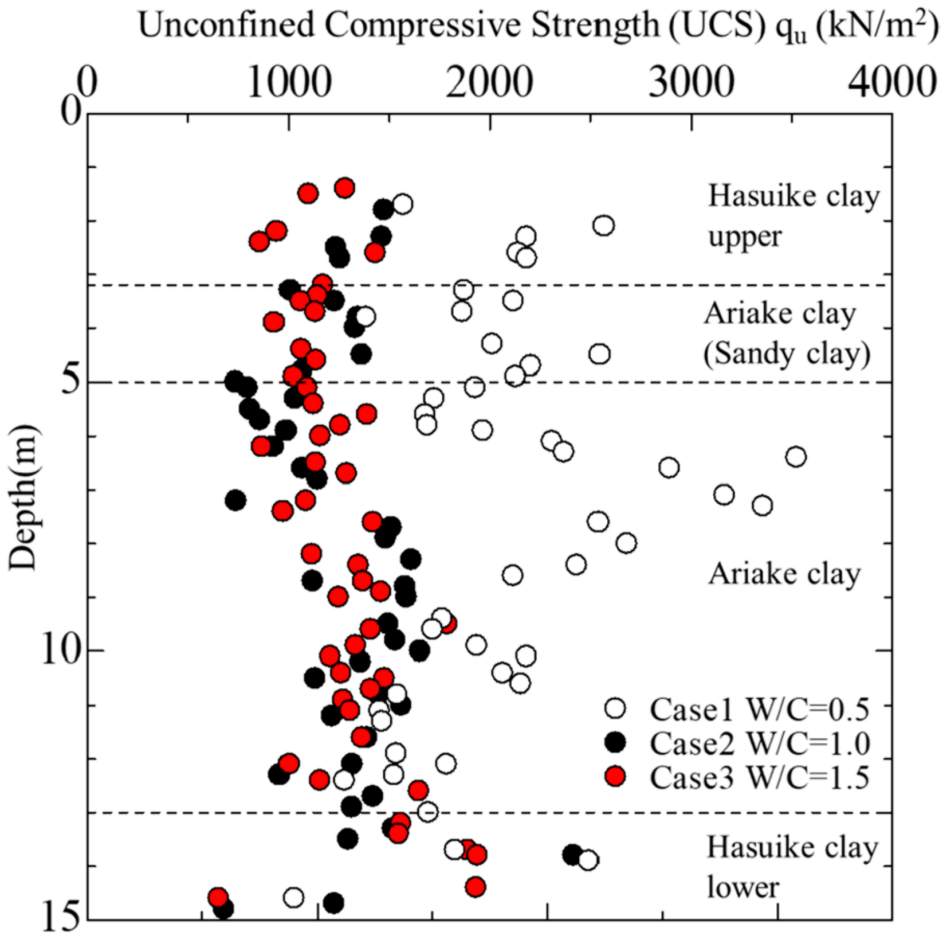


Figure 2.22: Unconfined Compressive Strength at Various Depth and Different Water Cement Ratio (W/C) (Usui et al., 2024)

Deep Cement Mixing columns were installed for Undredged Offshore Land Redemption (Yin et al., 2022). Variation in Unconfined Compressive Strength (UCS), Moisture Content and Density of the columns with depth were observed (Figure. 24). Also, the factors affecting Unconfined Compressive Strength (UCS) including tidal level fluctuations,

soil types, volumes of injected water and cement slurries, mixing times, curing ages, and moisture contents at different curing periods were observed and significant impact has been found which have been shown in Figure. 25.

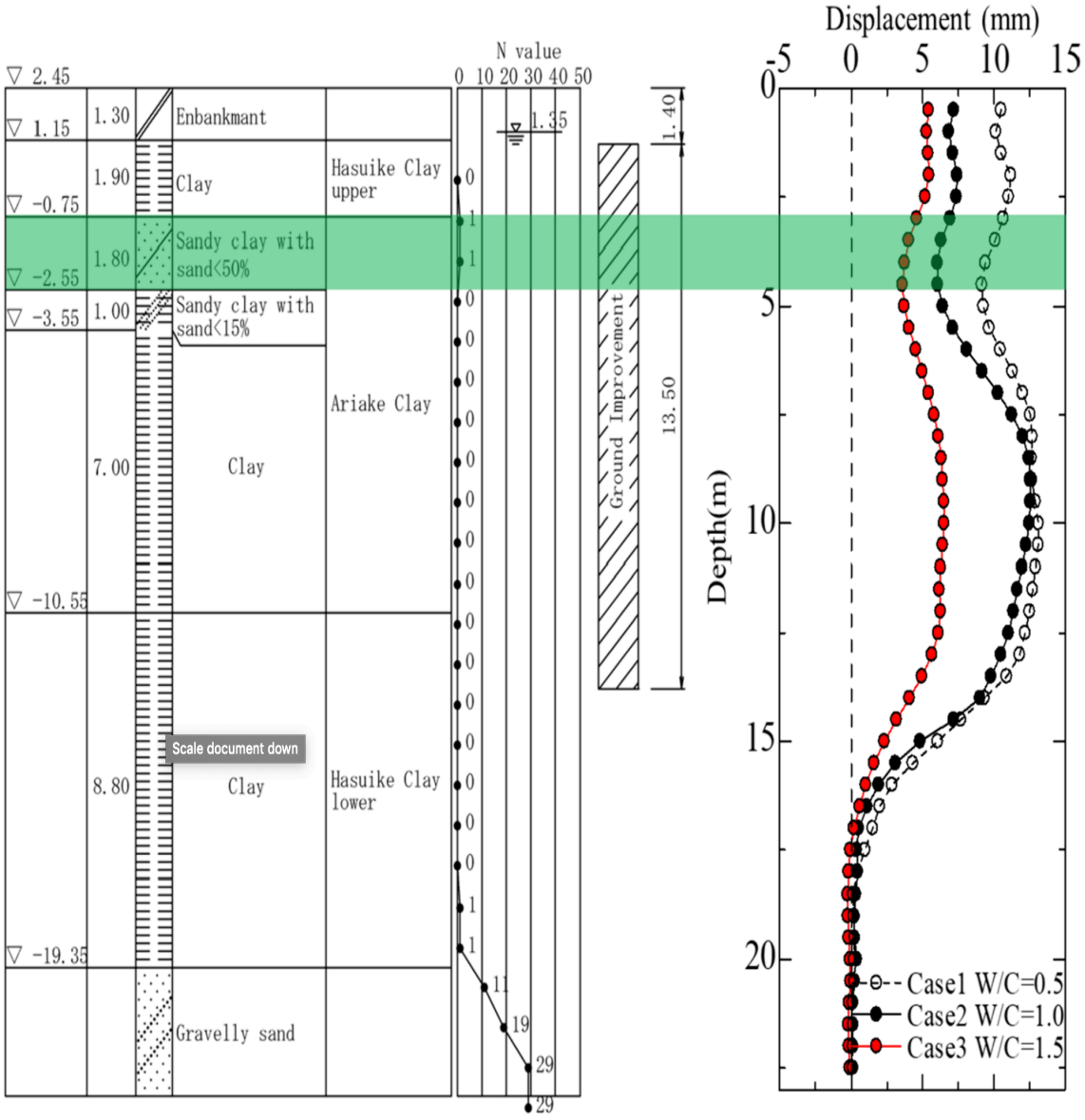


Figure 2.23: Displacemnet of Deep Mix Column at Various Depth (Usui et al., 2024)

2.4 GEOPOLYMER

The term "geopolymer" was first used by Joseph Davidovits in 1976. Geopolymerization is a polycondensation reaction of the geopolymeric cement due to alumino-silicate binders (Davidovits, 2005). It forms a three-dimensional structure. The general empirical formula for geopolymers is Mn[-(SiO2)z-

AlO2]n·wH2O, where M is a cation such as K, Na, or Ca; n is the polycondensation degree; and z is the molar ratio of Si/Al and varies in values of 1, 2, 3, or higher. These names are called polysialates, where "sialate" describes the silicon-oxo-aluminate building unit. In the sialate chain, the SiO4 and AlO4 tetrahedra are connected with each other through a shared oxygen atom. The negative charge of aluminum in 4-fold coordination is balanced by positive ions Na+, K+, Ca2+, etc. Si-O-Al bridges form links and rings in the sialate structure.

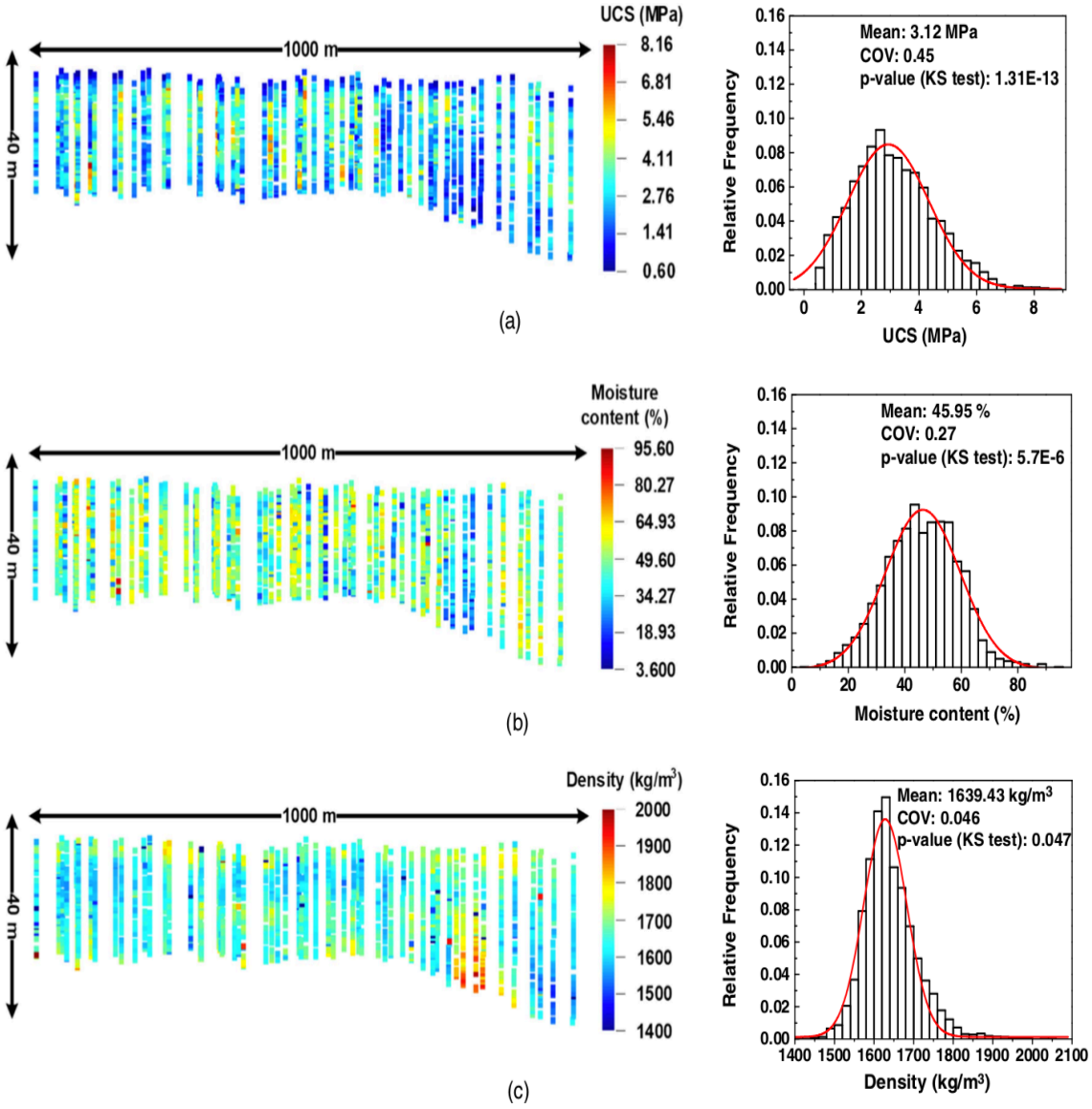


Figure 2.24: Frequency of various (a) Unconfined Compressive Strength (UCS), (b) Moisture Content, and (c) Density (Yin et al., 2022)

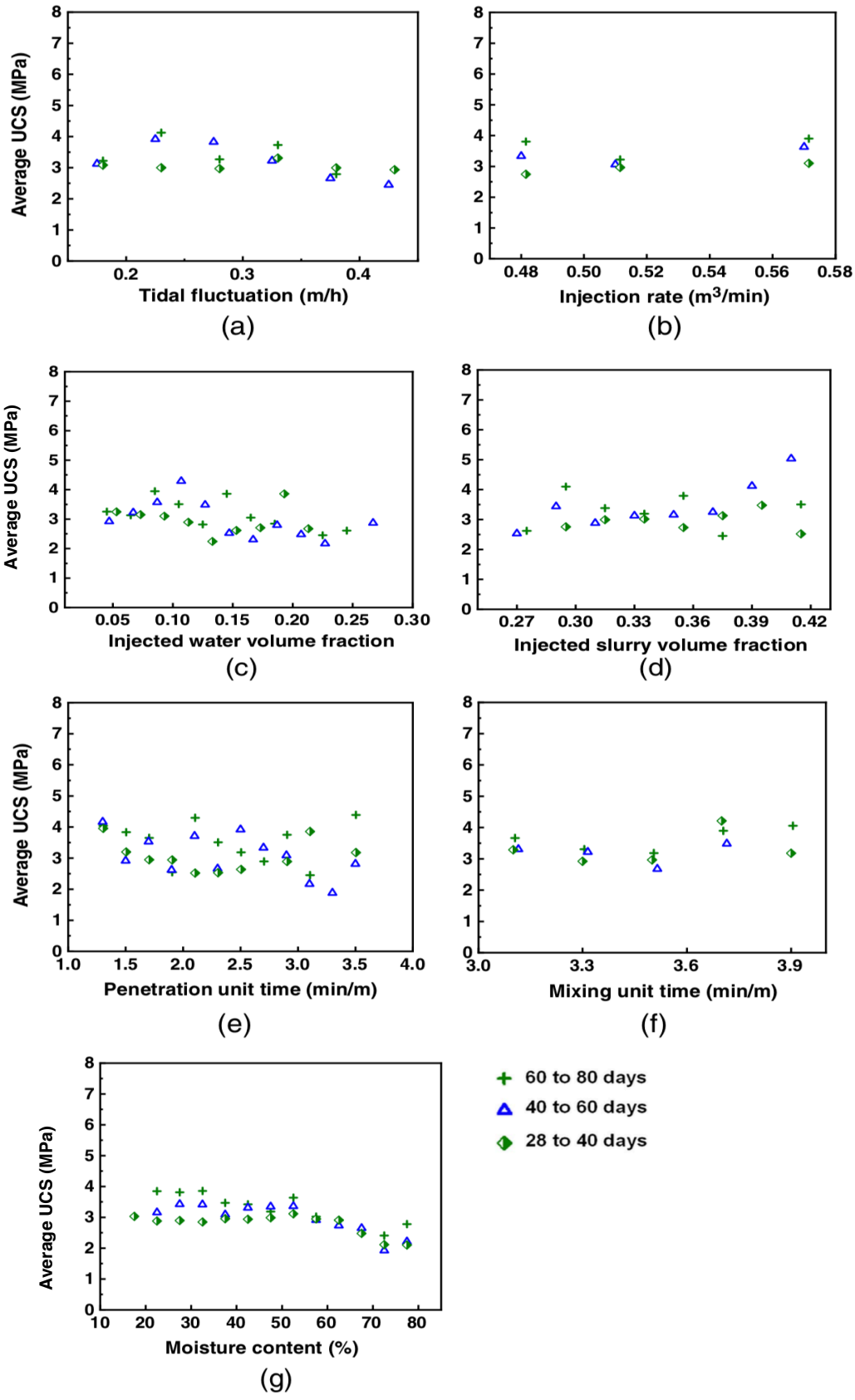


Figure 2.25: Variation of Unconfined Compressive Strength (UCS) with (a) Tidal Fluctuation, (b) Injection Rate, (c) Water Volume, (d) Slurry Volume, (e)Penetration Time, (f) Mixing Time, and (g) Moisture Content (Yin et al., 2022)

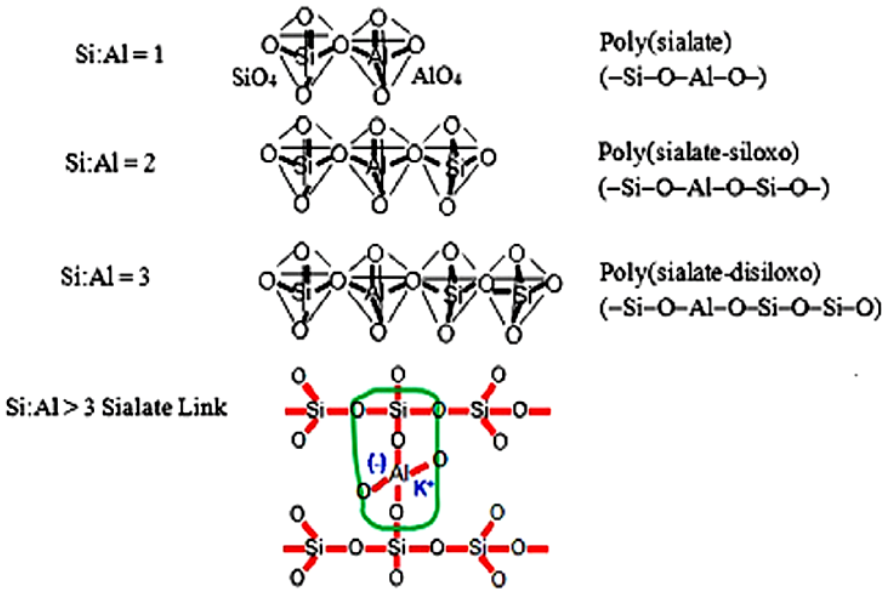


Figure 2.26: Formation of Geopolymer (Davidovits, 2005)

The chemical name "Poly(sialate)" was coined for geopolymers obtained from silico-aluminates. The term "sialate" is abbreviated for silicon-oxo-aluminate and polysialates are the polymer chains and rings consisting of Si4+ and Al3+ ions in IV-fold coordination with oxygen. Such polymers are from amorphous to semi-crystalline, while the obtained three-dimensional silico-aluminate framework is geopolymers.

2.4.2 Geopolymer as an Alternate of Cement

Portland Cement production is energy-intensive and, therefore, contributes substantially to greenhouse gas emissions (Phummiphan et al., 2016). The microstructure and mechanical properties of geopolymers depend on the composition of their raw materials and the type and concentration of the alkaline solutions used. The use of geopolymer binders is becoming increasingly relevant as an alternative to OPC due to the large amounts of waste materials rich in aluminosilicates produced by industries and agriculture, which pose a serious challenge in their disposal. This has led to the development of geopolymer-based soil stabilization as an effective alternative to traditional cement stabilization methods (Part et al., 2015). Geopolymers are

inorganic materials that exhibit aluminosilicates, which, with water, produce strong bonds among themselves. The process, generally referred to as geo-polymerization, is initiated with the addition of an activator to less reactive binders. Conventional materials such as fly ash, blast furnace slag, and silica are mixed together with alkali activators like sodium hydroxide NaOH and sodium silicate Na_2SiO_3 to form geopolymers for soil stabilization. Class F Fly Ash is an abundant by-product from coal-based power plants that could serve as a substitute for cement in various geopolymer-based stabilizations of soils. Geostatic stress on compressibility and strength development of submerged geopolymer-stabilized columns, with particular emphasis on various combinations of fly ash and slag precursors under different curing stresses, has been studied (Yaghoubi et al., 2020). With increased geopolymer content, unconfined compressive strength increases, whereas permeability reduces with increasing stress and increases with higher geopolymer content.

Performance of Micro-silica (MS) as Geopolymer

Recent research has shown that the inclusion of micro-silica (MS) in deep soil mixing columns improves the Unconfined Compressive Strength and Modulus of Elasticity in loose sandy soils, with optimum performance achieved using 15% micro-silica and a water-to-cement ratio of 0.8 (Esmaeili et al., 2020). The variation of strength and elasticity with water to cement ratio have been shown in Figure 2.27. Scanning Electron Microscope images are showing the agglomeration of the compounds formed during the stabilization process which results densification and void reduction (Figure 2.28 and 2.29).

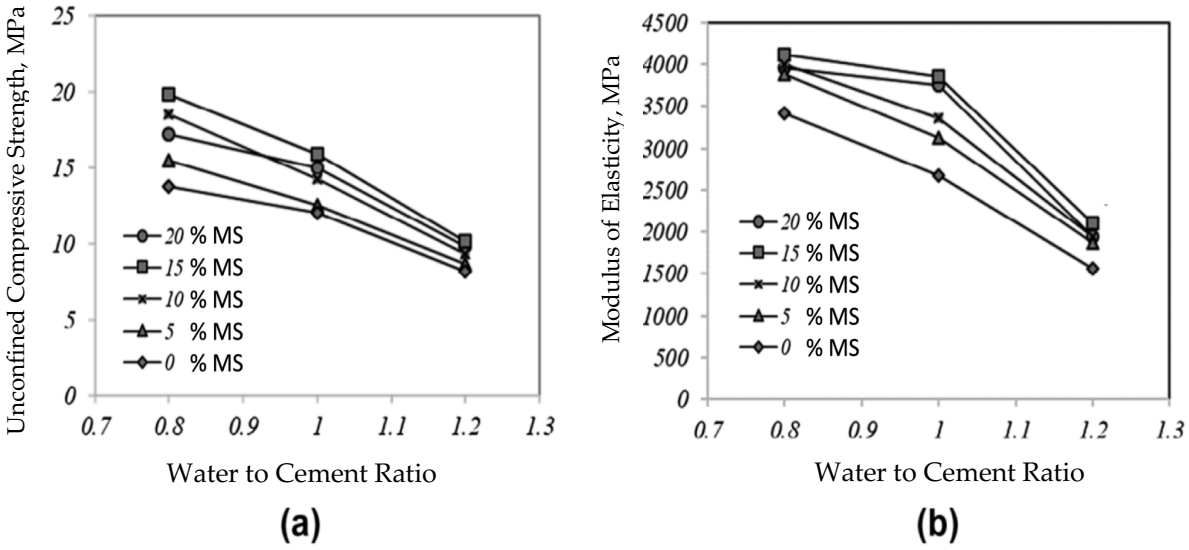


Figure 2.27: Effect of Water-to-Cement Ratio and Various Micro-Silica (MS) Percentages on (a) Unconfined Compressive Strength (UCS) and (b) Modulus of Elasticity of the Deep Mix Columns (Esmaeili et al., 2020).

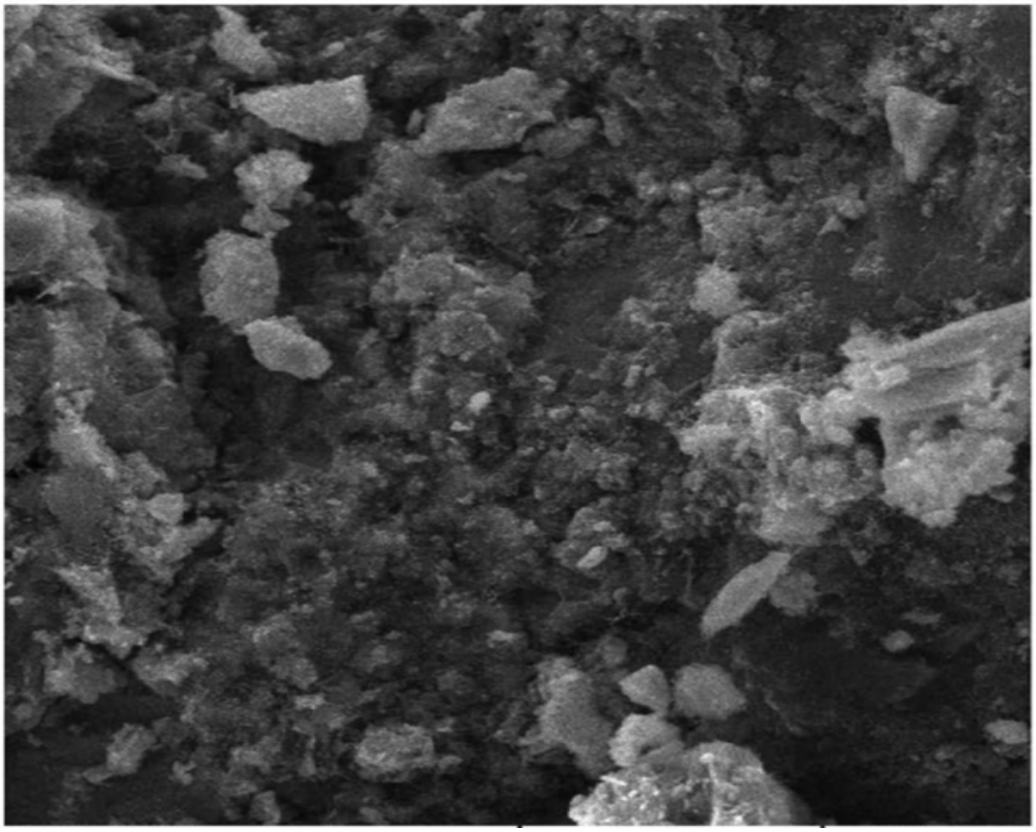


Figure 2.28: Scanning Electron Microscopy (800x Enlarged) Images of Deep Mix Column Having 15% Microsilica (Esmaeili et al., 2020)

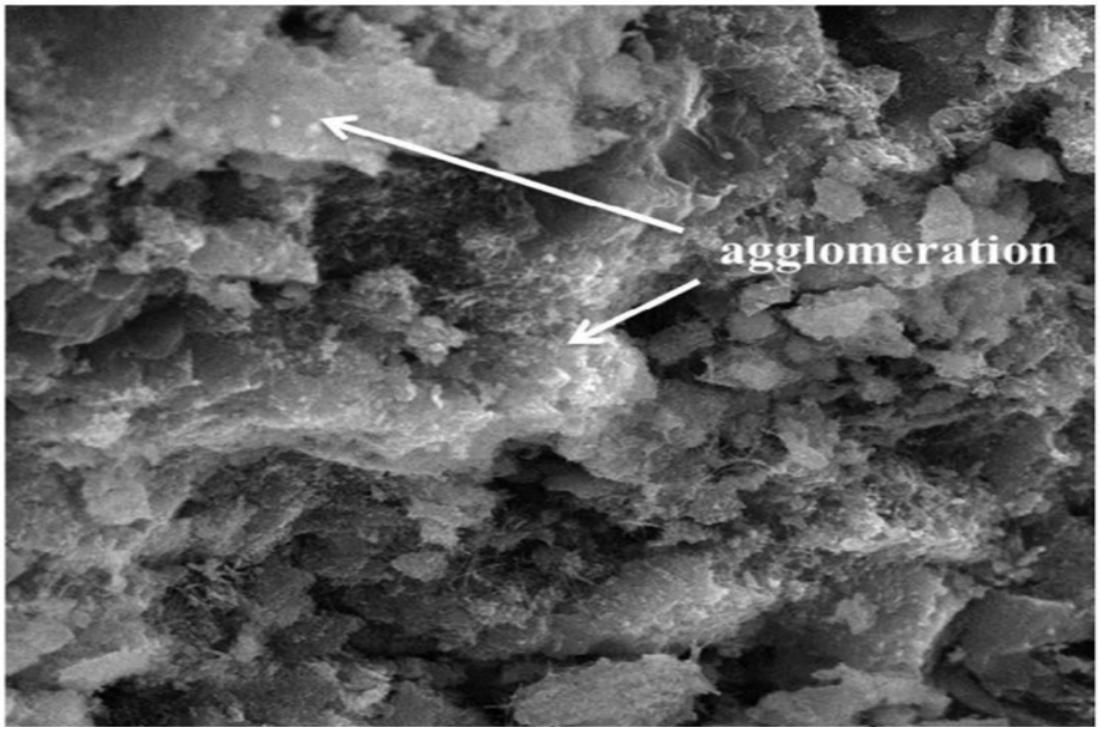


Figure 2.29: Scanning Electron Microscopy (800x Enlarged) Images of Deep Mix Column Having 20% Microsilica (Esmaeili et al., 2020)

Ground Granulated Slag as Geopolymer

The influence of different fly ash percentage as main precursor material on strength gain in geopolymer-stabilized clay was investigated under a fixed Activator to Fly Ash ratio of 40%, with various proportions of Binder to Total Dry Mix ratio, SM/DM such as 10, 20, and 30%. The results, as presented in Figure. 30 (Abdullah, Shahin, and Sarker, 2019), indicate that with both 7-day and 28-day curing periods, an increase in the percentage of fly ash produces increased Unconfined Compressive Strength, UCS of geopolymer-treated clay for all mixes. It was demonstrated in the study that adding only 10% fly ash to the clay increased the Strength Development Index, SDI (the ratio of treated to untreated soil strength) by 1.2 and 2 for the curing periods of 7 days and 28 days, respectively. With a further increase in the fly ash content to 20%, an increase of 2.1 and 0.5 in SDI for the respective curing periods was achieved. This is highly pronounced at higher fly ash concentration and with extended curing times. These results are in good agreement with those reported in the

literature previously (e.g. (Cristelo et al., 2013; Sargent et al., 2013)) and could be attributed to the introduced cementitious properties by the activated fly ash in the form of Sodium-Alumino-Silicate-Hydrate (N-A-S-H) geopolymer gel.

Table 2.3: Proportioning of Deep Mix Column Panels (Abdullah, Shahin, and Sarker, 2019)

Sample Designation	Binder (SM) (Fly Ash + Slag) to Total Mix (DM) ratio, SM/DM (%)	Slag to Total Binder (SM) ratio, S/SM (%)	Activator (A) to Total Binder (SM) ratio, A/SM (%)
M(10-20-0)	10	20	0
M(10-20-40)	10	20	40
M(10-20-80)	10	20	80
M(20-20-0)	20	20	0
M(20-20-40)	20	20	40
M(20-20-80)	20	20	80
M(30-20-0)	30	20	0
M(30-20-40)	30	20	40
M(230-20-80)	30	20	80

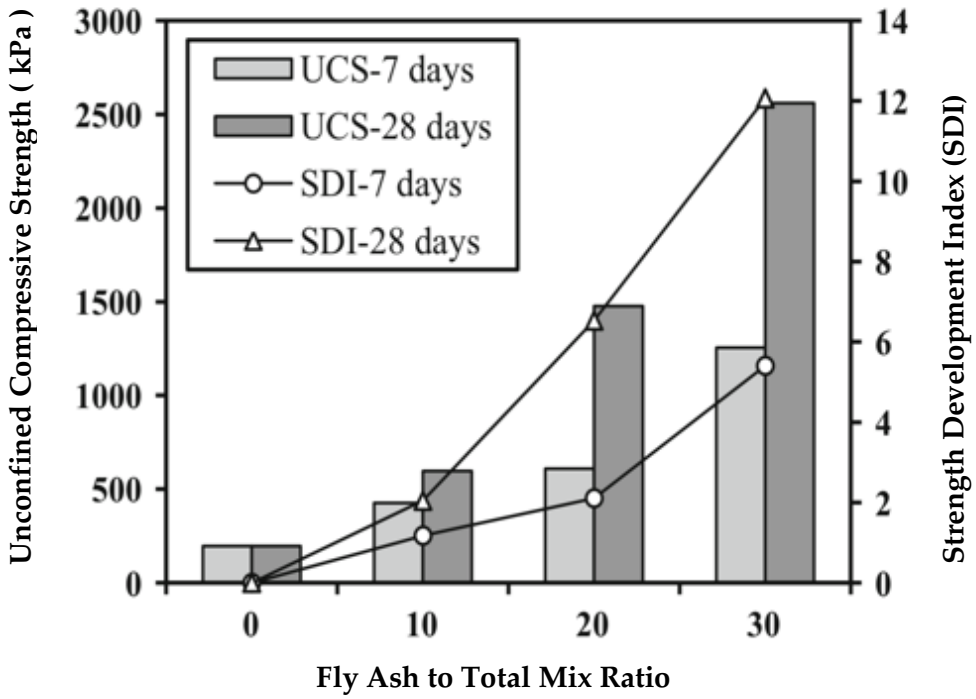


Figure 2.30: (a) Development of Strength with Fly Ash Geopolymer; (Abdullah, Shahin, and Sarker, 2019).

Figure 2.34 compares different geopolymer-stabilized clay specimens prepared with various mix compositions cured for 7 and 28 days to investigate the effect of the activator at different A/SM ratios. With A/SM = 0, representing zero activator concentration, no gain in UCS improvement over the untreated clay in all mixes could be identified due to minimum pozzolanic reaction and little self-cementitious activity from the raw material. When the value of A/SM > 0, a substantial improvement in strength may be found. Mixes with A/SM ratios of 40% and 80% obtained the highest strength gains, probably due to the higher reactivity of the source material (Cristelo et al., 2012). For the case of the M(10-20-A/SM) mixture, no more significant increase in UCS beyond 40% activator concentration after 7- and 28-day curing, as the majority of the available material had already reacted.

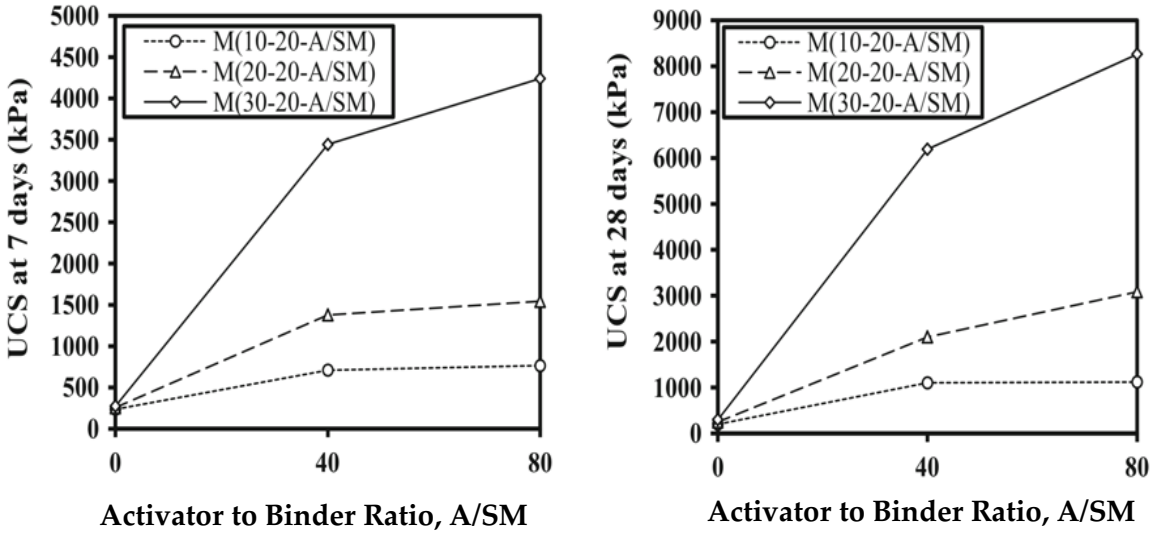


Figure 2.31: Effect of Activator on Unconfined Compressive Strength (UCS) (Abdullah, Shahin, and Sarker, 2019)

In contrast, mix M(20-20-A/SM) exhibited a 12% gain in UCS for the increased A/SM ratio from 40% to 80% after 7 days of curing and an improved UCS of 47% after 28 days. Similarly, mix M(30-20-A/SM) showed a 23% improvement in UCS over the same activator ratio increase after 7 days and an improved 33% after 28 days. These differences in strength gain could be

indicative of the limited short-term reactivity of kaolin clay when exposed to the activator.

Rice Husk Ash (RHA) and Cement Kiln Dust (CKD) as Geopolymer

The addition of Cement Kiln Dust (CKD) with soil improved Unconfined Compressive Strength (UCS) and California Bearing Capacity Ratio (CBR) of soil significantly (Adeyanju et al., 2020). Table 2.4 shows the material proportioning and Figure 2.32 shows the improvement in both UCS and CBR. On the whole, these enhancements translated into advantages of over 2500%. Accordingly, 15% CKD addition gave the maximum percentage soaking CBR of the native soil CBR value, increasing from 0.557 to 16.82%. The result suggests that 10% CKD by dry weight gave the optimum CBR. In general, the maximum CBR peaked at 16.8% after the addition of 15% CKD, while optimization can demonstrate the optimality of 10%. Addition of Rice Husk Ash (RHA) along with CKD shows decreased value in both UCS and CBR.

Table 2.4: Mix Proportion of Soil with CKD and RHA (Adeyanju et al., 2020)

ID	Soil, %	Cement Kiln Dust (CKD), %	Rice Husk Ash (RHA), %
NAT	100	-	-
CKD 1	92.5	7.5	-
CKD 2	90	10	-
CKD 3	87.5	12.5	-
CKD 4	85	15	-
GRHA1	86	10	4
GRHA 2	84	10	6
GRHA 3	82	10	8
GRHA 4	80	10	10

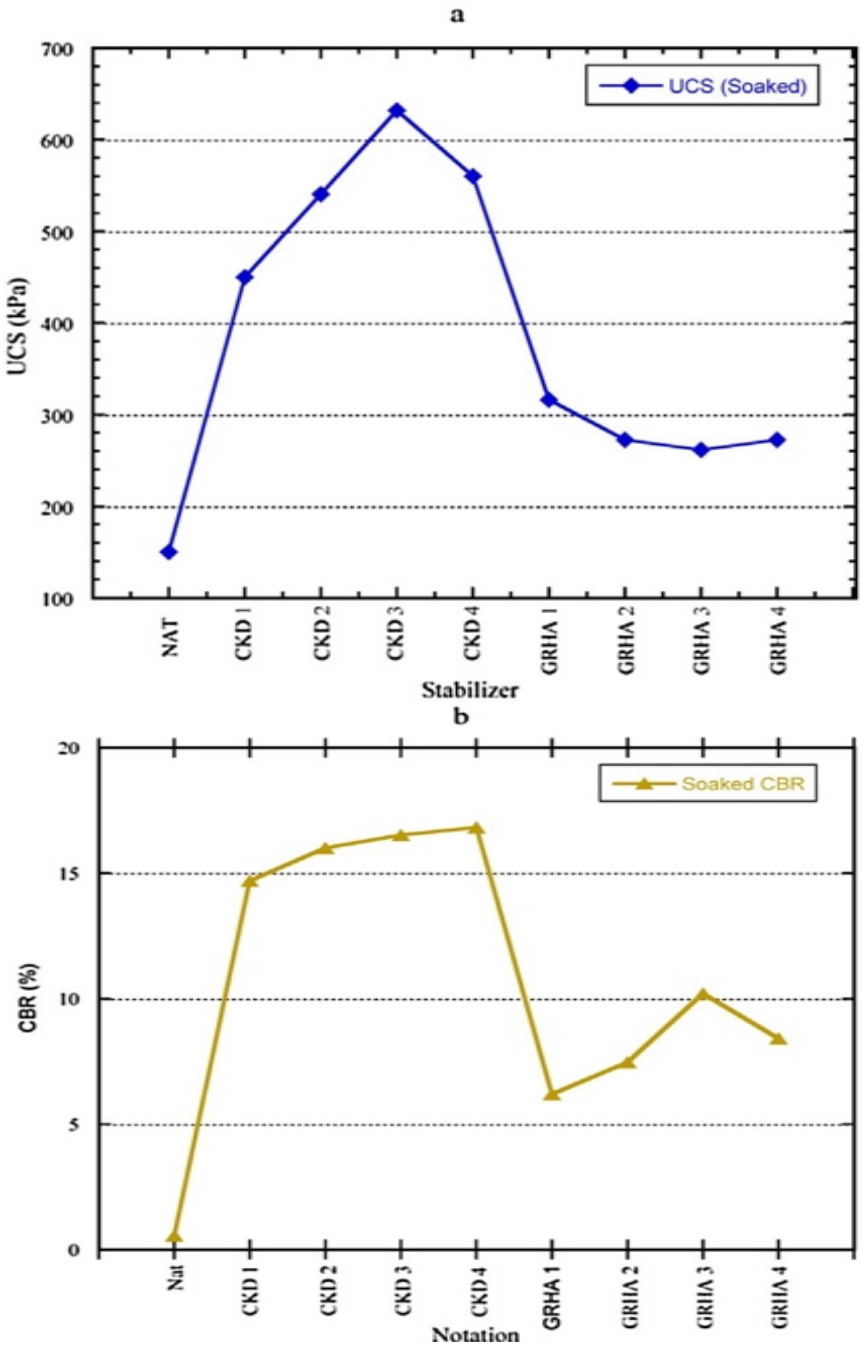


Figure 2.32: Effect of Stabilizers on (a) Unconfined Compressive Strength (UCS), (b) Soaked California Bearing Capacity Ratio (CBR) (Adeyanju et al., 2020)

Meta-Kaolin (MK) as Geopolymer

Soils that are very compressible, possess very low shear strength and low permeability are termed soft soils. Understandably, the engineering properties of soft soils are improved using conventional stabilizers like lime or cement with metakaolin based geopolymer (Wassie and Demir, 2024). Unconfined

Compressive Strength (UCS) test conducted on specimens cured for 7 days showed in Figure 2.33(a) that the soil stabilised with cement (with no metakaolin) had the largest yield stress (Figure 2.33(a)). Figure 2.33(b) shows that, in the triaxial shear test, the metakaolin stabilized soft soil showed the greatest deviator stress as compared to lime stabilized soil and untreated soil.

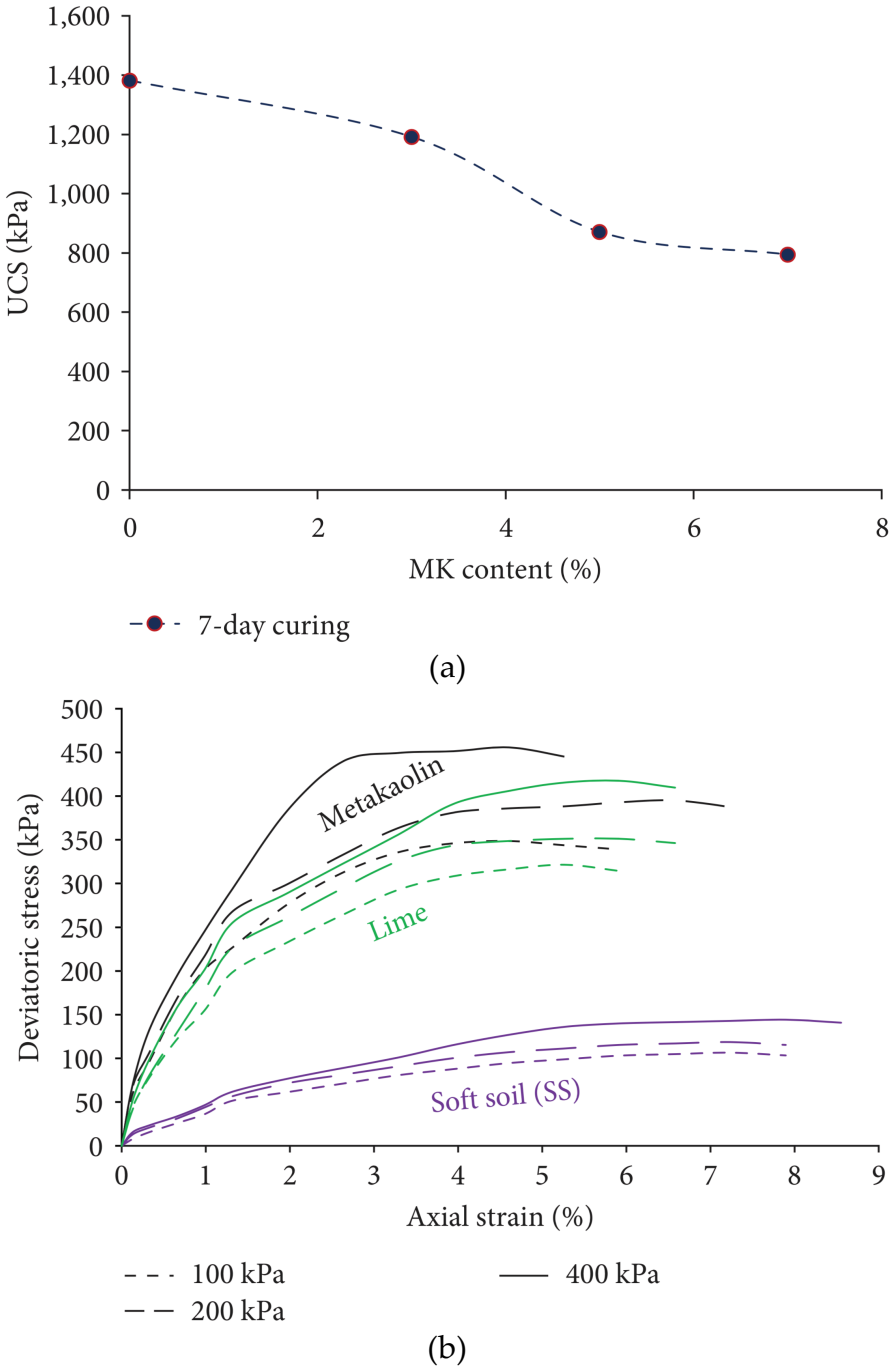


Figure 2.33: (a) Unconfined Compressive Strength (UCS) at Different Metakaolin (MK) Content Added to Cement, (b) Deviatoric Stress-Strain (Wassie and Demir, 2024)

2.4.5 Efficiency of Fly Ash by Various Investigations

A number of research have been conducted on ground improvement with fly ash based geopolymer. The changes of soil properties due to stabilization have been observed. The most common properties that change with fly ash geopolymer stabilization are described in the following subsections.

Unconfined Compressive Strength (UCS)

When evaluating the strength of soil treated with geopolymers, the unconfined compressive strength (UCS) test is most frequently used ((Abdullah, Shahin, and Sarker, 2019), (Adeyanju et al., 2020), (Bellato et al., 2020), (Esmaeili et al., 2020), (Onur et al., 2022)). All things considered, the study shows that incorporating geopolymers into the soil matrix increases the unconfined compressive strength (Phummiphan et al., 2016). The soil geopolymer combination performs better in terms of strength development the higher the fly ash content (Cristelo et al., 2011). For the 50% fly ash mixture, the optimal activator-to-fly ash ratios were determined to be 0.8 and 0.9 for curing periods of 7 and 28 days, respectively. These ratios were identified while incorporating fly ash at proportions of 20%, 30%, and 40%, respectively, in the mixture. The results indicate that an increase in the activator content enhances the early-age strength development of the geopolymerized soil. Figure 2.34 further illustrates the strength gain trends observed after 7 days of curing under varying activator-to-fly ash ratios and curing conditions. It is evident that the strength improved significantly within this initial period. However, after 28 days of curing, particularly under normal and buried curing conditions, the strength of the 50% fly ash mixture with an activator-to-fly ash ratio of 0.9 exhibited a noticeable decline. This suggests that excess activator may have caused a porous or brittle structure, reducing long-term strength.

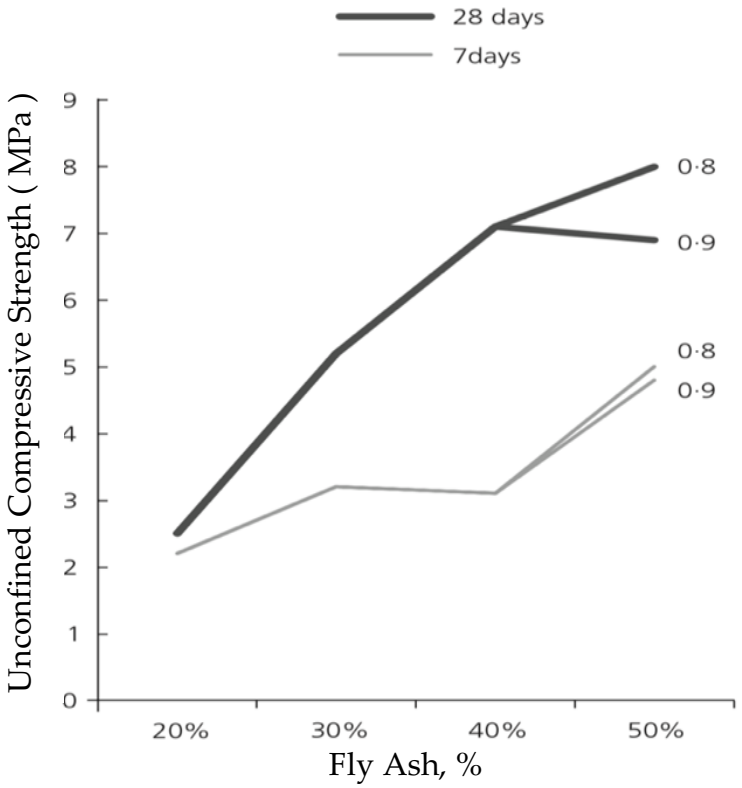


Figure 2.34: Comparison Between 20, 30, 40 and 50% Fly Ash Mixtures (Cristelo et al., 2011)

Figure 2.35 compares cement and alkaline grouts directly. The w/c ratio of 1.0 was adopted because this is the most common in practice. Longer curing periods than 28 days had to be compared since it is well known that the majority of the final strength for traditional Portland cement-based binders is achieved after 28 days of curing, while for the alkaline activator samples that period proved to be too short to develop substantial strength. substantial strength. Investigation on the stabilisation of loess soil (mostly composed of silt and clay delivered by wind) with fly ash activated by potassium hydroxide (KOH) and sodium hydroxide (NaOH) was carried out (Liu et al., 2016). The UCS value of geopolymer stabilised samples rises when the same alkaline activator precursor is added (Figure 2.36). This might be explained by the production of geopolymer, which offers strong cementation between loess particles and contributes to the strength of stabilised loess.

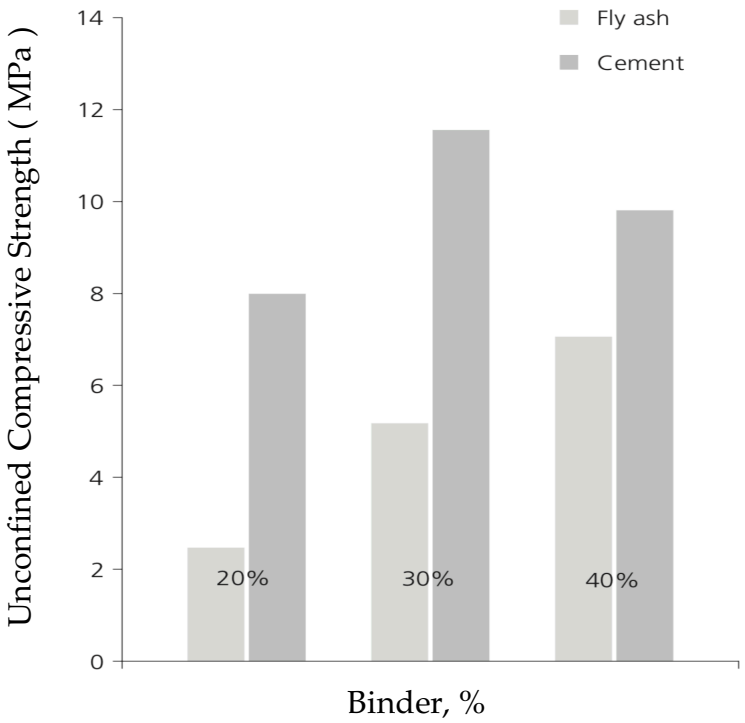


Figure 2.35: Comparison between Cement and 12·5 Molal Cold Activator with Fly Ash at 28 Days Curing (Cristelo et al., 2011)

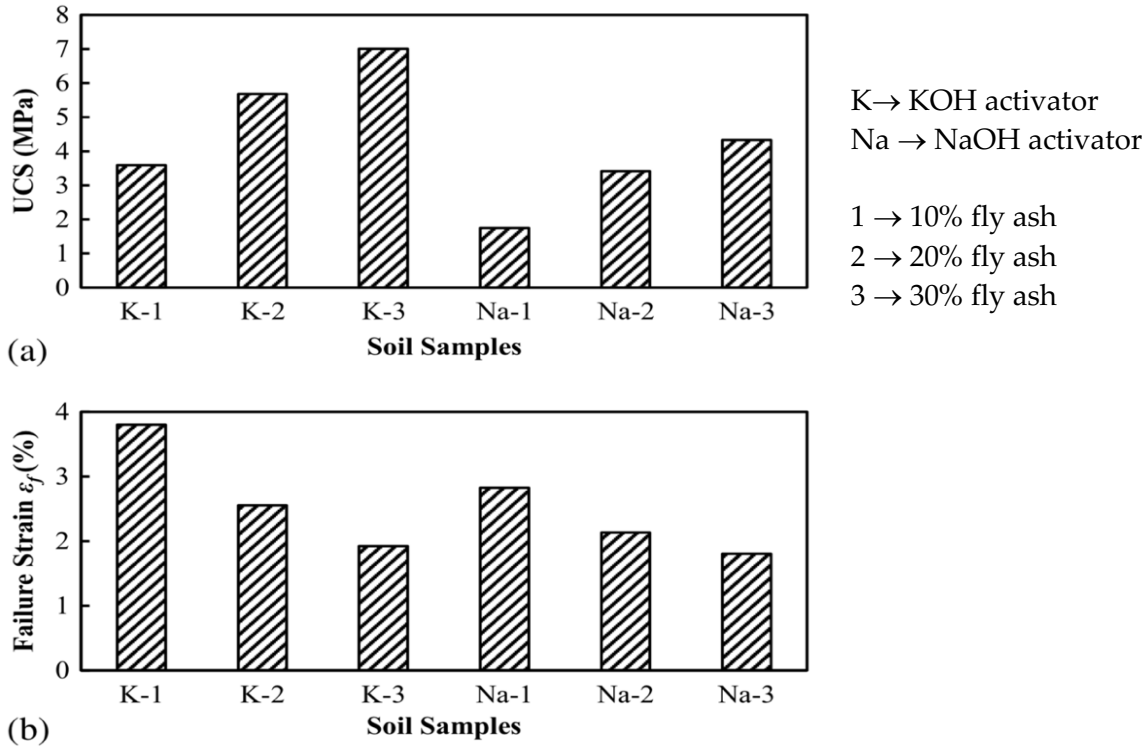


Figure 2.36: (a) Unconfined Compressive Strength (UCS); (b) Failure Strain(Liu et al., 2016)

Recently, an experimental study has been conducted to substantiate the use of Fly Ash as a partial replacement of cement in the deep mixing pile (Ekmen et al., 2020). The pattern of strength development along with the axial strain is described in Figure 2.37 and 2.38.

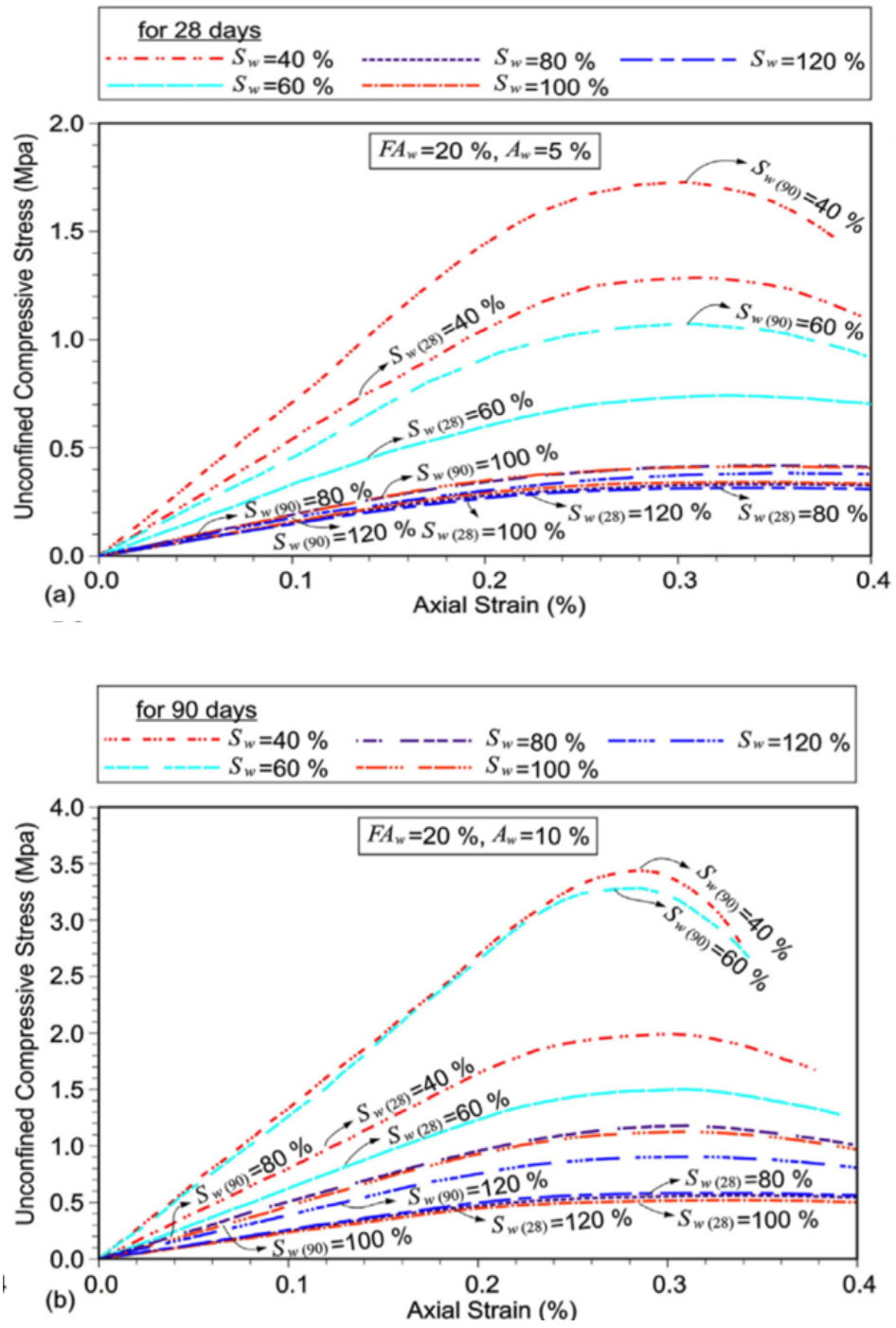


Figure 2.37: Unconfined Compressive Strength Test Results for Clayey, Silty Sand Stabilized with Cement and the Addition of 20% Fly Ash; (a)Aw = 5%, (b) Aw = 10% (Ekmen et al., 2020)

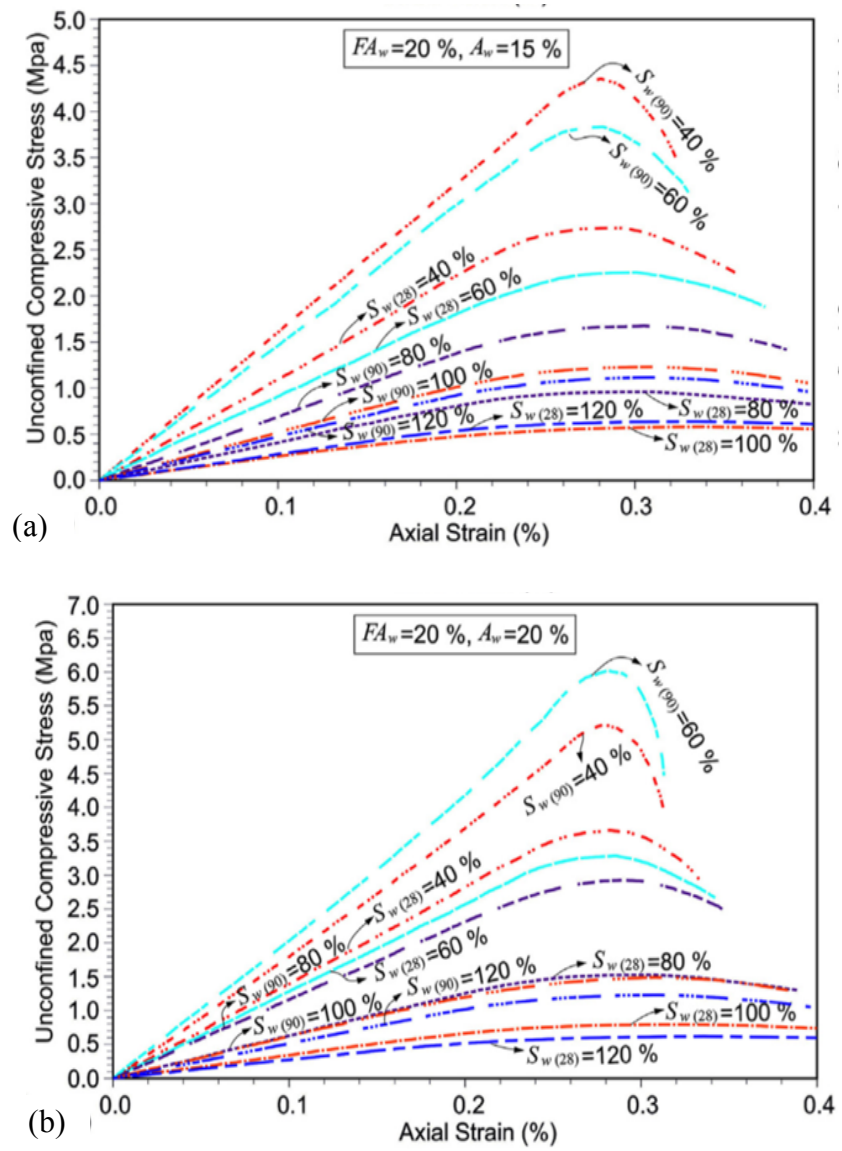


Figure 2.38: Unconfined Compressive Strength Test Results for Clayey, Silty Sand Stabilized with Cement and the Addition of 20% Fly Ash; (a)Aw = 15%, (b) Aw = 20% (Ekmen et al., 2020)

Tri axial Test

From the triaxial test results on silty sand presented in Figure. 2.39 and. 2.40, very stiff stress-strain curves and a significant dilatation after an initial volume decrease. are described (Rios et al., 2016). The triaxial test results on silty sand revealed extremely stiff stress-strain curves, with a significant dilatation after an initial volume decrease. Mixture M1 exhibited higher dilatation compared to the other mixes, as well as higher initial stiffness (lower

strain at peak stress) and higher peak deviator stresses. In any case, the abrupt strain softening as depicted in the volumetric strain may confirm that strain localization during shearing took place for all specimens.

Table 2.5 Material Proportioning. (Rios et al., 2016)

ID	Ash/solids (wt.)	Activator[a] (%)	Activator/Ash (wt.)
M1	0.15	11.7	0.781
M2	0.20	15.6	0.781
M3	0.25	19.5	0.781

[a]For Sodium Sillicate/Sodium Hydroxide ratio of 0.5

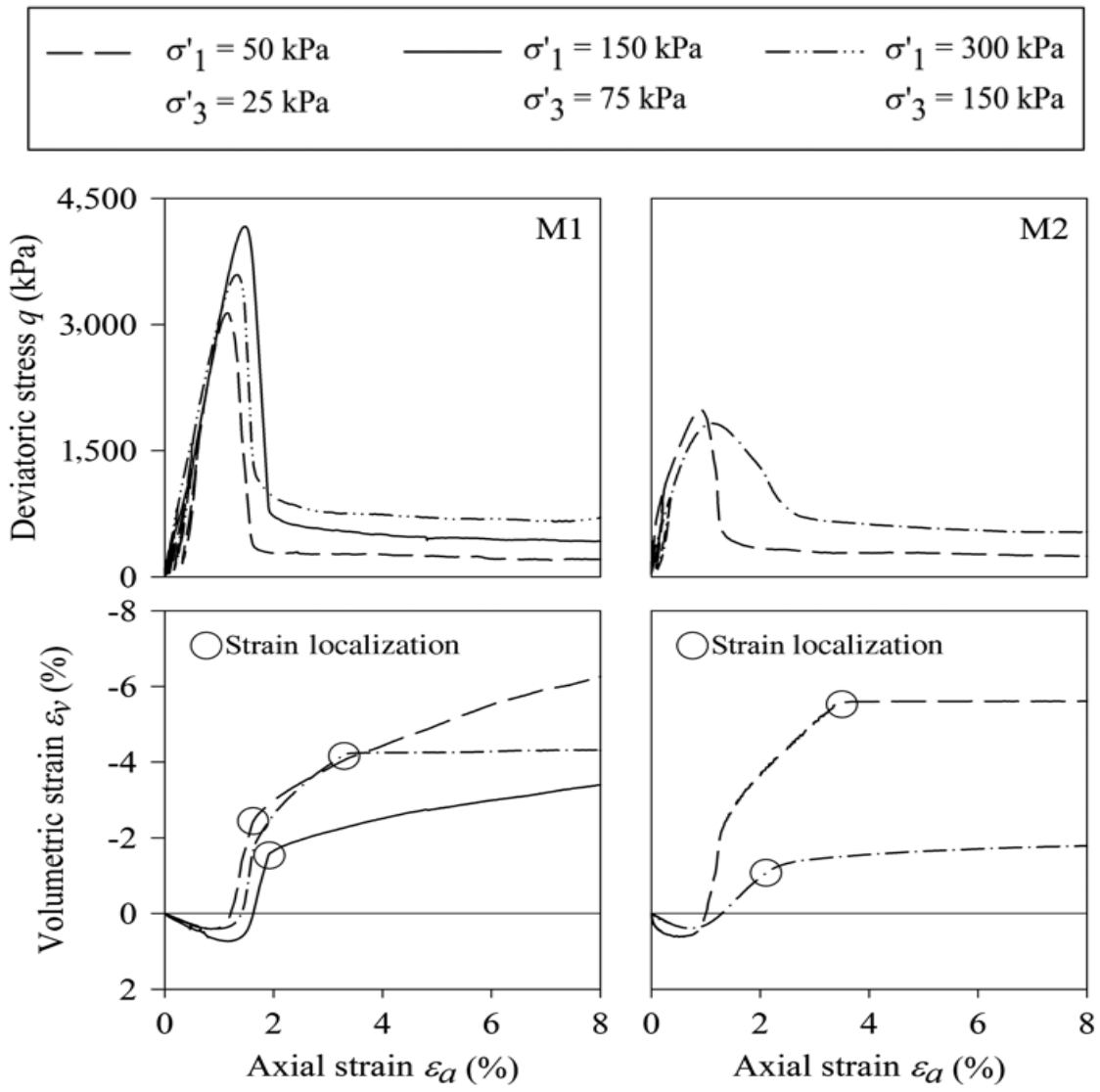


Figure 2.39: Variation of Deviatoric Stress and Volumetric Strain with Axial Strain in Triaxial Compression Tests at 28 Days of Curing (Rios et al., 2016)

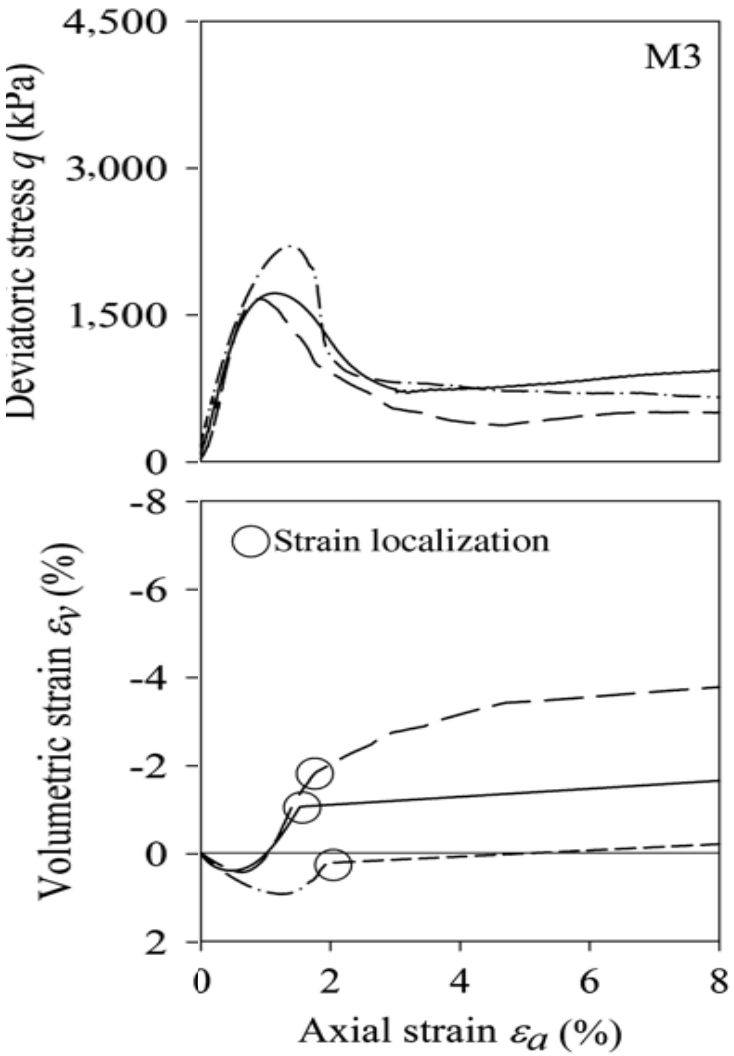


Figure 2.40: Variation of Deviatoric Stress and Volumetric Strain with Axial Strain in Triaxial Compression Tests at 28 Days of Curing (Rios et al., 2016)

The pre-shear consolidation pressure, p'_c, significantly affects the stress-strain behavior of the geopolymer-treated clay (Abdullah, Shahin, and Walske, 2019) Yield stress significantly increases under increased confining pressures due to only minor de-structuring of the cemented soil during consolidation, such that behavior remains dominated by cementitious bonds and friction (MR Coop, 1993). When the confining pressure is 100 kPa, the de-structuration of the stabilized soil subjected to consolidation will be very slight, and its yield stress is determined mainly by the cementation bond between clay particles. By increasing the confining pressures to 200 kPa and 400 kPa, the cementation structure of the specimen may be slightly damaged by the consolidation

process; however, strength remains predominantly controlled by cementitious bonds, while the frictional component in the response due to consolidation-induced volumetric change is very small. The magnitude of post-peak residual strength is determined predominantly by frictional response. In undrained shearing, the rise in mean total stress, associated with the volume change tendency of the specimen, causes the generation of excess pore water pressure, Δu.

For untreated kaolin, the positive pore water pressure was produced for the strain values of 0-2%, beyond which it showed a slight reduction at higher strains with no peak stress developed as seen in Figure 2.41a. It contracts at low strain followed by slight dilation at higher strains, although it was not observed in these tests due to its excessively ductile nature. Untreated clay changed from a contractive to a slightly dilative behavior and showed quasi-over-consolidated response typical of consolidation at higher pressures (Jackson, 2015). For 10% geopolymer-treated specimens, Figure 2.41b, the specimen first contracts at the strain corresponding to peak stress before dilating. At peak deviator stress, Δu exhibited higher positive values where the behavior was transitioning from contractive to dilative, followed by a reduction during strain softening, into over-consolidation. When the geopolymer content was raised to 20%, negative pore pressure readings became dominant in Figure 2.42, indicating a stronger tendency for dilatation during shearing. Such increased dilation may be an indication of the fact that, during shearing, the geopolymer is increasingly involved in modifying the size of voids and clusters of fractures and, accordingly, affects the residual frictional response

California Bearing Ratio (CBR)

CBR value has been increased due to geo-polymerization with fly ash in various degree of expansive soil both in soaked (Figure 2.43) and unsoaked condition (Debanath, 2019). Soaked CBR increased in higher rate compared to

the unsoaked CBR which might be considered as positive sign of elimination of problems arise from submerged effect in road or embankment due to flood or any other fluctuation of water table.

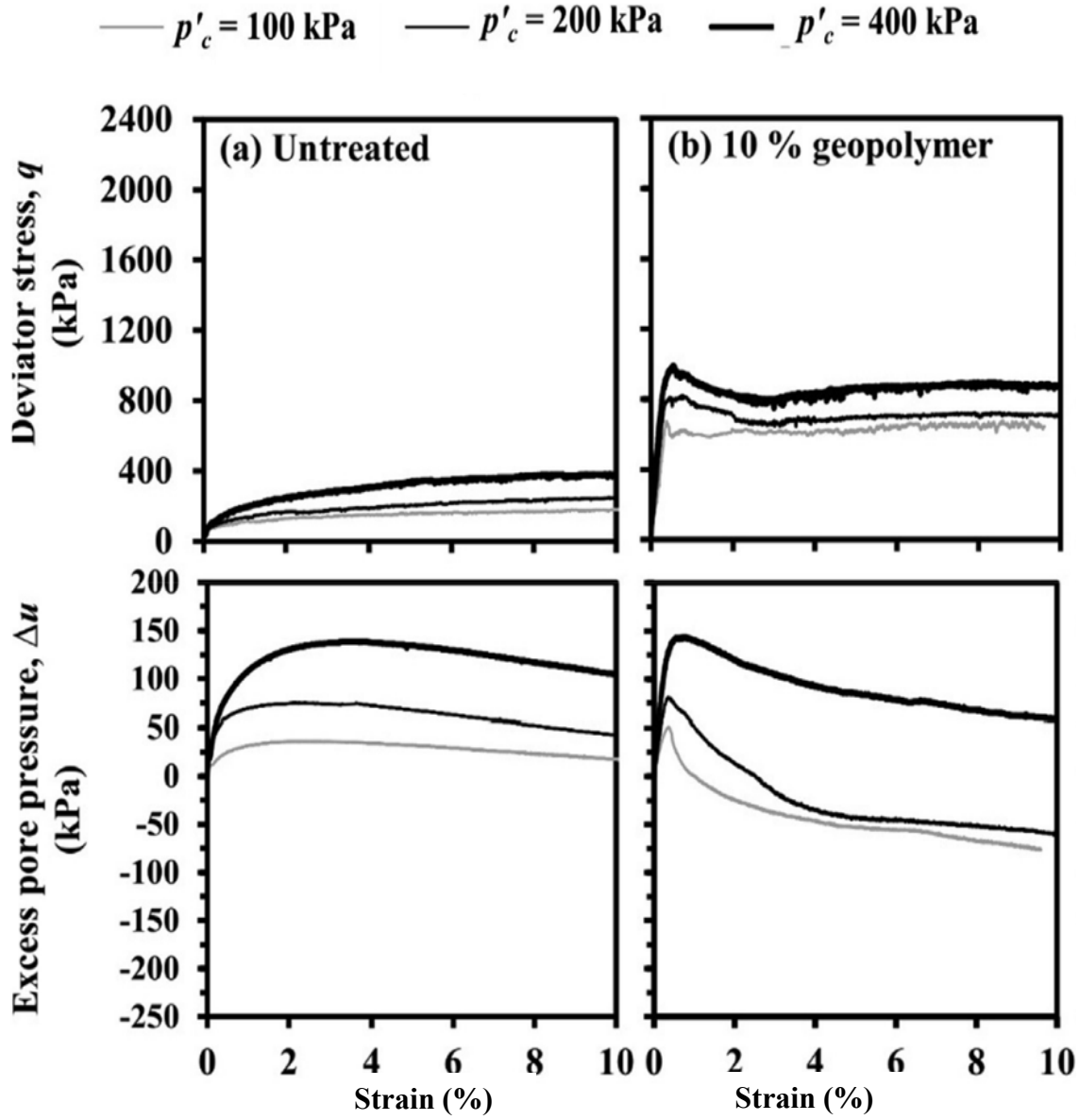


Figure 2.41: Typical CU Triaxial Compression Test Results for Untreated and Treated Kaolin Clay with Various Geopolymer Contents at 100, 200, and 400 Kpa Confining Pressures (28 Days): (a) Untreated; (b) 10% Geopolymer (Abdullah, Shahin, and Walske, 2019)

Consolidation

On a laboratory scale FA-replaced cement DM columns measuring 30 cm in diameter and 80 cm in length were installed in clayey soils using DM equipment(Yenginar and Olgun, 2024). Since the strengths of hardened soilcrete

are significantly higher than the maximum stress in the consolidation test, the consolidation curves of design 14 and the ideal design continue linearly at low slopes and lack a yield point. Furthermore, given the same design, the hardened soilcrete's compression index (Cc) falls with increasing curing time.

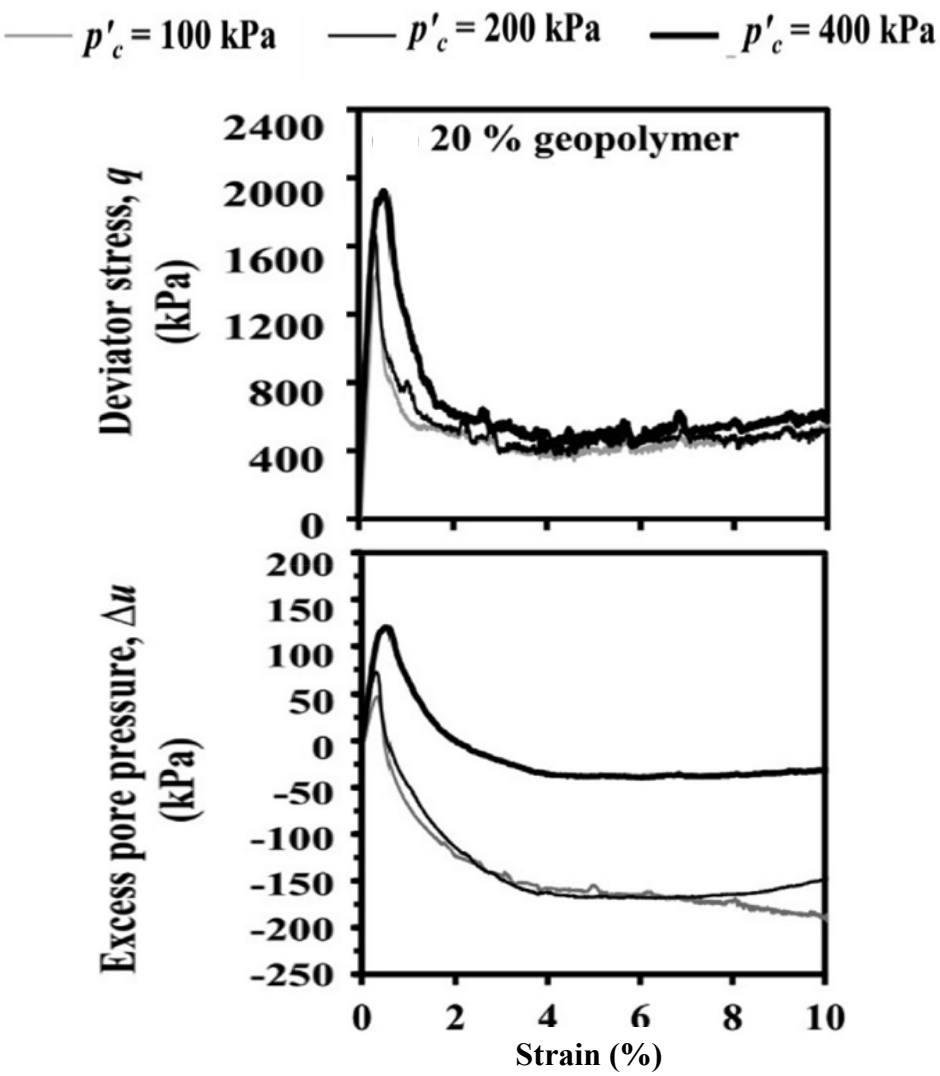


Figure 2.42: Typical CU Triaxial Compression Test Results for Untreated and Treated Kaolin Clay with Various Geopolymer Contents at 100, 200, and 400 Kpa Confining Pressures (28 Days): 20% Geopolymer (Abdullah, Shahin, and Walske, 2019)

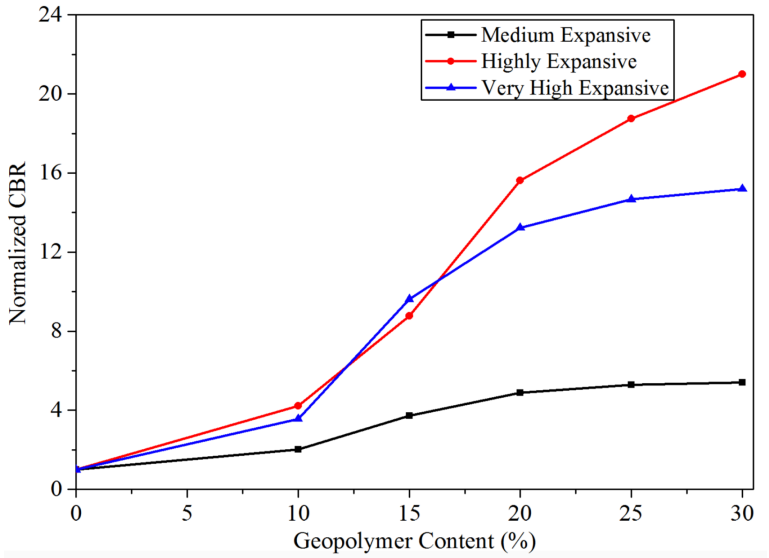


Figure 2.43: Soaked CBR Value of Geopolymer Treated Soils (Debanath, 2019)

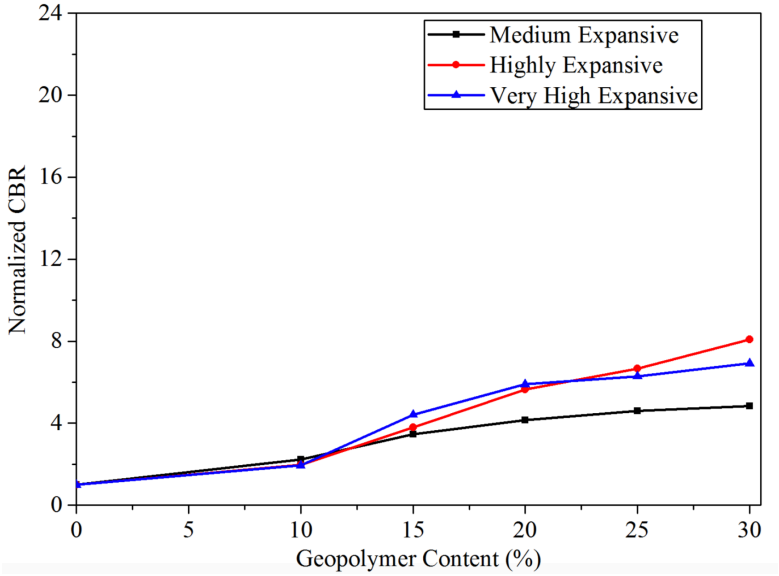


Figure 2.44: Unsoaked Value of Geopolymer Treated Soils (Debanath, 2019)

XRD Analysis

Microstructural bond formation in treated soil with both cement and fly ash was observed by Ekmen et al. (2020). The geopolymerized soil shows the peak intensity of both soil and binder material which shows the compounds formed due to reaction between the binder and soil.

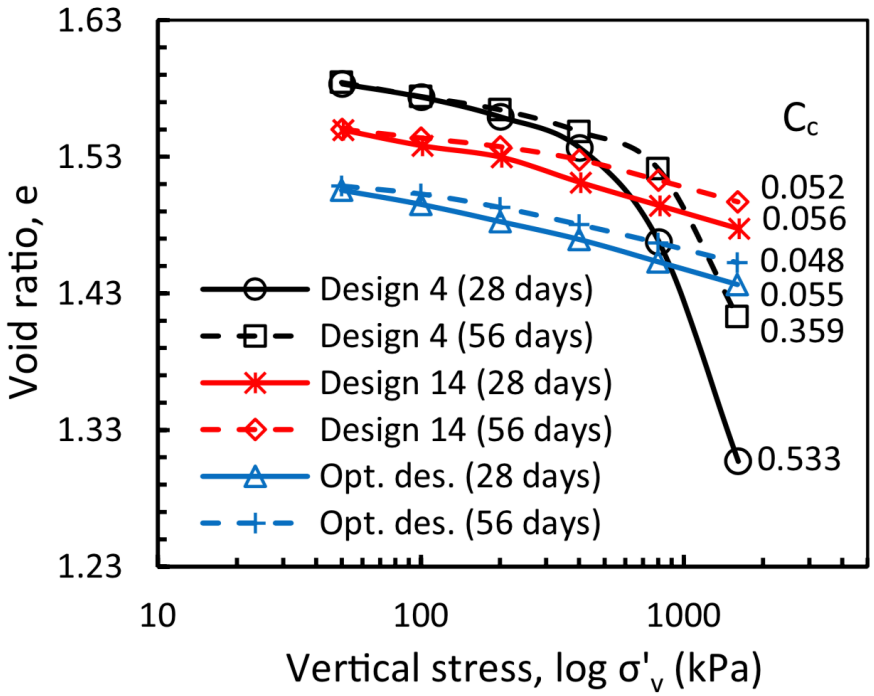


Figure 2.45: Consolidation curve (Yenginar and Olgun, 2024)

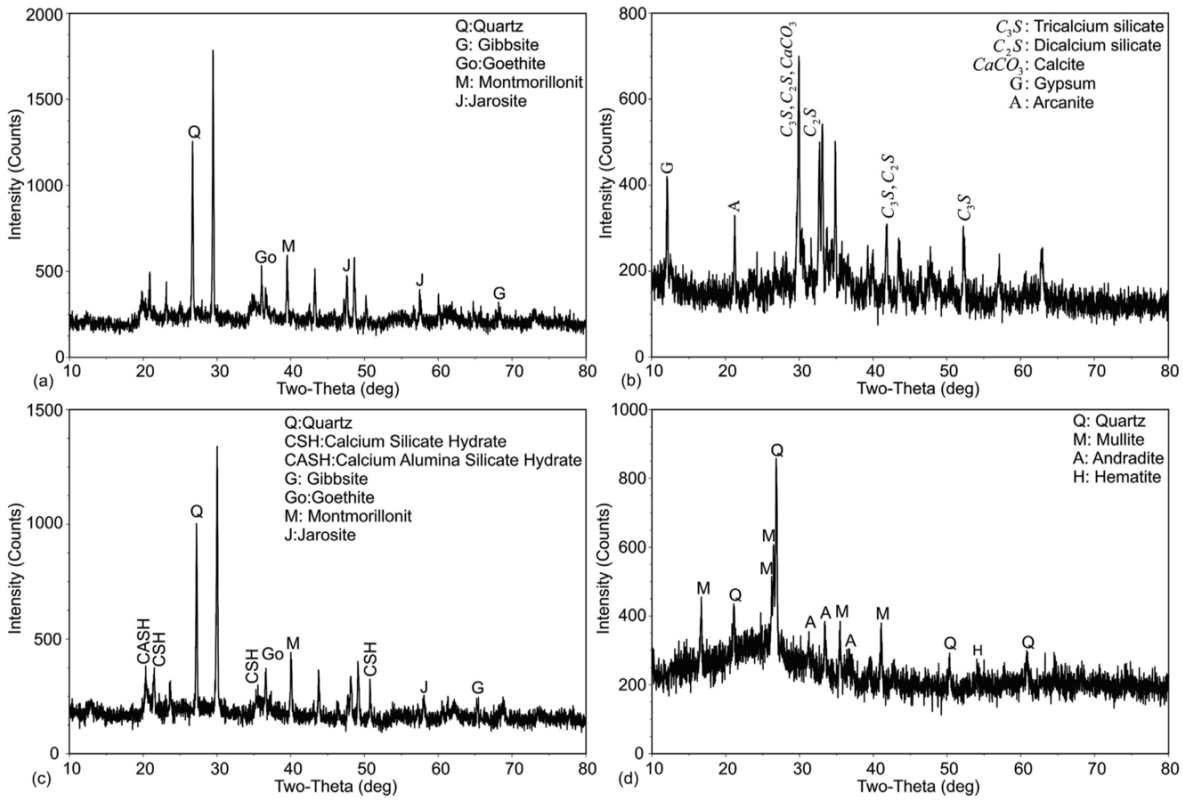


Figure 2.46: XRD Analyses of (a) the Base Soil (< 75 μm), (b) Cement, (c) Soil Treated with Cement and Fly Ash, and (d) Fly Ash (Ekmen et al., 2020)

2.5 CONCLUDING REMARKS

The limited development of mechanised deep mixing in Bangladesh as a method for enhancing the strength of soft soils for civil engineering purposes remains a problem. Most of the few studies that have been done have dealt with cement or lime based binder reinforcement of soft. However, basic research and practical application are still much needed in order to solve local problems. The vast deltaic plains of Bangladesh contain soft and weak clayey soils, which are highly compressible and unsuitable for any kind of construction without ground improvement. The Deep Mixing Method (DMM) may provide such a solution in the case of stabilization of these soils, more so in towns and cities along the coasts. The DMM can improve the soil characteristics and enable the buildings system heavy buildings. Transport networks which are important strategically often pass through areas with marginal soils; the DMM can help mitigate settlements and enhance the bearing pressure. In general, the DMM is more eco-friendly as it incorporates more earthbound components like fly ash and slag than simple cement combined with raw earth. Moreover it is also quite appealing as an approach in sensitive areas because of its limited destruction to the environment in comparison to the rest of the techniques. Due to the high incidence of flooding and tectonic activities in the area, the DMM will also assist in minimizing the risks caused by liquefaction through enhancing the stabilizing and strengthening of soils. Coastal and river delta areas in Bangladesh are prone to erosion and soft soil problems. The DMM can be a very useful technique in such cases for land balancing, sill support and for enhancing the bottom soil quality of the coastal structures.

On the other hand, fly ash is a major waste produced in the coal power plant in Bangladesh. It is very difficult to dispose of this huge amount of fly ash. When fly ash is dumped in open ground, the small particulates of fly ash can pollute air, and water by runoff (Kanchan et al., 2015) and percolation

(Dandautiya et al., 2018). By inhaling and drinking fly ash contaminated air and water, people can have serious respiratory problem and other diseases. If fly ash geo-polymerized by alkali activator can be used as an alternative of cement to strengthen loose soil, the construction of foundation or embankment will be economic as well as the environmental pollution will also be reduced which is a prime criterion of any development project. Hence, the study will be conducted using fly ash as binder material to improve ground strength by deep mixing method with an aim to make eco-friendly, sustainable, and economic foundation.

Chapter 3 : TEST PROGRAMME AND PROCEDURES

3.1 GENERAL

Geopolymer is an organic substance prepared by alkali-activated fly ash, which might improve properties when mixed with soil. Hence, it is used as an alternative to conventional cement stabilization by which a sustainable, economic, and environment-friendly (Zhang et al, 2022) foundation on poor soil could be achieved. A series of laboratory experiments were conducted on different proportions of geopolymer-stabilized soil at different proportions to observe the effects of geopolymer on strength development. In addition, microscopic evaluation and material characterization were conducted to understand the bond formation of geopolymer addition to the parent soil. This chapter focuses on material collection, material properties, sample preparation, and experimental design that are in the subsequent sections. Figure 3.1 shows the overview of the test program involved in the study.

3.2 MATERIALS

Clayey soil samples were used as parent material, aiming to stabilize with the addition of geopolymer. Geopolymer includes fly ash, which is considered as precursor added with an alkali activator, considered a binder. A designed amount of water (FHA manual, 2013) was added to the mixture to prepare the wet mix of the sample with varying proportions of geopolymer under different soil moisture conditions to estimate the increase in strength of soil.

3.2.1 Soil

Soil Sample was collected from the nearby area of Chittagong University of Engineering and Technology (CUET), pointing to the aim of getting soft, cohesive soils, which are found in the typical alluvial deposition. A bulk quantity of samples was taken from approximately 1.5m below the ground level

to get the original deposition of soft soils. The Standard Penetration Test at that level was found to be very low, hence implicitly depicting the consistency as very soft soils. Upon bringing it to the laboratory, its physical and index properties, and chemical composition were determined and shown in Figure 3.2, and Table 3.1 and 3.2.

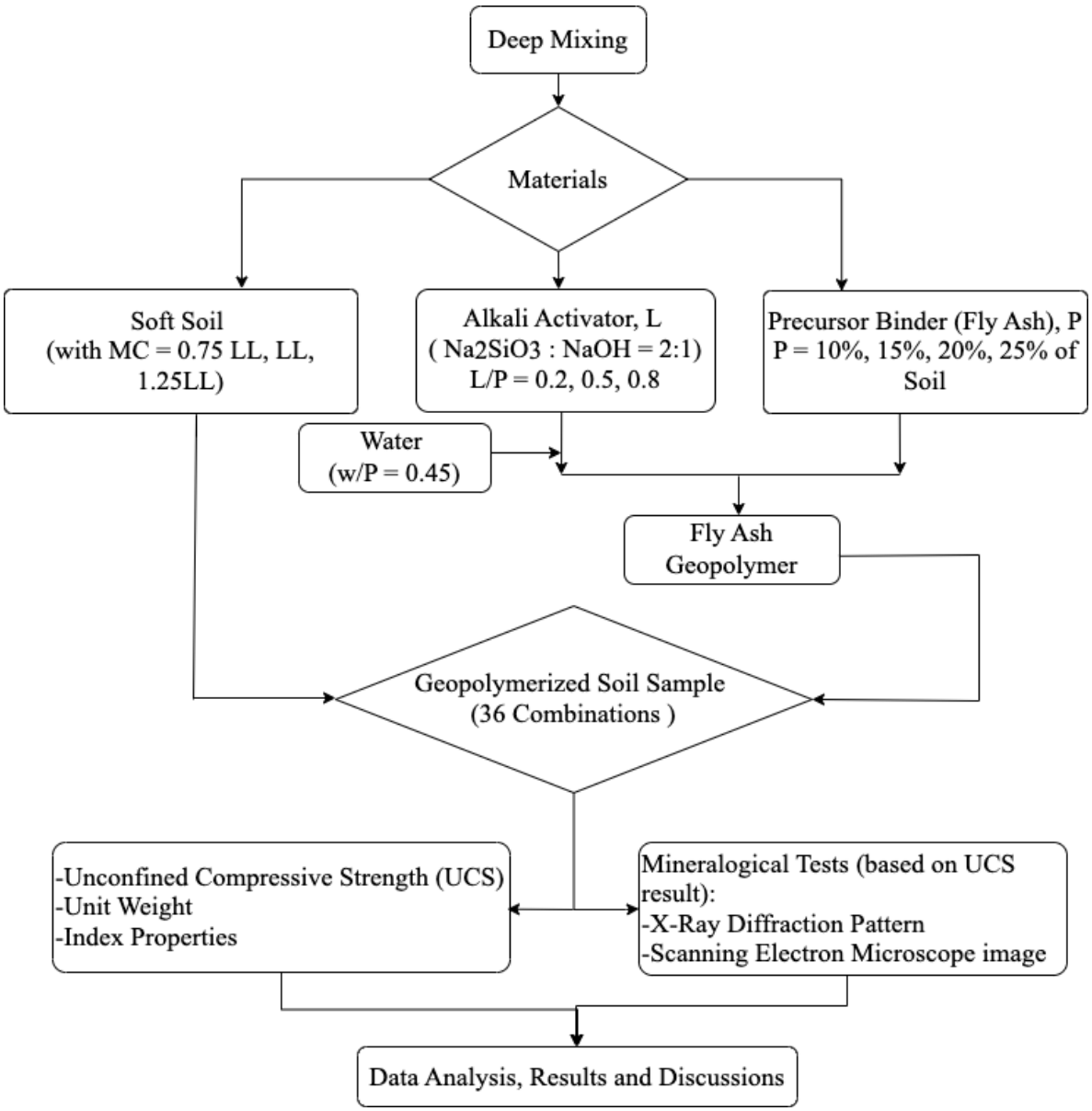


Figure 3.1: Flow Diagram of Test Programme

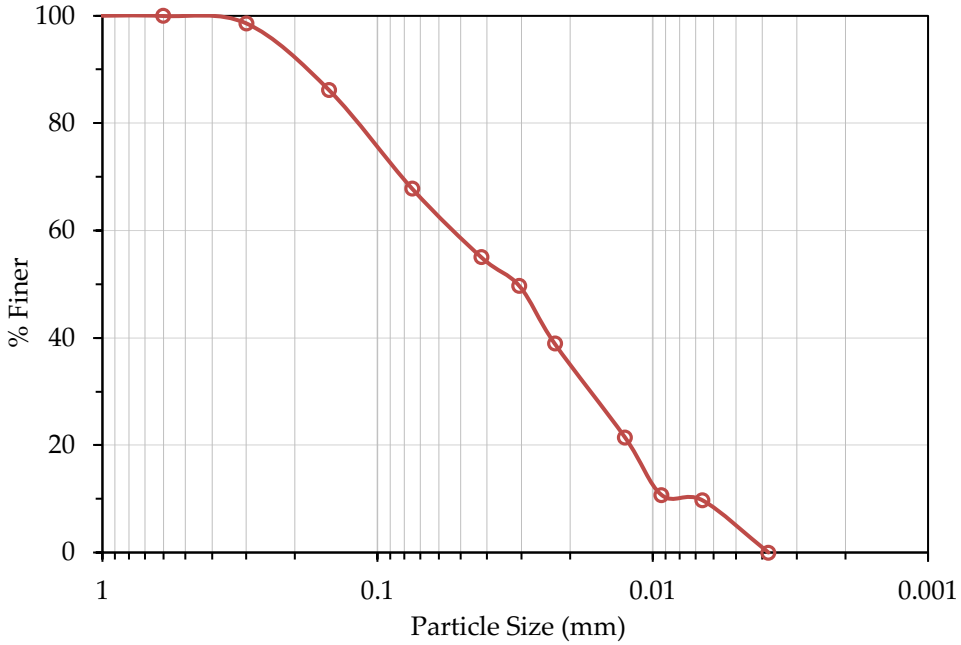


Figure 3.2: Grain Size Distribution Curve for Parent Soil

Table 3.1: Properties of Parent Soil

Parameters		**Value**	**Standard**
Specific Gravity		2.70	ASTM D854-14
Grain Size Distribution	Sand (%)	32.18	ASTM D6913
	Coarse Sand (%)	0	
	Medium Sand (%)	0.82	
	Fine Sand (%)	31.36	
	Fines (%)	67.82	
	Silt (%)	62.82	ASTM D7928
	Clay (%)	5	
	D_{10} (mm)	0.0068	ASTM D2487-11
	D_{30} (mm)	0.017	
	D_{60} (mm)	0.054	
	C_c	0.787	
	C_u	7.94	
Plasticity of Soil	Liquid Limit	30	ASTM D4318-10
	Plastic Limit	23	
	Plasticity Index	7	
Soil Classification		ML (Sandy Silt)	ASTM D2487-11

3.2.2 Precursor Binder

Fly Ash (FA) is a biproduct of coal combustion in coal-fired boilers from where it is driven out with other flue gases. Its major ingredients are SiO_2, Al_2O_3, Cao, Fe_2O_3 etc. The American Society for Testing and Materials (ASTM) classifies fly ash into two types: Class C and Class F (ASTM 618) (Little and Nair, 2009). Class F fly ash has less than 10% calcium oxide (CaO), whereas Class (C) fly ash contains more than 20% calcium (Khale and Chaudhary, 2007). Low calcium fly ash contains more silica and alumina, which may encourage geopolymer synthesis with superior mechanical qualities (Hardjito and Rangan, 2005). As a result, Class F fly ash is preferred for geopolymer production over Class C fly ash. Class F fly ash was used as precursor binder which varies from 10 to 25% of dry soil in the current study and some alkali activators are introduced into the soil-fly ash mix to increase the cementing properties. Typical grain size analysis of the fly ash sample is shown in Figure 3.3. Chemical composition of fly ash is shown in Table 3.2 the images of fly ash (both in normal and microscopic scale) are shown in Figure 3.4.

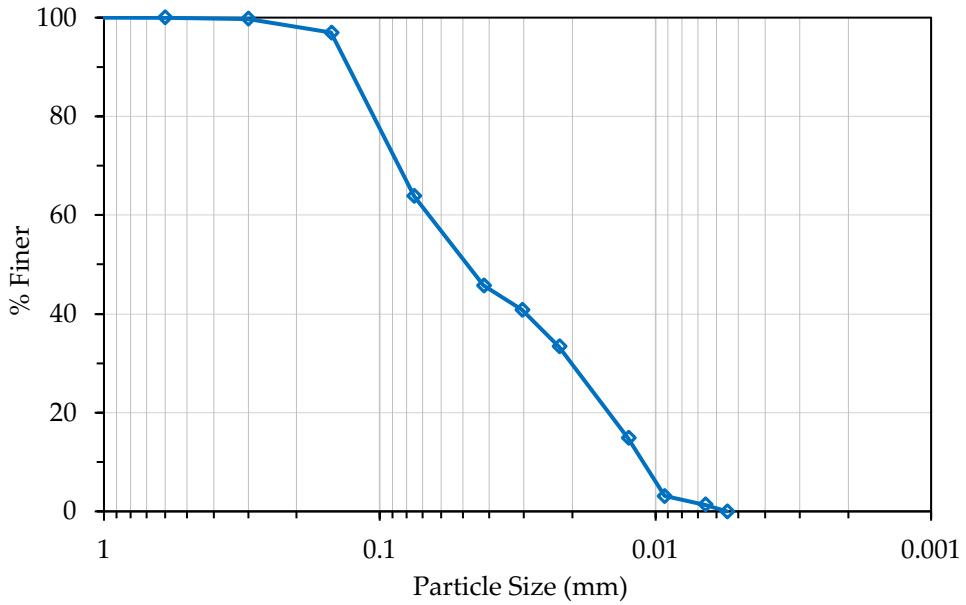
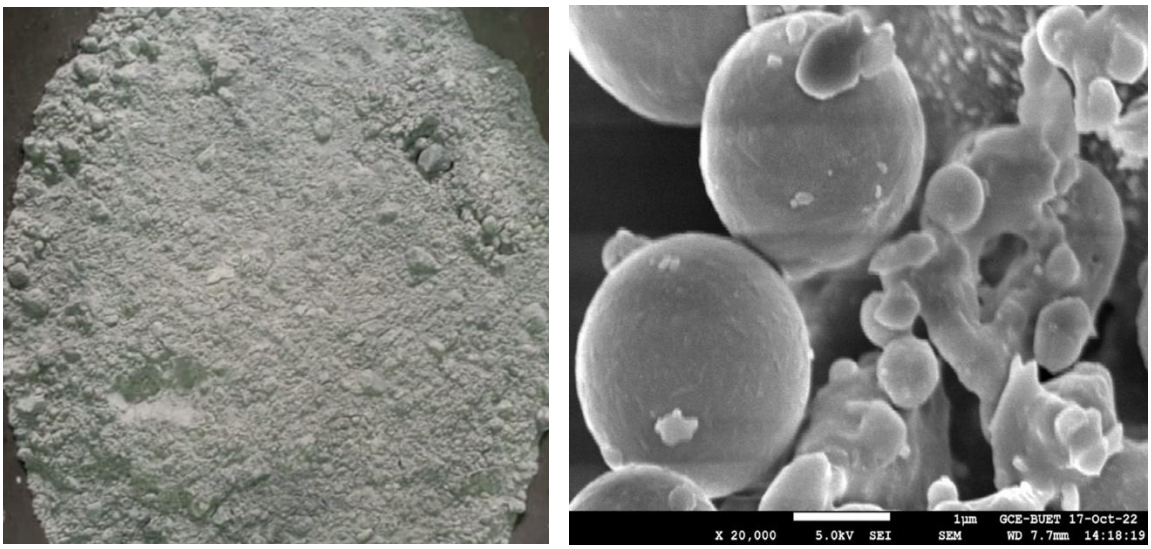


Figure 3.3: Grain Size Distribution of Fly Ash

Table 3.2: Chemical Composition of Parent Soil and Fly Ash

Elements	Elemental Concentration (mg/kg)		Oxides	Oxide Concentration, %	
	Soil	Fly Ash		Soil	Fly Ash
Ti	4052	7462	**SiO_2**	64.5737	62.9881
Cr	<5.2	<5.2	**Al_2O_3**	13.5577	22.4790
Mn	471.772	439.236	**Fe_2O_3**	8.7541	5.2066
Fe	58450	37340	**TiO_2**	1.3325	2.7280
Co	<0.03	<0.03	**K_2O**	4.5745	2.4903
Ni	<0.19	<0.19	**CaO**	0.6262	1.6078
Cu	<0.95	<0.95	**P_2O_5**	0.1357	1.0702
Zn	91.669	121.670	**MgO**	2.3799	0.6634
As	<4.17	<4.17	**SO_3**	2.9261	0.2817
Se	<0.18	<0.18	**BaO**	----	0.1320
Rb	97.449	71.558	**Na_2O**	0.9247	0.1156
Sr	80.893	217.278	**Cr_2O_3**	0.0322	0.0583
Y	38.445	54.379	**MnO**	0.0801	0.0558
Zr	204.913	358.646	**SrO**	0.0174	0.0454
Pb	<1.35	<1.35	**ZrO_2**	0.0396	0.0433
--	--	--	**Rb_2O**	0.0250	0.0187
--	--	--	**ZnO**	0.0205	0.0158

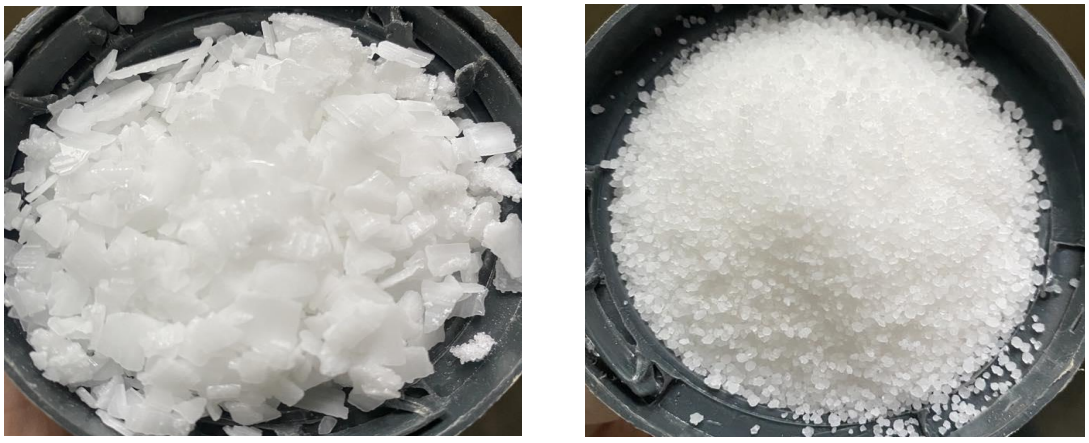


(a) (b)

Figure 3.4: (a) Fly Ash; (b) Scanning Electron Microscope (SEM) Image of Fly Ash

3.2.3 Additives

The most common alkaline activator used in geopolymerization is a solution of sodium hydroxide (NaOH) or potassium hydroxide (KOH) with sodium or potassium silicate (Hardjito and Rangan, 2005). Sodium Hydroxide (NaOH) and Sodium Silicate (Na_2SiO_3) pellets (Figure 3.5) were used in the current study since these are the most powerful activators during geopolymer synthesis (Siyal et al., 2024). These activators strongly promote the dissolution of aluminosilicate precursors, enhance the geopolymerization, and lead to a more solid and durable matrix. As an alkaline activator, sodium silicate solution was added to the sodium hydroxide solution to improve the interaction between the source material and the solution (Xu and Van Deventer, 2000). In the presence of NaOH in the activating solution, the process accelerates and the gel becomes less smooth (Duchesne et al., 2010) The most effective alkali activator combination as suggested by Bakri et al. (2012) is 2:1 to 2.5:1 for Na_2SiO_3:NaOH for the activation process of binders, and the ratio of Na_2SiO_3: NaOH was taken as 2:1 in the current study. Alkali activator to binder ratio of 0.45 to 0.6 was studied with where 0.55 was concluded as the optimum dose (Adam et al., 2019). To observe the effect of alkali activator with wider range of activator to binder ratio (L/P), the ratio has been taken as 0.2, 0.5 and 0.8 in various combinations in the current study.



(a) (b)

Figure 3.5: (a) Sodium Hydroxide (NaOH) and (b) Sodium Silicate (Na_2SiO_3) pellets

3.2.4 Water

To prepare the sample, normal drinking water was used with the soil-geopolymer mix. The water quality is shown in Table 3.3.

Table 3.3. Water Quality Parameters

Parameters	**Unit**	**Concentration present**	**Bangladesh Standards for Drinking Water** (The Environment Conservation Rules, 1997)
Salinity	mg/L	23.5	No Guideline
pH	- - -	7.0	6.5 – 8.5
Colour	PCU	15.0	15
Alkalinity	mg/L (as $CaCO_3$)	40.0	No Guideline
Chloride	mg/L	13.0	150 – 600 (1000 for Coastal Areas)
TDS	mg/L	110.0	1000
SS	mg/L	20.0	10
Turbidity	NTU	7.5	10
Hardness	mg/L (as $CaCO_3$)	100.0	200 – 500
CO_2	mg/L	5.5	No Guideline
Iron	mg/L	1.0	0.3 – 1.0
Manganese	mg/L	0.020	0.1
Odour	- - -	Odourless	Odourless
Total Coliform	N/100mL	0.0	0
Fecal Coliform	N/100mL	0.0	0
Sulphate	mg/L	1.0	400
Nitrate	mg/L	0.1	10
Arsenic	mg/L	0.0	0.05

3.3 FLY ASH GEOPOLYMERIZATION PROCESS

When fly ash is added to an alkaline solution, the Al and Si dissolve (Fernández-Jiménez et al., 2005). Then the higher molecules condense into the gel (polymerization and nucleation), and alkali assault opens the spheres, exposing little spheres on the interior that will also dissolve until the spheres are nearly completely dissolved with the creation of reaction products within and outside the sphere (Figures 3.6 and 3.7). The activation of fly ash is a

process that may be called a zeolitization in which the final phase does not occur because the experimental circumstances lead to extremely fast dissolving and condensation reactions but a lesser one when hardening takes place (Palomo et al., 2004).

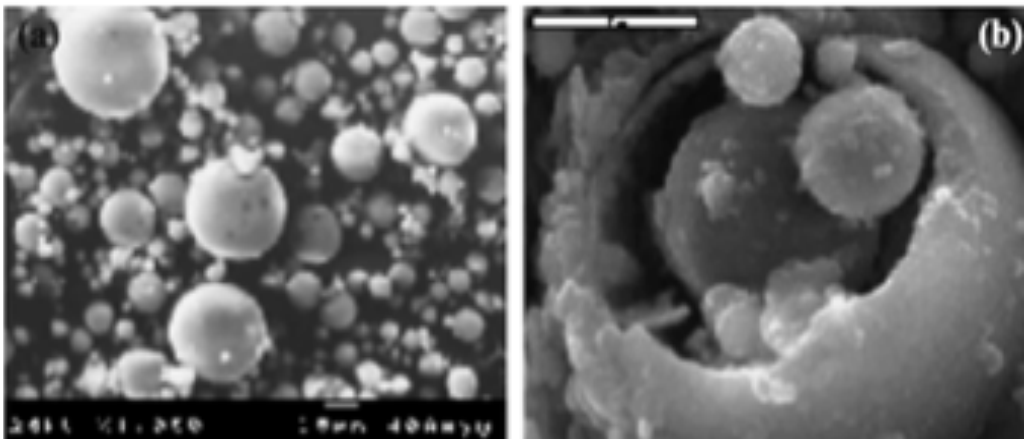


Figure 3.6: Broken spheres after activated with sodium hydroxide (Pacheco-Torgal et al., 2008)

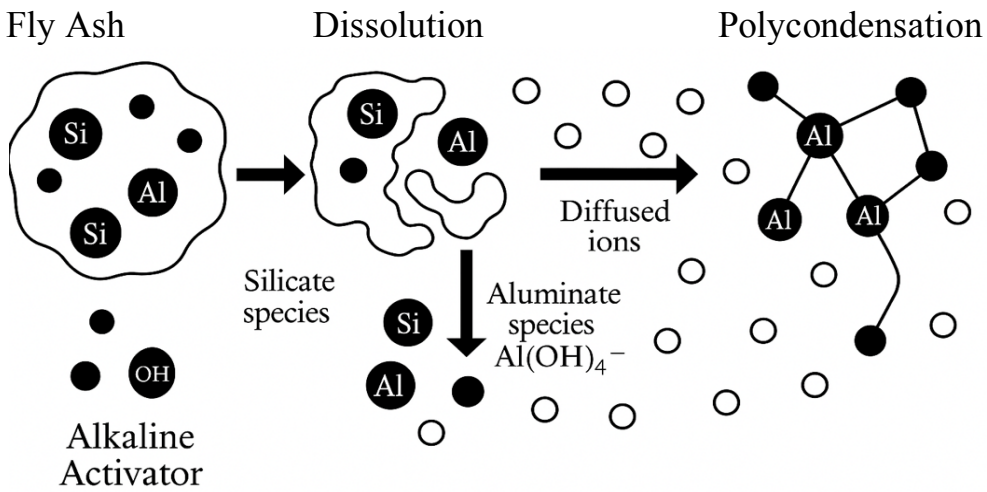


Figure 3.7: Alkali Activation Process of Fly Ash

With an alkaline aluminosilicate as the main reaction product, the activation of FA is a process very different from Portland cement hydration but comparable to the chemical principles involved in the creation of many different kinds of zeolites (Criado et al., 2005). Alkali cations balance the negative electric charge and Al3+ replaces Si4+ in polymeric chains, resulting in the tetrahedral

coordination of silica and aluminium. The aluminosilicate species decompose during the first nucleation phase of the alkali attack on the aluminosilicate material. The nuclei start crystallising at a critical size but that is a gradual process and it may take quite a long time to be completed. The entire process of fly ash geo-polimerization was described using flow chart in Figure 3.8.

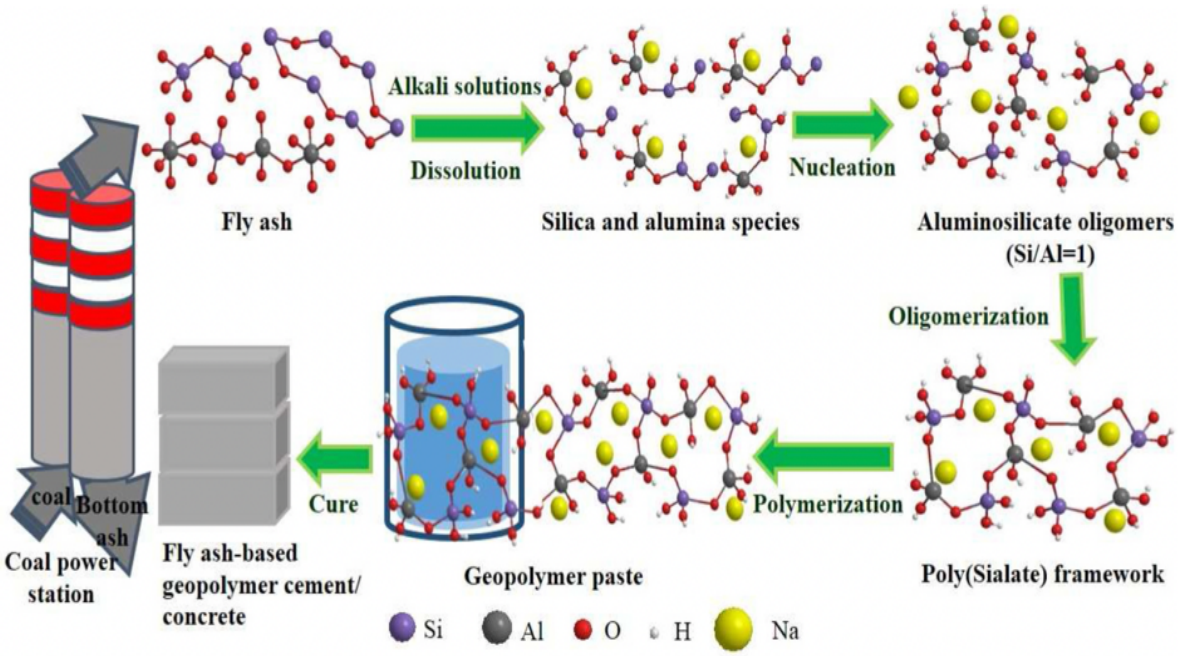


Figure 3.8: Geopolymerization Process (Singh, 2018)

3.4 EXPERIMENTAL PROGRAMME

As stated in the preceding section, parent soils, fly ash, and alkali activators were stored in cool and dry places. Soil-geopolymer samples were prepared in proportions as described in Figure 3.1 and Table 3.4 for necessary testing.

3.4.1 Material Proportioning

Soils were treated with 10-25% fly ash of dry weight of parent soil which acts as a precursor, as evidenced by previous studies, where it shows the strength decrement after 20-25% of fly ash addition in most of the improvement options ((Debanath, 2019; Abdullah et al., 2019; Ekmen et al., 2020,) In aid to enhancing the binding, an alkali-activator, i.e., a 2:1 mixture of Sodium Silicate

(Na_2SiO_3) and Sodium Hydroxide (NaOH), was used with each combination. To clutch the wide variation of the scenario, different combinations of activator and precursor were considered in this study. Based on the literature review and practical consideration, three different activator-to-precursor ratios, 0.2, 0.5, and 0.8, were considered in the preparation of soil samples. In most practical instances, water content plays a dominant role in strength development; hence, the effects of water on the strength development of geopolymer-treated samples need to be explicitly evaluated for effective use in deep mixing methods. Samples were prepared at three different water contents with respect to the liquid limit of the soils to understand the response on both the dry side (0.75LL) and wet side (1.25LL) of the liquid limit. Due to the slow geo-polymerization process of fly ash geopolymer (Singh and Middendorf, 2020), the samples were tested at longer curing ages: 14 days, 28 days, and 56 days to observe the effect of the curing period on strength development. The material proportioning is described in Table 3.4.

Table 3.4. Material Proportioning for Sampling

Sample Designation	**Dry Soil (%)**	**Binder (Fly Ash), P (% of Dry Soil)**	**Alkali Activator, L (Na_2SiO_3:NaOH=2:1) (% of Dry Soil)**				**Water in Geopolymer (w/P=0.45) (% of Dry Soil)**
			L/P	**Total (%)**	**Na_2SiO_3 (%)**	**NaOH (%)**	
F10L20	100	10	0.2	2	1.33	0.67	4.5
F15L20	100	15		3	2.00	1.00	6.75
F20L20	100	20		4	2.67	1.33	9.0
F25L20	100	25		5	3.33	1.67	11.25
F10L50	100	10	0.5	5	3.33	1.67	4.5
F15L50	100	15		7.5	5.00	2.50	6.75
F20L50	100	20		10	6.67	3.33	9.0
F25L50	100	25		12.5	8.33	4.17	11.25
F10L80	100	10	0.8	8	5.33	2.67	4.5
F15L80	100	15		12	8.00	4.00	6.75
F20L80	100	20		16	10.67	5.33	9.0
F25L80	100	25		20	13.33	6.67	11.25

3.4.2 Method of Sample Preparation

Fly Ash was mixed with soil as percentages of dry soil mass from 10% to 25% with an interval of 5% to act as binder. All these combinations were conducted for each variation of water content, 75%, 100%, and 125% of Liquid Limit. Alkali activators used 20%, 50% and 80% of precursor to increase cementation to the mix. Among the two methods of Deep Mixing (i.e. Dry method when soil having moisture content greater than 60% and Wet method for moisture content less than 60%), the Wet method was used since the water content of the soil was less than 60% % (Han, 2015). A water-to-binder ratio of 0.45 was used to prepare the geopolymer slurry so that it can meet the pumping capability (FHA Manual, 2013).

First, the chemical additives (NaOH and Na_2SiO_3) were dissolved in the water and rested for 5-10 minutes to reduce heat as the chemical reaction takes place in an exothermic reaction. The precursor binder was then mixed with the solution using a precursor mixer to form a slurry (Figure 3.9.a). On the other hand, dry soil was mixed with the desired water content (i.e., 75%, 100%, and 125% of liquid limit) in another mixer. After that, the two mixes were combined and mixed for 10 minutes in an automated mixer to get a homogenous paste (Figure 3.9.b). The mixed paste was poured into previously prepared PVC tube moulds with an internal diameter of 37.5 mm and a height of 75 mm.

The samples were made in three layers and protruded gently without compaction with thin rods to remove air pockets so that the actual condition of the deep mix column in the field prevails in the sample. The top surface of the specimen was leveled with screeding so that the load distribution during the experiment become uniform. Three identical samples were prepared for each combination. The moulds were sealed and wrapped with polythene to make them airtight (Figure 3.10) and kept in a desiccator and water bath to ensure

desirable humidity and temperature (Figure 3.11). Samples were prepared according to the Federal Highway Administration Manual (FHA Manual, 2013) to conform to the practical scenario for their possible use in reality.



(a) (b)

Figure 3.9: (a) Geopolymer Slurry; (b) Soil-Geopolymer Mix

3.4.3 Test Procedures

Samples were removed from the mold just before the test, and Unconfined Compressive Strength (UCS) was tested by applying compressive load in an automated machine, maintaining a strain rate of 1 to 1.5 mm per minute for all curing ages, i.e., 14days, 28days and 56 days. For each combination, three samples were tested, and an average was taken as corresponding compressive strength, confirming that the variation of results in each sample shall not exceed 10%. In case of substantial variation, samples were prepared again and cured as per experimental design to determine the compressive strength. The samples having a height to diameter ratio lower than two were corrected by multiplying with the correction factor according to ASTM C-42 as prescribed in the Federal Highway Administration manual (FHA Manual, 2013). Figure 3.12 shows the experimental condition of the samples.



Figure 3.10: Sealed Sample in Mould



(a) (b)

Figure 3.11: Samples in (a) Desiccator and (b) Water Bath for curing

Later, selected samples having significant increase in Unconfined Compressive Strength (UCS) were taken for mineralogical analysis i.e., X-ray Diffraction (XRD) Pattern and Scanning Electron Microscope (SEM) Image to observe the microstructural bond formation due to geo-polymerization.

(a)



(b)



(c)



Figure 3.12: (a) Cured Sample Prior to Test; (b) Sample Being Tested in Unconfined Compressive Strength Test Machine; (c) Broken Samples After Test

Chapter 4 : RESULTS AND DISCUSSIONS

4.1 GENERAL

A detailed experimental program was conducted to study the effect of geopolymer on the development of strength of the Deep Mix Column. Samples were prepared for each case, as delineated in the previous chapter and standard curing procedure was taken for the entire experimental program. Mostly, Unconfined Compressive Strength tests were conducted on each category to estimate the development of strength of geopolymer treated soils. In addition, samples were tested to estimate the physical and index properties (liquid limit, plastic limit, plasticity index) of treated soils in all cases, the addition of geopolymer shows higher strength and acceptable physical properties that implicitly justify the effectiveness of geopolymer in Deep Mix Column. Microscopic tests and material characterization were conducted to understand the bond formation of treated soils. Predictions models have also been developed. The performed tests are summarized in the table 4.1.The details are discussed in this chapter in subsequent sections.

Table 4.1: Summary of Analysis on Deep Mixing Method

Name of the Analysis	**Test(s) Performed**
Strength	Unconfined Compressive Strength (UCS)
Physical Properties	Unit Weight
Index Properties	Liquid Limit, Plastic Limit, Plasticity Index
Mineralogy	Scanning Electron Microscopy (SEM), X-ray Diffraction Pattern
Prediction Model	Statistical Model

4.2 PROPERTIES OF GEOPOLYMER TREATED SOILS

To improve the strength of soft soils, fly ash based geopolymer was added to the parent soils with the proportion of 10 to 25% by weight of soils. The Unconfined Compressive Strength (UCS) test was conducted in an automated machine at an axial strain rate of 1 to 1.5 mm/min per minute as per ASTM D 2166. The effects of binder (fly ash), water and activator to binder ratio (L/P) at three different curing ages: 14 days, 28 days, and 56 days have been discussed in this section.

4.2.1 Effect of Precursor Binder on Unconfined Compressive Strength

The Unconfined Compressive Strength at various proportion of materials (i.e. binder, additive, soil moisture) has been tabulated in Table 4.2. Figure 4.1 shows the effects of precursor on Unconfined Compressive Strength (UCS) for three Activator to Binder ratio (L/P) where the water content was chosen at the liquid limit. Strength has been found to be increasing with the increase in precursor binder (fly ash) content with a maximum strength at maximum binder content of 25% at L/P is 0.2. The rate of increase is approximately linear with precursor binder content (fly ash), whereas a slight increase in rate is observed when precursor content increases from 15% to 20%.

A similar increasing trend was seen when the L/P ratio was 0.5, and peak strength was found for maximum precursor content. A slight reverse result was found in strength between 10% and 15% fly ash content at 14 days of curing age. Soil mix having 15% fly ash has shown lower strength than 10% fly ash. It might be caused by more air voids present in the soil mix. The increasing rate in strength followed almost a linear pattern from 15 to 25% binder. For 28-day and 56-day strength, the UCS has always been increasing with binder content. The initial increasing rate in strength is somewhat lower when the fly ash content increases from 10% to 15% for 28-day strength, whereas strength at 15% to 25% binder (fly ash) content has shown a close to constant rate.

Table 4.2: Variation of Unconfined Compressive Strength at different proportion of materials

Sample ID	Moisture Content/ Liquid Limit ratio	Binder, P (%)	Additive / Binder, (L/P)	Unconfined Compressive Strength, UCS (KPa) at		
				14 days	28 days	56 days
F10L20	0.75	10	0.20	170	175	240
F10L50			0.50	317	355	361
F10L80			0.80	268	468	726
F15L20		15	0.20	158	194	229
F15L50			0.50	338	615	747
F15L80			0.80	465	679	695
F20L20		20	0.20	307	349	353
F20L50			0.50	691	1059	1099
F20L80			0.80	647	967	1153
F25L20		25	0.20	335	400	467
F25L50			0.50	1002	1148	1400
F25L80			0.80	454	926	1030
F10L20	1.0	10	0.20	54	66	68
F10L50			0.50	178	265	286
F10L80			0.80	135	319	467
F15L20		15	0.20	78	93	95
F15L50			0.50	158	366	488
F15L80			0.80	384	583	652
F20L20		20	0.20	134	168	199
F20L50			0.50	456	678	852
F20L80			0.80	540	642	822
F25L20		25	0.20	213	229	246
F25L50			0.50	904	1082	1143
F25L80			0.80	487	791	823
F10L20	1.25	10	0.20	23	25	27
F10L50			0.50	62	97	115
F10L80			0.80	72	140	258
F15L20		15	0.20	32	34	44
F15L50			0.50	172	259	335
F15L80			0.80	162	242	293
F20L20		20	0.20	72	82	95
F20L50			0.50	323	476	612
F20L80			0.80	191	285	387
F25L20		25	0.20	84	91	92
F25L50			0.50	346	370	426
F25L80			0.80	461	784	822

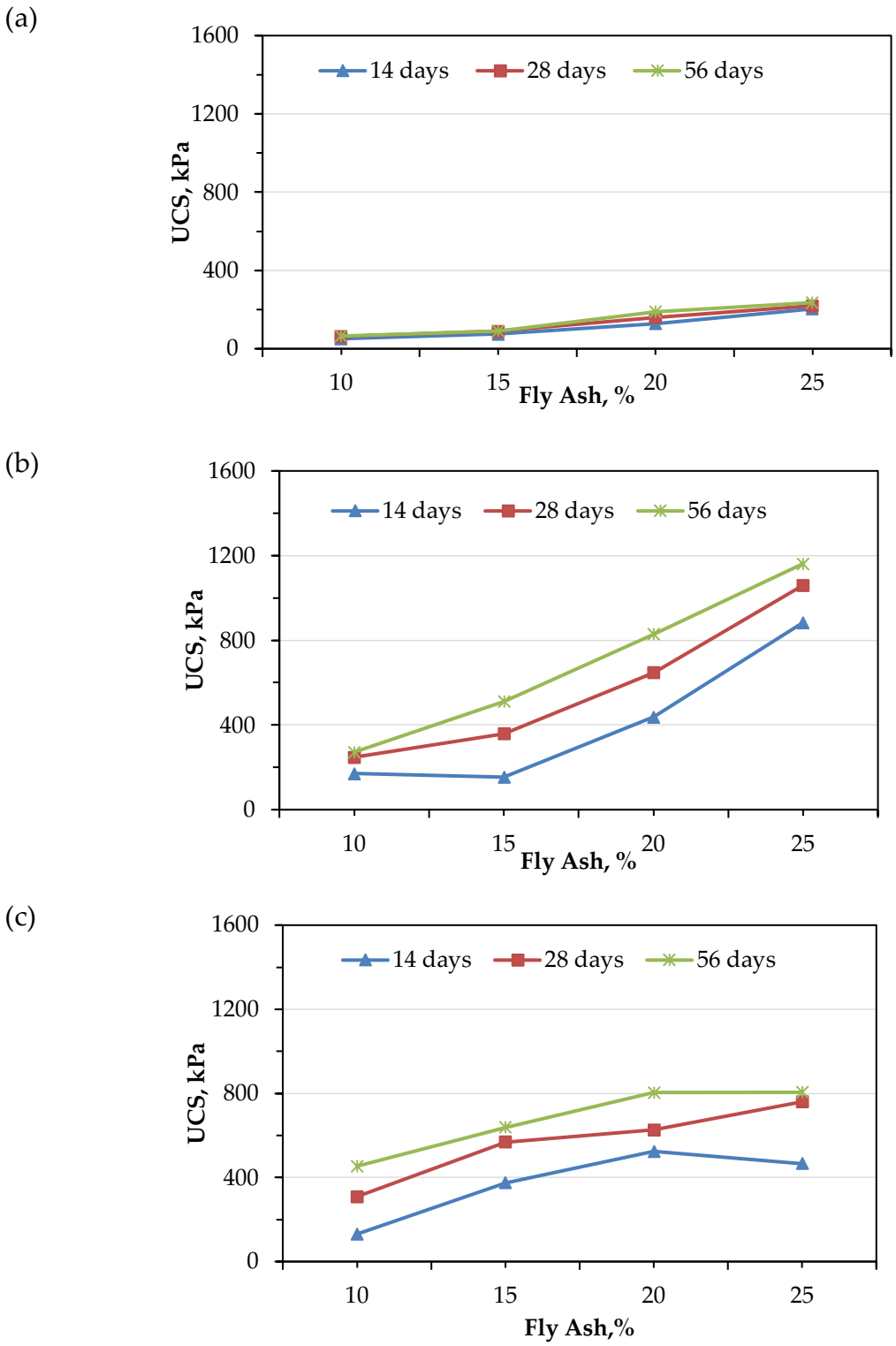


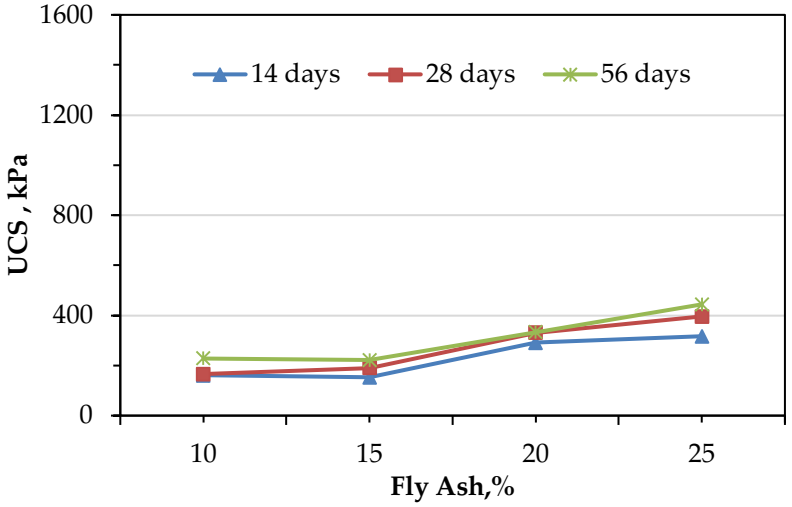
Figure 4.1: Variation of Unconfined Compressive Strength (UCS) with Fly Ash Content at Liquid Limit and Activator to Binder Ratio (L/P) of (a) 0.2, (b) 0.5, (c) 0.8

With the increase in L/P ratio to 0.8, the strength follows the pattern of increasing in lower binder content. The strength tends to decrease from 20% to 25% binder for 14 days and remains unchanged for 56 days strength, whereas

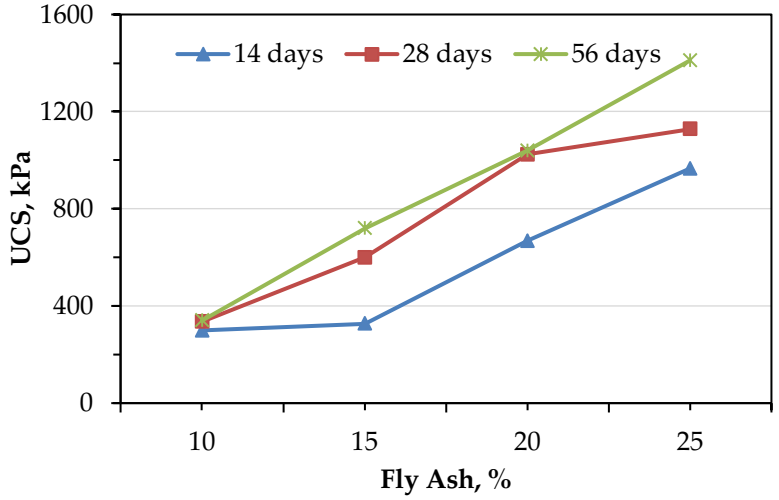
an increasing pattern has been observed for 28 days strength. When different additive to the precursor (FA) ratios (L/P) are compared, strength generally shows an increasing trend with increasing fly ash contents, though in some cases, strength decreases beyond 20% fly ash contents. Similar trends are generally seen in fly ash -treated improvement cases.

However, it is interesting that even though additives are added to enhance the bonding, the strength development was not found to be significant after saturation; for this study, it was found at an L/P ratio of 0.5. The unchanged or decreasing strength at higher L/P might be an indication of excess geopolymer present in the soil mix, which has not got enough ions from the soil to react with. Too much fly ash and alkali activator might decrease UCS as a result of high porosity, incomplete geo-polymerization, and excessive unreacted particles. High alkali disrupts gel formation, and excess fly ash dilutes the strength-providing geopolymer gel, which consequently affects load transfer and structural integrity (Turan et al., 2022). When the soil has a moisture content less than the liquid limit, a similar pattern of strength development was observed. The pattern is illustrated in Figure. 4.2. Strength tends to increase with the increasing precursor content and the highest strength was observed at the highest FA content. At L/P ratio =0.5, the strength rises linearly with a slight variation of 14-day strength having 10 to 15% fly ash, and 28-day strength having 20 to 25% FA. The increasing rate of strength is slightly lower in these two cases. Lack of geopolymer and/or water and the presence of a void might be the possible reasons. The scattered variation was seen in the L/P ratio of 0.8, where maximum precursor content did not portray the highest strength. Strength reaches its optimum level at 20% precursor content, and further increase causes a fall in UCS. A decrease in 56-day strength at 15% binder compared to 10% has been observed in this case. The presence of tiny air pockets or improper mixing might result in this fall. When soil having moisture

(a)



(b)



(c)

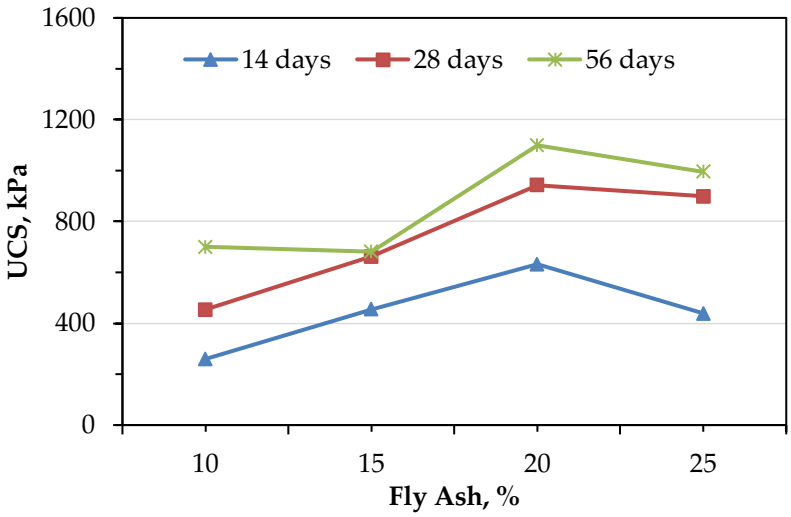
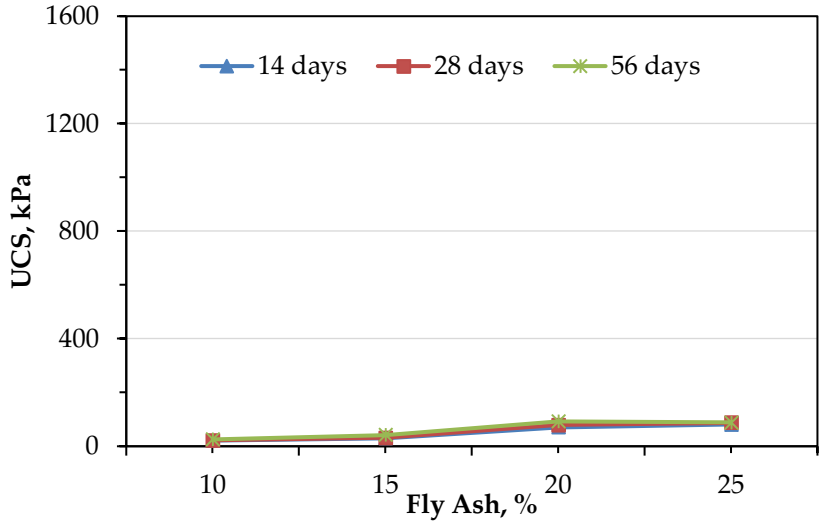
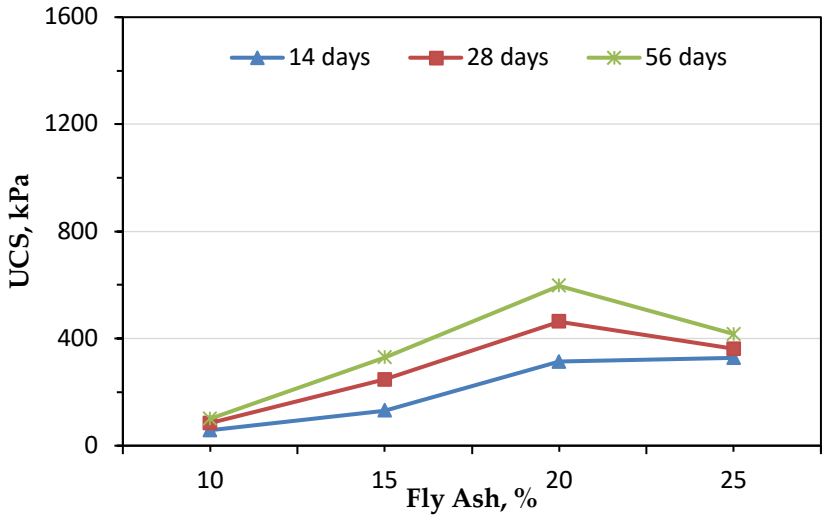


Figure 4.2: Variation of Unconfined Compressive Strength (UCS) with Fly Ash Content at 0.75xLiquid Limit and Activator to Binder Ratio (L/P) of (a) 0.2, (b) 0.5, (c) 0.8

(a)



(b)



(c)

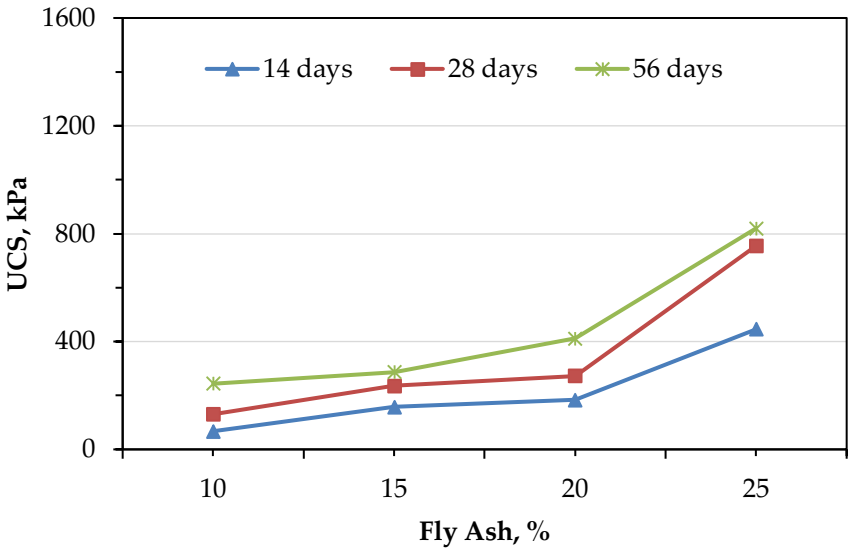


Figure 4.3: Variation of Unconfined Compressive Strength (UCS) with Fly Ash Content at 1.25xLiquid Limit and Activator to Binder Ratio (L/P) of (a) 0.2, (b) 0.5, (c) 0.8

moisture content greater than the liquid limit gets mixed with geopolymer, it shows a different pattern of strength development. A very little strength gain was observed when treated with the minimum proportion of alkali additives (i.e., L/P=0.2), as shown in Figure. 4.3. A significant amount of strength gain with almost a linear pattern has been observed when treated with a larger amount of additives (i.e., L/P=0.5). The UCS tends to fall after reaching an optimum level at a binder content of 20%, and a further rise in precursor causes decay in strength. The peak strength was developed at the maximum fly ash content of 25% when activated with additives to precursor ratio of 0.8. The rate of strength gain is almost linear up to 20% precursor and a sudden rise of rate was observed after that.

4.2.2 Effects of Water on Unconfined Compressive Strength

Water might have effect on the development of strength with geopolymer in the deep mixing method. It reacts with the precursor binder and soil mass to form complex compounds that strengthen the soil mix. However, excessive water present in the soil makes the soil softer and less strong. The reaction with water takes place in two stages. Firstly, the water of 45% of binder weight (w/P = 0.45) was added to fly ash and alkali activators to form a geopolymer. After that, the geopolymer was mixed with the wet soil where it gets more water to react with. The total mixing water has been taken as the summation of added water to the geopolymer and the water present in the soil. The relation between Unconfined Compressive Strength (UCS) and the total mixing water-to-binder ratio (Figure. 4.4, 4.5 and 4.6) shows an exponential decay function, similar to the UCS vs. water-to-cement ratio in conventional ground improvement with cement treatment (Figure. 4.7).

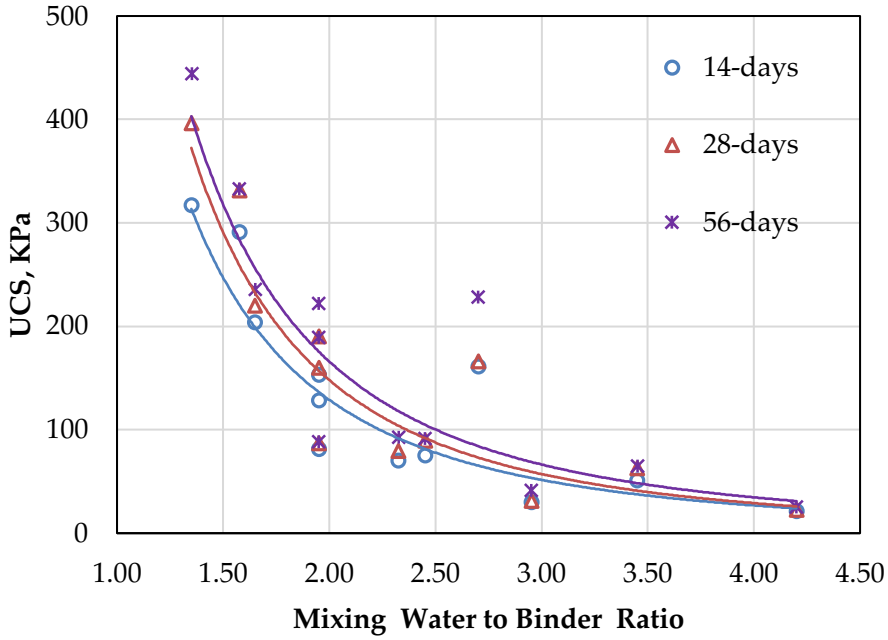


Figure 4.4: Variation of Unconfined Compressive Strength (UCS) with Water at Activator to Binder Ratio (L/P) = 0.2

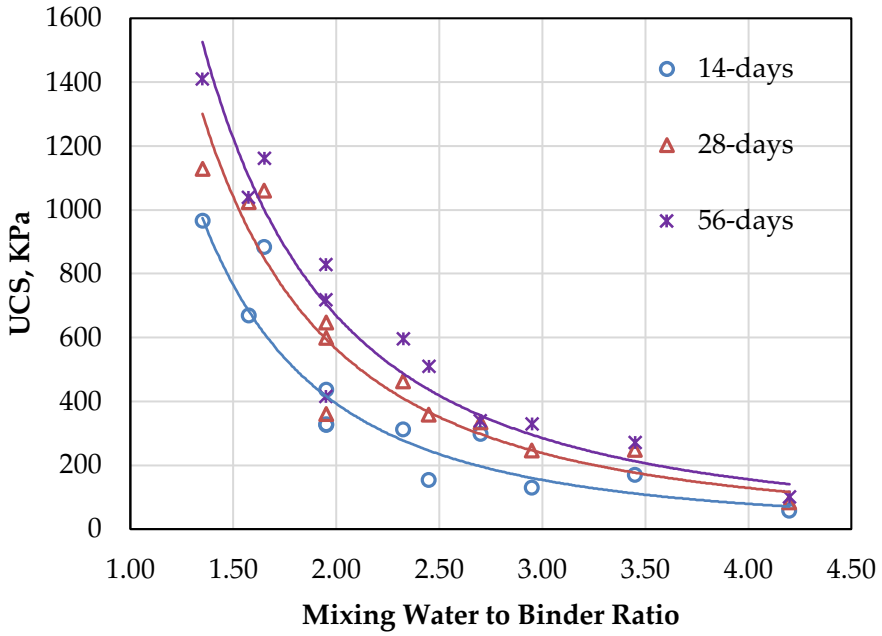


Figure 4.5: Variation of Unconfined Compressive Strength (UCS) with Water at Activator to Binder Ratio (L/P) = 0.5

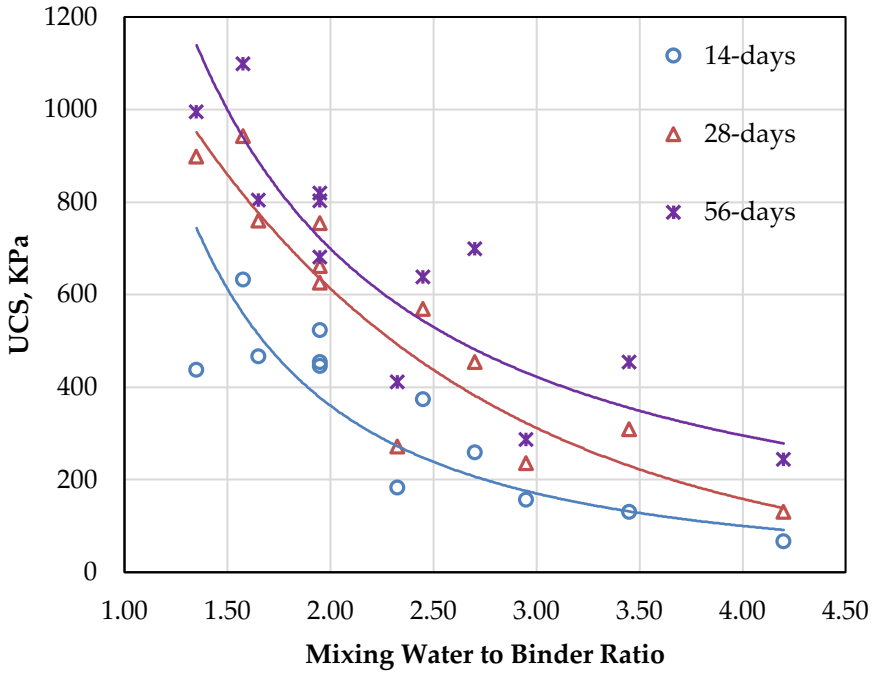


Figure 4.6: Variation of Unconfined Compressive Strength (UCS) with Water at Activator to Binder Ratio (L/P) = 0.8

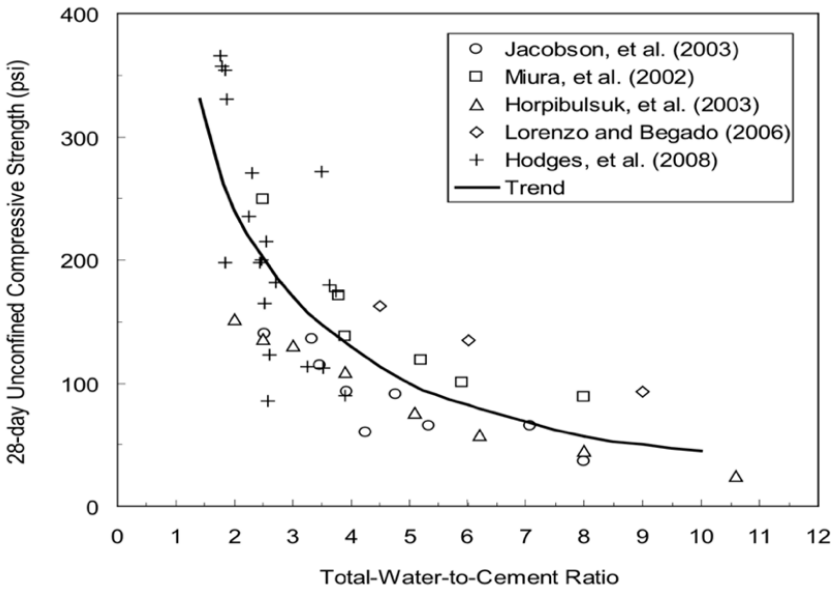


Figure 4.7: Unconfined Compressive Strength (psi) vs. Water to Cement Ratio in Different Studies (FHA Manual, 2013)

The Unconfined Compressive Strength (UCS) vs total mixing water to binder (fly ash) ratio curve is very useful in designing durable, efficient, and cost-effective mixes for a sustainable ground improvement technique. It helps in finding the optimal value of the water to fly ash ratio at which maximum compressive strength for a given mix is obtained. When the ratio is too low, the

concrete becomes inadequately workable; on the other hand, with a higher ratio, there is an increase in the porosity during the hardened. state, reducing strength.

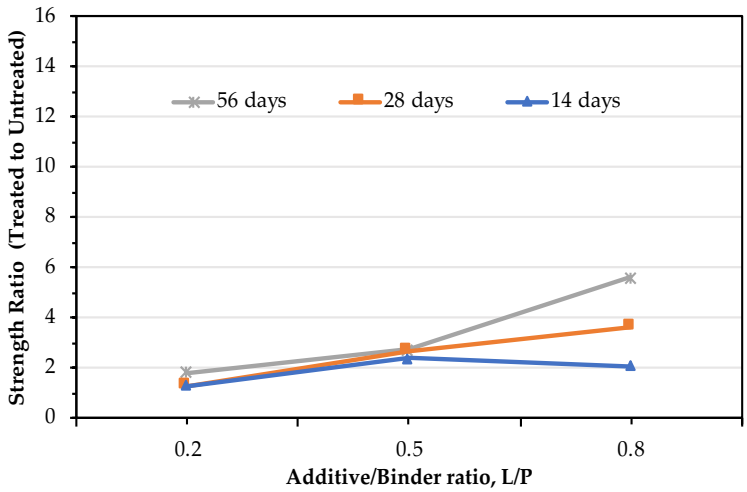
A balance of strength versus workability is crucial for Mix design targeting specific structural needs. The cure also details strength behavior on a deeper level. Exceeding the optimum dose of water leads to exponential decay in strength due to higher porosity and weaker hydration bonds. On the other hand, insufficient water results in incomplete hydration and reduced strength. Such understandings are fundamental to engineers and contractors in ensuring that the engineering properties of deep mixed soil meet the design expectations.

4.2.3 Effects of Additives on Unconfined Compressive Strength

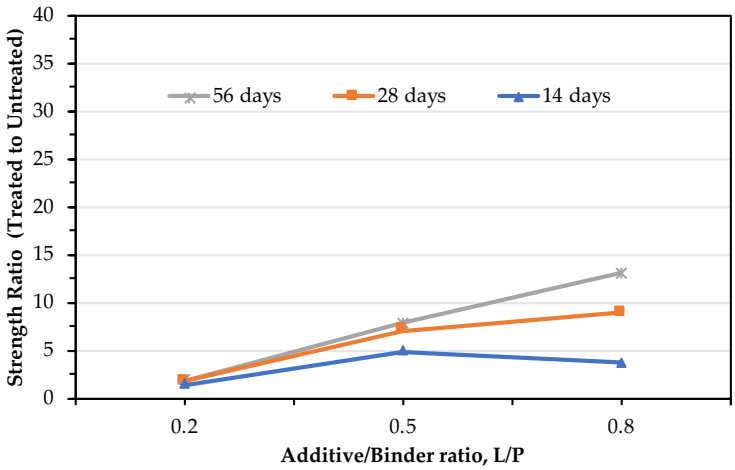
To comprehensively illustrate the effects of various additives on the strength development of treated soil, the strength ratio is determined. This strength ratio is calculated by dividing the strength of the treated soil by the strength of the untreated soil. A higher strength ratio indicates a more significant improvement in soil strength due to the addition of stabilizers. The graphical representation of the strength ratio variation is provided in Figure 4.8, which visually depicts the influence of the additives on soil strength enhancement. Additionally, the effects of these additives under two different moisture content levels are demonstrated in Figure 4.9 and Figure 4.10. These figures help in understanding how moisture content plays a crucial role in determining the overall performance of the stabilization process. From the above discussion, it can be concluded that achieving the maximum improvement in soil strength requires an optimum dose of the additive. This optimum dose is not fixed but rather varies depending on the water content present in the soil. Notably, when the water content is constrained to the soil's

liquid limit, the most effective dosage of the additive corresponds to an additive-to-binder ratio (L/P) of 0.5.

(a)



(b)



(c)

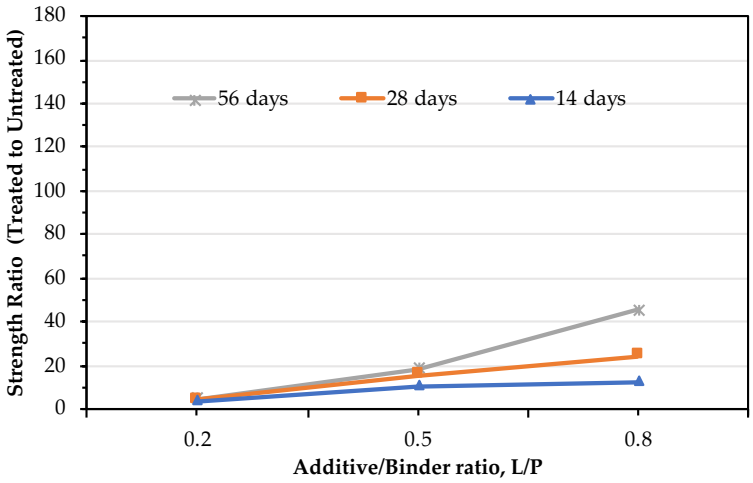
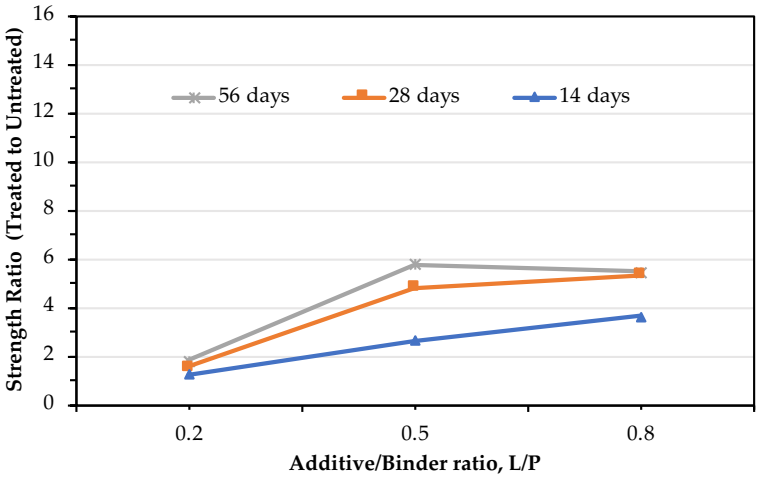
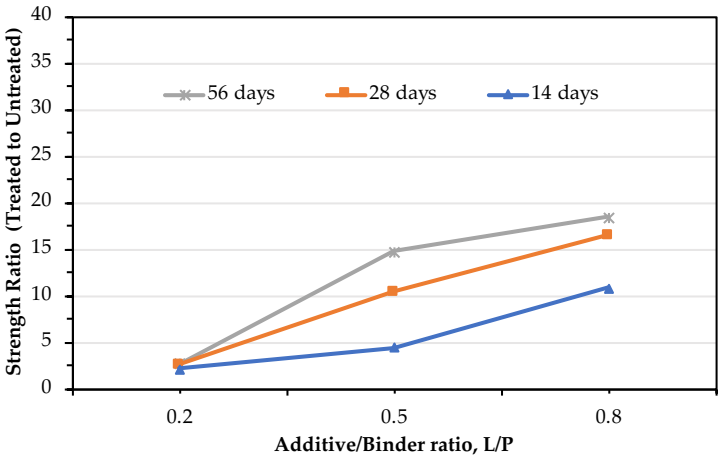


Figure 4.8: Variation of Unconfined Compressive Strength (UCS) Ratio with Alkali Additive (Activator) to Binder Ratio (L/P) at Fly Ash =10% and MC of (a) 0.75LL (b) LL and (c)1.25LL

(a)



(b)



(c)

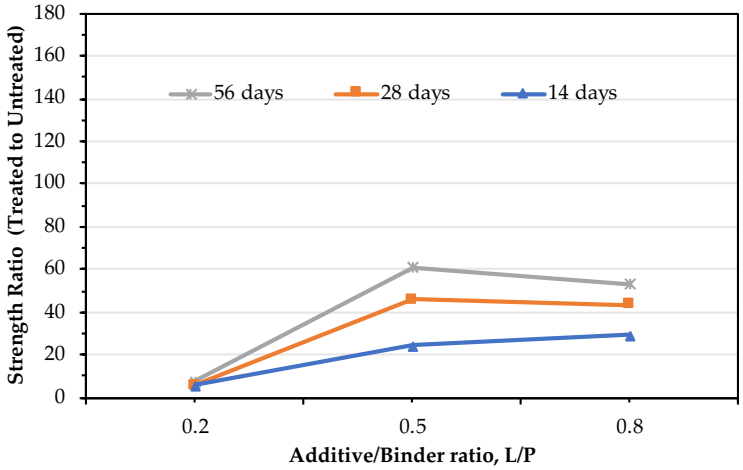
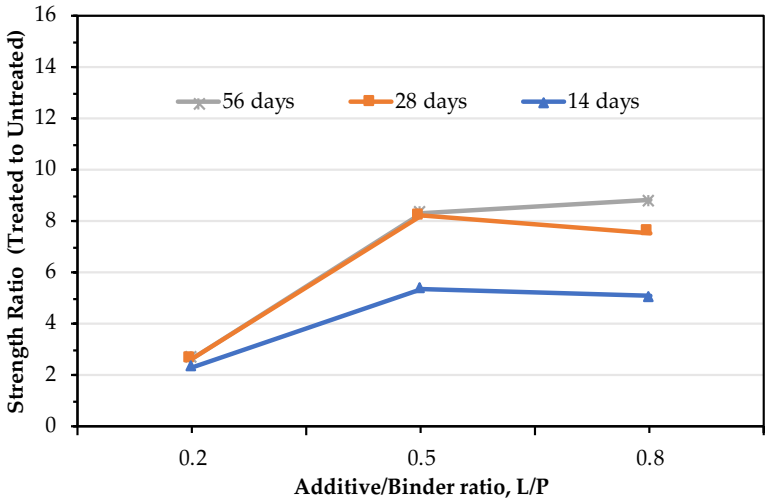
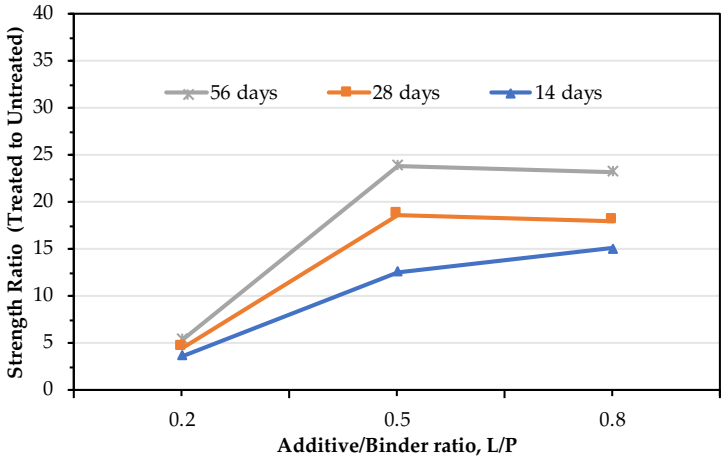


Figure 4.9: Variation of Unconfined Compressive Strength (UCS) Ratio with Alkali Additive (Activator) to Binder Ratio (L/P) at Fly Ash =15% and MC of (a) 0.75xLiquid Limit (b) Liquid Limit and (c) 1.25xLiquid Limit

(a)



(b)



(c)

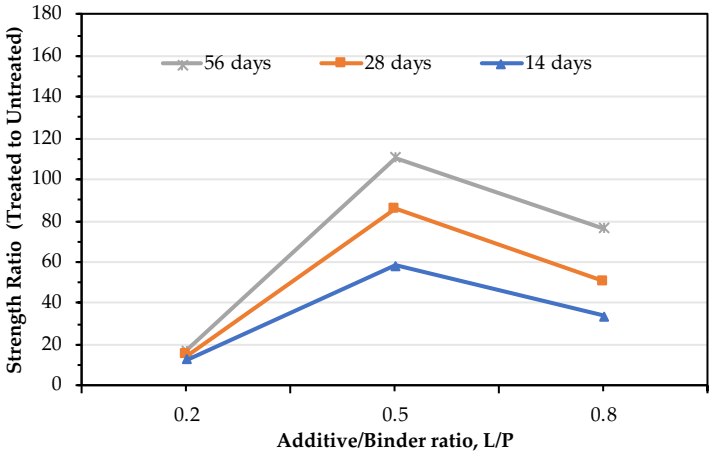
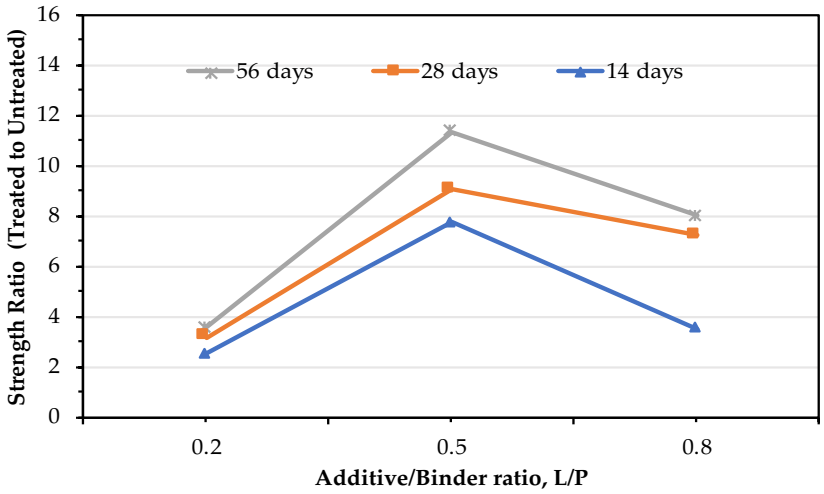
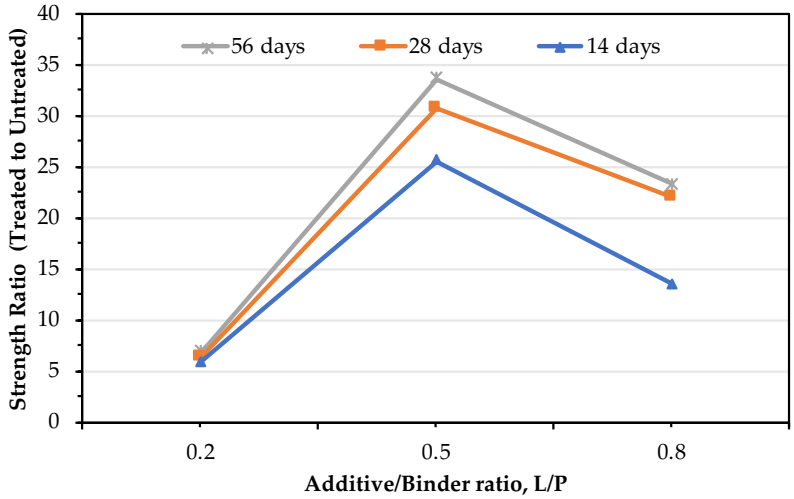


Figure 4.10: Variation of Unconfined Compressive Strength (UCS) Ratio with Alkali Additive (Activator) to Binder Ratio (L/P) at Fly Ash =20% and MC of (a)) 0.75xLiquid Limit (b) Liquid Limit and (c) 1.25xLiquid Limit

(a)



(b)



(c)

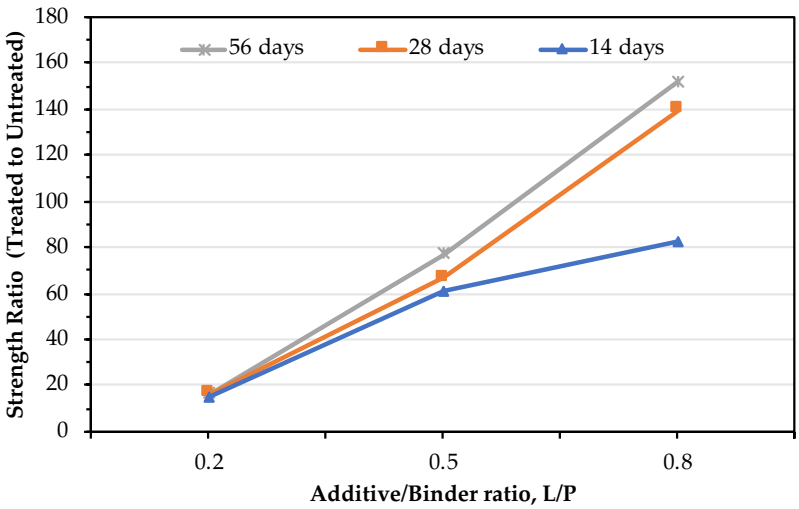


Figure 4.11: Variation of Unconfined Compressive Strength (UCS) Ratio with Activator to Binder Ratio (L/P) at Fly Ash =25% and MC of (a)) 0.75xLiquid Limit (b) Liquid Limit and (c) 1.25xLiquid Limit

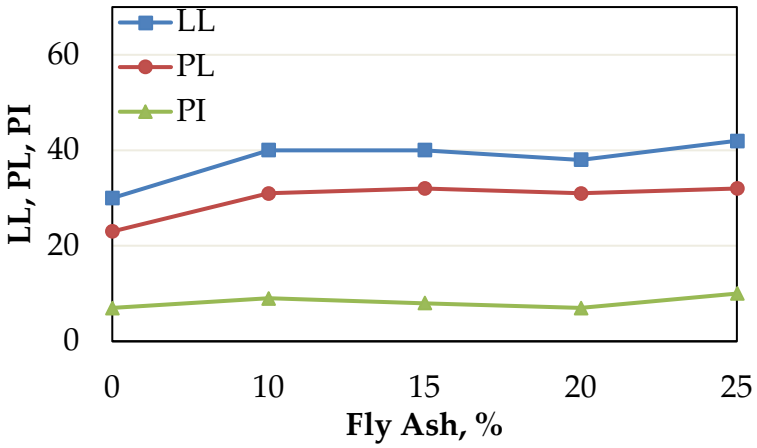
4.3 VARIATION OF INDEX PROPERTIES

The index properties (i.e. liquid limit, plastic limit and plasticity index) of the geo-polymerized soil have been determined on the 56-days cured and crushed sample. The Liquid Limit (LL) increases with increased geopolymer content, which indicates that the soil-geopolymer mix of that particular proportion needs more water to make the stabilized soil flow. Plasticity is proportional to LL and cohesion. Hence, higher LL stipulates a rise in cohesion as well as the strength, since cohesion provides strength to the soil. Soil mix having higher geopolymer content exhibits higher LL; in other words, higher strength which supports the discussions above. Plastic Limit (PL) and Plasticity Index (PI) also show the similar pattern with a little variation in some cases. Figure 4.12 shows the effect of geopolymer on Atterbergs' limits and plasticity index.

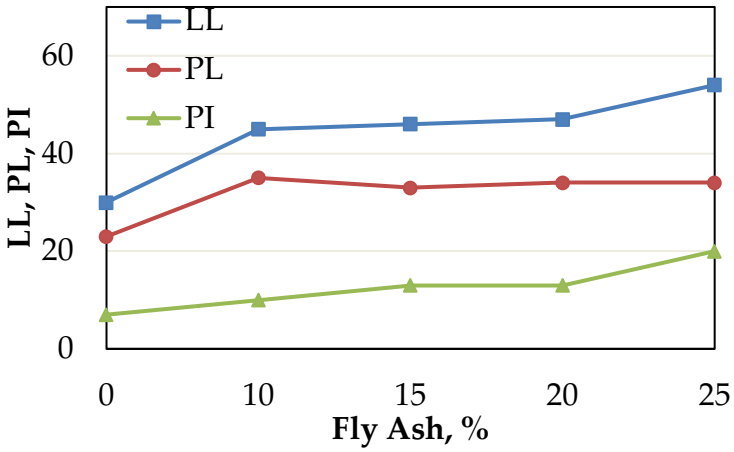
Table 4.3: Variation of Index Properties at Different Proportion of Materials

Sample ID	Binder, P (%)	Additive / Binder Ratio	Index Properties		
			Liquid Limit (LL)	Plastic Limit (PL)	Plasticity Index (PI)
Untreated	---	---	30	23	7
F10L20	10	0.2	40	31	9
F15L20	15		40	32	8
F20L20	20		38	31	7
F25L20	25		42	32	10
F10L50	10	0.5	45	35	10
F15L50	15		46	33	13
F20L50	20		47	34	13
F25L50	25		54	34	20
F10L80	10	0.8	52	40	12
F15L80	15		58	37	21
F20L80	20		57	36	21
F25L80	25		61	48	13

(a)



(b)



(c)

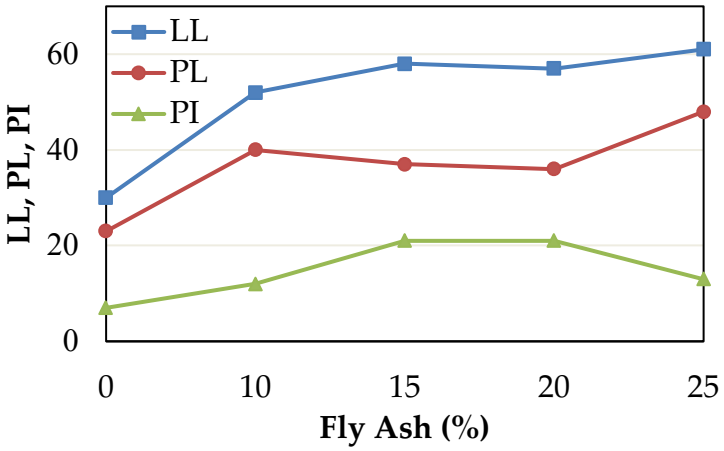


Figure 4.12: Variation of Liquid Limit (LL), Plastic Limit (PL) and Plasticity Index (PI) at Activator to Binder ratio (L/P) of (a) 0.2, (b) 0.5, (c) 0.8

At the L/P ratio 0.2, increase in LL and PL have been observed whereas minor increase in PI has been seen when the geopolymer content increased from 0 to 10% due to the added cohesion provided by geopolymer. After that, the increase in geopolymer has affected very little up to 20%. At 25%, the three

parameters have increased. Similar rising trend has been observed in case of. activator to binder ratio (L/P) of 0.5. The initial pattern follows the previous one's. There has been a sharp increase in LL at the highest geopolymer level. Previous discussion also showed the highest strength in this condition.

The observed increase and decrease in Atterbergs' limits and plasticity index at L/P = 0.8 to similar to the UCS increase and decrease curve. At 15% and 20% geopolymer, the PL decreases whereas LL increased. At 25%, PL has increased significantly. Increased LL signifies growth in cohesion and rise in PL signifies the brittleness of mix. The brittleness has also been observed in stress-strain behavior (Figure A.1 to Figure A.3). The increase in PI is a sign of greater workability results in better mixing with in situ soil, homogeneous distribution of binder, lesser segregation, and hence homogeneous and stable soil-binder matrix. This can also accommodate variable moisture, minimize the chances of voids, and can pump and inject smoothly through equipment which might be helpful during construction phases.

4.4 VARIATION OF UNIT WEIGHT

Geopolymerized soil has lower voids as various bonds formed between soil and geopolymer which densified the material. The voids content in the parent soil has been filled up with the allumino-sillicate compounds which are formed due to ion-exchange reaction results in greater unit weight in soil-geopolymer mix. In some cases, strength decreases with increasing geopolymer content. The reasons might be the presence of tiny air pockets, lack of bond formation due to insufficient water to react with or inability to fill the voids due to insufficient mixing. The improvement in unit weight after geo-polymerization has been shown in figure 4.13. From this analysis, the material amount can be predicted prior to the field construction.

Unit weight analysis in geopolymers of different proportions is indeed essential to optimize the process for soil stabilization, ensuring ground improvement techniques are effective. This allows the engineer to design a mix which will achieve desired density, strength, and durability with minimal material use, considering the economical and sustainable issues of the process. Based on this, unit weight can show the quality of compaction, and thus soil stiffness will ensure that structural stability is achieved by providing adequate load-bearing capacity of the treated ground. Changes in unit weight also provide information about durability by indicating the resistance to some factors, such as water infiltration, freeze-thaw cycles, and chemical attacks.

Table 4.4: Variation of Unit Weight at Different Proportion of Materials

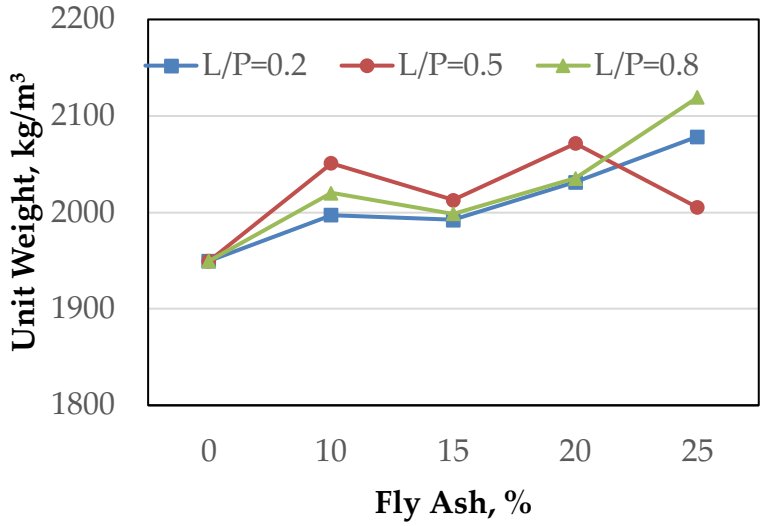
Sample ID	**Binder, P (%)**	**Additive / Binder Ratio**	**Unit Weight (kg/m^3) at Moisture Content/ Liquid Limit Ratio MC/LL)**		
			MC/LL= 0.75	**MC/LL= 1.00**	**MC/LL= 1.25**
Untreated	---	---	1950	1963	1905
F10L20	10	0.2	1997	1994	1899
F15L20	15		1992	2085	1955
F20L20	20		2031	1925	1931
F25L20	25		2079	1921	2148
F10L50	10	0.5	2051	2123	2086
F15L50	15		2013	1935	2001
F20L50	20		2071	1938	1957
F25L50	25		2005	1926	1953
F10L80	10	0.8	2020	1989	2066
F15L80	15		1999	1931	2075
F20L80	20		2035	1896	2065
F25L80	25		2119	2006	2010

4.5 MINERALOGICAL ANALYSIS

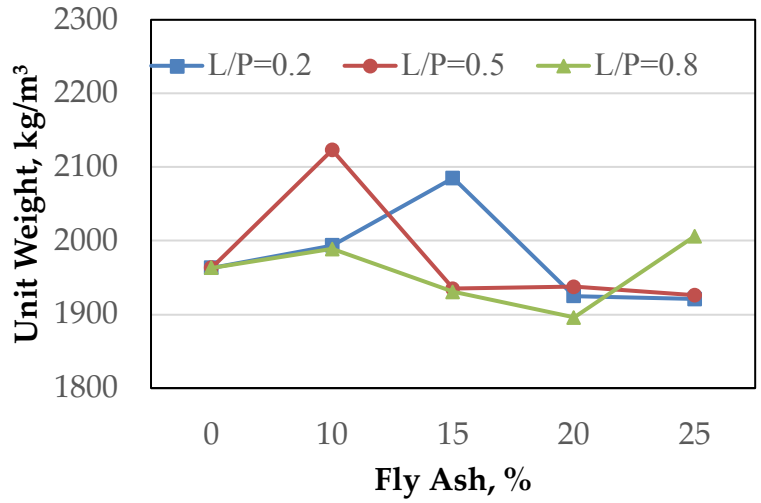
Bond formation at the microstructural level, which actually results in strength gain, can be observed in mineralogical analysis. In the current study, the densification of material has been viewed with a Scanning Electron

Microscope (SEM) image, and the chemical details of the stabilized soil were analyzed with an X-ray diffraction (XRD) pattern.

(a)



(b)



(c)

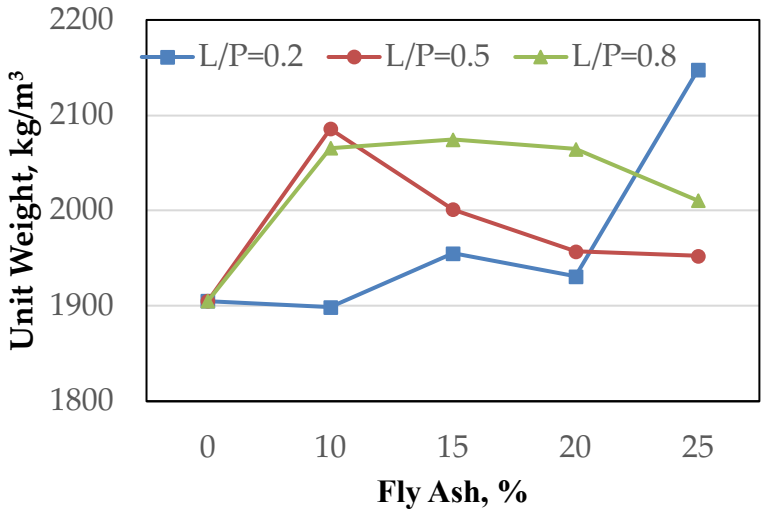


Figure 4.13: Unit Weight at 56-Days Curing Period and Moisture Content of (a) 0.75LL, (b) LL, (c) 1.25LL

4.5.1 SEM Analysis

Scanning Electron Microscopy (SEM) analysis enables the observation of surface features and internal structure at high magnification, which provides critical information about the hydration and polymerization processes, and the interaction between the geopolymer binder and the soil particles. It can show the voids and microcracks present in the mix. Figure 4.27 to 4.30 show the magnified images of parent soil and geo-polymerized soils.

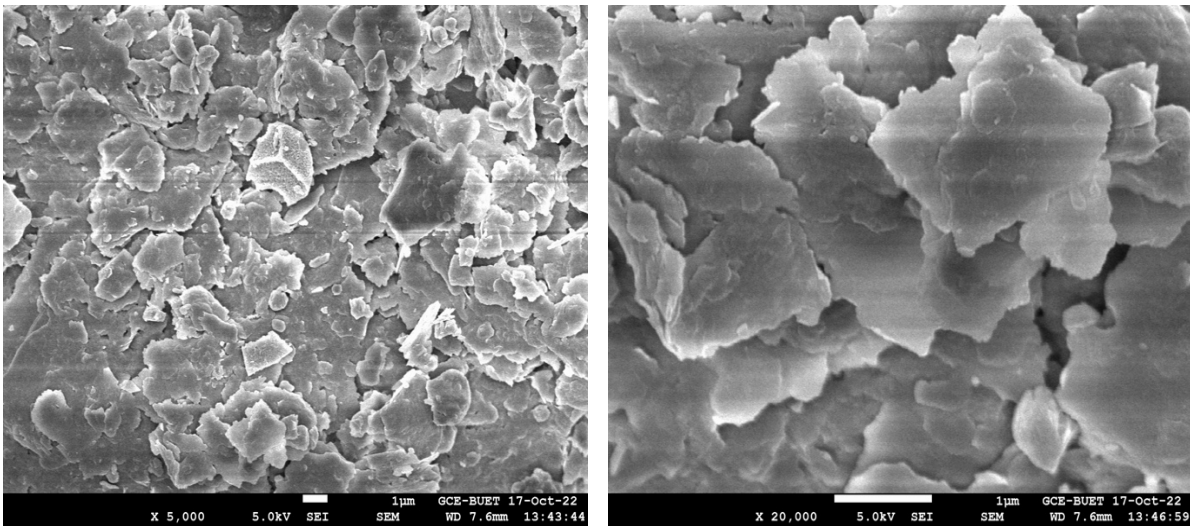
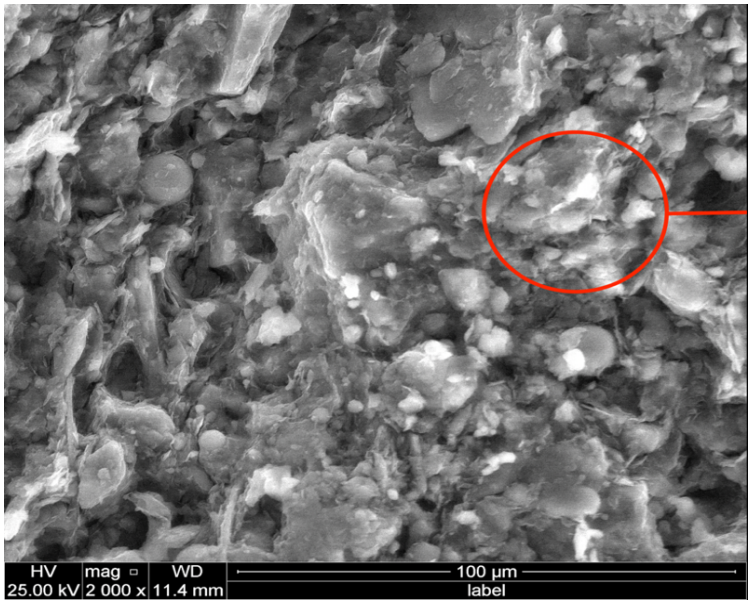


Figure 4.14: SEM image of parent soil

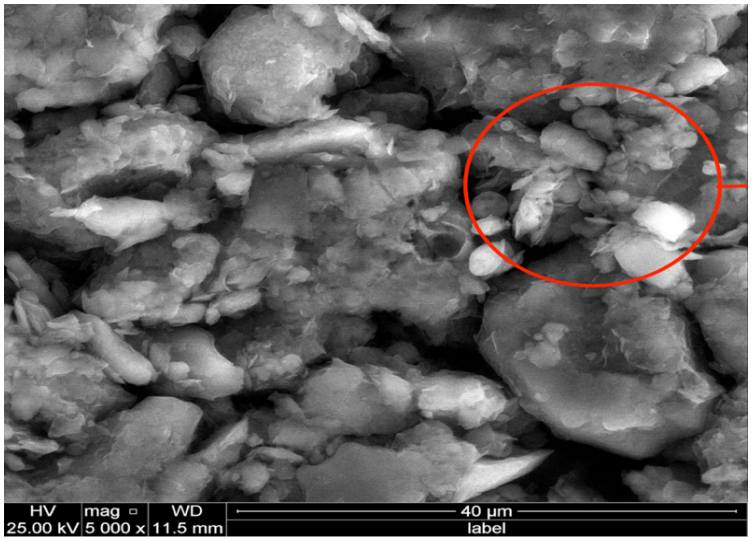
SEM observation of the parent soil indicates that the particles are well dispersed and highly porous with no strong inter-particle bonding and loosely packed structure, resulting in low strength. In contrast, SEM observation of geo-polymerized soil samples indicates a significant change, with the particles being closely packed and less porous and in clustered forms. The microstructure development is due to ion exchange reactions between the geopolymer binder and soil at their interface. The less stable cations are substituted by alkali ions during this process, facilitating the formation of stable chemical bonds. The particles are strengthened by these bonds, and a strong networked structure is formed, significantly increasing the treated soil strength.

(a)



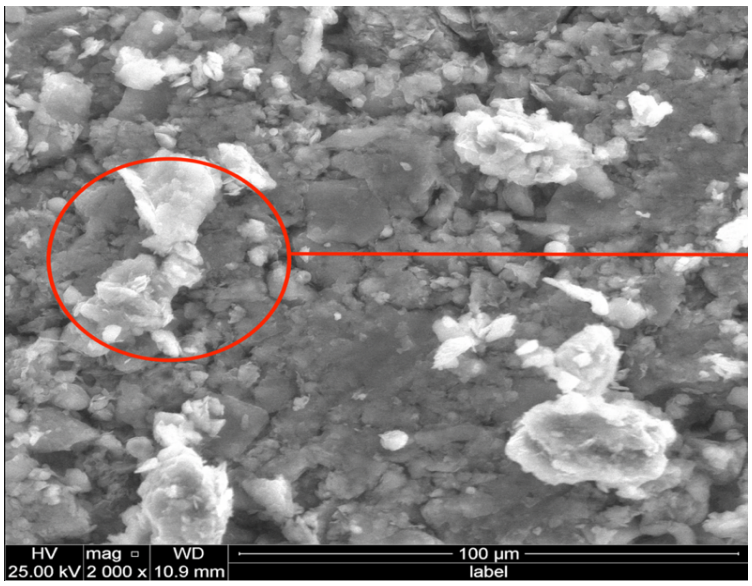
Soil Geopolymer Cluster

(b)



Soil Geopolymer Cluster

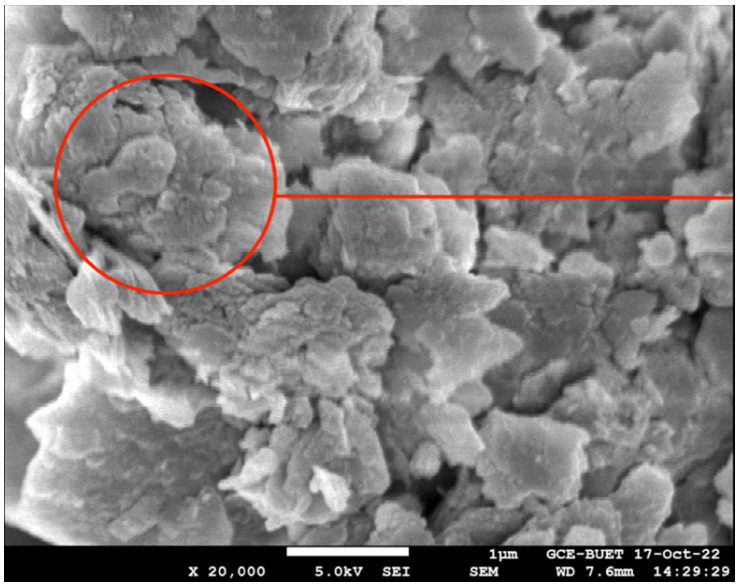
(c)



Flocculated Soil Geopolymer Cluster

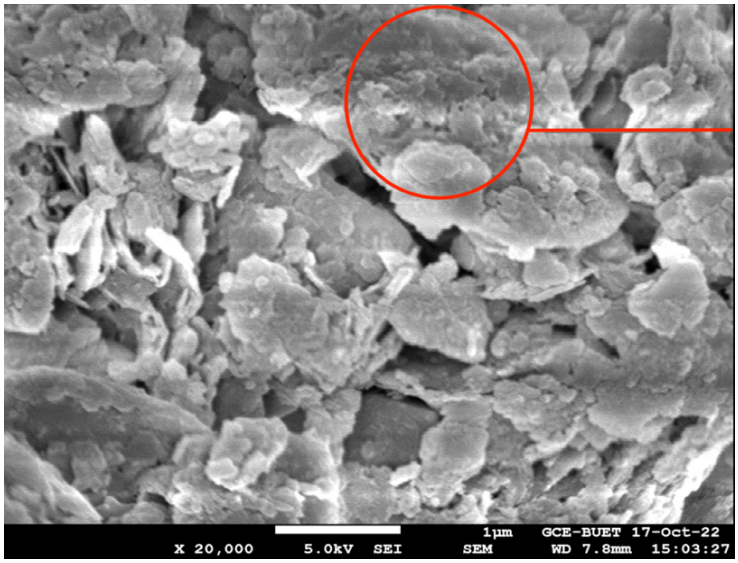
Figure 4.15: SEM image of stabilized soil at 25% Binder Content, L/P=0.2 and (a) w/LL=0.75 (b) w/LL=1.0 and (c) w/LL=1.25

(a)



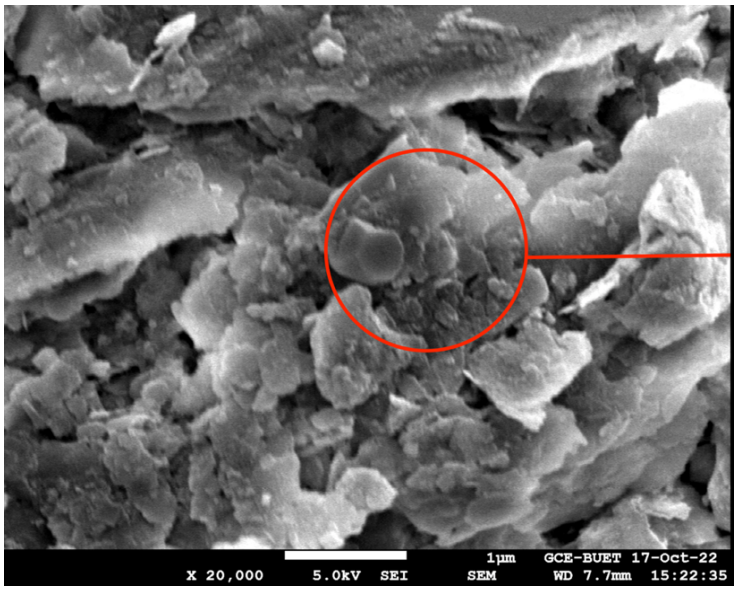
Densified Stabilized Soil

(b)



Densified Stabilized Soil

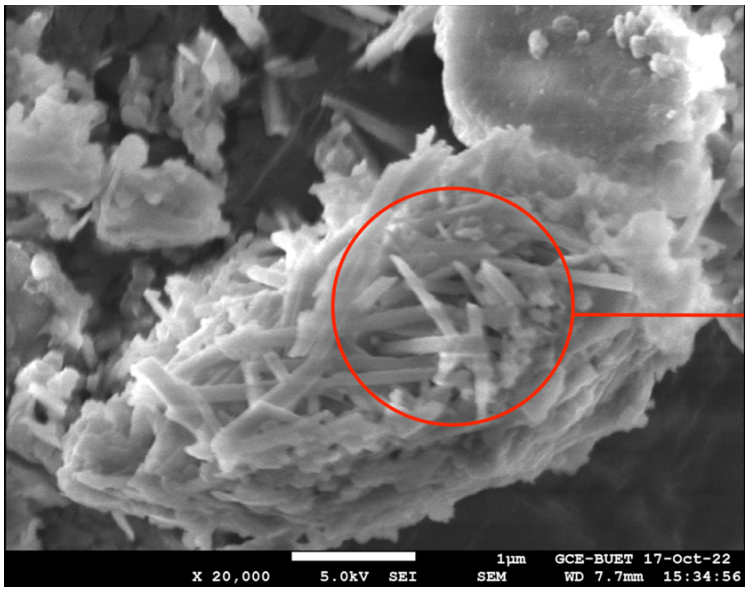
(c)



Densified Stabilized Soil with less void

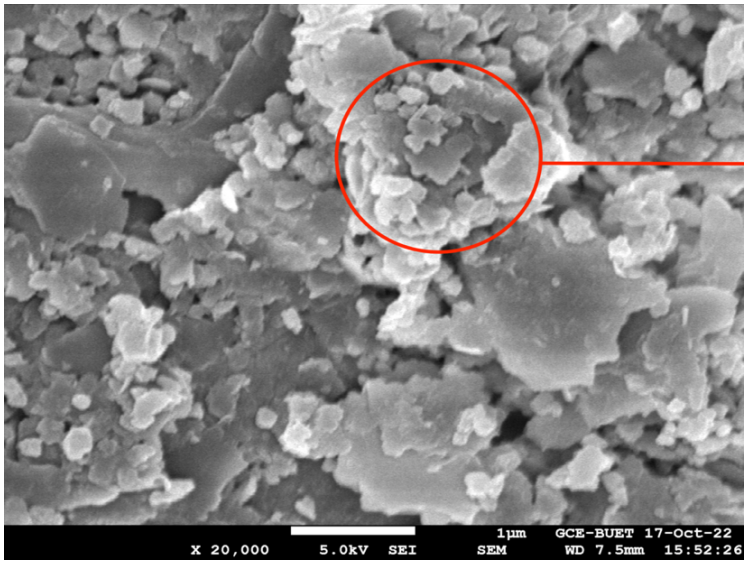
Figure 4.16: SEM image of stabilized soil at 25% Binder Content, L/P=0.5 and (a) w/LL=0.75 (b) w/LL=1.0 and (c) w/LL=1.25

(a)



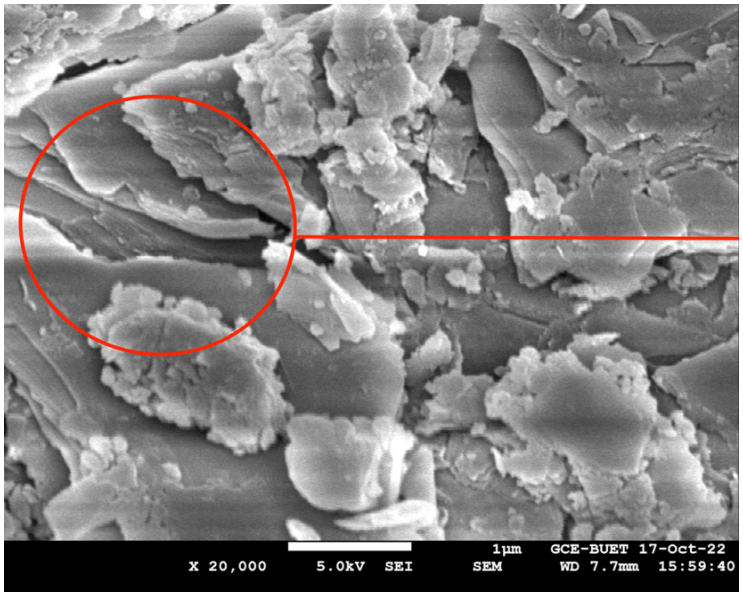
Interlocking Geopolymer Cluster

(b)



Flocculated Geopolymer Cluster

(c)



Densified Stabilized Soil

Figure 4.17 SEM image of stabilized soil at 25% Binder Content, L/P=0.8 and (a) w/LL=0.75 (b) w/LL=1.0 and (c) w/LL=1.25

With the increase of additive content, densification, and void reduction phenomena are more visible in the microstructural images. With additive to binder ratio of 0.8 and water content of 75% of liquid limit, a flocculated geopolymer cluster of spaghetti shape, is found, which might be the excess geopolymer that is not bonded with soil. The lesser amount of water available in the soil might restrict the geopolymer from forming a bond with the soil. At the same additive level with 125% of the liquid limit, very dense and compacted particles are shown in SEM image. Also, no micro-crack has been observed.

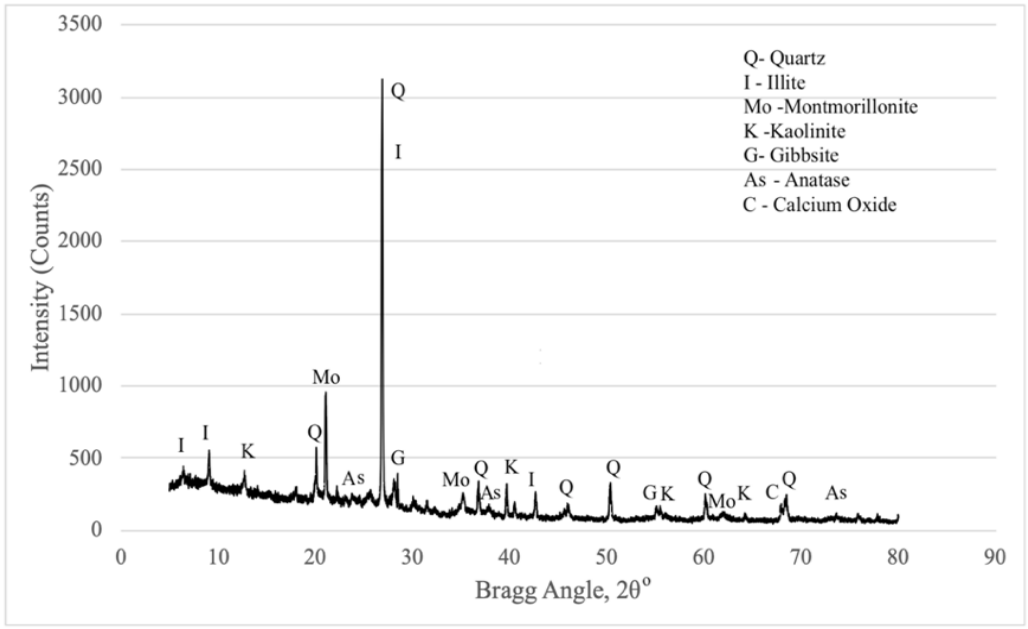
4.6.1 X-Ray Diffraction Pattern (XRD) Analysis

X-Ray Diffraction Pattern (XRD) is a powerful analytical technique used in the identification and characterization of the crystalline structure, phase composition, and other structural properties of materials. It works by directing X-rays at a material and analyzing the patterns of diffraction produced as the X-rays interact with the atomic lattice of the sample. X-ray diffraction could act as a powerful tool in order to assess the effects of chemical attacks on geopolymer-treated soils in deep mixing.

XRD Pattern of Parent Soil and Fly Ash

From X-Ray Diffraction Pattern, it is found that the parent soil is abundant with Quartz [SiO_2)] which shows the maximum peaks. Montmorillonite [$(OH)_4Si_8Al_4O_{20}{\cdot}nH_2O$], Illite $(K,H_3O)(Al,Mg,Fe)_2(Si,Al)_4O_{10}$ [$(OH)_2$,(H_2O)], Kaolinite [$Al_2(OH)_4Si_2O_5$] are also present and show some peaks. There are some small peaks of Gibbsite [Al_2O_3], Anatase [TiO_2] and Calcium Oxide [$Ca(OH)_2$] also. Quartz is also in maximum proportion in fly ash and shows maximum peak in XRD pattern. Some peaks have come from Mullite [$Al_6Si_2O_{13}$], Andradite [$Ca_3Fe_2(SiO_4)_3$], Hematite [Fe_2O_3] etc.

(a)



(b)

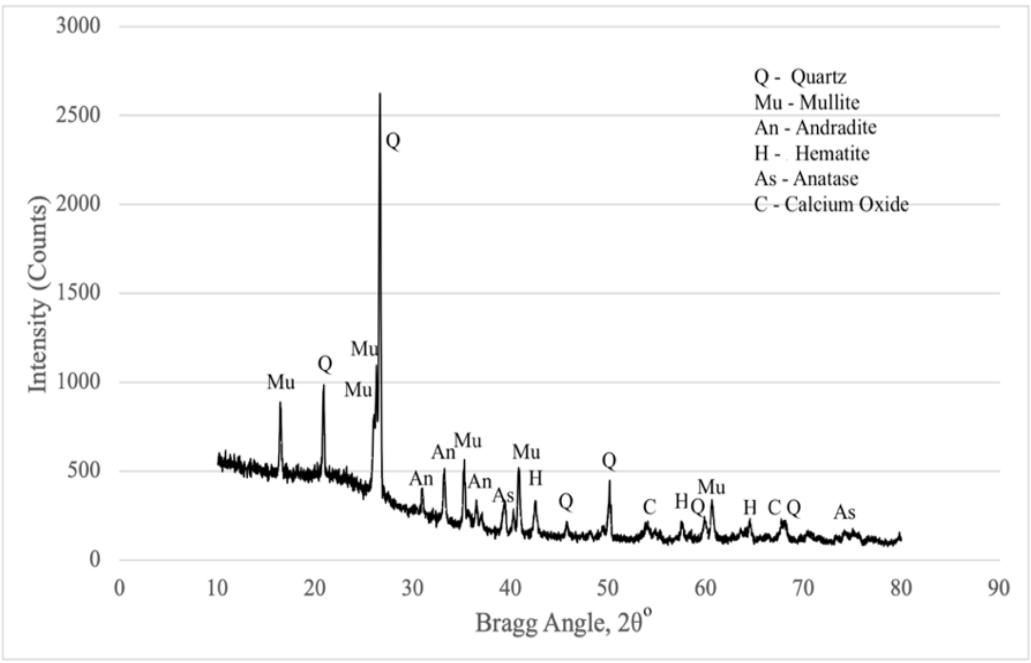
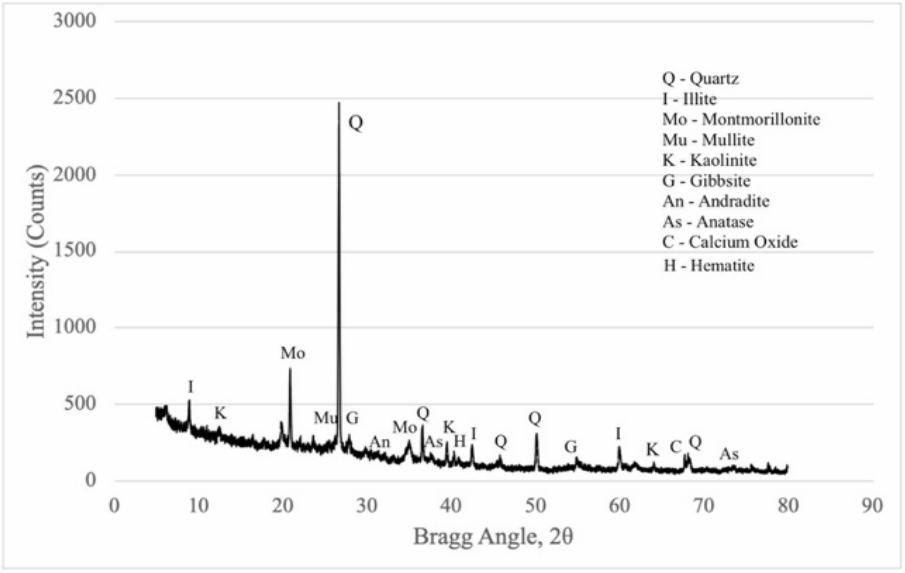


Figure 4.18: XRD pattern of (a) soil and (b) Fly Ash

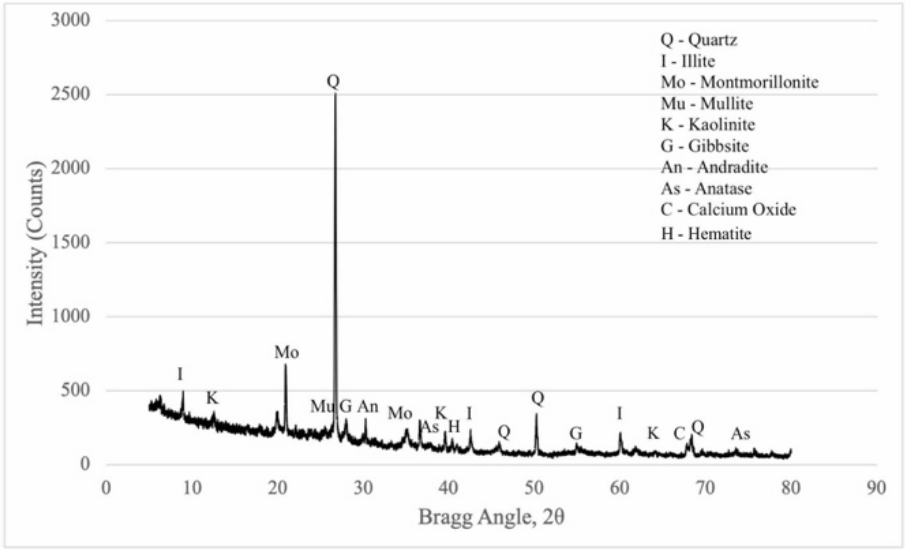
XRD Patterns of Stabilized Soils

In the stabilized soil sample, the mineral composition mostly resembles the composition of parent soil. The maximum peak comes from Quartz as the parent soil and the fly ash. Some peaks come from other minerals as like as the soil. Some smaller peaks also come from the minerals of Fly Ash such as Mullite, Andradite, Hematite etc.

(a)



(b)



(c)

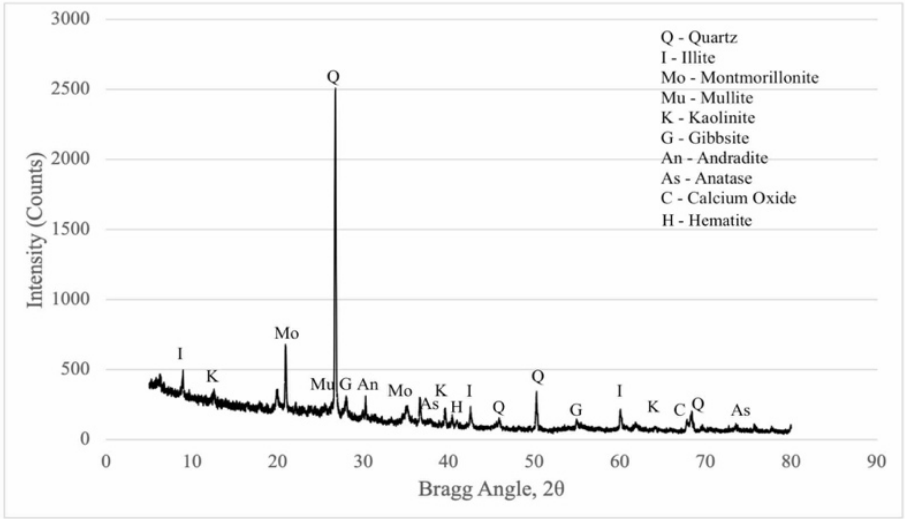
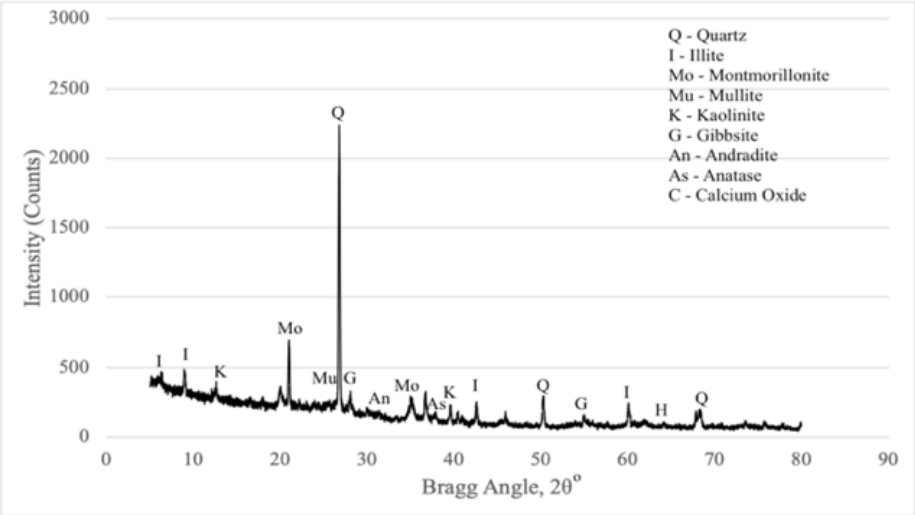
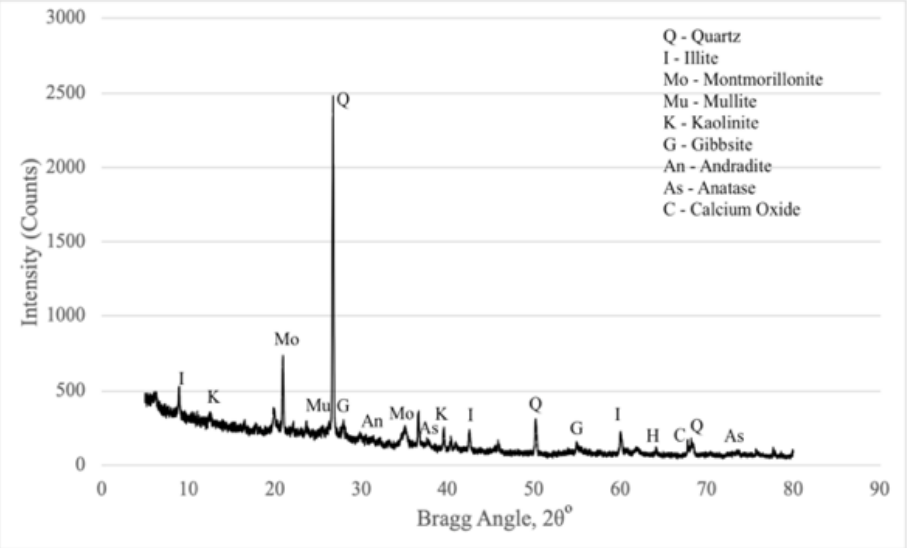


Figure 4.19: XRD Pattern of Stabilized Soil at MC = 0.75xLL and (a) L/P=0.2, (b)L/P=0.5, and (c) L/P=0.8

(a)



(b)



(c)

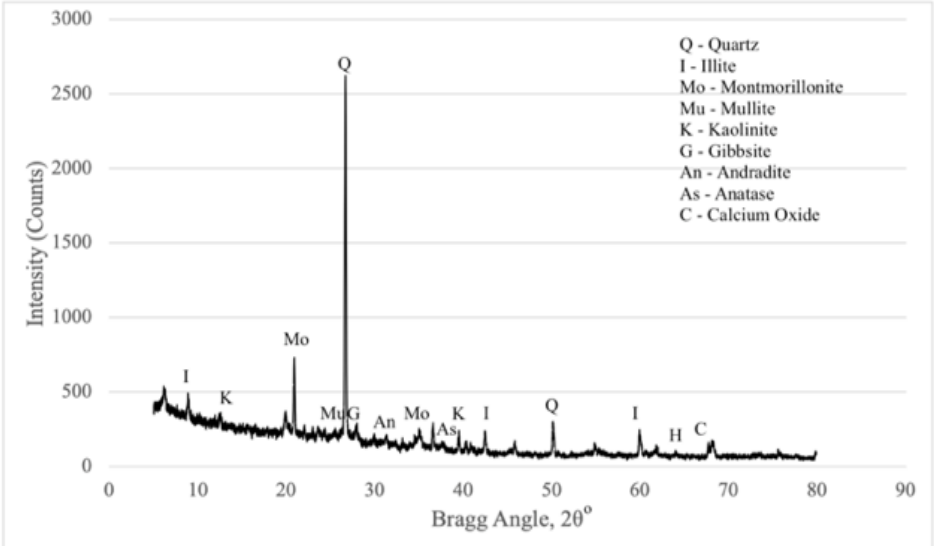
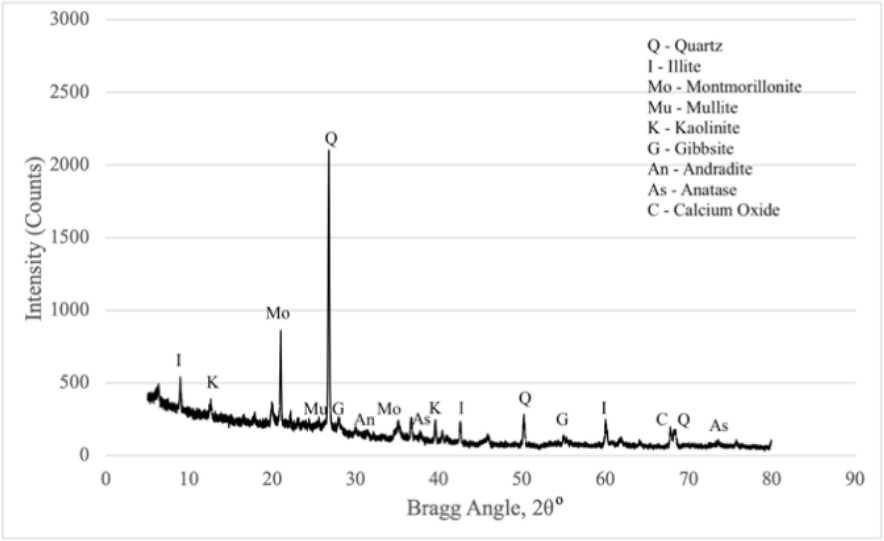
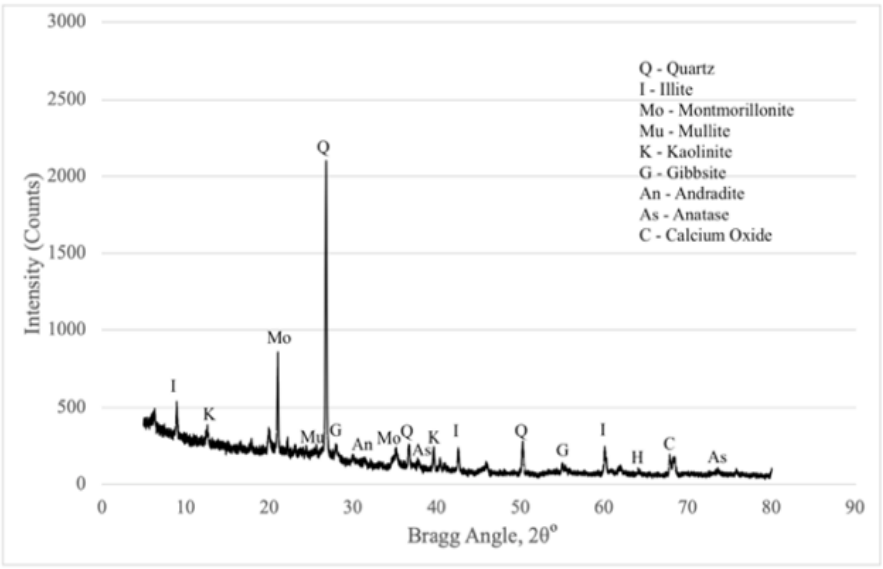


Figure 4.20: XRD Pattern of Stabilized Soil at MC =LL and (a) L/P=0.2, (b)L/P=0.5, and (c) L/P=0.8

(a)



(b)



(c)

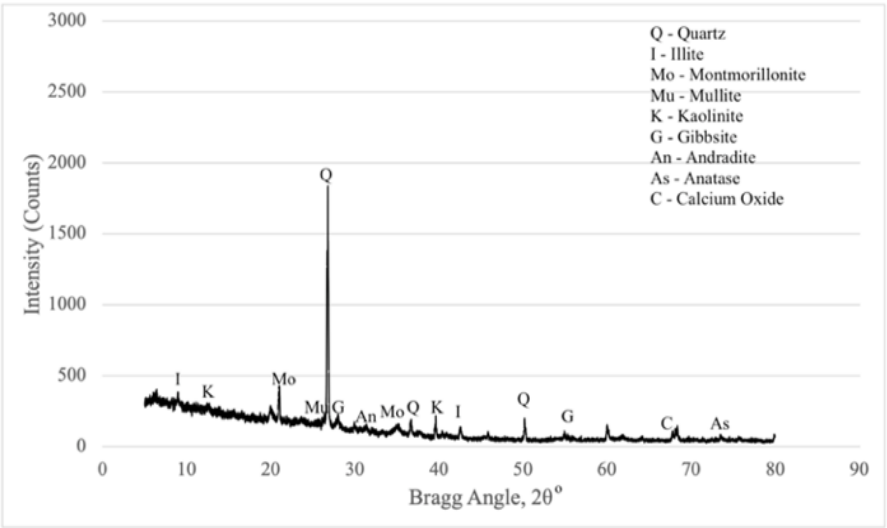


Figure 4.21: XRD Pattern of Stabilized Soil at MC = 1.25xLL and (a) L/P=0.2, (b)L/P=0.5, and (c) L/P=0.8

Geopolymers are characterized by very high resistance against chemical attacks, but some long-term performance may also be affected because of the aggressive nature of sulfates, chlorides, or acidic conditions. XRD helps in identifying and quantifying mineralogical changes in the geopolymer matrix and soil owing to chemical attacks, thus helping get important information about durability. XRD detects the formation of harmful phases, such as gypsum or ettringite upon exposure to sulfates, which may cause expansion and cracking by analyzing the diffraction patterns. It also identifies chloride-induced changes, including the formation of Friedel's salt, that may affect structural integrity. In acidic environments, XRD reveals either the leaching of aluminosilicates or the formation of secondary phases that indicate degradation. The XRD pattern before and after chemical exposure allows engineers to assess the resistance of the geopolymer mix, work out an optimized formulation for better durability, and long performance in challenging situations.

Among the compounds found in the XRD analysis, Quratz, Anatase, Hematile and Mullite are highly stable and can resist adverse environmental effect to prevent decay. Whereas , Montmorillonite, Kaolinite, Gibbsite can have ion exchange reaction with sulphate or chlorine present in the environment. The study of XRD can provide a direction of taking action against decay when there is a possibility of chemical attack.

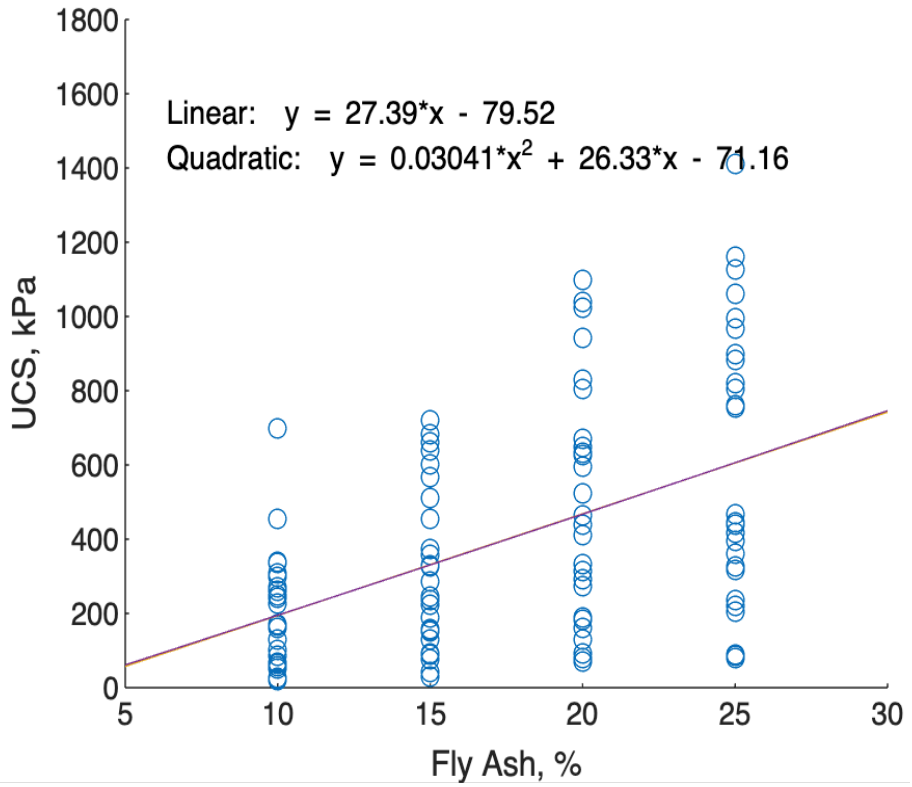
4.6 DEVELOPMENT OF PREDICTION MODEL

A number of factors are responsible for the strength gaining of geo-polymerized soil. The effects of water, binder, additives, and curing period have been taken into account in the current study. For an instant prediction or a preliminary investigation, a model addressing the above-mentioned parameters

might be useful to predict strength before going for experimental investigation. The benefit of models are listed below:

i. Models predict a future outcome, for instance, forecasting how soil or structure would act in the future.
ii. They simplify complex systems to represent interactions. For example, a soil behavior due to moisture and load.
iii. They allow for inexpensive testing virtually before the actual implementation of any method.
iv. They allow for decisions based on quantitative information and optimization of material or method use.
v. Models uncover the risks, hence making planning and safety more effective.
vi. New materials, systems, and methods are driven by models.
vii. They extend results to larger applications in new conditions.
viii. Models reduce costs: They reduce the need to actually test and try.

The relationship among the variables should be understood to generate models. In the current study, the input variables are fly ash content, activator to binder ratio, mixing water to binder ratio and curing age, and the output variable is unconfined compressive strength (UCS). Figure 4.22 to 4.25 show the relationships between the output and input variables. Both linear and nonlinear (quadratic) fit have been shown in the figures. It is clearly visible from the values of Correlation, R^2 and Coefficient of Variance, COV that the output parameter cannot be explained well by a single input parameter. Generation of models addressing all the input parameters have been approached.



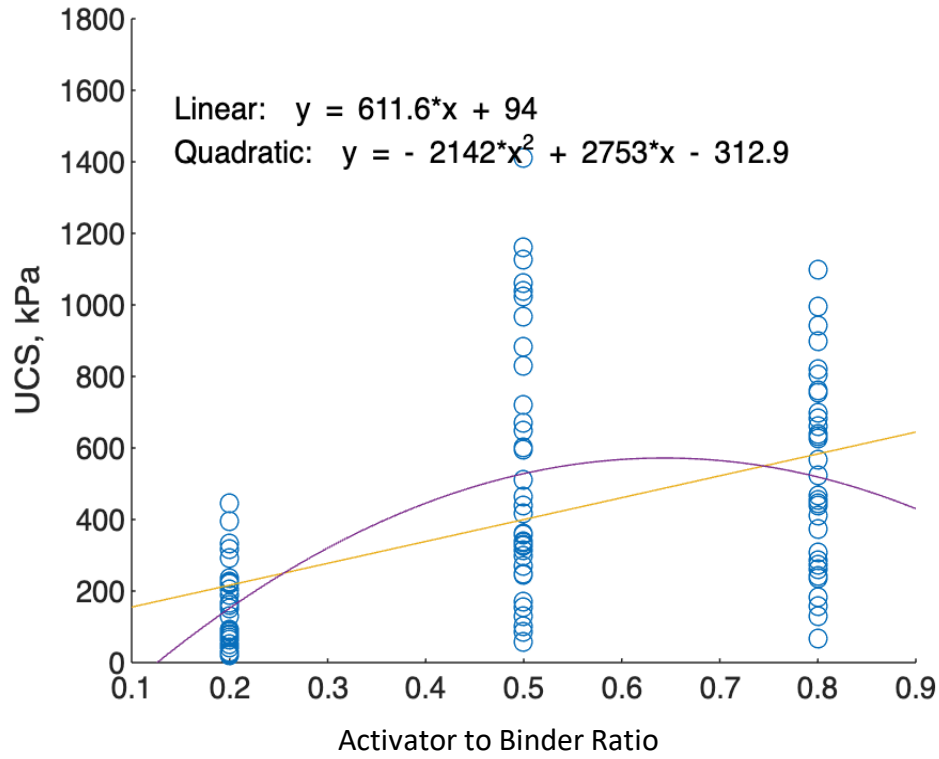
Linear:

$R^2 = 0.235$
COV (%)= 69.73

Quadratic:

$R^2 = 0.235$
COV (%) = 70.06

Figure 4.22: Relationship between Unconfined Compressive Strength (UCS) and Fly Ash Content



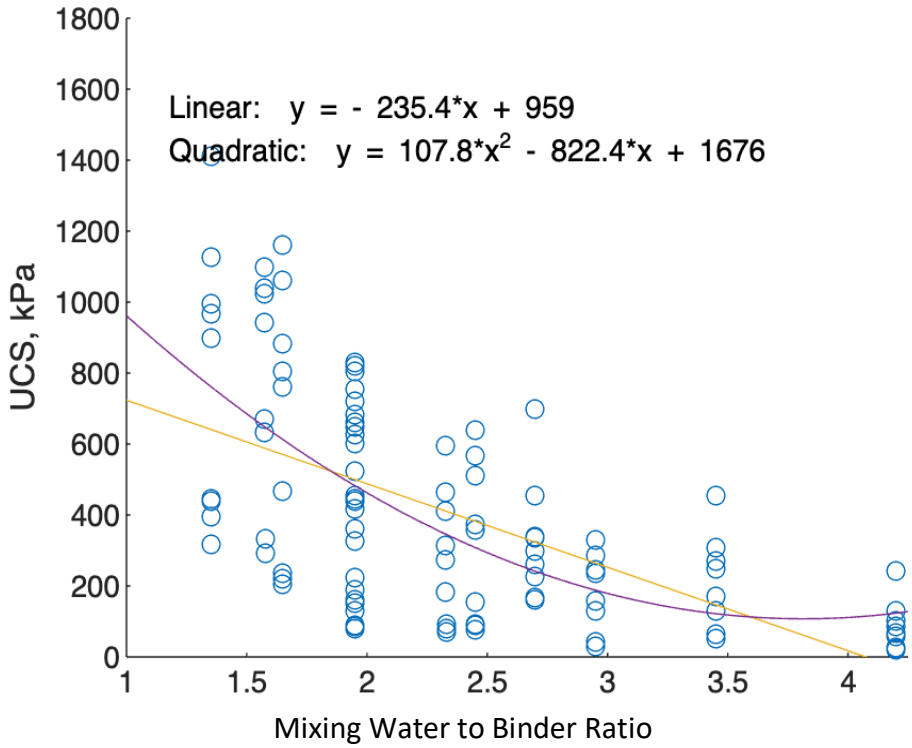
Linear:

$R^2 = 0.225$
COV (%)= 70.18

Quadratic:

$R^2 = 0.308$
COV (%)= 66.64

Figure 4.23: Relationship between Unconfined Compressive Strength (UCS) and Activator to Binder Ratio



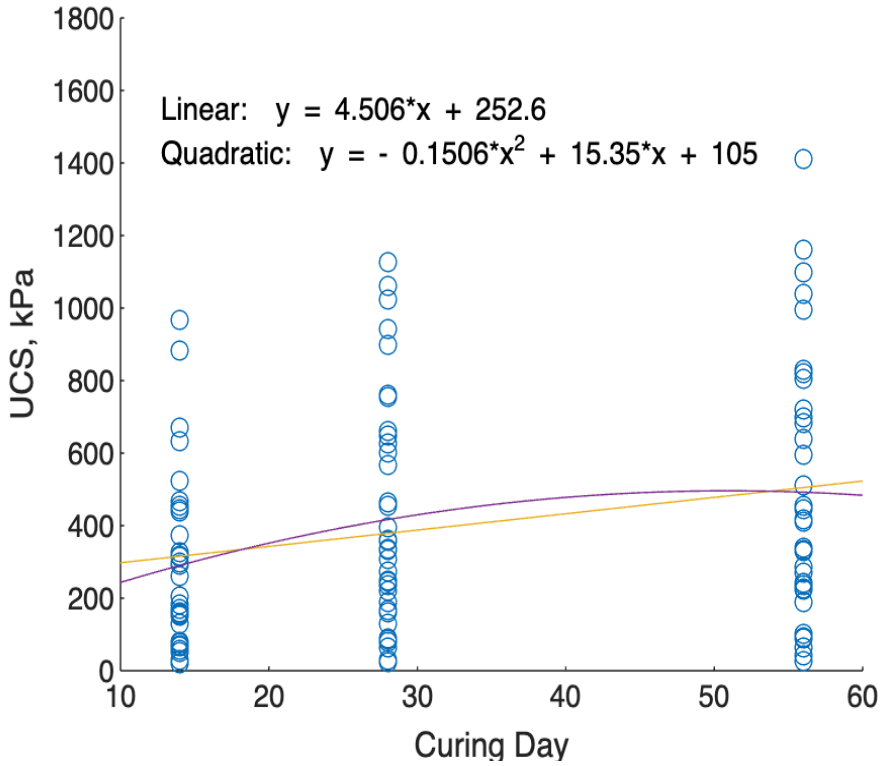
Linear:

R^2 = 0.356
COV (%)= 63.98

Quadratic:

R^2 = 0.412
COV (%)= 61.42

Figure 4.24: Relationship between Unconfined Compressive Strength (UCS) and Mixing Water to Binder Ratio



Linear:

R^2 = 0.062
COV (%) = 77.21

Quadratic:

R^2 = 0.07
COV (%) = 77.27

Figure 4.25: Relationship between Unconfined Compressive Strength (UCS) and Curing Day

Several comprehensive Statistical Regression (both equation based and machine learning) Models (Figure 4.26) have been developed to predict the desired parameters governed by multiple influencing factors. In Deep Mixing Method, the estimation of unconfined compressive strength is a crucial parameter since this parameter determines the improved ground condition and required spacing, and other parameters. The models are trained with 90% of total data and tested with the rest 10% data. The performance of the model has been evaluated with Correlation, R^2 and Root Mean Square Error (RMSE) values. The model accuracy is defined by the response to test data set since it is unseen data for the model.

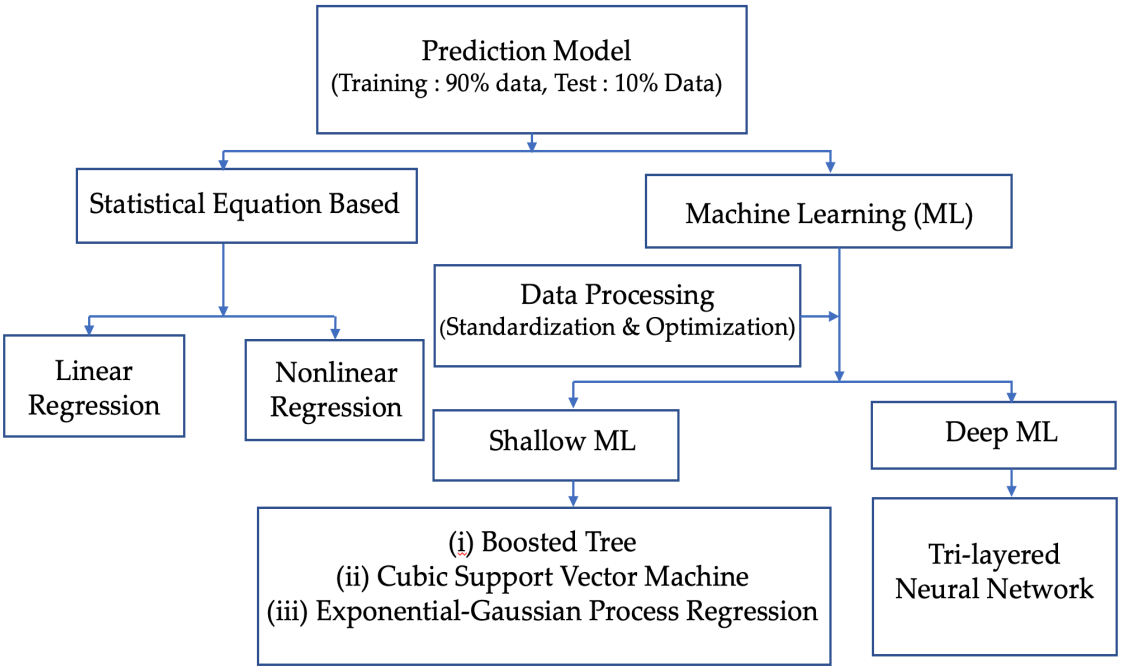


Figure 4.26: Summary of Generated Prediction Models

4.6.1 Linear Regression Model

At first, a linear regression model has been tried with a normal straight line equation of

$$Y = b_0 + \sum_{i=1}^{n} b_i X_i$$

Where, Y= Dependent (Output) variables

X_i = Independent (predictor) variables,

b_0 = Intercept term,

b_i = Regression coefficients for each predictor

The prediction equation:

$$Y = b_0 + b_1 X_1 + b_2 X_2 + b_3 X_3 + b_4 X_4$$

Where, Y = Unconfined Compressive Strength, UCS (kPa),

X_1 = P=Fly Ash (%),

X_2 = w/P = Mixing Water to Binder ratio,

X_3 = D = Curing Age (Days),

X_4 = L/P = Additives to FA ratio

From MATLAB linear fit analysis,

$$\text{UCS (kPa)} = 27.138 + 309.73P + 309.73 \left(\frac{w}{P}\right) + 4.3851\ D - 533.52 \left(\frac{L}{P}\right) \quad (4.1)$$

The model response has been explained with the Figure 4.27. The R^2 value for test data set has been observed as 0.63 which indicates a moderate fit model with an ability to explain 63% of the data.

Limitations of Linear Model

There are some limitations of linear regression model. Those are:

i. The linear model cannot disclose complex relationships, especially non-linear relationships.
ii. The estimates of regression coefficients are biased by outliers that might be far away from the bulk of data points.
iii. When independent variables are highly interrelated, separating the individual effect of each predictor gives rise to unreliable estimates.

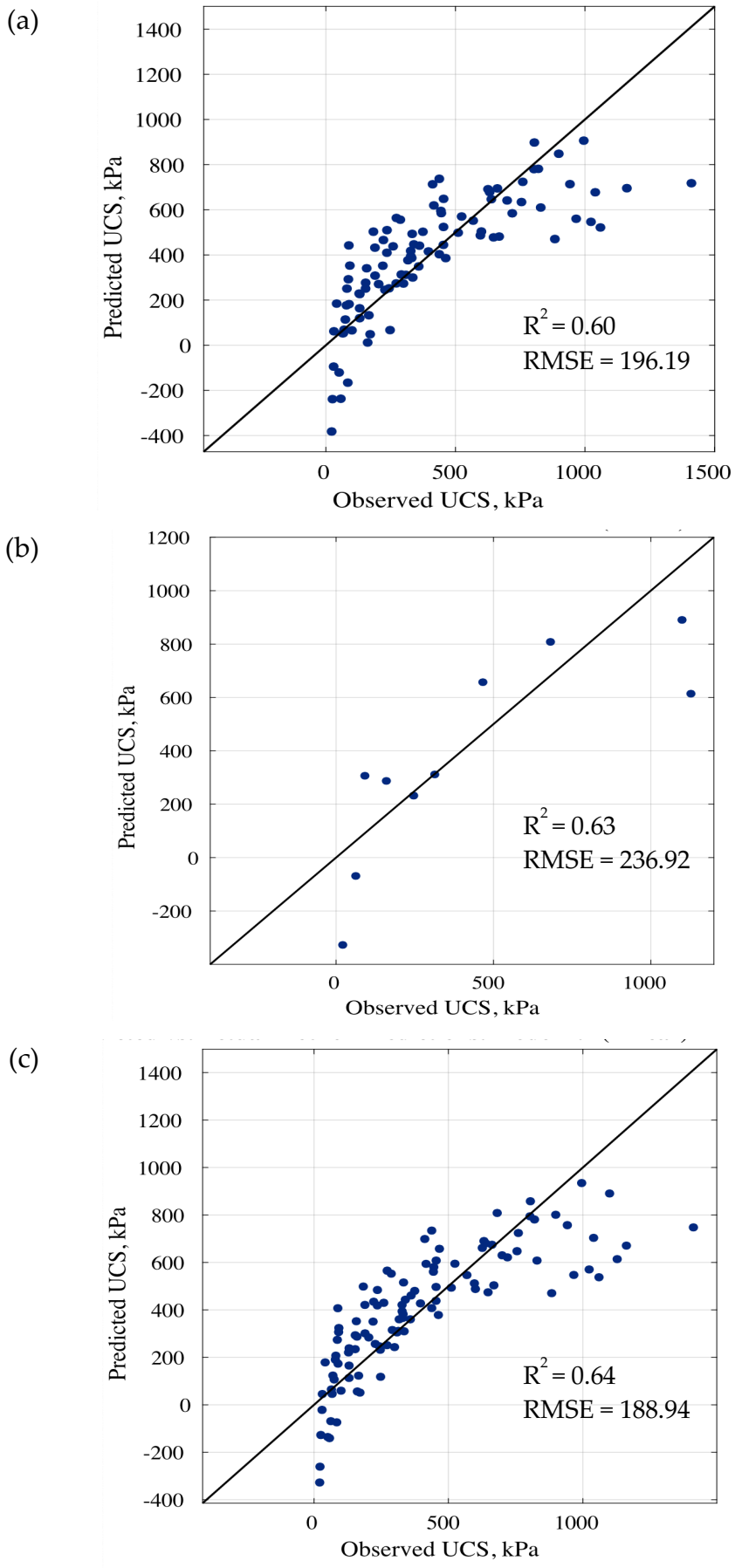


Figure 4.27: Linear Regression Model Analysis on (a) Training, (b) Test, (c) All data

4.6.2 Non-linear (Quadratic) Regression Model

The quadratic equation of nonlinear regression model according to the relationship among output and input variables may be presented as:

$$Y = b_0 + b_1X_1 + b_2X_2 + b_3X_2^2 + b_4X_3 + b_5X_3^2 + b_6X_4 + b_7X_4^2$$

Where, Y = Unconfined Compressive Strength, UCS (kPa),

X_1 = P=Fly Ash (%),

X_2 = w/P = Total Water to Binder ratio

X_3 = D = Curing Age (Days)

X_4 = L/P = Additives to FA ratio

$b_0, b_1 \ldots b_7$ = intercept and coefficients

Since, the linear and quadratic fit merge together in UCS vs Fly Ash curve, the relation. With fly ash has been taken as linear in the quadratic model.

One Step Non-linear (Quadratic) Regression Model

From MATLAB non-linear fit analysis,

$$\text{UCS (kPa)} = 1171.9 - 9.6859\,P + 2538.9\left(\frac{L}{P}\right) - 1920.1\left(\frac{L}{P}\right)^2 + 968.32\left(\frac{w}{P}\right) - 123.83\left(\frac{w}{P}\right)^2 + 12.214\,D - 0.1118\,D^2 \quad (4.2)$$

Where, test data set have a Root Mean Square Error (RMSE) = 224.34 and Correlation R^2 =0.686

Step-wise Non-linear (Quadratic) Regression Model

To get a better fit model, the whole data set has been divided into two parts as:

Set 1: $L/P \leq 0.5$

Set 2: $L/P > 0.5$

The two data set have been fitted with the same predicted quadratic equation and the equations become:

$$\text{UCS (kPa)} = 1305.1 - 7.4429\,P + 1265.7\left(\frac{L}{P}\right) - 107.26\left(\frac{L}{P}\right)^2 + 923.37\left(\frac{w}{P}\right) - 123.38\left(\frac{w}{P}\right)^2 + 8.5928\,D - 0.080392\,D^2 \quad [\text{When, } L/P \leq 0.5] \quad (4.3)$$

$$UCS\ (kPa) = 674.66 - 14.403\ P + 843.32\left(\frac{L}{P}\right) + 1054.1\left(\frac{L}{P}\right)^2 + 1026.5\left(\frac{w}{P}\right) + 126.12\left(\frac{w}{P}\right)^2 + 20.044\ D - 0.18475\ D^2 \quad [When,\ L/P > 0.5] \qquad (4.4)$$

The predicted UCS (kPa) found from both the equations are merged together and plotted against the observed UCS (kPa) to understand the model accuracy (Figure 4.28). The R^2 value has been found greater than 0.80 in training data set and all data set for both fit. Hence, model responses are less accurate in case of test data set i.e.R^2 <0.70 indicating the inability of explaining more than 30% of unseen data with the model. Also higher values Root Mean Square Error (RMSE) have been found.

4.6.3 Trial-based Non-linear Regression Model

Based on numbers of trial on different nonlinear equations, a simplified empirical equation has been taken as follows:

$$Y = b_0 + b_1 X_1^{\,b2}\ X_2^{\,b3}\ X_3^{\,b4}\ X_4^{\,b5}$$

Single Step Trial-based Non-linear Regression Model (TNR)

From MATLAB non-linear fit analysis,

$$UCS\ (kPa) = 2254.6\ P^{-0.22877}\left(\frac{w}{P}\right)^{-1.0961} D^{0.20741}\left(\frac{L}{P}\right)^{0.38142} - 356.54 \qquad (4.6)$$

The model fits with a greater accuracy with R^2 value of 0.88 and RMSE of 136.28 on test data.

Step-wise Trial-based Non-linear Regression Model (S-TNR)

Further increase in accuracy with an R^2 value of 0.97 and RMSE of 85.64 on test data has been achieved when the data has been divided into two parts.

Set 1: $L/P \leq 0.5$, and

Set 2: $L/P > 0.5$

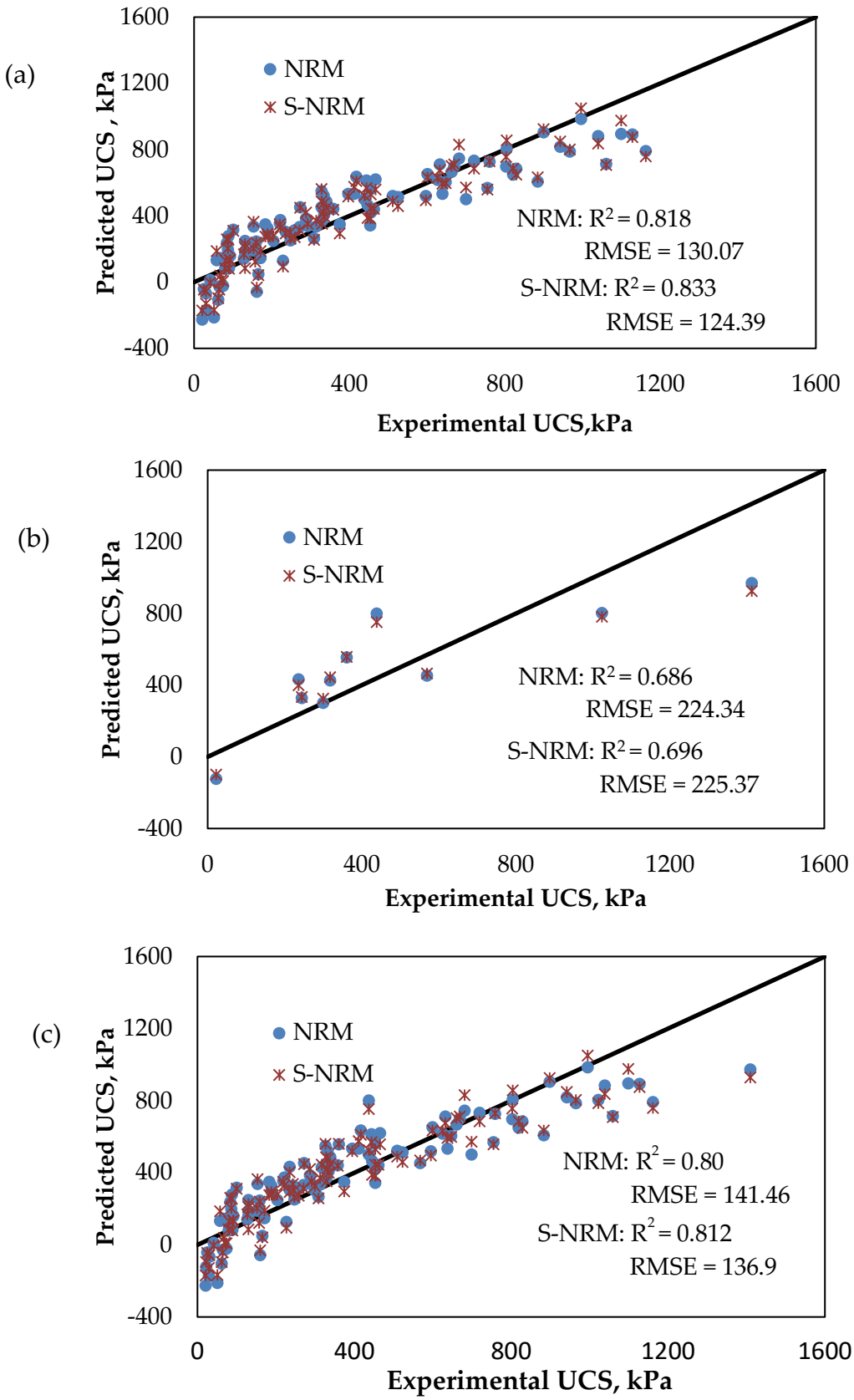


Figure 4.28: Comparison of Nonlinear Regression Model (NRM) and Step-wise Nonlinear Regression Model (S-NRM) on (a)Training Data ,(b) Test Data, (c) All Data

The equations from MATLAB nonlinear fit analysis found:

$$\text{UCS (kPa)} = 3625.7\ P^{-0.17072} \left(\frac{w}{P}\right)^{-2.0251} D^{0.28176} \left(\frac{L}{P}\right)^{1.2313} - 33.351, \text{ [When, } L/P \leq 0.5] \quad (4.7)$$

$$\text{UCS (kPa)} = 753.19\ P^{-0.129} \left(\frac{w}{P}\right)^{-0.4773} D^{0.12744} \left(\frac{L}{P}\right)^{-5.3425} - 1290.4, \text{ [When, } L/P > 0.5] \quad (4.8)$$

Figure 4.29 It shows the predicted Unconfined Compressive Strength (UCS) in kPa versus the actual UCS in kPa, so as to assess how correct the developed regression models are. The Single-Step Trial-based Non-linear Regression Model (TNR) performs well with a prediction accuracy of 88% for new data. However, the Step-wise Trial-based Non-linear Regression Model (S-TNR) performs better with a remarkable 97% accuracy of predicting new data. This demonstrates its ability to generalize and explain unseen data exceptionally well. Moreover, the S-TNR model shows remarkable consistency in achieving more than 91% accuracy when tested on the training data and combined dataset, proving to be robust and reliable in capturing the relationship among variables. The values of RMSE for the S-TNR model are much lower than those in previous models. This indicates that it has better predictive capability and accuracy.

The following three-dimensional (3-D) plots in Figures 4.30 to 4.32 provide more analysis. They compare the observed UCS values with those predicted by the new models. The experimental results, being based on observed data, are somewhat irregular and scattered. In contrast, the predicted results by the models show a smoother and more consistent trend but, at the same time, preserve a similar general pattern to the experimental observations. This alignment proves that the models actually do understand how the data behaves, even with the noise and unevenness in the experimental results.

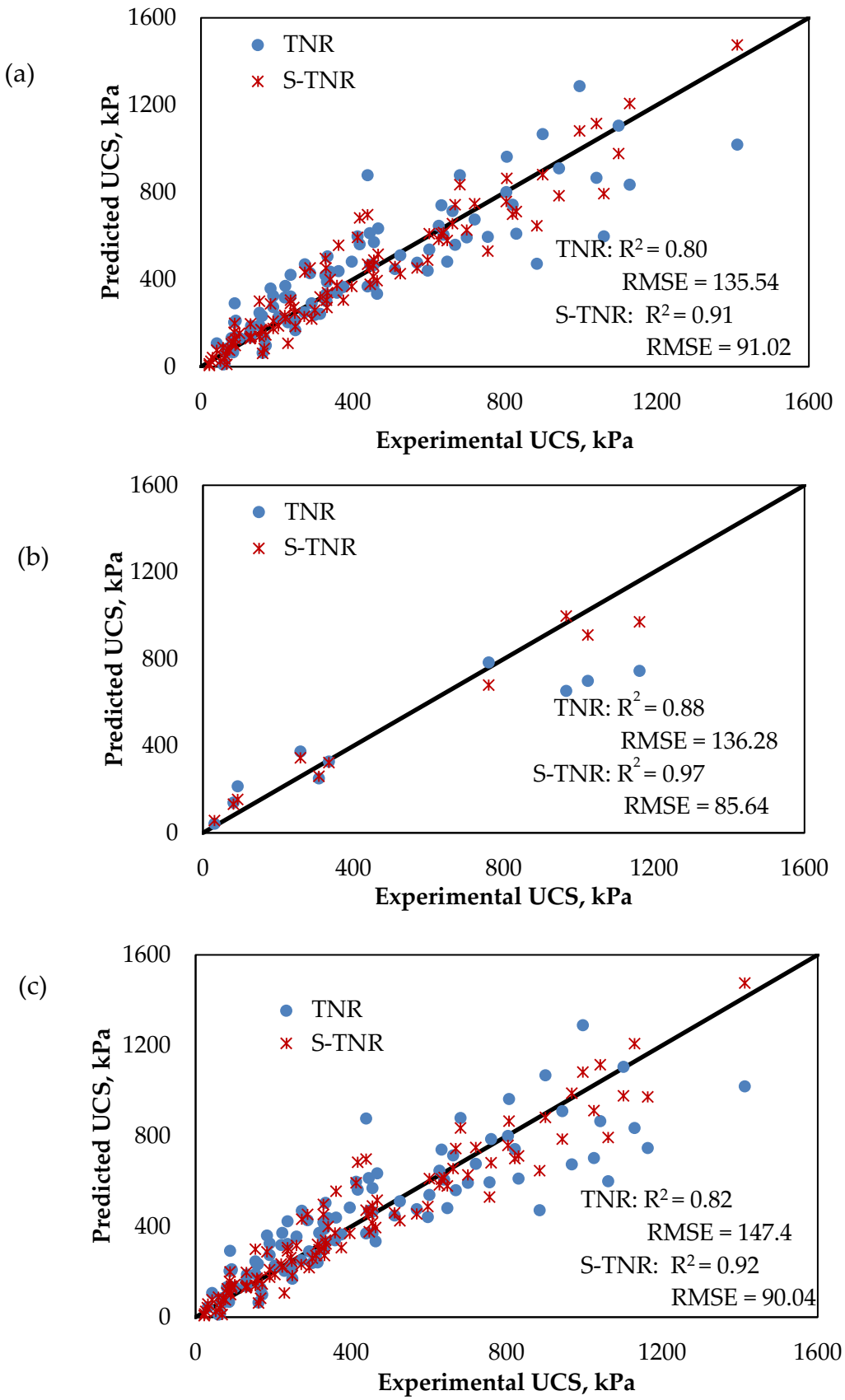
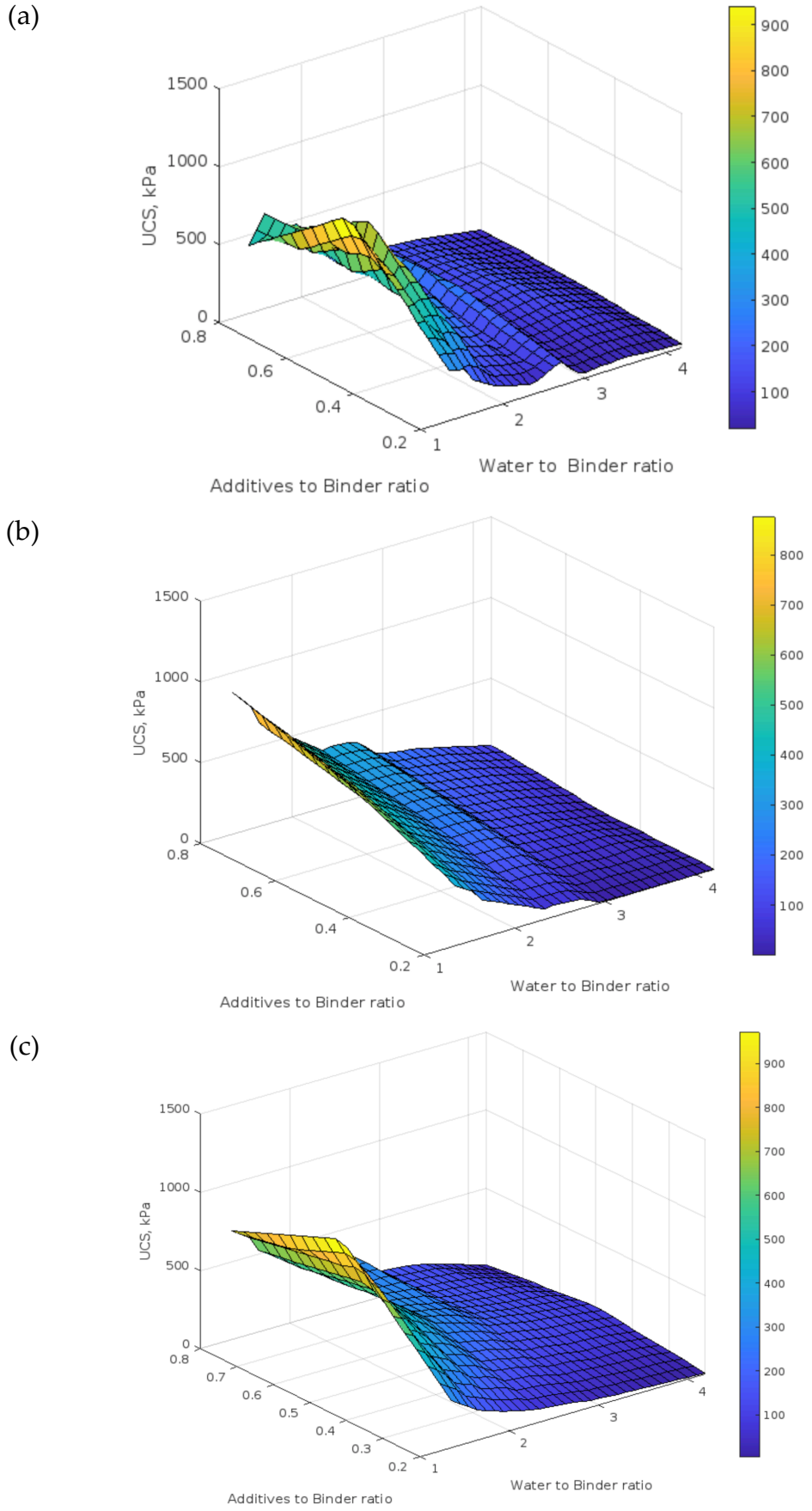


Figure 4.29: Comparison of Trial-based Nonlinear Regression Model (TNR) and Step-wise Trial-based Nonlinear Regression Model (S-TNR) on (a)Training Data ,(b) Test Data, (c) All Data



. Figure 4.30: UCS (kPa) at 14-days Curing period (a) Experimental UCS, kPa (b) Trial-based UCS, kPa (c) Step-wise Trial-based UCS, kPa

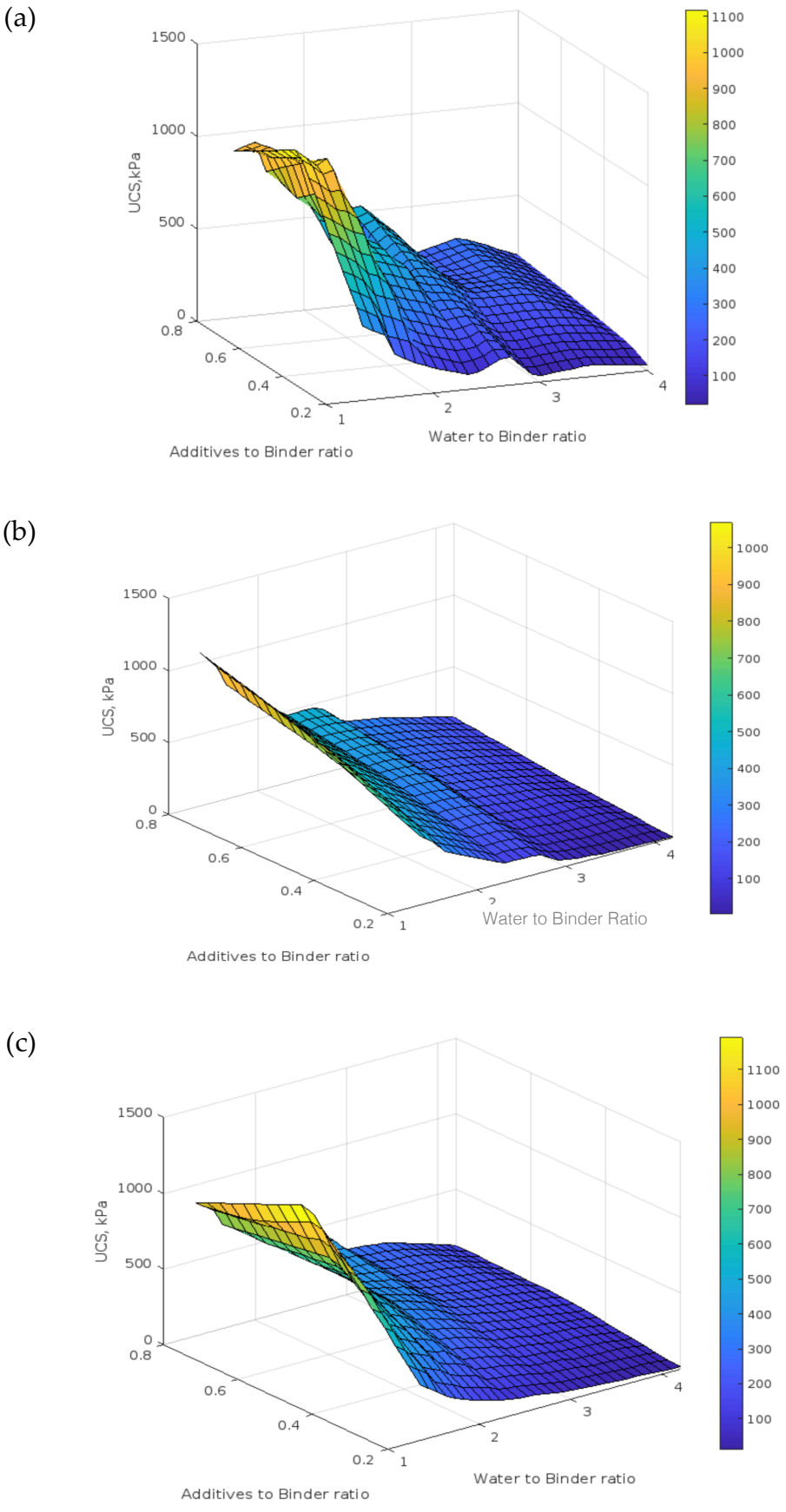


Figure 4.31: UCS (kPa) at 28-days Curing period (a) Experimental UCS, kPa (b) Trial-based UCS, kPa (c) Step-wise Trial-based UCS, kPa

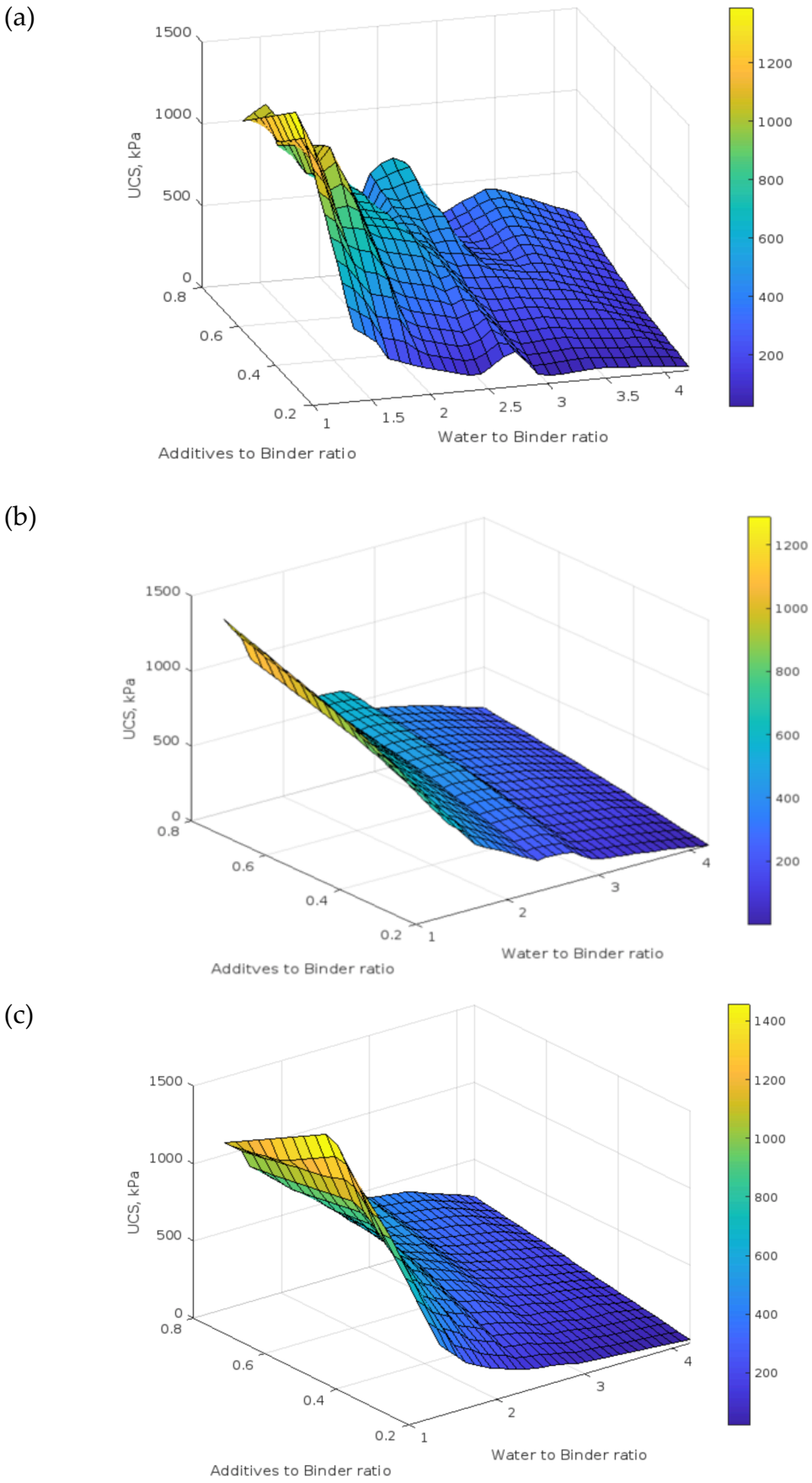


Figure 4.32: UCS (kPa) at 56-days Curing period (a) Experimental UCS, kPa (b) Trial-based UCS, kPa (c) Step-wise Trial-based UCS, kPa

Limitations of Equation-based Model

There are some limitations of prefixed equation-based empirical models. These are:

i. They are often specific to the dataset or conditions they were developed from, limiting generalization to new scenarios.
ii. Prefixed equations may oversimplify complex relationships, ignoring non-linearities or interactions between variables.
iii. They cannot adapt or improve with additional data or changing conditions.
iv. Poor-quality or biased data can lead to inaccurate models.
v. These models focus on statistical relationships rather than underlying physical or causal mechanisms.

These limitations can be overcome if the models are developed with machine learning algorithms.

Machine Learning Model

Machine learning models are computational systems that use algorithms to look for patterns, relationships, or trends from data and make predictions or action based on the data. Comparison of Prediction Models. There are several benefits of machine learning models which includes:

i. Capture complex, non-linear relationships between variables.
ii. Identify and mitigate the impact of outliers.
iii. Reduce manual intervention by automatically identifying patterns.
iv. Handle large datasets efficiently.
v. Provide highly accurate predictions, especially for complex problems.
vi. Applicable across various domains

Optimization

Optimization is a core part of machine learning; it is the process of minimizing or maximizing an objective function—possibly including a loss function—by changing the parameters of a model. Commonly used algorithms are Gradient Descent and its variants (SGD, Adam, RMSProp), which adjust parameters iteratively using gradients. Many problems arise, such as non-convex loss landscapes, vanishing or exploding gradients, and overfitting, so different strategies must be used, like regularization, dropout, or adaptive learning rates. Recent developments, such as Bayesian optimization and hyperparameter tuning techniques, have improved the performance and generalizability of models. These optimization strategies are critical for training resilient and effective machine learning models.

Standardization

Standardization is an important preprocessing technique in machine learning that scales features to have zero mean and unit standard deviation, enhancing the performance of the model as well as the numerical stability. It is also necessary for algorithms sensitive to feature scaling, such as Support Vector Machines and Gradient Descent-based methods.

The standardized value:

$$z = \frac{x - \mu}{\sigma}$$

Where, μ : average

σ : amount of variation

This allows the model to learn faster and perform better on new data.

Validation in Machine Learning Model

K-fold cross-validation method has been applied in machine learning models in this study with K value of 5. K-fold cross-validation is a resampling methodology that will estimate how well a model will generalize to an entirely new, unseen data.

In 5-fold cross-validation, dataset is divided into 5 equal or nearly equal parts (also known as "folds"). Later, the model is trained on 4 folds (training set) and validated on the remaining fold (validation set). This process is then repeated 5 times, with each of the 5 folds being used once as the validation set and 4 times as part of the training set.

Steps Involved in 5-Fold Cross-Validation:

i. Divide the whole dataset into 5 parts (folds).
ii. Train the model on 4 of the folds (80% of the data) and validate it on the remaining 1 fold (20% of the data).
iii. Repeat this whole process for each fold so that each fold serves as the validation set once.
iv. Finally, take an average of the performance metrics (such as R^2 RMSE etc.) from each fold to obtain an overall performance estimate.

Hyperparameter

In machine learning, a hyperparameter is a variable that is set before the training process begins and is used to control the behavior of the learning algorithm. Hyperparameters are not learned from the data; instead, they are fixed by the practitioner and directly influence how the model learns from the data. The machine learning models and the hyperparameters used to develop the models are tabulated in Table 4.2.

Table 4.5: Hyperparameters of Machine Learning Models

Model Name	**Hyperparameters**
Boosted Tree (BT)	Minimum Leaf Size: 8, Numbers of learners: 30, Learning rate:0.1
Cubic Support Vector Machine (C-SVM)	Kernel function: Cubic, Kernel Scale: Automatic, Box constraint: Automatic, Epsilon: Auto, Standardized data: Yes
Exponential Gaussian Process Regression (E-GPR)	Basis function: Constant, Kernel function: Exponential, Use isotropic kernel: yes, Kernel Scale: Automatic, Signal Standard deviation: Automatic, Sigma: Automatic, Standardized data: Yes, Optimized numeric parameters: Yes. (Bayessianopt)
Tri-layered Artificial Neural Network (T-ANN)	Number of fully connected layers: 3, First layer size:10, Second layer size: 10, Third layer size:10, Activation: ReLU, Iteration limit: 1000, Regularization strength :0, Standardized data: Yes

4.6.4 Boosted Tree (BT) Model

Boosting is an ensemble-based machine learning model that combines a number of weak learners, usually decision trees, for a strong predictive model. Boosting works by additively training models in a sequence, with subsequent models correcting the errors made in previously trained models (Figure 4.33). The main aim is to reduce the overall prediction error by emphasizing those misclassified or poorly predicted instances in subsequent iterations. Boosted models have been applied much in practice due to a reduction of bias and great variability in giving very accurate predictions.

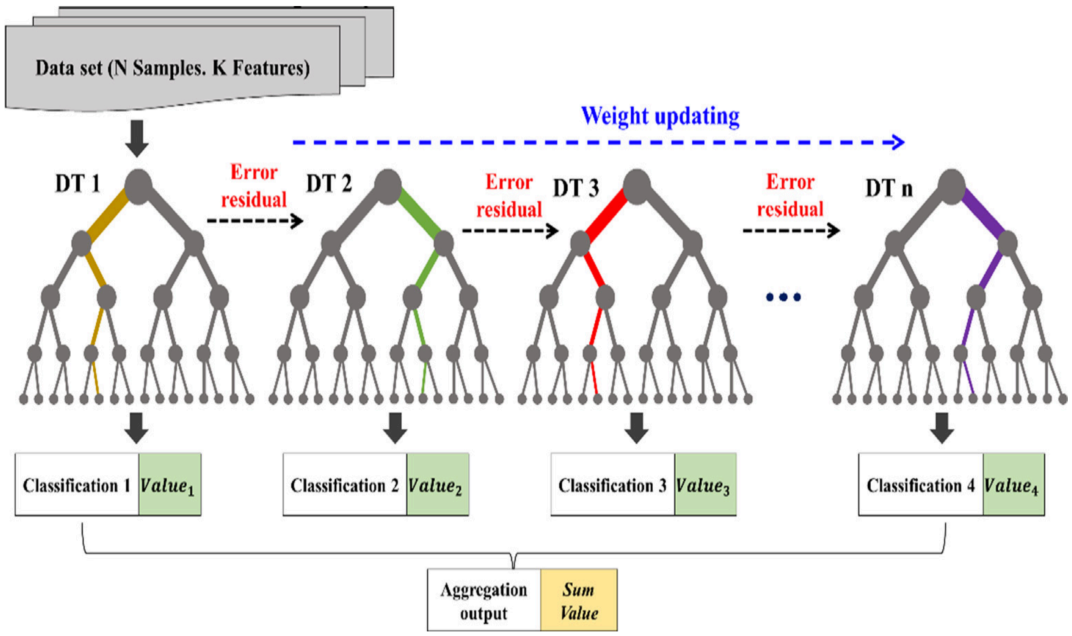


Figure 4.33: Mechanism of Boosted Tree Model (Chen et al., 2021)

General Equation:

$$F(x) = F_0(x) + \sum_{m=1}^{N} \gamma_m h_m(x)$$

Where, $F(x)$: The final prediction of the boosted model for input x.

$F_0(x)$: The initial prediction

M: The total number of trees (iterations).

$h_m(x)$: The prediction from the m-th weak learner (decision tree).

γ_m: The weight or learning rate for the mmm-th tree (typically determined during training).

$\sum_{m=1}^{N} M$: The cumulative contribution of all M weak learners

Initializing the Model:

$$F_0(x) = \arg\min (c) \sum_{i=1}^{N} L\ (y_i, c)$$

Where, $L(y_i, c)$= Loss function for the true label y_i and prediction c.

Updating with Weak Learners:

$$h_m(x) = \arg\min (h)\ \sum_{i=1}^{N} (\text{Gradient}_i \cdot h(x_i) + \text{Regularization})$$

Update the Model:

$$F_m(x) = F_{m-1}(x) + \gamma_m h_m(x)$$

Figure 4.34 shows the performance of boosted. Tree model on training, test and all data set. The is well fitted with the training data with an R^2 value of 0.81 and all data with R^2 value of 0.90. The model accuracy is evaluated with the response to unseen data. In test data set, which is unseen by the model while training, model fits excellently with a predictability of 92%. The value of root mean square error (RMSE) has also been lowered by the model.

4.6.5 Cubic Support Vector Machine (C-SVM) Model

A Support Vector Machine (SVM) is a supervised machine learning model used for classification and regression tasks. SVM works by finding the optimal hyperplane that separates data points belonging to different classes with the largest possible margin. It aims to minimize classification errors while maximizing the margin between the closest data points (called support vectors) and the decision boundary. Figure 4.35 shows the mechanism of classifying data with hyper plane.

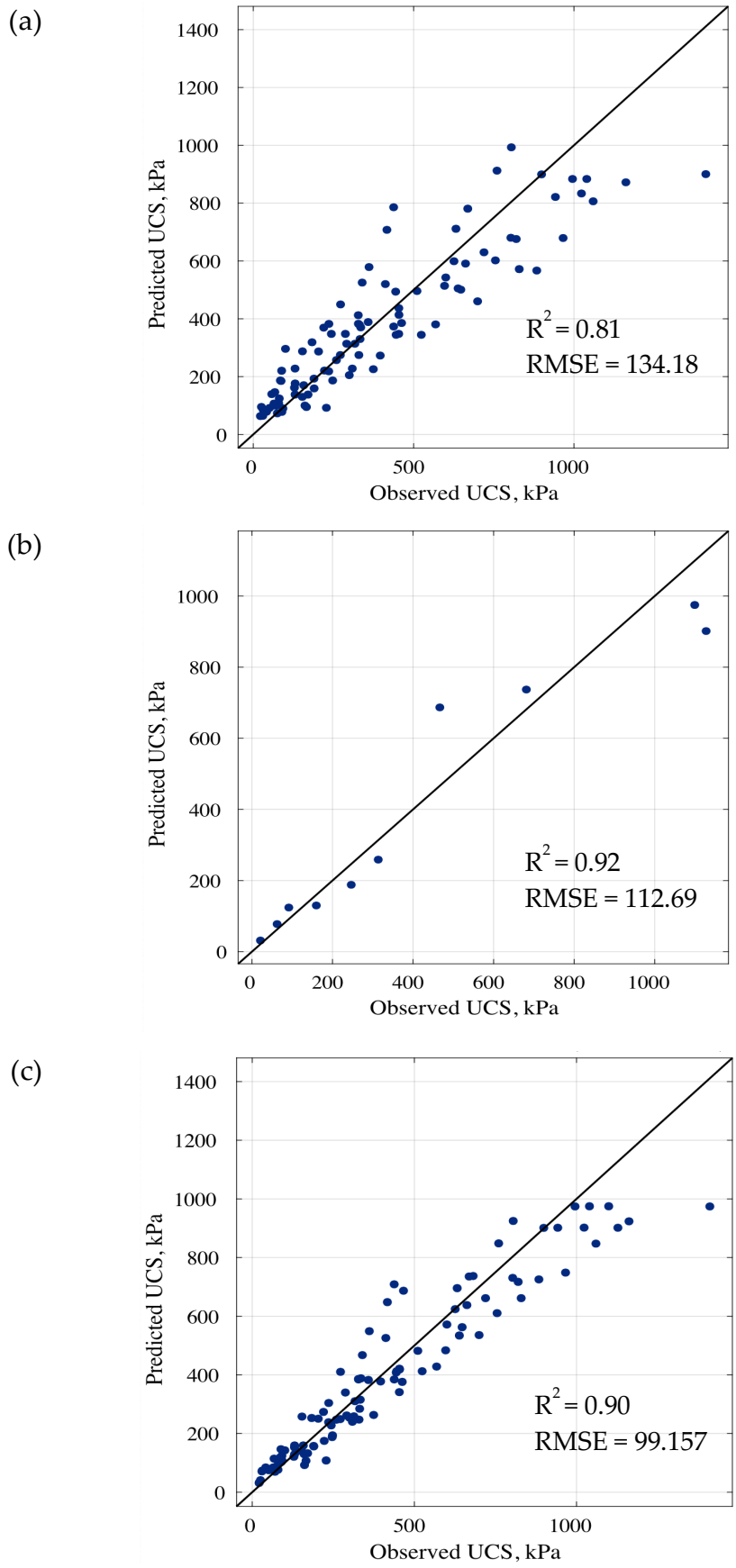


Figure 4.34: Boosted Tree Model Analysis on (a) Training, (b) Test, (c) All data

The Cubic Support Vector Machine (C-SVM) is a variation of the standard Support Vector Machine (SVM) model that uses a cubic kernel function. The cubic kernel maps input data into a higher-dimensional feature space using polynomial transformations, allowing the model to capture more complex relationships in the data. This makes C-SVM suitable for datasets with nonlinear separations. Figure 4.36 shows the model performance.

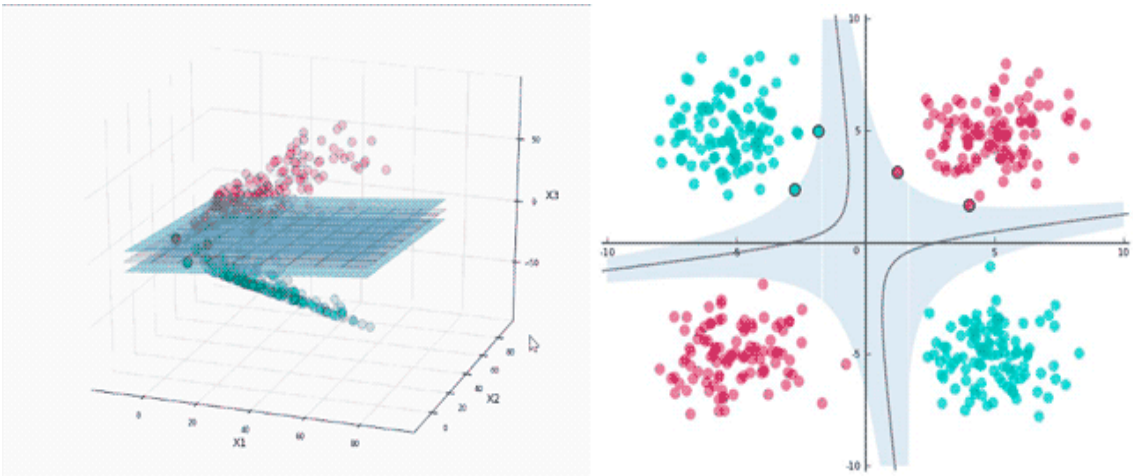


Figure 4.35: Mechanism of C-SVM Model (Source: https://medium.com/cube-dev/support-vector-machines-tutorial-c1618e635e93)

Equation in Support Vector Machine:

$$\min(w,b,\xi)\ \frac{1}{2}\|w\|^2 + C\sum_{i=1}^{n}\ \xi i$$

Subject to:

$$y_i(w\cdot x_i+b)\geq 1-\xi_i,\ \ \xi_i\geq 0,\quad \text{for } i=1,\ldots,n$$

Where, w : weight vector,

b : bias term,

ξ_i : slack variables that allow for some misclassification,

C : the regularization parameter

y_i : the class label of the i-th training sample (+1 or −1),

x_i : the feature vector of the i-th training sample.

Cubic Kernel Function:

$$K(x,y) = (x \cdot y + c)^3$$

Where, K(x,y): the kernel function

' · ' denotes the dot product of the vectors x and y,

c : constant

The Cubic Support Vector Machine Model fits well with the training data with an R^2 value of 0.85 and all data with R^2 value of 0.85. The model accuracy is evaluated with the response to unseen data. In test data set, which is unseen by the model while training, model fits excellently with a predictability of 91%. The value of root mean square error (RMSE) has also been lowered by the model than the linear regression model.

4.6.6 Exponential Gaussian Process Regression (EGPR) Model

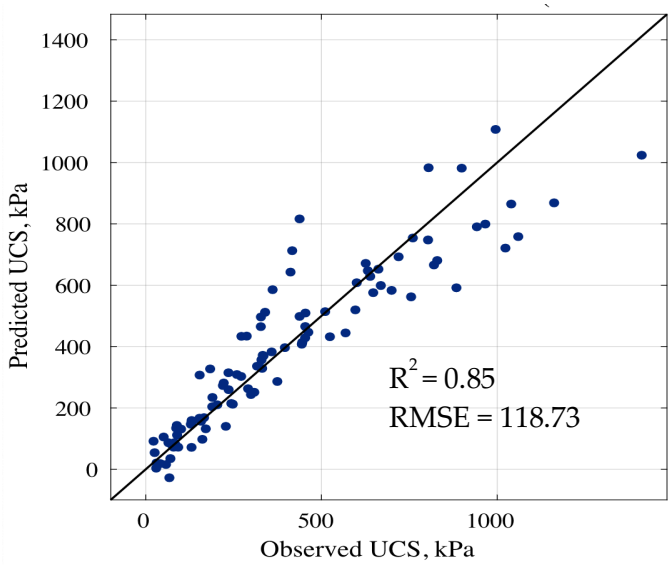
Gaussian Process Regression (GPR) is a non-parametric, Bayesian approach to regression that is particularly useful for predicting unknown functions. It assumes that the observed data can be described by a set of random variables that follow a joint Gaussian distribution. The Exponential Gaussian Process Regression (EGPR) model is a variant of the Gaussian Process Regression (GPR) technique that incorporates an exponential kernel function. EGPR is a non-parametric, probabilistic machine learning model widely used for regression tasks. It is particularly effective for capturing non-linear relationships between variables and quantifying uncertainty in predictions. The exponential kernel function ensures smoothness in the prediction while effectively modeling complex patterns in the data.

General Prediction Formula:

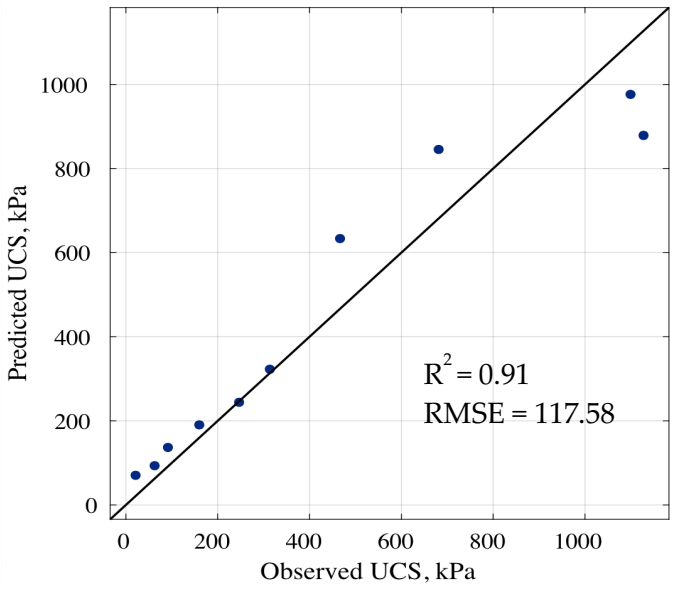
The prediction for a Gaussian Process is given as

$$\hat{y}(x_*) = K(x_*,X)[K(X,X)+\sigma_n^2 I]^{-1} y$$

(a)



(b)



(c)

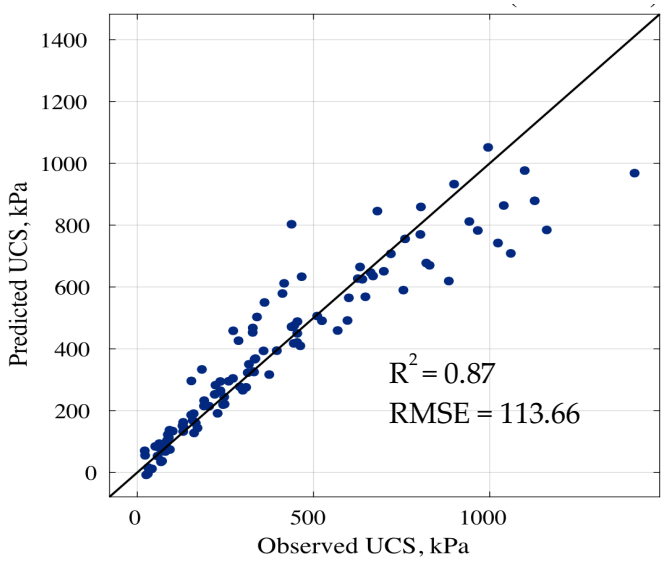


Figure 4.36: Cubic Support Vector Machine Model Analysis on (a) Training, (b) Test, (c) All data

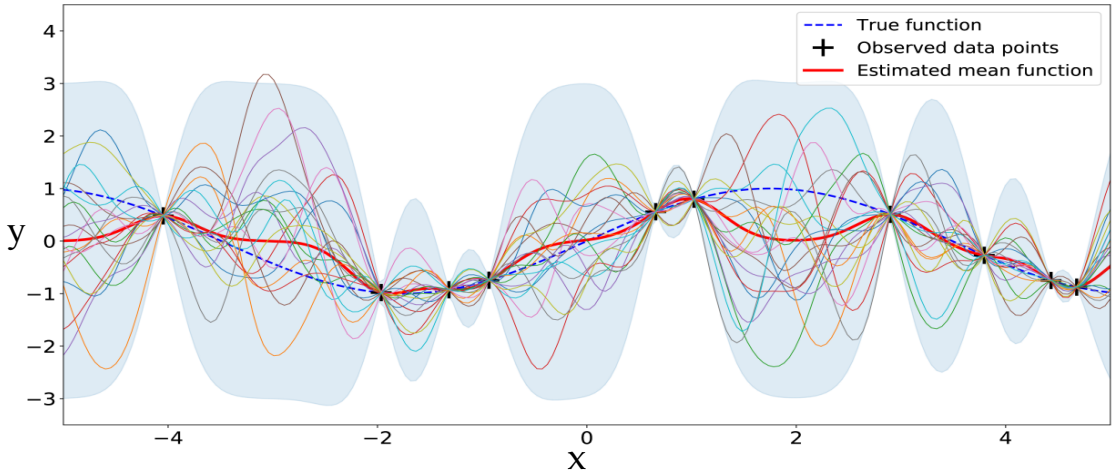


Figure 4.37: Illustration of Gaussian Process Regression Model (Source: https://arxiv.org/html/2009.10862v5)

Where, $\hat{y}(x_*)$: Predicted output for a new input x_*,

$K(x_*,X)$: Kernel function between the test input x_* and training inputs X

K(X,X): Kernel matrix computed for training data

σ_n^2: Noise variance.

y: Observed training outputs.

Exponential Kernel Function:

The kernel function $K(x_i,x_j)$ in EGPR is defined as:

$$K(x_i,x_j) = \exp(-||x_i-x_j||^2/2l^2)$$

Where, $||x_i-x_j||^2$: Euclidean distance between inputs x and x_i and x_j.

l: Length scale parameter that controls the smoothness of the function.

Posterior Variance (Uncertainty):

$$Var(x_*)=K(x_*,x_*)-K(x_*,X)\,[K(X,X)+\sigma_n^2 I]^{-1}K(X,x_*)$$

This equation provides the uncertainty of the prediction at x_*.

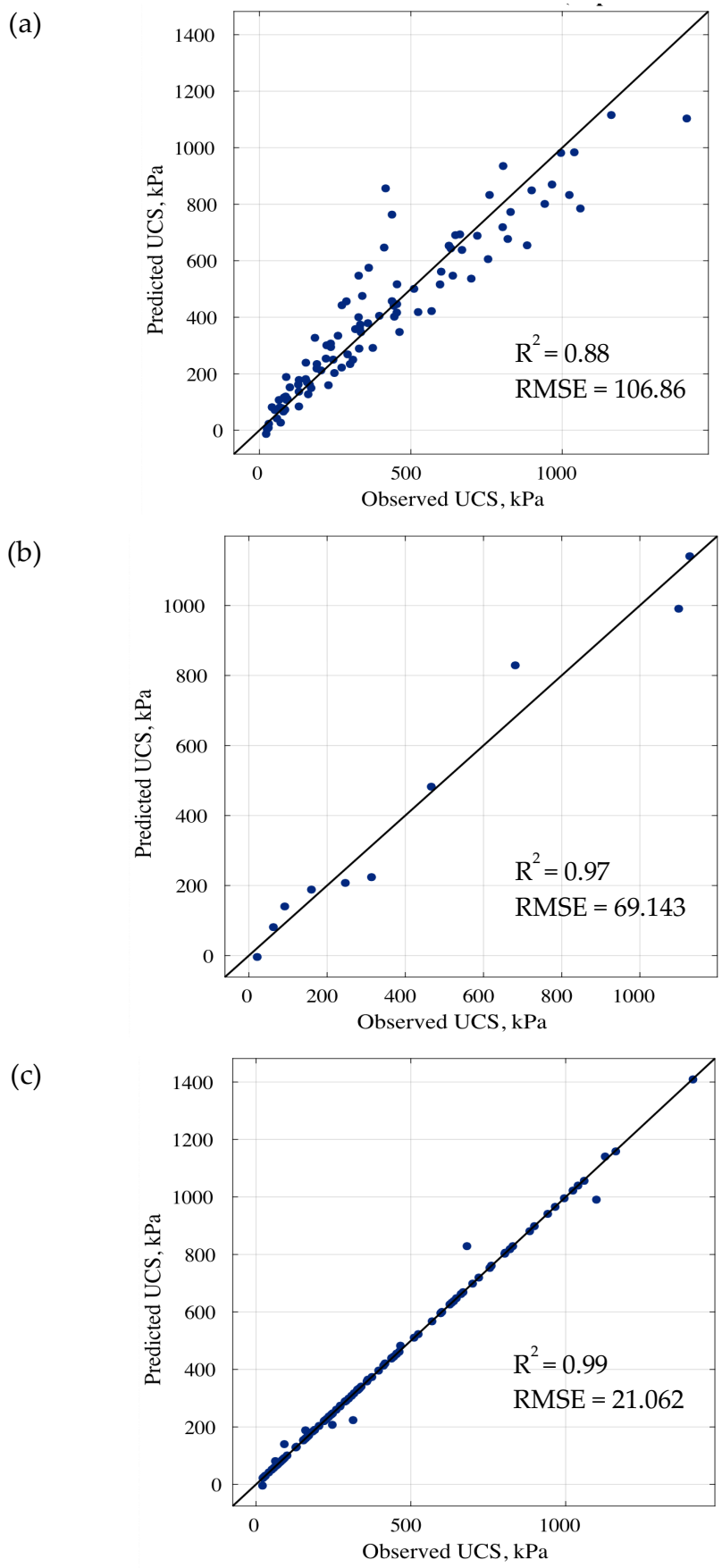


Figure 4.38: Exponential Gaussian Process Regression Model Analysis on (a) Training, (b) Test, (c) All data

Figure 4.38 shows the performance of the Exponential Gaussian Process Regression (EGPR) model in predicting Unconfined Compressive Strength (UCS) across the training, test, and combined datasets. The model demonstrates an excellent fit with the training data and whole data set , achieving a strong R^2 value of 0.88 and 0.99, reflecting its ability to generalize effectively across all observed data points. In the test dataset, the model showcases exceptional predictability with an R^2 value of 0.97. The RMSE value is also significantly lower compared to those of other models examined in this study.

4.6.7 Tri-layered Artificial Neural Network (T-ANN) Model

An Artificial Neural Network (ANN) is a deep machine learning algorithm inspired by the structure and functioning of the human brain. It is designed to recognize patterns, learn from data, and make decisions or predictions based on the learned information. It consists of an input layer (features), hidden layers (processes data), and an output layer (predictions) (Figure 4.39).

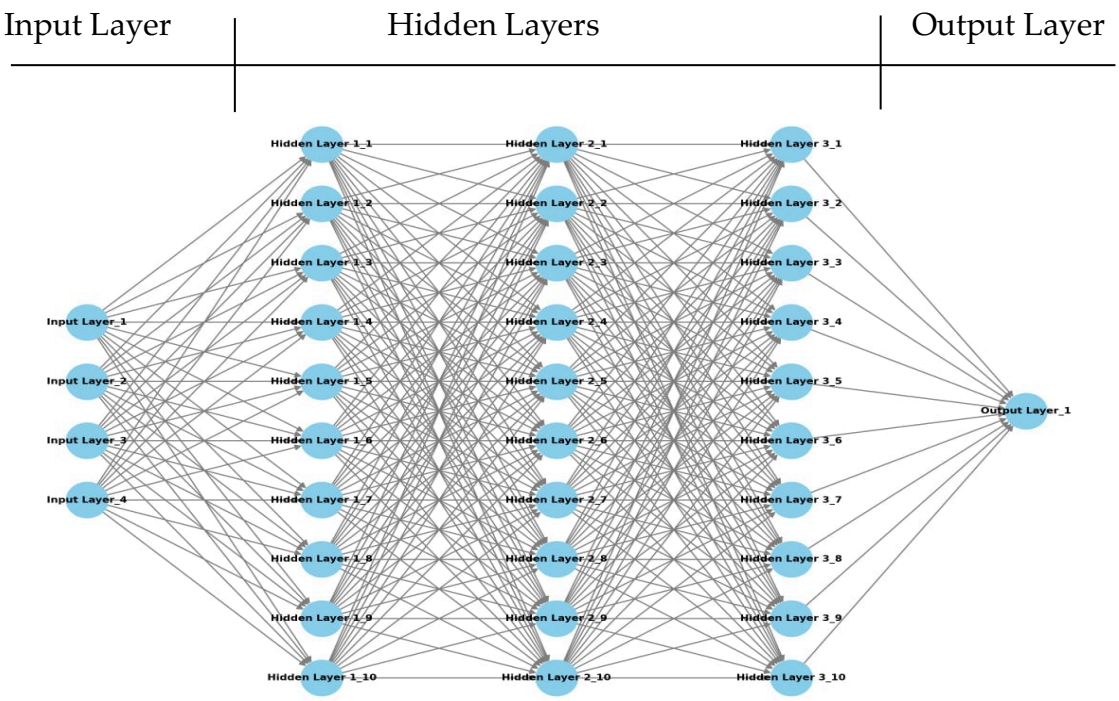


Figure 4.39: Architecture of Tri-layered Artificial Neural Network Model

Tri-layered Artificial Neural Network has 3 hidden layers for which it is named 'tri-layered'. Neurons in the layers are connected with weights and biases, and activation functions (ReLU, in this study) introduce non-linearity. Data flows forward through the network (forward propagation**),** and errors are minimized through backpropagation and optimization.

Input Layer:

Each neuron in a layer computes a weighted sum of its inputs:

$$z_j = \sum_1^n w_{ij}\, x_i + b_j$$

Where, z_j : Weighted sum for neuron j,

x_i :Input i to the neuron.

w_{ij} : Weight associated with input x_i and neuron j.

b_j: Bias term for neuron j.

n: Number of inputs.

Activation Function:

The output of the neuron is obtained by applying an activation function f:

$$a_j = f(z_j)$$

Where:, f: Activation function (ReLU).

a_j : Activation (output) of neuron j.

Output Layer:

The outputs from the last layer combine to produce the final prediction:

$$\hat{y} = \sum_{k=1}^m w_k\, a_k + b$$

Where, $\hat{y}$:Final output of the network.

a_k : Activations from the last hidden layer.

w_k: Weights connecting the last hidden layer to the output.

m: Number of neurons in the last hidden layer

Complete Form:

For a multilayer ANN with L layers, the general form of the network is:

$$a^{(l)} = f^{(l)} (W^{(l)}a^{(l-1)}+b^{(l)})$$

Where, l: Index of the layer.

$W^{(l)}$: Weight matrix for layer l.

$b^{(l)}$: Bias vector for layer l.

$a^{(l)}$: Activations from layer l.

$f^{(l)}$: Activation function for layer l

Figure 4.40 shows the performance of the Tri-layered Artificial Neural Network (T-ANN) Model in predicting Unconfined Compressive Strength (UCS) across the training, test, and combined datasets. The model demonstrates a good fit with the training data with a strong R^2 value of 0.71. It fits excellently with whole data set with R^2 value of 0.98, reflecting its ability to generalize effectively across all observed data points. In the test dataset, the model showcases exceptional predictability with an R^2 value of 0.96. This remarkable performance highlights the robustness of the T-ANN model and its capacity to accurately predict unseen data.

4.6.8 Comparison of Model Performances

A comparison chart showing all the model with their performance on the basis of R^2 and RMSE has been shown in the Figure 4.41. Among the equation based models, step-wise trial based non-linear model shows the highest value of R^2 and lowest value of models RMSE for every type of data set. Exponential Gaussian Process Regression (EGPR) Model has the highest performance with an $R^{2.}$ of 0.99 for all data set and 0.97 for test data set.

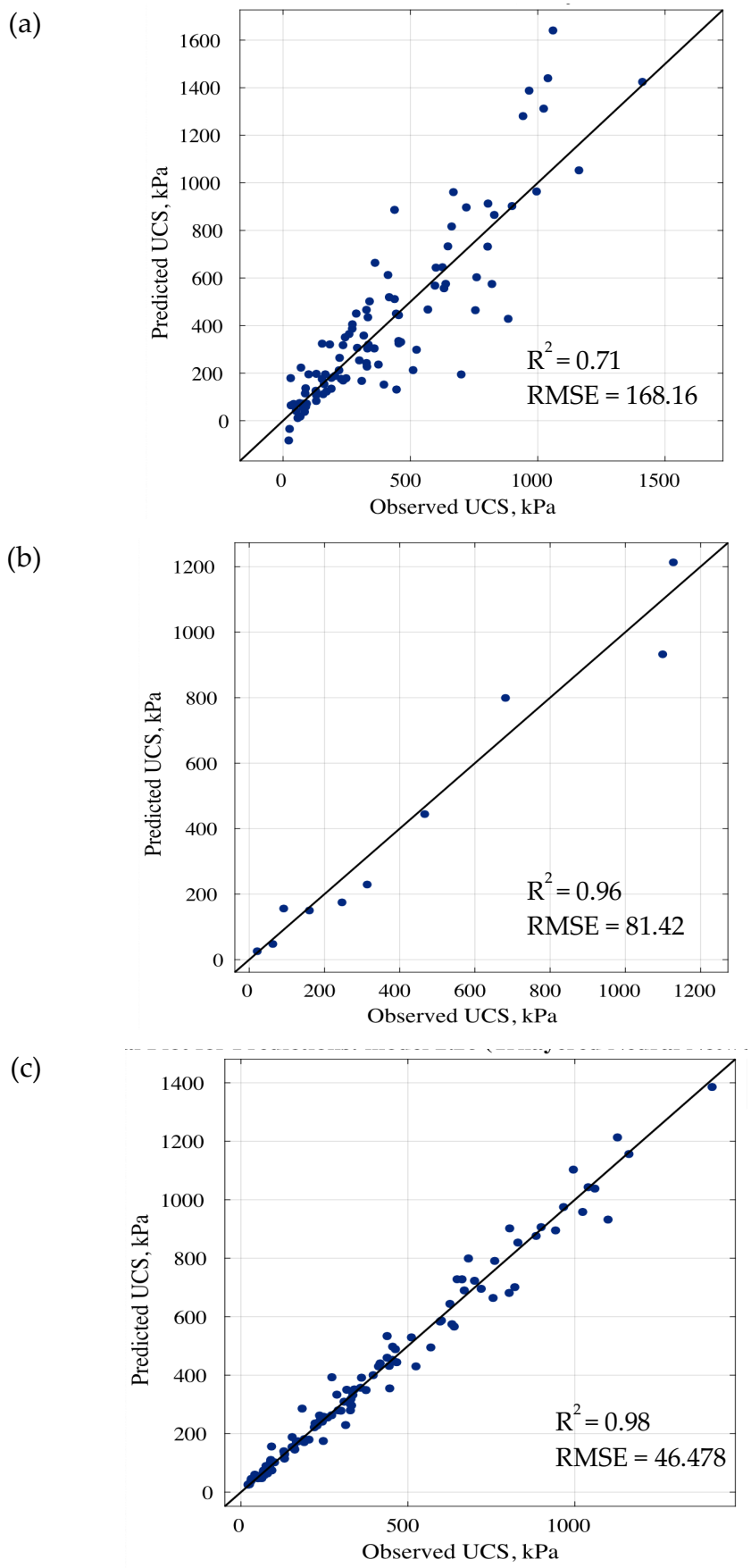


Figure 4.40: Tri-layered Artificial Neural Network Model Analysis on (a) Training, (b) Test, (c) All data

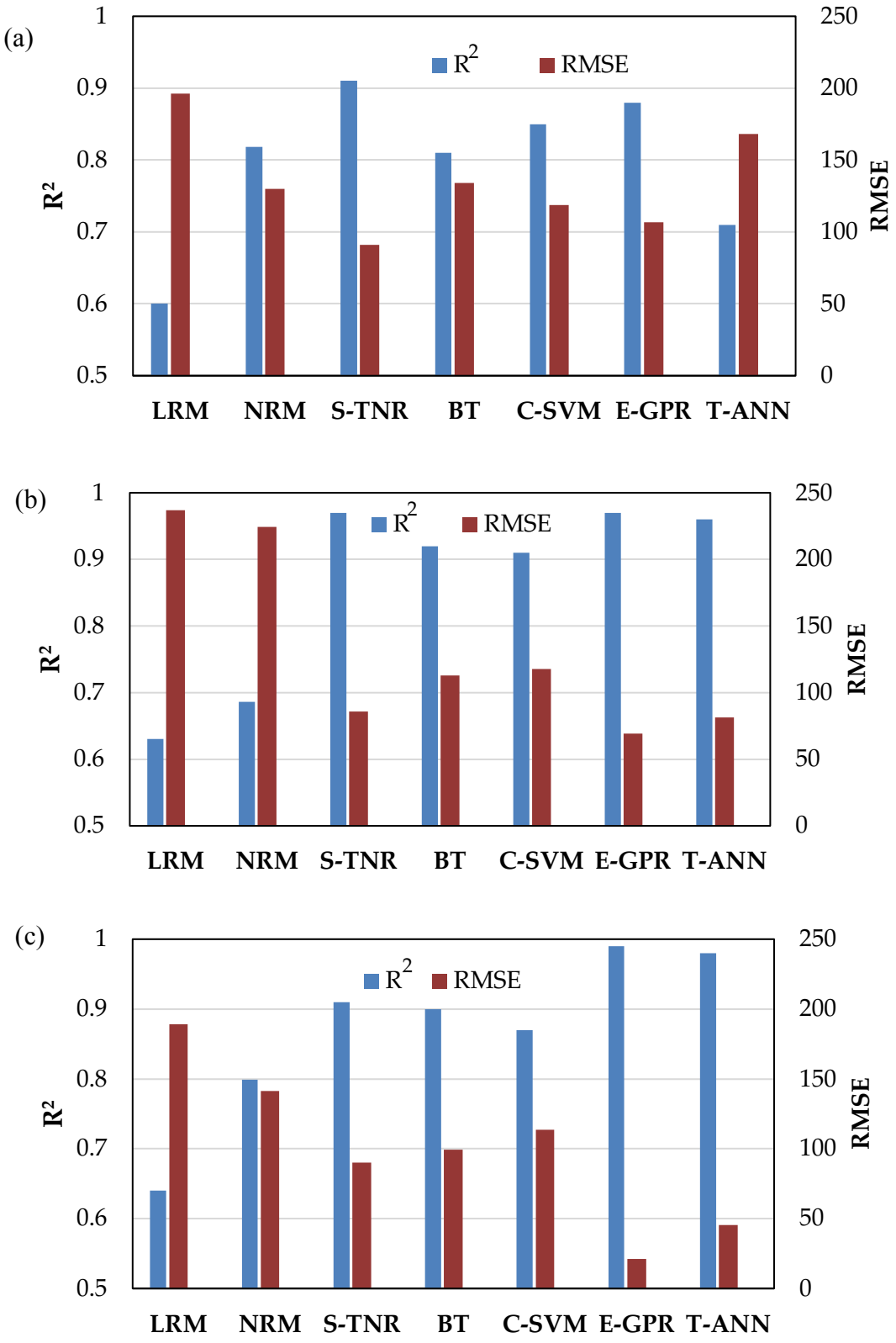


Figure 4.41: Comparison of Prediction Models on (a)Training Data ,(b) Test Data, (c) All Data

Considering the limitations in fixed equation based model and the ability of capturing complex relationship among the variables by the machine learning model, Exponential Gaussian Process Regression (EGPR) Model can be used for predicting the unconfined compressive strength (UCS).

Chapter 5 : CONCLUSIONS

5.1 GENERAL

This study aimed to observe the suitability of a geopolymer-based deep mixing method for soil improvement. Soil with varying degrees of geopolymer content and different proportions of precursor and water was mixed, and laboratory investigation and microstructural analysis were carried out. This chapter summarizes the major findings and discusses the scope of further research in this field.

5.2 KEY FINDINGS

The findings of the present study can be summarized as follows:

i. The unconfined compressive strength was maximum when the fly ash content is at maximum proportion (i.e. 25% of dry soil weight) with activator content of 50% of the binder (fly ash) and soil moisture content is 75% of liquid limit.

ii. Geopolymer-treated soil provides 11 times and 26 times larger unconfined compressive strength than the untreated soil having a water content of 75% of liquid limit and equal to liquid limit respectively at the highest binder content (i.e., 25% of dry soil weight) and optimum additives of 50% of binder. An increase of 102 times in strength has been provided by the geopolymer of 25% binder and additive of 80% of the binder at a moisture content of 125% of the liquid limit.

iii. Additive content is most effective at 50% of binder weight in all moisture conditions.

iv. Significant change in Atterberg's limit was found in treated soil, which becomes more stable as liquid limit and Plasticity index increase with the increase of Geopolymer.

v. In most cases, the unit weight of the treated soil increases with the increase of Geopolymer content, which indicates densified and less porous soil after stabilization.

vi. Densification of soil with the bond with geopolymer has been observed in Scanning Electron Microscope (SEM) images and also in X-ray diffraction Pattern analysis.

vii. Regression analysis (both empirical equation based and machine learning) models have been developed. The best fitted model has been provided by Exponential Gaussian Process Regression with an R^2 value of 0.97, which indicates that 97% of experimented data can be explained by the model.

5.3 LIMITATIONS OF THE STUDY

There are some limitations of the study which are listed below:

i. The precursor binder content has been limited to 25% of dry soil weight according to previous study and the maximum unconfined compressive strength has been observed at that level of binder in this study. The effect of further increase in binder has not been addressed.

ii. The model is fitted only for this particular soil type. This may not be valid for different types of soil.

iii. Soil properties are not addressed in this model. Any change of the properties of soil might need re-modelling.

iv. The reactivity of the chemicals might be different depending on the source and level of purity which are not addressed. Only the amount of chemical used in soil stabilization has been taken as one of the input variables in the model.

5.4 RECOMMENDATIONS FOR FURTHER STUDY

This study was focused only on the low-plastic soils of a particular location and some fixed proportion of materials. The development of strength might be different for other types of soil and the regression model may also vary. The study can be continued with:

i. A wide category of soils, such as clay, organic soil, etc.,
ii. Different proportion of materials (i.e. fly ash, alkali activator, water)
iii. Addressing the reactivity of chemical activator by analyzing its properties.
iv. Observing other properties of geo-polymerized soil (i.e. shear strength, consolidation, permeability etc.)
v. Other kind of geopolymer (i.e. slag, rice husk ash, micro and/or nano-silica, coconut coir ash, bamboo ash etc.)
vi. Laboratory trial on small scale model of deep mixing column.
vii. In-situ trial to observe the properties of geo-polymerized soil
viii. Larger data set to build more precise Machine Learning model

References

Abdullah, H. H., Shahin, M. A., and Sarker, P. (2019). Use of Fly-Ash Geopolymer Incorporating Ground Granulated Slag for Stabilisation of Kaolin Clay Cured at Ambient Temperature. Geotechnical and Geological Engineering, 37(2), 721–740. https://doi.org/10.1007/s10706-018-0644-2

Abdullah, H. H., Shahin, M. A., and Walske, M. L. (2019). Geo-mechanical behavior of clay soils stabilized at ambient temperature with fly-ash geopolymer-incorporated granulated slag. Soils and Foundations, 59(6), 1906–1920. https://doi.org/10.1016/J.SANDF.2019.08.005

Adam, A. A. (2019). The Effects of Water to Solid Ratio, Activator to Binder Ratio, and Lime Proportion on the Compressive Strength of Ambient-Cured Geopolymer Concrete. Journal of the Civil Engineering Forum, 5(2), 161. https://doi.org/10.22146/jcef.43878

Adeyanju, E., Okeke, C. A., Akinwumi, I., and Busari, A. (2020). Subgrade Stabilization using Rice Husk Ash-based Geopolymer (GRHA) and Cement Kiln Dust (CKD). Case Studies in Construction Materials, 13. https://doi.org/10.1016/j.cscm.2020.e00388

Al-Qaisi, M. S., and Al-Waily, M. J. M. (2022). Experimental Study of Soft Clay Soil Improvement by Deep Mixing Method. Mathematical Modelling of Engineering Problems, 9(1), 224–232. https://doi.org/10.18280/mmep.090128

Bakri, A. M. Mustafa Al., Kamarudin, H., M., Bnhussain, A., Rafiza, R., and Zarina, Y. (2012). Effect of Na2SiO3/NaOH Ratios and NaOH Molarities on Compressive Strength of Fly-Ash-Based Geopolymer. 109(5), 503–508.

Bellato, D., Marzano, I. P., and Simonini, P. (2020). Microstructural Analyses of a Stabilized Sand by a Deep-Mixing Method. Journal of Geotechnical and

Geoenvironmental Engineering, 146(6), 1–10. https://doi.org/10.1061/(asce)gt.1943-5606.0002254

Chen, J., Huang, H. W., Cohn, A. G., Zhang, D. (2021) Machine Learning-based classification of Rock Discontinuity Trace : SMOTE Oversampling Integrated with GBT Ensemble Learning, International Journal of Mining Science and Technology, http://DOI: 10.1016/j.ijmst.2021.08.004

Criado, M., Palomo, A., and Fernández-Jiménez, A. (2005). Alkali activation of fly ashes. Part 1: Effect of curing conditions on the carbonation of the reaction products. Fuel, 84(16), 2048–2054. https://doi.org/10.1016/J.FUEL.2005.03.030

Cristelo, N., Glendinning, S., Fernandes, L., and Pinto, A. T. (2013). Effects of alkaline-activated fly ash and Portland cement on soft soil stabilisation. Acta Geotechnica, 8(4), 395–405. https://doi.org/10.1007/s11440-012-0200-9

Cristelo, N., Glendinning, S., Miranda, T., Oliveira, D., and Silva, R. (2012). Soil stabilisation using alkaline activation of fly ash for self compacting rammed earth construction. Construction and Building Materials, 36, 727–735. https://doi.org/10.1016/J.CONBUILDMAT.2012.06.037

Cristelo, N., Glendinning, S., and Pinto, A. T. (2011). Deep soft soil improvement by alkaline activation. Proceedings of the Institution of Civil Engineers: Ground Improvement, 164(2), 73–82. https://doi.org/10.1680/grim.900032

Dandautiya, R., Singh, A. P., and Kundu, S. (2018). Impact assessment of fly ash on ground water quality: An experimental study using batch leaching tests. Waste Management and Research, 36, 0734242X1877548. https://doi.org/10.1177/0734242X18775484

Davidovits, J. (2005). Geopolymer chemistry and sustainable development. https://www.researchgate.net/publication/284514069

Debanath, O. C. (2019). Performance Evaluation of Geopolymer Stabilized Soil. Department of Civil Engineering, Chittagong University of Engineering and Technology. .

Dehghanbanadaki, A., Rashid, A. S. A., Ahmad, K., Yunus, N. Z. M., Shahu, J. T., and Mohanty, M. (2022). Ultimate Bearing Capacity of Soft Soil Improved by DCM Columns: A Comparative Review. KSCE Journal of Civil Engineering, 26(6), 2653–2661. https://doi.org/10.1007/s12205-022-1463-9

Duchesne, J., Duong, L., Bostrom, T., and Frost, R. (2010). Microstructure study of early in situ reaction of fly ash geopolymer observed by environmental scanning electron microscopy (ESEM). Waste and Biomass Valorization, 1(3), 367–377. https://doi.org/10.1007/s12649-010-9036-4

Ekmen, A. B., Algin, H. M., and Özen, M. (2020). Strength and stiffness optimisation of fly ash-admixed DCM columns constructed in clayey silty sand. Transportation Geotechnics, 24. https://doi.org/10.1016/j.trgeo.2020.100364

Esmaeili, M., Astaraki, F., and Khajehei, H. (2020). Laboratory investigation on the effect of microsilica additive on mechanical properties of deep soil mixing columns in loose sandy soils. European Journal of Environmental and Civil Engineering, 24(3), 321–335. https://doi.org/10.1080/19648189.2017.1382394

Federal Highway Administration (FHA) Design Manual: Deep Mixing for Embankment and Foundation Support. (2013).

Fernández-Jiménez, A., Palomo, A., and Criado, M. (2005). Microstructure development of alkali-activated fly ash cement: a descriptive model. Cement and Concrete Research, 35(6), 1204–1209. https://doi.org/10.1016/J.CEMCONRES.2004.08.021

Frikha, W., Zargayouna, H., Boussetta, S., and Bouassida, M. (2017). Experimental Study of Tunis Soft Soil Improved by Deep Mixing Column.

Geotechnical and Geological Engineering, 35(3), 931–947. https://doi.org/10.1007/s10706-016-0151-2

Hamdhan, I. N., Anugrah, R. F. V., and Nurhalizaa, S. (2024). the Effect of Soil Improvement Patterns Using Deep Cement Mixing (Dcm) on Soft Soil Settlement. International Journal of GEOMATE, 27(119), 120–126. https://doi.org/10.21660/2024.119.4525

Han, J. (2015). Principles and Practices of Ground Improvement. ISBN 978-1-118-25991-7 (hardback); 978-1-118-41960-1 (ebk.); 978-1-118-42130-7 (ebk.)

Han, J., Oztoprak, S., Parsons, R. L., and Huang, J. (2007). Numerical analysis of foundation columns to support widening of embankments. Comput. Geotech., 34(6), 435–448.

Hardjito, D., and Rangan, B. (2005). Studies on fly ash-based geopolymer concrete. In Proc. 4th World … (Issue November). Curtin University of Technology.

Hodges, D.K., Filz, G.M., and Weatherby, D.E. (2008). Laboratory Mixing, Curing, and Strength Testing of Soil-Cement Specimens Applicable to the Wet Method of Deep Mixing, CGPR Report No. 48, Virginia Tech Center for Geotechnical Practice and Research, Blacksburg, VA.

Horpibulsuk, S., Miura, N. and Nagara, T.S. (2003). "Assessment of Strength Development in Cement-Admixed High Water Content Clays with Abrams' Law as a Basis," Geotechnique, 53(4), 439

Jackson, R. (2015). Manual of Soil Laboratory Testing. Environmental and Engineering Geoscience, 21(3), 247–248. https://doi.org/10.2113/gseegeosci.21.3.247

Jacobson, J.R., Filz, G.M., and Mitchell, J.K. (2003). Factors Affecting Strength Gain in Lime Cement Columns and Development of a Laboratory Testing Procedure, Virginia Transportation Research Council, Charlottesville, VA.

Kacemi, T., Atif Nawaz, M., Bakhtyar, B., and Nawaz, A. (2017). A Review on Carbon Emissions in Malaysian Cement Industry International Journal of Energy Economics and Policy A Review on Carbon Emissions in Malaysian Cement Industry. International Journal of Energy Economics and Policy , 7(3), 282–286. http:www.econjournals.com

Kanchan, S., Kumar, V., Yadav, K., Gupta, N., and Arya, S. (2015). Effect of Fly Ash Disposal on Ground Water Quality near Parichha Thermal Power Plant, Jhansi: A Case Study. Current World Environment, 10(2), 572–580. https://doi.org/10.12944/cwe.10.2.21

Khale, D., and Chaudhary, R. (2007). Mechanism of geopolymerization and factors influencing its development: A review. Journal of Materials Science, 42(3), 729–746. https://doi.org/10.1007/s10853-006-0401-4

Kitazume, M., Okano, K., and Miyajima, S. (2000). Centrifuge model tests on failure envelope of column type mixing method improved ground. Soils and Foundations 40(4).

Liu, Z., Cai, C. S., Liu, F., and Fan, F. (2016). Feasibility Study of Loess Stabilization with Fly Ash–Based Geopolymer. Journal of Materials in Civil Engineering, 28(5). https://doi.org/10.1061/(asce)mt.1943-5533.0001490

Lorenzo, G.A. and Bergado, D.T. (2003). "New Consolidation Equation for Soil-Cement Pile Improved Ground," Canadian Geotechnical Journal, 40, 265–275.

Luo, Yiping. , M. Jinhao. , W. Defa. , J. Lin. , X. Guobin. (2022). Experimental study on mechanical properties and microstructure of metakaolin based geopolymer stabilized silty clay. Construction and Building Materials, 316.

MR Coop, J. A. (1993). The mechanics of cemented carbonate sands. Geotechnique 43(1).

Miura, N., Horpibulsuk, S., and Nagaraj, T.S. (2002). "Engineering Behavior of Cement Stabilized Clay at High Water Content," Soils and Foundations, 41(5), 33–45.

Nguyen, T. N. (2024). Exploring Optimal Cement Deep Mixing Column Arrangements For Soft Ground Improvement: A Simplified Approach Investigation. International Journal of Scientific Research in Science, Engineering and Technology, 11(1), 1–7.

Onur, M. İ., Bıçakcı, M., Kardoğan, P. S. Ö., Erdağ, A., and Aghlmand, M. (2022). LABORATORY MODEL DESIGN FOR DEEP SOIL MIXING METHOD. Elektronički Časopis Građevinskog Fakulteta Osijek, 13(24), 59–69. https://doi.org/10.13167/2022.24.6

Pacheco-Torgal, F., Castro-Gomes, J., and Jalali, S. (2008). Alkali-activated binders: A review. Part 1. Historical background, terminology, reaction mechanisms and hydration products. In Construction and Building Materials (Vol. 22, Issue 7, pp. 1305–1314). https://doi.org/10.1016/j.conbuildmat.2007.10.015

Palomo, Á., Alonso, S., Fernandez-Jiménez, A., Sobrados, I., and Sanz, J. (2004). Alkaline activation of fly ashes: NMR study of the reaction products. Journal of the American Ceramic Society, 87(6), 1141–1145. https://doi.org/10.1111/j.1551-2916.2004.01141.x

Part, W. K., Ramli, M., and Cheah, C. B. (2015). An overview on the influence of various factors on the properties of geopolymer concrete derived from industrial by-products. Construction and Building Materials, 77, 370–395. https://doi.org/10.1016/J.CONBUILDMAT.2014.12.065

Phummiphan, I., Horpibulsuk, S., Sukmak, P., Chinkulkijniwat, A., Arulrajah, A., and Shen, S.-L. (2016). Stabilisation of marginal lateritic soil using high calcium fly ash-based geopolymer. Road Materials and Pavement Design, 17(4), 877–891. https://doi.org/10.1080/14680629.2015.1132632

Puppala, A. J., Madhyannapu, R. S., Nazarian, S., Yuan, D., and Hoyos, L. (2008). Deep Soil Mixing Technology for Mitigation of Pavement Roughness. FHWA/TX-08/0-5179-1, FHWA, Wash- Ington, DC.

Raftari, M., Dehghanbanadaki, A., Rashid, A. S. A., Kassim, K. A., and Mahjoub, R. (2024). Long-Term Compressibility and Shear Strength Properties of Cement-Treated Clay in Deep Cement Mixing Method. Transportation Infrastructure Geotechnology, 3381–3401. https://doi.org/10.1007/s40515-024-00414-6

Recommended Practice for Stabilization of Subgrade Soils and Base Materials. (2009). https://doi.org/10.17226/22999

Rios, S., Cristelo, N., Viana da Fonseca, A., and Ferreira, C. (2016). Structural Performance of Alkali-Activated Soil Ash versus Soil Cement. Journal of Materials in Civil Engineering, 28(2). https://doi.org/10.1061/(asce)mt.1943-5533.0001398

Sargent, P., Hughes, P. N., Rouainia, M., and White, M. L. (2013). The use of alkali activated waste binders in enhancing the mechanical properties and durability of soft alluvial soils. Engineering Geology, 152(1), 96–108. https://doi.org/10.1016/J.ENGGEO.2012.10.013

Singh, N. B. (2018). Fly ash-based geopolymer binder: A future construction material. In Minerals (Vol. 8, Issue 7). MDPI AG. https://doi.org/10.3390/min8070299

Singh, N. B., and Middendorf, B. (2020). Geopolymers as an alternative to Portland cement: An overview. Construction and Building Materials, 237, 117455. https://doi.org/10.1016/J.CONBUILDMAT.2019.117455

Siyal, A. A., Radin Mohamed, R. M. S., Shamsuddin, R., and Ridzuan, M. B. (2024). A comprehensive review of synthesis kinetics and formation mechanism of geopolymers. In RSC Advances (Vol. 14, Issue 1, pp. 446–462). Royal Society of Chemistry. https://doi.org/10.1039/d3ra06205h

The Environment Conservation Rules, 1997 .

Turan, C., Javadi, A. A., Vinai, R., and Russo, G. (2022). Effects of Fly Ash Inclusion and Alkali Activation on Physical, Mechanical, and Chemical Properties of Clay. Materials, 15(13). https://doi.org/10.3390/ma15134628

Usui, H., Some, D. D., Sindete, M. J., and Hino, T. (2024). Sustainable construction and quality of improved columns with three types of water-cement ratios on deep mixing method in Saga Lowland, Kyushu, Japan. Smart Construction and Sustainable Cities, 2(1). https://doi.org/10.1007/s44268-024-00030-w

Wassie, T. A., and Demir, G. (2024). Mechanical Strength and Microstructure of Soft Soil Stabilized with Cement, Lime, and Metakaolin-Based Geopolymer Stabilizers. Advances in Civil Engineering, 2024. https://doi.org/10.1155/2024/6613742

Xu, H., and Van Deventer, J. S. J. (2000). The geopolymerisation of alumino-silicate minerals. International Journal of Mineral Processing, 59(3), 247–266. https://doi.org/10.1016/S0301-7516(99)00074-5

Yaghoubi, M., Arulrajah, A., Miri Disfani, M., Horpibulsuk, S., and Leong, M. (2020). Compressibility and strength development of geopolymer stabilized columns cured under stress. Soils and Foundations, 60(5), 1241–1250. https://doi.org/10.1016/j.sandf.2020.07.005

Yamashita, E., Aristo Cikmit, A., Tsuchida, T., and Hashimoto, R. (2020). Strength estimation of cement-treated marine clay with wide ranges of sand and initial water contents. Soils and Foundations, 60(5), 1065–1083. https://doi.org/10.1016/j.sandf.2020.05.002

Yanase, S. (1968). Stabilization of marine clays by quicklime. Report of the Port and Harbour Research Institute. (in Japanese)., 7(4), 85–132.

Yenginar, Y., and Olgun, M. (2024). Physical, mechanical, and microstructural characteristics of fly ash replaced cement deep mixing columns. Bulletin of Engineering Geology and the Environment, 83(8), 1–24. https://doi.org/10.1007/s10064-024-03800-z

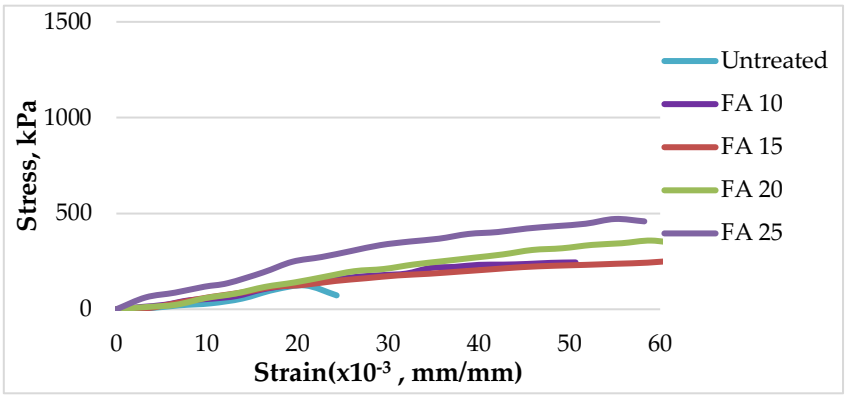
Yi, J. T., Goh, S. H., and Lee, F. H. (2013). Effect of sand compaction pile installation on strength of soft clay. Geotechnique, 63(12), 1029–1041. https://doi.org/10.1680/geot.12.P.108

Yin, K. S., Zhang, L. M., Zou, H. F., Luo, H. Y., and Lu, W. J. (2022). Key Factors for Deep Cement Mixing Construction for Undredged Offshore Land Reclamation. Journal of Geotechnical and Geoenvironmental Engineering, 148(8), 1–11. https://doi.org/10.1061/(asce)gt.1943-5606.0002848

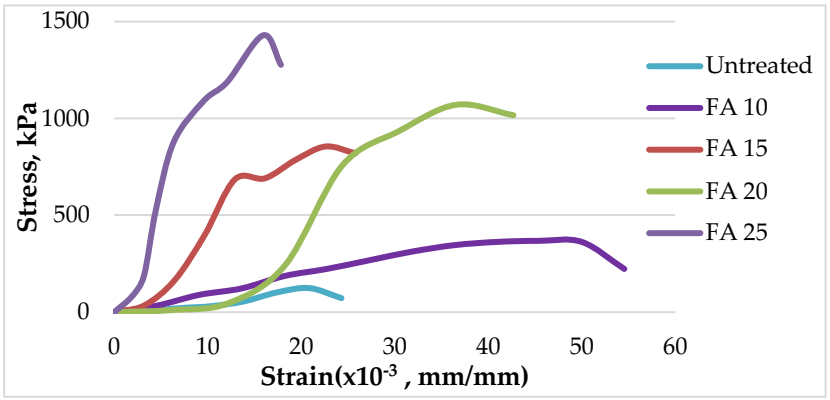
Zakaria, M. M., Mohamed, H. K., Hamdy, W., Kamash, E., Moubarak, A. H., Mohamed, [, Zakaria, M., Kamal, M., Hafez, W., Hamdy, E., Kamash, A., and Hassan, M. (2020). Stabilization of Soft Clay Soil by Deep Mixing. Life Sci J, 17(3), 1–15. https://doi.org/10.7537/marslsj170320.01

Appendices

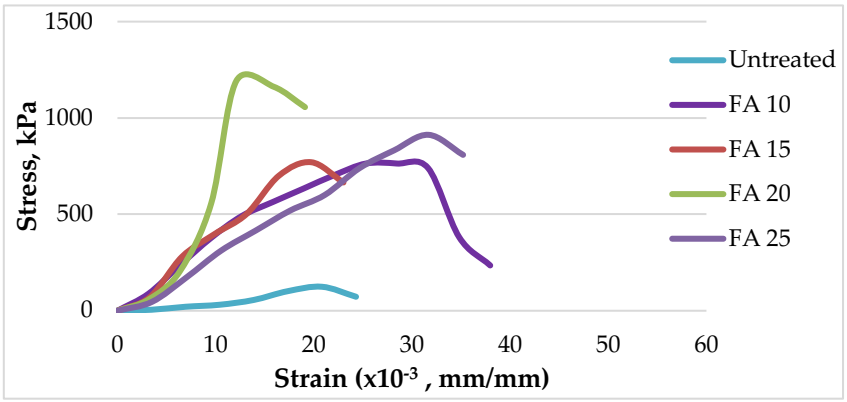
Appendix A: [Stress-Strain relationship of geo-polymerized Soil]



(i)

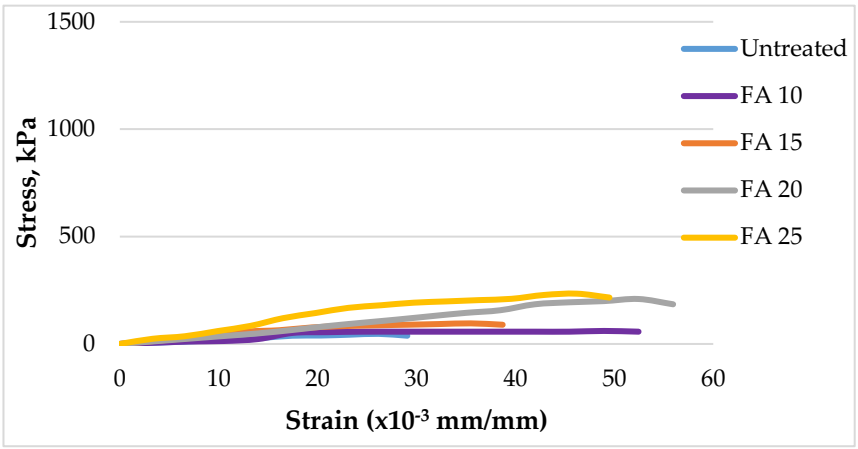


(ii)

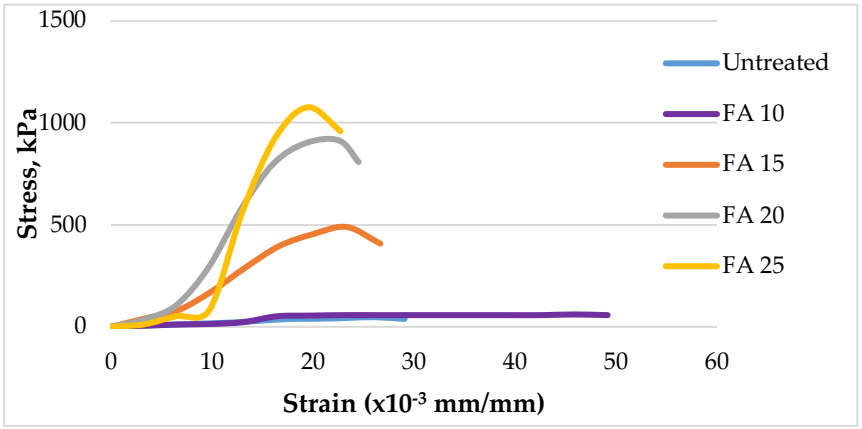


(iii)

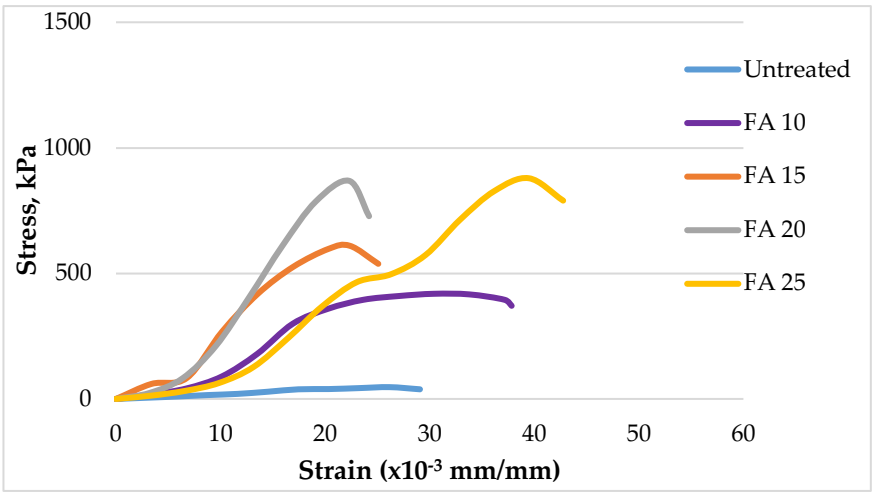
Figure A.1: Stress vs Strain Curve for Water Content=0.75 x Liquid Limit (i) L/P=0.2 (ii) L/P=0.5 (iii) L/P=0.8



(i)

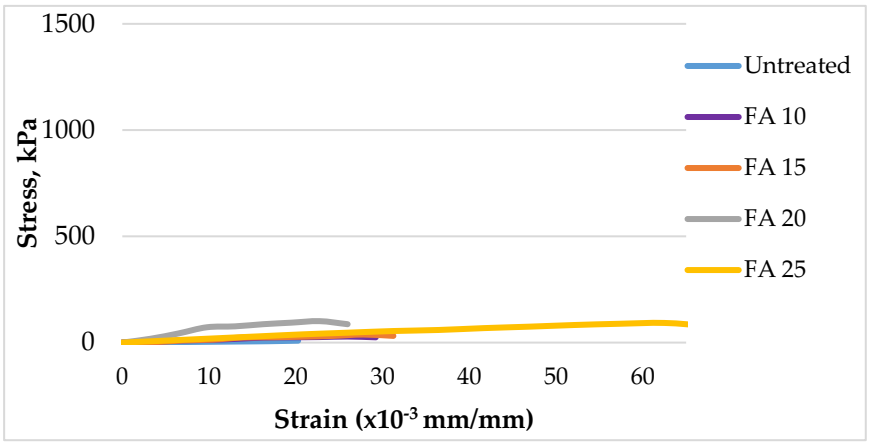


(ii)

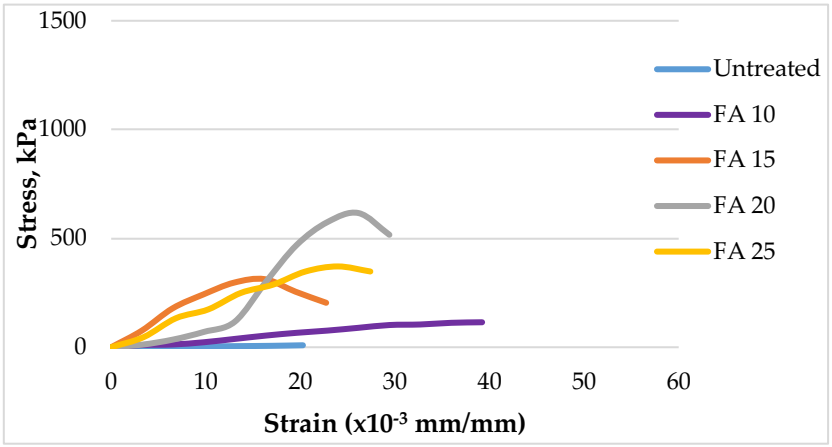


(iii)

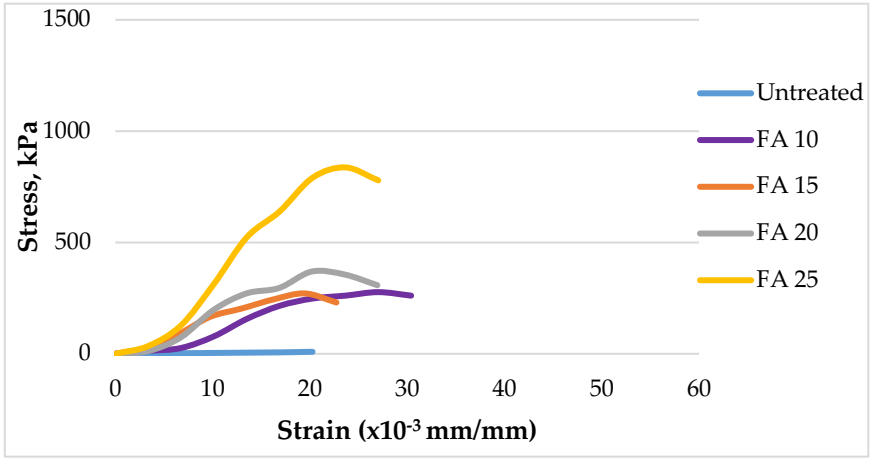
Figure A.2: Stress vs Strain Curve for Water Content = Liquid Limit (i) L/P=0.2 (ii) L/P=0.5 (iii) L/P=0.8



(i)



(ii)



(iii)

Figure A.3: Stress vs Strain Curve for Water Content =1.25 x Liquid Limit (i) L/P=0.2 (ii) L/P=0.5 (iii) L/P=0.8